



Fakultät für Physik  
Institut für Theorie der Kondensierten Materie

---

# **Ab-initio-Simulation von STM-Experimenten unter Verwendung von Clusterrechnungen mit Anwendung auf die Fullerene $C_{60}$ and $C_{58}$**

Diplomarbeit

von

**Melanie Stendel**

11.Juni.2012

Referent: Prof. (apl.) Dr. F. Evers  
Korreferent: Prof. Dr. W. Wulfhekel



---

Ich erkläre hiermit, dass ich diese Arbeit selbständig verfasst und keine anderen als die angegebenen Hilfsmittel verwendet habe.

Karlsruhe, den 11.Juni.2012



# Deutsche Zusammenfassung

Im Jahre 1985 wurde in der Gruppe von Kroto ein Molekül entdeckt, das aus 60 Kohlenstoffatomen besteht, welche eine geschlossene Käfig Struktur bilden. Da diese Struktur der geodätischen Kuppel von Buckminster Fuller ähnelt, wurde das gefundene Molekül  $C_{60}$  Buckminsterfulleren genannt. Darüber hinaus wurde eine ganze Klasse von sphärischen Kohlenstoffstrukturen gefunden, welche sich in der Anzahl der Kohlenstoffatome unterscheiden. Diese Klasse von Molekülen wird Fullerene oder Buckyballs genannt.

Fullerene zeigen strukturelle und elektronische Eigenschaften, die einzigartig sind. Mit ihrer Entdeckung öffnete sich ein neuer Forschungsbereich. Die Bedeutung der Entdeckung dieser Klasse von Molekülen wurde im Jahre 1996 durch die Verleihung des Nobel-Preises in Chemie an ihre Entdecker Kroto, Curl und Smalley hervorgehoben. Eine verwandte faszinierende Molekülstruktur, die nur aus Kohlenstoffatomen besteht, sind die sogenannten Kohlenstoff-Nanoröhren (CNTs, aus dem Englischen “carbon nanotubes”). Diese Struktur wurden im Jahre 1991 von Iijima gefunden. Für diese Entdeckung wurde ihm 2008 der Kavli-Preis in Nanowissenschaften verliehen. Fullerene und Kohlenstoff-Nanoröhren sind heutzutage von großem Interesse in vielen Bereichen der Wissenschaft, wie zum Beispiel in der Physik, der Chemie, den Materialwissenschaften und den Ingenieurwissenschaften.

Elektronische Bauteile wurden in den letzten Jahren immer kleiner. Die Größe solcher Komponenten ist mittlerweile im Nanometerbereich angelangt. Aus diesem Grund werden auch Fullerene und Kohlenstoff-Nanoröhren auf ihre Anwendbarkeit untersucht. So wurde zum Beispiel gezeigt, dass es möglich ist, einen elektromechanischen Transistor aus einzelnen  $C_{60}$  Molekülen oder einzelnen Kohlenstoff-Nanoröhren zu bauen. Die Dimension eines solchen Transistors ist circa 50 nm. Ausserdem finden Fullerene und Kohlenstoff-Nanoröhren auch Anwendungsmöglichkeiten im Bereich der Dünnschicht Technologie. So wurden kürzlich Geräte in der Photovoltaic und als Photodetektor vorgeschlagen, welche aus einer heterogenen Dünnschicht-Verbindung aus Kohlenstoff-Nanoröhren und  $C_{60}$  bestehen.

Fullerene  $C_n$  mit mindestens 60 Kohlenstoffatomen ( $n \geq 60$ ) wurden bereits experimentell und theoretisch intensiv untersucht. Dagegen wurden kleinere Fullerene lange Zeit als hoch chemisch reaktiv und daher als instabil angesehen. Aufgrund dessen ist ihnen bisher sehr viel weniger Aufmerksamkeit geschenkt worden. Dies hängt vor allem mit den Herstellmöglichkeiten des jeweiligen Fullerenes zusammen. Durch die von Krätschmer im Jahre 1990 entwickelte Methode wurde es möglich,  $C_{60}$  in großen Mengen herzustellen. Kleinere

Fullerene werden aus  $C_{60}$  gewonnen, in dem  $C_{60}$  mit Elektronen beschossen wird, woraufhin sich ein geradzahliges Vielfaches von  $C_2$  herauslöst. Die resultierenden Fullerene werden anschliessend mittels preparativer Massen-Spektrometrie selektiert. Dieses Verfahren wurde im Laufe der letzten Jahren verbessert, so dass heutzutage auch kleinere Fullerene wie  $C_{58}$  zugänglich sind.

Die vorliegende Arbeit wurde insbesondere durch STM-Experimente (Rastertunnelmikroskopie, vom Englischen “scanning tunneling microscopy”) mit Fullerenen motiviert, welche aktuell in Karlsruhe durchgeführt wurden. Dabei sind sowohl  $C_{60}$  als auch  $C_{58}$  Moleküle auf einer Goldoberfläche experimentell untersucht worden. Wir erstellen im Rahmen dieser Arbeit einen Katalog mit simulierten Topographie Bildern für  $C_{60}$  and  $C_{58}$  auf Au(111). Dafür untersuchen wir  $C_{60}$  mit ikosahedraler Symmetrie und zwei Isomere von  $C_{58}$  mit  $C_{3v}$ - bzw.  $C_s$ -Symmetrie. Durch Vergleich der simulierten Bilder mit den experimentellen Aufnahmen, wollen wir die Bindungsgeometrie dieser Fullerene auf der Au(111) Oberfläche bestimmen.

Zur Untersuchung der Moleküle  $C_{60}$  und  $C_{58}$  verwenden wir die Dichtefunktionaltheorie (Kohn-Sham-Formulierung, B-P86-Funktional; TURBOMOLE Implementierung). Dabei tritt ein wesentliches Problem bedingt durch die lokalen Näherungen in den Austausch-Korrelations-Funktionalen auf. Das Bindungsverhalten der Fullerene auf Goldoberflächen ist bestimmt durch van-der-Waals Wechselwirkungen. Allerdings werden diese Beiträge im verwendeten GGA-Funktional nicht korrekt beschrieben. Daher verwenden wir empirische Korrekturterme (DFT-D) um diese Wechselwirkung zu berücksichtigen. Um die elektronischen Eigenschaften der Moleküle auf der Oberfläche zu untersuchen, modellieren wir die Oberfläche zuerst als ein endliches Goldcluster. Dieses erweiterte Molekül kann dann durch eine Einteilchen-Greensfunktion beschrieben werden. Die makroskopische Oberfläche wird mittels eines Formalismus der Green’schen Funktion (Selbstenergie; absorbierende Randbedingungen) hinzugefügt. Dieser “embedding”-Formalismus ist im Rahmen dieser Diplomarbeit aus einem bestehenden Transport-Formalismus entwickelt worden. Die elektronischen Eigenschaften des Moleküls auf einer endlichen Oberfläche bestimmen wir wie bereits erwähnt mittels der Dichtefunktionaltheorie. Für ein System endlicher Größe sind die Zustände diskret. Diese diskreten Zustände des erweiterten Moleküls erfahren auf einer sehr großen Oberfläche im Vergleich zur Größe des Moleküls eine Verbreiterung. Somit gehen die diskreten Niveaus in einen kontinuierlichen Verlauf der lokalen Zustandsdichte (LDOS, aus dem Englischen “local density of states”) über. Um diese Einfluß der Oberfläche auf das erweiterte Molekül zu berücksichtigen, ist es notwendig eine “unendlich“ große Oberfläche in den Rechnungen zu integrieren. Die Modellierung dieser unendlichen Oberfläche wird durch den erwähnten “embedding”-Formalismus erreicht. Ausserdem haben wir das Programm erweitert. Es ist nun möglich, die ortsaufgelöste Zustandsdichte in einer Ebene oberhalb des Moleküls zu berechnen. Die ortsaufgelöste Zustandsdichte ist in erster Näherung proportional zum Tunnelstrom in den STM-Experimenten. Daher ist ein Vergleich zwischen den simulierten Topographie Bildern und den experimentellen STM Aufnahmen nützlich.

Unsere Analyse von  $C_{60}$  als auch  $C_{58}$  gliedert sich in zwei Teile. Zuerst untersuchen wir

die elektronischen Eigenschaften der Moleküle in der Gasphase. Anschliessend prüfen wir mögliche Bindungsgeometrien der Moleküle auf der Goldoberfläche. Die Bindungsgeometrien erstellen wir, indem wir die in der Gasphase optimierte Struktur des Fulleren auf die Goldoberfläche (Au(111)) setzen. Kohlenstoffatome nehmen bei der Bindung mit Goldoberflächen Positionen direkt oberhalb der Goldatome ein, sogenannte “on-site” Positionen. Daher rotieren wir das Molekül auf der Oberfläche so, dass ein Polygon des Moleküls parallel zur Oberfläche ist und Kohlenstoffatome dieses Polygons on-site Positionen einnehmen. Da die Goldoberfläche allerdings eine Kraft auf die Kohlenstoffatome des Fulleren ausübt, führen wir anschliessend eine Optimierung des Moleküls auf der Oberfläche durch, wobei die Positionen der Goldatome allerdings festgehalten werden.

Unsere Untersuchung beginnt mit  $C_{60}$ . Dieses klassische Fulleren bestehend aus Hexagonen und Pentagonen besitzt ikosahedrale Symmetrie. Diese hohe Symmetry bringt eine hohe Entartung der Energieniveaus in der Gasphase mit sich. DFT-Rechnungen ergeben eine Energielücke von 1.6 eV zwischen dem höchsten besetzten Orbital (HOMO, vom Englischen “highest occupied molecular orbital”) und dem niedrigsten unbesetzten Orbital (LUMO, “lowest unoccupied molecular orbital”). Dieser Wert ist kleiner als der experimentelle Wert von 2.2 eV. Die Differenz ist teilweise eine Folge des verwendeten GGA-Funktional in den DFT-Rechnungen, da dieses die Energielücke unterschätzt.

Wir erstellen zwei Bindungsgeometrien für  $C_{60}$  auf Au(111), mit einem Hexagon und mit einem Pentagon parallel zur Oberfläche. Anschliessend führen wir für beide Geometrien eine systematische Untersuchung des Bindungsabstands durch um die Bindungsgeometrie mit der maximalen Bindungsenergie zu ermitteln. So finden wir, dass die Bindungsenergie für das Hexagon größer ist als für das Pentagon. Für beide Geometrien berechnen wir die ortsaufgelöste Zustandsdichte an der Fermikante. Die experimentellen STM Bilder von  $C_{60}$  auf Au(111) zeigen eine sechszählige Symmetrie. Diese Symmetrie finden wir in unseren simulierten Topographie Bildern ebenfalls, wenn das höchste Polygon des Fulleren ein Hexagon ist.

Da sich die von uns verwendete Methode für  $C_{60}$  auf Au(111) bewährt hat, wenden wir diese auf  $C_{58}$  an. Wir untersuchen in dieser Arbeit zwei Isomere von  $C_{58}$ . Zum einen ein Isomer mit  $C_{3v}$ -Symmetrie, welches ein klassisches Fulleren ist, bestehend aus Hexagonen und Pentagonen. Zum anderen ein Isomer mit  $C_s$ -Symmetrie, welches neben Hexagonen und Pentagonen ein Heptagon besitzt, daher ein sogenanntes nicht-klassisches Fulleren ist. Wir beginnen unsere Analyse mit der Untersuchung der elektronischen Eigenschaften der beiden Isomere in der Gasphase. Der Grundzustand des Isomers mit  $C_{3v}$ -Symmetrie ist ein Triplett-Zustand, während der Grundzustand des Isomers mit  $C_s$ -Symmetrie ein Singulett-Zustand ist. Ausserdem ist das Isomer mit  $C_{3v}$ -Symmetrie in der Gasphase stabiler als das Isomer mit  $C_s$ -Symmetrie. Weiterhin ist die HOMO-LUMO-Lücke für das Isomer mit  $C_s$ -Symmetrie mit 0.6 eV doppelt so groß wie die des Isomers mit  $C_{3v}$ -Symmetrie.

Da die Symmetrie der beiden untersuchten Isomere von  $C_{58}$  sehr viel geringer ist als die ikosahedrale Symmetrie von  $C_{60}$ , ergeben sich sehr viel mehr mögliche Bindungsgeometrien. Deswegen treffen wir für beide Isomere eine Auswahl an Geometrien die wir untersuchen. Die Bindungsgeometrien werden ebenfalls so erstellt, dass jeweils ein Polygon parallel

zur Oberfläche ist und dass Kohlenstoffatome on-site Positionen einnehmen. Insbesondere untersuchen wir die Bindungsgeometrie des Isomers  $C_s$  mit dem Heptagon parallel zur Oberfläche. Wir finden, dass das Isomer mit  $C_{3v}$ -Symmetrie die Bindung zur Oberfläche mit einem Hexagon bevorzugt gegenüber einer Bindung mit einem Pentagon. Das Isomer mit  $C_s$ -Symmetrie hingegen bevorzugt die Bindung mit dem Heptagon. Ausserdem bindet das Isomer mit  $C_s$ -Symmetrie mit dem Heptagon besser zur Oberfläche als das Hexagon des Isomers mit  $C_{3v}$ -Symmetrie.

Für die von uns untersuchten Bindungsgeometrien von  $C_{58}$  auf der Au(111) Oberfläche berechnen wir die orts aufgelöste Zustandsdichte um einen Katalog von simulierten Topographie Bildern zu erstellen. Die experimentellen STM Bilder zeigen je nach angelegter Spannung eine ringartige Struktur oder ein zentrales Maximum. Da diese Bilder für verschiedene Spannungen aufgenommen wurden, integrieren wir die Zustandsdichte ausserdem über den entsprechenden Energiebereich. Unsere simulierten Topographien zeigen viele verschiedene Charakteristika. Allerdings finden wir auch die Eigenschaften der experimentellen Bilder wieder für eine Bindungsgeometrie. Das zugehörige Isomer hat die  $C_s$ -Symmetrie und bindet mit dem Heptagon zur Oberfläche.

Wir haben in dieser Arbeit einen Hinweis dafür gegeben, dass sich  $C_{58}$  auf der Oberfläche im Experiment befindet. Weiterhin haben wir die Bindungsgeometrien von  $C_{60}$  und  $C_{58}$  mit Hilfe der Topographie Aufnahmen und Vergleich mit dem Experiment identifiziert. Da man annehmen darf, dass die Struktur der LDOS-Muster, die im Katalog auftreten, nicht stark vom Substrat abhängen, wird man erwarten, daß der Katalog auch für die Identifizierung von Bindungsgeometrien auf anderen Substraten, zum Beispiel Au(100), nützlich sein kann.



Fakultät für Physik

Institut für Theorie der Kondensierten Materie

---

**Ab-initio simulations of STM experiments  
employing finite cluster studies and  
application to the fullerenes  $C_{60}$  and  $C_{58}$**

Diplomathesis

by

**Melanie Stendel**

June 11th, 2012

Referent: Prof. (apl.) Dr. F. Evers  
Coreferent: Prof. Dr. W. Wulfhekel



---

# Contents

<b>1</b>	<b>Introduction</b>	<b>5</b>
1.1	Atomic Structure of Fullerenes . . . . .	6
1.2	Recent Experiments on Fullerenes . . . . .	9
1.3	Motivation underlying this Thesis and Overview . . . . .	12
<b>2</b>	<b>Formalism</b>	<b>15</b>
2.1	Density Functional Theory . . . . .	15
2.1.1	The Kohn-Sham Equations . . . . .	16
2.1.2	Approximations for the exchange-correlation-functional . . . . .	18
2.1.3	Empirical Corrections for Dispersive Interactions . . . . .	20
2.1.4	Contracted Gaussian Type Orbitals . . . . .	23
2.2	Embedding Formalism . . . . .	24
2.2.1	Embedding Green's Function Formalism . . . . .	24
2.2.2	Self-Energy . . . . .	25
2.2.3	Local Density of States . . . . .	25
2.2.4	Tunnel Current . . . . .	26
<b>3</b>	<b>Electronic Structure of <math>C_{60}</math></b>	<b>29</b>
3.1	$C_{60}$ in Vacuum . . . . .	29
3.2	$C_{60}$ on Au(111) . . . . .	30
3.2.1	Geometry Optimisation . . . . .	31
3.2.2	Local Density of States . . . . .	34
3.2.3	Simulated Topography . . . . .	36
3.2.4	Comparison with Literature . . . . .	38
<b>4</b>	<b>Electronic Structure of <math>C_{58}</math></b>	<b>41</b>
4.1	$C_{58}$ in Vacuum . . . . .	41
4.2	$C_{58}$ on Au(111) . . . . .	44

4.2.1	Geometry Optimisation of $C_{58}$ with $C_{3v}$ Symmetry . . . . .	44
4.2.2	Geometry Optimisation of $C_{58}$ with $C_s$ Symmetry . . . . .	47
4.2.3	Summary regarding Geometry Optimisation . . . . .	51
4.2.4	Local Density of States . . . . .	52
4.2.5	Simulated Topography . . . . .	56
<b>5</b>	<b>Summary and Outlook</b>	<b>59</b>
<b>A</b>	<b>Atomic Coordinate Files</b>	<b>65</b>
<b>B</b>	<b>Catalogue</b>	<b>85</b>
	<b>Bibliography</b>	<b>143</b>

# Chapter 1

## Introduction

In 1985 a molecule was discovered by Kroto et. al. [1]. This molecule consists of 60 carbon atoms which form a closed cage structure. Since this structure resembles the geodesic domes build by Buckminster Fuller, it is named the buckminsterfullerene. Furthermore, a whole class of spherical carbon structures that differ in the number of carbon atoms have been found. Such spherical molecules are called fullerenes or buckyballs.

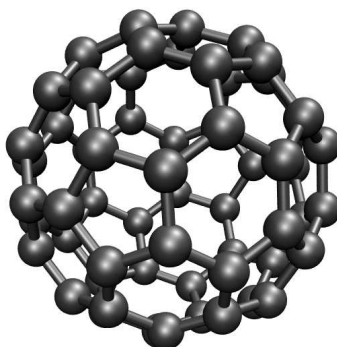


Figure 1.1: Atomic structure of the buckminsterfullerene C<sub>60</sub>

Fullerenes opened a new field of research because of their unique structural and electronic properties [2]. The importance of the discovery of the fullerenes was acknowledged by presenting Kroto, Curl and Smalley with the Nobel Prize in Chemistry in 1996. Another fascinating structure formed of carbon atoms, the carbon nanotubes (CNTs), was found in 1991 by Iijima [3]. For this finding, he was awarded with the Kavli Prize in Nanoscience 2008. Today, both fullerenes and carbon nanotubes are still of great interest in various fields of research like physics, chemistry, material science and device engineering [4].

The miniaturisation of electronic devices requires smaller and smaller electronic building devices. However, the size of such devices has reached the nanometre scale, restricting the size of a device to the size of a single molecule. This calls for research on single molecules like

fullerenes and carbon nanotubes. It has been shown, that a  $C_{60}$  electromechanical transistor [5] as well as a carbon nanotube transistor [6] are scalable to dimensions well below 50 nm [7]. Furthermore, fullerenes and carbon nanotubes do not only find an applicability as single molecules but also as thin-films. Efficient photovoltaic and photodetector devices constructed of a thin-film carbon nanotube and  $C_{60}$  heterojunction have been proposed recently [8].

## 1.1 Atomic Structure of Fullerenes

As mentioned above, fullerenes are closed cage structures which consist of only carbon atoms (Fig. 1.1). Each atom forms a covalent bond with three neighbouring atoms forming a curved  $\pi$ -conjugation. In chemical structural formulae this is usually displayed by two single bonds and one double bond. Therefore fullerenes with an odd number of carbon atoms have at least one atom with a dangling, unsatisfied valence. Consequently, fullerenes with an odd number of carbon atoms have not been isolated, yet [9, 10].

Fullerenes are classified as either classical or non-classical. Classical ones are built of only pentagons and hexagons, whereas the non-classical ones also contain tetragons and heptagons. In general, non-classical fullerenes are less stable than classical ones.

A good 2-dimensional illustration of the 3-dimensional fullerene, called Schlegel Graph (Fig. 1.2), is obtained by stretching the vertices of a chosen polygon, until the polyhedron becomes planar. This image is helpful because the structure of the fullerene is immediately obvious. However, the projection is not unique since it depends on the chosen polygon. Usually, the polygon through which the highest symmetric axis runs is chosen. However, this is not always possible as the highest symmetric axis can also be through an atom or an edge.

In mathematical terms, fullerenes can be described as convex polyhedra. Euler's polyhedron formula [11]

$$V - E + F = 2 \quad (1.1)$$

gives a connection between the number of vertices  $V$ , edges  $E$  and faces  $F$  of a polyhedron. It applies to spherical polyhedra like fullerenes, too. A fullerene  $C_n$  with  $n$  carbon atoms has  $V = n$  vertices. Since each carbon atom is bound to three neighbours and with the correction that each bond is counted twice, the number of edges is given by

$$E = \frac{3n}{2}. \quad (1.2)$$

The number of faces  $F$  is therefore

$$F = E - V + 2 = \frac{n}{2} + 2. \quad (1.3)$$

For a classical fullerene with  $p$  pentagons and  $h$  heptagons, the expression for the vertices

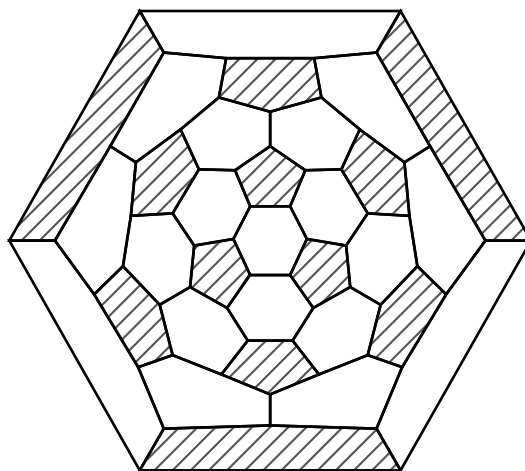


Figure 1.2: Example of a Schlegel Graph: the buckminsterfullerene  $C_{60}$

and the faces can be rewritten as

$$V = \frac{5p + 6h}{3}, \quad (1.4)$$

$$F = p + h. \quad (1.5)$$

Inserting (1.4) into (1.3) gives

$$F = \frac{5p + 6h}{6} + 2 \stackrel{!}{=} p + h \quad (1.6)$$

and finally results in a constant number of 12 pentagons in each classical fullerene. The number of hexagons is therefore given by

$$h = \frac{n}{2} - 10. \quad (1.7)$$

Thus, the smallest classical fullerene possible is the dodecahedron  $C_{20}$  which has 12 pentagonal faces and no hexagonal face. Non-classical fullerenes have not only a variable number of hexagons, but also a variable number of pentagons.

The number of classical isomers of a fullerene  $C_n$  grows rapidly with  $n$ , for example  $C_{20}$  has only one isomer,  $C_{50}$  271 isomers,  $C_{58}$  1205 isomers and  $C_{60}$  already 1812 isomers [12]. The stability of an isomer obeys some rules which depend on the arrangement of the pentagons within the fullerene:

- Isolated Pentagon Rule (IPR) [13, 14]: Connected pentagons lead to a higher local bending of the cage which results in a strong bond-angle strain and is therefore energetically unfavourable. Hence, the most stable fullerenes are those where the pentagons are separated from each other. The most famous and smallest IPR fullerene

is the icosahedral buckminsterfullerene  $C_{60}$ . All fullerenes with adjacent pentagons (AP) are called non-IPR fullerenes.

- Pentagon Adjacency Penalty Rule (PAPR) [15, 16]: Isomers with the smallest number of adjacent pentagons are energetically more favourable. The energy within a set of isomers grows linearly with the number of pentagon adjacencies by  $80 - 100 \frac{\text{kJ}}{\text{mol}}$  per adjacency. Furthermore, the lost energy grows with increasing cage size because the perturbation of two adjacent pentagons is even higher. Thus, non-classical isomers can happen to be energetically more favourable than the destabilised non-IPR ones. Especially, non-classical one-heptagon isomers are competitive in energy with classical isomers [17].

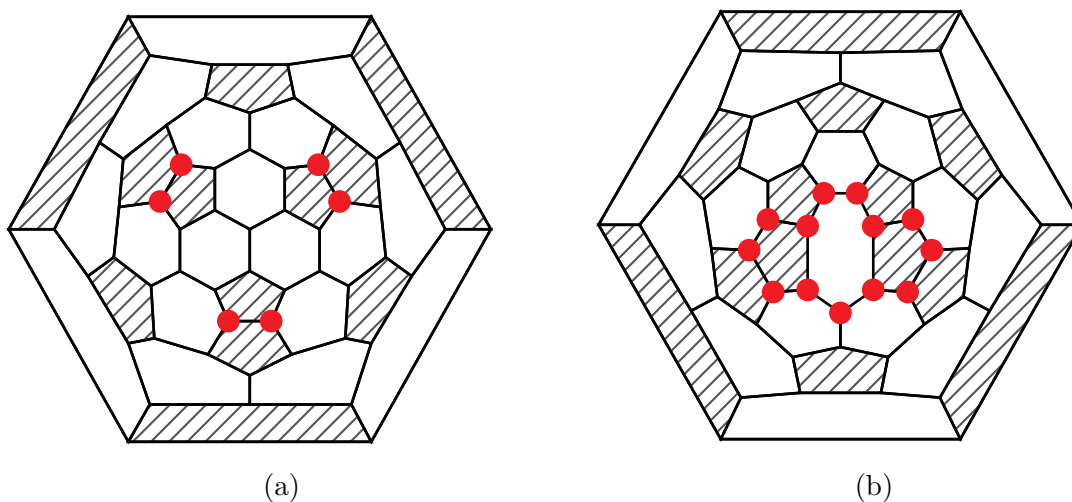


Figure 1.3: Schlegel Graphs of the two investigated isomers of  $C_{58}$ : (a) Classical non-IPR isomer with  $C_{3v}$  symmetry and three pairs of adjacent pentagons (3 x 2AP). (b) Non-classical isomer with  $C_s$  symmetry and a heptagon as well as two chains of three adjacent pentagons (2 x C3AP). The reactive carbon atoms are coloured in red for both isomers.

These rules are explained by the behaviour of molecular orbitals. The  $sp^2$  hybridised carbon atom prefers to establish planar  $\sigma$ -bonds with its neighbours. Then the  $p_\pi$ -bond is perpendicular to the  $\sigma$ -bonds resulting in a  $\pi$ -conjugation. However, in fullerenes, the  $\sigma$ -bonds are not planar but pyramidalized causing the angle  $\Theta_{\sigma\pi}$  between the  $\sigma$ -bond and the  $p_\pi$ -bond to be larger than  $90^\circ$ . A measure for the local weakening of the  $\sigma$ -framework due to the curvature of the carbon surface is the pyramidalization angle  $\Theta_p = \Theta_{\sigma\pi} - 90^\circ$  [18, 19]. For icosahedral  $C_{60}$  the pyramidalization angle is equal for all carbon atoms  $\Theta_p \approx 11.6^\circ$ , but it is always larger for smaller fullerenes. Consequently, a larger pyramidalization angle leads to a higher reactivity towards other reactions and to a more unstable structure of the fullerene. Especially adjacent pentagons exhibit the largest pyramidalization angle and

thus they present highly reactive sites [2, 20]. Furthermore, rings different from hexagons and pentagons are expected to lead to a higher reactivity too [21].

In this study, we investigate the buckminsterfullerene  $C_{60}$  and two isomers of  $C_{58}$ . The buckminsterfullerene  $C_{60}$  as illustrated in Figure 1.2 is the smallest possible IPR fullerene. It is constructed of 12 pentagons and 20 hexagons and exhibits icosahedral symmetry. Furthermore, we examine a classical non-IPR fullerene of  $C_{58}$  which possesses  $C_{3v}$  symmetry as illustrated in Figure 1.3a. This isomer has three pairs of adjacent pentagons (3 x 2AP) and is constructed of 12 pentagons and 19 hexagons. Moreover, a non-classical non-IPR isomer of  $C_{58}$  with  $C_s$  symmetry is analysed. It contains a heptagon, 12 pentagons and 16 hexagons. Furthermore, it exhibits two chains of three adjacent pentagons (2 x C3AP) as illustrated in (Fig. 1.3b). These two isomers of  $C_{58}$  are shown to be the most stable ones with essentially the same stability [22].

## 1.2 Recent Experiments on Fullerenes

Recent experiments on the fullerenes  $C_{60}$  and  $C_{58}$  have been performed in Karlsruhe [23]. Before we present the results of these experiments, we first describe the synthesis of fullerenes as well as the experimental setup.

It is possible to produce macroscopic amounts of IPR fullerenes using a method developed by Krätschmer in 1990 [24]. Thereby, a carbon soot is produced by evaporating pure graphite electrodes in helium gas at reduced pressure. The soot contains a few percent of IPR fullerenes which are then extracted from the soot in a multistep procedure.

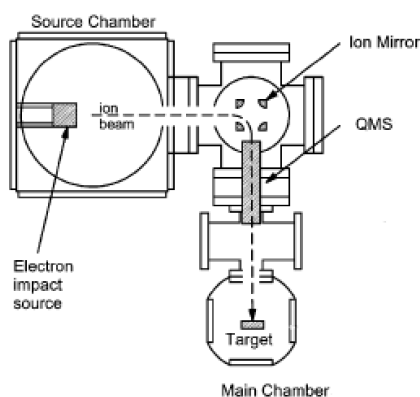


Figure 1.4: The experimental setup: the electron impact ionisation source creates a fullerene ion beam which is then bent by 90° in an ion mirror, mass selected by a quadrupole mass filter (QMS), decelerated and soft landed on a target surface (Picture taken from [25]).

Smaller fullerenes, which can also be non-IPR ones, are produced by electron-impact induced ionisation of those IPR fullerenes (Fig. 1.4). Thereby, an even multiple of  $C_2$  is extracted from the IPR fullerenes such that a smaller positive ion is obtained, for example



The resulting positive ion beam is then deflected by  $90^\circ$  in an ion mirror in order to prevent neutral fullerenes from reaching the surface. Afterwards, the ions are mass selected in a quadrupole mass filter in order to remove all undesired ions. Finally, they are decelerated and soft landed on a target surface where they are neutralised depending on the surface [25].

In order to explore the surface topography of a sample, scanning tunneling microscopy (STM) is used. It was invented by G. Binnig and H. Rohrer in 1981 [26]. This technology allows for atomic resolution of single molecules as well as whole layers. In 1986, Binnig and Rohrer were awarded with the Nobel Prize in Physics for their invention.

The underlying principle of STM is the quantum mechanical tunneling effect. A conducting tip scans the sample surface while a bias is applied causing electrons to tunnel between the tip and the sample creating a tunnel current. Thereby, the position of the tip is piezoelectric controlled in all three directions. Furthermore, the STM has two operation modes:

- *constant height mode* (Fig. 1.5a): The height, i.e. the  $z$  position, of the tip to the surface is kept constant while the tunnel current is recorded. Thus, the tunnel current in dependence of the  $(x, y)$  position of the tip is mapped. Even though this mode allows to scan the sample quickly, it always bears the risk that the tip might crash into the surface.
- *constant current mode* (Fig. 1.5b): The sample is scanned at a constant tunnel current by recording the  $z$  position of the tip. If the current increases due to a change in height of the surface, then the tip is lifted in order to keep the current at a constant value. Thus, the topography of the surface is revealed. A feed-back loop is used which reads out the tunnel current and adjusts the height of the tip accordingly. This mode operates with a slower speed than the *constant height mode* but it avoids tip crashes with the surface.

The study of nanostructures like fullerenes requires several conditions to the experimental setup such that unwanted influences are reduced allowing for a high sensitivity of the STM. In order to avoid a contamination of the sample with perturbing adsorbates, the preparation of the sample as well as the measurement are carried out in ultra high vacuum (UHV). Furthermore, the whole system is decoupled from external noise effects by a damping system. In order to reduce thermal effects, in particular the mobility of the fullerenes on the surface, the drift of the tip relative to the surface as well as thermal fluctuations of the examined properties, the experiments are performed at low temperatures.

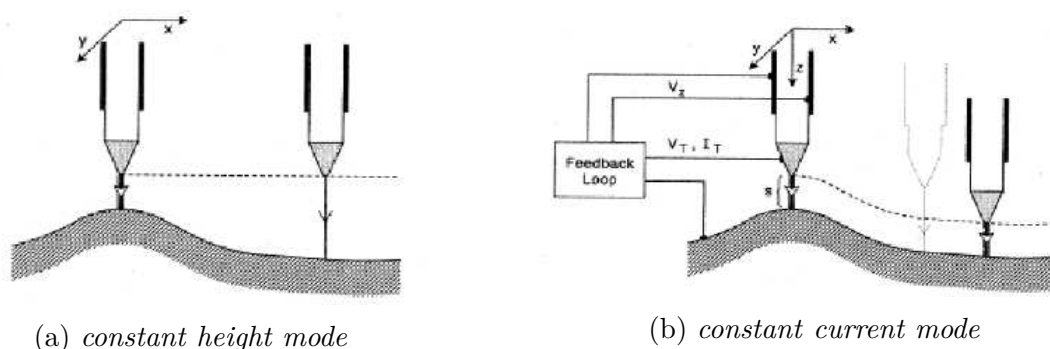


Figure 1.5: Illustration of the two operating modes of a STM: the *constant height mode* and the *constant current mode* (Pictures taken from [26]).

The STM images presented in Figure 1.6 and Figure 1.7 of  $C_{60}$  and  $C_{58}$  are obtained by a self-made STM instrument in the *constant current mode* [23]. This setup consists of three chambers, namely the load-lock, the preparation and the STM chamber. Since the preparation of a sample and the measurements are performed under UHV, the load-lock chamber allows to insert samples into the system without breaking the UHV of the two other chambers. The loaded samples are then transferred into the preparation chamber where unwanted adsorbates are removed. Furthermore, a gold surface is prepared and  $C_{60}$  or  $C_{58}$  fullerenes are deposited. As said above, the STM operates on low temperatures in order to reduce thermal effects. Thus, the STM chamber contains the STM which is coupled to a liquid He bath cryostat which allows for a working temperature of 4.2 K. To reduce the  $He^4$  consumption, a  $N_2$  cryostat is mounted around the  $He^4$  one. The sensitivity of the STM is approximately 0.002 nm depth resolution and 0.1 nm lateral resolution [27, 28].



Figure 1.6: Experimental STM images of  $C_{60}$  on Au(111) obtained near zero bias. The single  $C_{60}$  in (b) is Laplace filtered. [23]

Moreover, the lateral sensitivity also depends on the form of the tip. In an ideal case, there is only a single atom at the tip apex which contributes to the tunnel current. Even then has the prepared tip an approximately pyramidal form so that not only one atom

might add to the tunnel current. Since the height of the tip is just a few Angström, molecules might jump from the surface onto the tip. This effect is reduced by covering the tip, fabricated of iridium-platinum, by gold atoms [23].

The resulting STM image of  $C_{60}$  on Au(111) (Fig. 1.6b) is Laplace filtered. This filter identifies regions in the STM image where the brightness changes sharply i.e. has discontinuities. Therewith, homogeneous areas are separated from one another by edges. Therefore, the structure of the STM image becomes more sharp.

STM images for  $C_{60}$  at the Fermi energy are presented in Figure 1.6. A sixfold symmetry is clearly visible. The results for  $C_{58}$  as presented in Figure 1.7 are obtained at different voltages. When applying a positive bias, the electrons tunnel from occupied states in the sample to unoccupied states in the tip. It is vice versa for negative voltages. They do not display a symmetry like  $C_{60}$ . Instead, there is a centric maximum for large voltages, i.e.  $\pm 2V$  which for smaller voltages becomes a ring like structure.

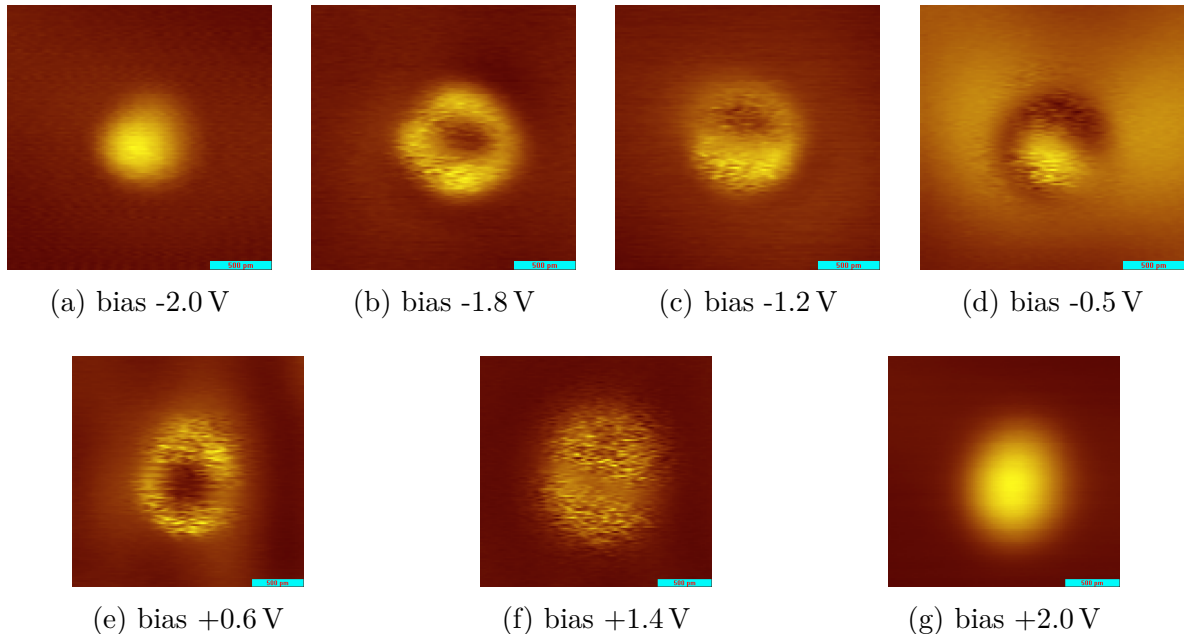


Figure 1.7: Experimental STM images of  $C_{58}$  on Au(111) obtained for different applied voltages [23]. The blue bar at the lower right corner represents the length scale of 500 pm.

### 1.3 Motivation underlying this Thesis and Overview

Fullerenes  $C_n$  with  $n \geq 60$ , especially IPR fullerenes, have been prepared and studied experimentally as well as theoretically [21]. Since smaller fullerenes are always non-IPR fullerenes, they were assumed to be unstable and highly reactive. Due to this prejudice,

they received less attention than the larger IPR fullerenes [22]. However, developments in synthesis and preparative mass spectrometry have made it possible to synthesise these smaller fullerenes such as  $C_{58}$  [25] and study their properties experimentally.

Motivated by the STM experiments on  $C_{60}$  and  $C_{58}$  presented in Figure 1.6 and Figure 1.7, we study these fullerenes from a theoretical point of view. Currently, it is not known which isomer of the fullerenes is present on the Au(111) surface in the experiments. Furthermore, the orientation of the molecules towards the surface cannot easily be extracted from the experimental STM images. Thus, a detailed investigation of several binding geometries of  $C_{60}$  and  $C_{58}$  to the Au(111) surface as well as the corresponding topography is needed. To this end, we aim to develop a catalogue that contains the major theoretically determined topographies for  $C_{60}$  and  $C_{58}$  which is presented in Appendix B. For this reason we investigate the most stable isomers of these fullerenes, namely the buckminsterfullerene  $C_{60}$  with icosahedral symmetry (Fig. 1.2) and two isomers of  $C_{58}$  which exhibit  $C_{3v}$  and  $C_s$  symmetry (Fig. 1.3). As will be shown, the molecule in the experiments as well as its binding geometry can be identified using our catalogue.

In detail we analyse several binding geometries of the above mentioned fullerenes on a Au(111) surface as well as the role of the reactive centres of  $C_{58}$  in binding to the surface. In order to simulate the STM measurements, we calculate the local density of states (LDOS). Since we use a quantum chemistry code, we have the opportunity to determine the electronic properties of the molecule in vacuum as well as on a finite-size surface with several basis sets. The use of different basis sets makes it possible to check if our results reached convergence. However, the LDOS of a finite system exhibits discrete states. In contrast on the real surface used in the experiments these discrete states experience a level broadening. In order to account for this effect, a bigger, effectively infinite surface needs to be included in our calculation. This embedding formalism, based on an existing transport code, is implemented during this study. Furthermore, the possibility to calculate the spatially resolved density of states in a plane above the molecule has been included in the code. Therefore, we are able to calculate the local density of states at four representative heights above the molecules for the investigated contact geometries and thus obtain the corresponding topographic images which can then be compared to the experimental ones.

In conclusion, the structure of this study is as follow: while this chapter mainly dealt with the experiments on fullerenes the proceeding chapters are concerned with theoretical calculations on fullerenes. In Chapter 2 we give an introduction into the formalism including the density functional theory as well as the newly implemented embedding formalism. Afterwards, the formalism is tested on the fullerene  $C_{60}$  in Chapter 3. Finally the results on  $C_{58}$  are presented in Chapter 4. A brief conclusion in Chapter 5 will summarise the study.



# Chapter 2

## Formalism

### 2.1 Density Functional Theory

In order to investigate the electronic ground state properties of many-body systems such as atoms, molecules and solids from first principles, density functional theory (DFT) has become a very successful tool [29]. In this method electronic systems are no longer described by a many-body wave function, a complicated function that depends on  $3N$  coordinates, where  $N$  is the number of electrons. Instead, these systems are characterised by the electron density  $n(\vec{r})$ , which depends only on three coordinates.

This approach of using the electron density is justified by the Hohenberg-Kohn-theorems [30]:

1. For electron gases with Coulomb interactions, the ground state is a unique function of the ground state electron density  $n_0(\vec{r})$ .
2. It is possible to define an energy functional

$$E_v[n(\vec{r})] = F[n(\vec{r})] + \int_{\mathbb{R}^3} v(\vec{r})n(\vec{r}) d\vec{r}, \quad (2.1)$$

where the functional  $F[n(\vec{r})]$  is independent of an external potential  $v$ . For the ground state density  $n_0(\vec{r})$  the energy  $E_v[n_0(\vec{r})]$  equals the correct ground state energy  $E_0$ . For each density  $n(\vec{r})$ , with the restrictions  $n(\vec{r}) \geq 0$  and  $\int n(\vec{r}) d\vec{r} = N$ , the condition for the energy functional

$$E_v[n(\vec{r})] \geq E_0[n_0(\vec{r})] \quad (2.2)$$

is fulfilled. This means, that the functional  $E_v[n(\vec{r})]$  assumes its minimum value for the correct ground state density corresponding to the external potential  $v$ .

The Hohenberg-Kohn theorems were initially restricted to non-degenerate ground states, but have been generalised to degenerate ground states as well [31].

Though the theorems give evidence for the existence of such an energy functional  $F[n(\vec{r})]$ , they provide no explicit form for it. The ground state energy can be divided into three parts, namely the functional for the ground state kinetic energy  $T[n(\vec{r})]$ , the electron-electron interaction energy  $U[n(\vec{r})]$  and the external potential energy  $V[n(\vec{r})]$ :

$$E[n(\vec{r})] = T[n(\vec{r})] + U[n(\vec{r})] + V[n(\vec{r})] . \quad (2.3)$$

The kinetic and interaction energy functional for a given system are not known exactly and therefore approximations for those have to be used in order to gain an energy functional with which the ground state properties are calculated approximately.

### 2.1.1 The Kohn-Sham Equations

Practical implementations of DFT in quantum chemistry are based on the Kohn-Sham (KS) Equations. The functional for the ground state kinetic energy  $T[n(\vec{r})]$  in the real system of  $N$  interacting electrons is approximated by the kinetic energy of a non-interacting model system  $T_s[n(\vec{r})]$  with the same electron density  $n_s(\vec{r}) = n(\vec{r})$ . The kinetic energy of the model system is the single particle kinetic energy

$$T_s[n(\vec{r})] = -\frac{\hbar}{2m} \sum_{i=1}^N \int_{\mathbb{R}^3} \phi_i^*(\vec{r}) \nabla^2 \phi_i(\vec{r}) d\vec{r} , \quad (2.4)$$

with the orbital wave functions  $\phi_i$ , called KS orbitals.

The kinetic energy of the interacting system is

$$T[n(\vec{r})] = T_s[n(\vec{r})] + T_c[n(\vec{r})] , \quad (2.5)$$

where  $T_c[n(\vec{r})]$  includes correlation effects. Hence, the energy functional can be rewritten:

$$E[n(\vec{r})] = T_s[n(\vec{r})] + U_H[n(\vec{r})] + V[n(\vec{r})] + E_{xc}[n(\vec{r})] . \quad (2.6)$$

Here, the electron-electron interaction  $U_H[n(\vec{r})]$  in the Hartree approximation is given by

$$U_H[n(\vec{r})] = \frac{e^2}{2} \int_{\mathbb{R}^3} \int_{\mathbb{R}^3} \frac{n(\vec{r}_1)n(\vec{r}_2)}{|\vec{r}_1 - \vec{r}_2|} d\vec{r}_1 d\vec{r}_2 . \quad (2.7)$$

The contribution to the energy functional not known is the so called exchange-correlation-functional

$$E_{xc}[n(\vec{r})] = T_c[n(\vec{r})] + U[n(\vec{r})] - U_H[n(\vec{r})] , \quad (2.8)$$

which often is somewhat smaller than the other terms in  $E[n(\vec{r})]$  [29]. Some approximations to treat  $E_{xc}[n(\vec{r})]$  are explained in Section 2.1.2.

So far, the form of the energy functional (2.6) is still exact.

The energy functional is now minimised with respect to the density and the functional derivative is required to vanish:

$$\frac{\delta E [n(\vec{r})]}{\delta n(\vec{r})} = \frac{\delta T_s [n(\vec{r})]}{\delta n(\vec{r})} + \frac{\delta U_H [n(\vec{r})]}{\delta n(\vec{r})} + \frac{\delta V [n(\vec{r})]}{\delta n(\vec{r})} + \frac{\delta E_{xc} [n(\vec{r})]}{\delta n(\vec{r})} \stackrel{!}{=} 0, \quad (2.9)$$

where  $\frac{\delta V [n(\vec{r})]}{\delta n(\vec{r})} = v(\vec{r})$  is the external potential in which the electrons move,  $\frac{\delta U_H [n(\vec{r})]}{\delta n(\vec{r})} = v_H(\vec{r}) = e^2 \int_{\mathbb{R}^3} \frac{n(\vec{r}')}{|\vec{r} - \vec{r}'|} d\vec{r}'$  is the interaction potential in the Hartree approximation and  $\frac{\delta E_{xc} [n(\vec{r})]}{\delta n(\vec{r})} = v_{xc}(\vec{r})$  is the exchange-correlation potential.

The kinetic energy of the interacting system is approximated by the single particle kinetic energy (2.4). Therefore, a model system of non-interacting electrons in an external potential  $v_s(\vec{r})$  is considered in the following. Since there is no interaction,  $U [n(\vec{r})] = 0$ , the energy functional reads, analogously to (2.3),

$$E_s [n(\vec{r})] = T_s [n(\vec{r})] + V_s [n(\vec{r})] \quad (2.10)$$

and the functional derivative

$$\frac{\delta E_s [n(\vec{r})]}{\delta n(\vec{r})} = \frac{\delta T_s [n(\vec{r})]}{\delta n(\vec{r})} + \frac{\delta V_s [n(\vec{r})]}{\delta n(\vec{r})} \stackrel{!}{=} 0, \quad (2.11)$$

in which  $\frac{\delta V_s [n(\vec{r})]}{\delta n(\vec{r})} = v_s(\vec{r})$ .

The KS ground state wave function is given by a Slater determinant with the orbital wave functions  $\phi_i$ , which fulfil the single-particle Schrödinger equation

$$\left( -\frac{\hbar^2}{2m} \nabla^2 + v_s(\vec{r}) \right) \phi_i(\vec{r}) = \varepsilon_i \phi_i(\vec{r}). \quad (2.12)$$

These equations can be solved and the density  $n_s(\vec{r})$  which solves the functional derivative (2.11) is defined as  $n_s(\vec{r}) = \sum_{i=1}^N |\phi_i(\vec{r})|^2$ . Since  $n_s(\vec{r}) = n(\vec{r})$ , this also satisfies the constraint of the functional derivative (2.9) of the interacting system.

Finally, returning to the interacting system with  $v_s(\vec{r}) = v(\vec{r}) + v_H(\vec{r}) + v_{xc}(\vec{r})$  the Kohn-Sham equations are derived:

$$\left( -\frac{\hbar^2}{2m} \nabla^2 + v(\vec{r}) + v_H(\vec{r}) + v_{xc}(\vec{r}) \right) \phi_i(\vec{r}) = \varepsilon_i \phi_i(\vec{r}). \quad (2.13)$$

Eventually, an interacting many-body system has been replaced by a non-interacting single-particle system in an effective potential  $v_s(\vec{r})$ .

The solution of the KS equations provides the correct ground state density of the real system of  $N$  interacting electrons. The wave function of the KS particles is given by the Slater determinant of the KS orbitals  $\psi_{\text{model}} = |\phi_1 \dots \phi_N|$ . Note, that this is not the correct wave function of the interacting system. If the exchange-correlation potential

$v_{xc}(\vec{r})$  is exact, the KS equations give the exact ground state density  $n_0(\vec{r})$ . In comparison to Hartree-Fock, which takes into account only an exchange operator, KS-DFT considers correlation effects additionally.

Since the Hartree potential  $v_H(\vec{r})$  and the exchange-correlation potential  $v_{xc}(\vec{r})$  also depend on the density  $n(\vec{r})$ , the KS equations need to be solved in an iterative way. An initial guess for the electron density is used to calculate the effective potential. Afterwards, the KS equations are solved and the computed orbitals define the new density, which again estimates the effective potential. As convergence criteria one usually uses the difference in energy or density between two iterations.

Our calculations are done with the quantum chemistry package TURBOMOLE [32–34]. In order to reduce computational cost, we used the RI approximation (resolution of identity) [35–37] and the MARI-J approximation (multipole accelerated resolution of identity) [38].

### 2.1.2 Approximations for the exchange-correlation-functional

The contribution to the energy-functional not known is the exchange-correlation-functional (2.8). In order to be able to do numerical calculations, this functional needs to be approximated. The most established approximations are described below.

#### Local Density Approximation

The *Local Density Approximation* (LDA) assumes the exchange-correlation-functional to be local:

$$E_{xc}^{\text{LDA}} [n(\vec{r})] = \int_{\mathbb{R}^3} \epsilon_{xc} (n(\vec{r})) \, d\vec{r}, \quad (2.14)$$

where  $\epsilon_{xc} (n(\vec{r}))$  is a function of the density but not of the derivative of the density. The exchange-correlation-functional can be decomposed into an exchange and a correlation term:

$$E_{xc} [n(\vec{r})] = E_x [n(\vec{r})] + E_c [n(\vec{r})]. \quad (2.15)$$

An expression for the exchange energy  $E_x [n(\vec{r})]$  is derived analytically for the homogeneous electron gas model. This expression is referred to as the Dirac-exchange functional [39]

$$E_x^{\text{Dirac}} [n(\vec{r})] = -\frac{3}{4} \left( \frac{3}{\pi} \right)^{\frac{1}{3}} \int_{\mathbb{R}^3} (n(\vec{r}))^{\frac{4}{3}} \, d\vec{r}. \quad (2.16)$$

Based on Quantum Monte Carlo simulations, several descriptions for the correlation part  $E_c [n(\vec{r})]$  have been proposed. The most accurate and therefore most employed form has been developed by Vosko, Wilk and Nusair (VWN) [40]. Thus, the exchange-correlation-functional is given by

$$E_{xc}^{\text{LDA}} [n(\vec{r})] = E_x^{\text{Dirac}} [n(\vec{r})] + E_c^{\text{VWN}} [n(\vec{r})]. \quad (2.17)$$

The LDA was the first feasible DFT method that examined exchange and correlation effects. On the one hand, it is successfully applied in solid-state physics. On the other hand, it describes properties in quantum chemistry poorly: inter-atomic distances are underestimated and binding energies are overestimated. Furthermore, it does not describe van-der-Waals interactions, which follow a power law, at all. The chemical accuracy of about 43 meV per particle in the binding energy is not achieved [29].

### Generalised Gradient Approximation

While the LDA only uses the electron density  $n(\vec{r})$ , the *Generalised Gradient Approximation* (GGA) includes the gradient  $|\nabla n(\vec{r})|$  of the density  $n(\vec{r})$  at position  $\vec{r}$  in order to model the spatially inhomogeneous behaviour of real systems:

$$E_{xc}^{\text{GGA}}[n(\vec{r})] = \int_{\mathbb{R}^3} f(n(\vec{r}), \nabla n(\vec{r})) \, d\vec{r}. \quad (2.18)$$

The exchange-correlation-energy depends on the choice of the function  $f(n(\vec{r}), \nabla n(\vec{r}))$ , and can therefore be quite diverse. Mostly, the exchange term  $E_x^{\text{GGA}}[n(\vec{r})]$  is a combination of the LDA exchange and a correction term. The function  $f(n(\vec{r}), \nabla n(\vec{r}))$  is obtained by trying to fulfil as many analytical properties of the exact functional as possible and furthermore by fitting parameters for some test systems.

We use the so called B-P86 energy-functional, that implies Becke's 1988 correction  $E_x^{\text{B88}}[n(\vec{r})]$  to the LDA exchange-functional [41], the correlation-functional from Vosko, Wilk and Nusair [40] and Perdew's 1986 correction  $E_c^{\text{P86}}[n(\vec{r})]$  to the correlation-functional [42]:

$$E_{xc}^{\text{BP86}}[n(\vec{r})] = E_x^{\text{LDA}}[n(\vec{r})] + E_x^{\text{B88}}[n(\vec{r})] + E_c^{\text{VWN}}[n(\vec{r})] + E_c^{\text{P86}}[n(\vec{r})]. \quad (2.19)$$

The GGA is an improvement of the LDA and provides much more reliable results in quantum chemistry than the LDA. It describes binding energies much better and underestimates inter-atomic distances only a little [43]. However, the power law behaviour of van-der-Waals interactions is still not included in the GGA either.

### Hybrid Functionals

Even better results are often gained by using hybrid functionals (for example [44]), which have become well-established in quantum chemistry. To the GGA exchange description a Hartree-Fock exchange term is admixed:

$$E_x^{\text{Hybrid}} = a E_x^{\text{GGA}}[n(\vec{r})] + b E_x^{\text{HF}}(\{\phi_i(\vec{r})\}). \quad (2.20)$$

Technically speaking, this functional is not a DFT-functional because the Hartree-Fock term depends on the orbitals  $\phi_i(\vec{r})$  and not only on the density  $n(\vec{r})$ . The exact form of the functionals depend on the choice of the GGA, as well as on the weight-factors  $a$

and  $b$ , which are determined by empirical considerations. Hartree-Fock does not contain correlation effects, therefore the correlation energy is still given through the GGA correlation contribution  $E_c^{\text{GGA}}[n(\vec{r})]$ . Thus, van-der-Waals interactions are not accounted for either. A disadvantage of hybrid functionals is the increased computational cost due to the Hartree-Fock term. We do not use Hybrid Functionals in our calculations for this reason.

### 2.1.3 Empirical Corrections for Dispersive Interactions

Van-der-Waals interactions play a major role in many chemical systems, but have not been accounted for so far. One way to include them into KS-DFT based structure calculations was introduced by Grimme [45–47] using empirical corrections (DFT-D).

In this approach, the dispersion corrected total energy of a system is given by

$$E_{\text{DFT-D}} = E_{\text{KS-DFT}} + E_{\text{dispersion}}. \quad (2.21)$$

Grimme’s expression for the dispersive energy  $E_{\text{dispersion}}$  has undergone several improvements over the past years; we refer to those as DFT-D1, DFT-D2 and DFT-D3 and discuss them in the following.

#### Initial Approaches DFT-D1 and DFT-D2

The dispersion interaction is assumed to result from induced dipoles, leading to a  $R^{-6}$  behaviour for the correction term. Following [45, 46] and taking the contribution of each atom-pairwise dispersive interaction of a system consisting of  $N_{\text{at}}$  atoms into account, the van-der-Waals contribution naively reads

$$E_{\text{dispersion}} = - \sum_{A=1}^{N_{\text{at}}-1} \sum_{B=A+1}^{N_{\text{at}}} \frac{C_6^{AB}}{|\vec{r}_A - \vec{r}_B|^6}, \quad (2.22)$$

with the position  $\vec{r}_A$  of atom  $A$  and the dispersion coefficient  $C_6^{AB}$ .

However, the  $R^{-6}$  behaviour is only valid if the overlap between the electron densities of two atoms is negligible. Therefore a damping function  $f_{\text{damp}}(|\vec{r}_A - \vec{r}_B|)$  is introduced which decreases fast enough to zero for inter-atomic distances too small for typical van-der-Waals distances:

$$f_{\text{damp}}(|\vec{r}_A - \vec{r}_B|) = \frac{1}{1 + \exp\left(-d \frac{|\vec{r}_A - \vec{r}_B|}{R_0} - 1\right)}, \quad (2.23)$$

where  $R_0$  is the sum over the atomic van-der-Waals radii,  $R_0 = c(R_{\text{vdW}}^A + R_{\text{vdW}}^B)$ . These van-der-Waals radii are derived from the radius of the  $0.01 a_0^{-3}$  electron density contour, which is estimated via mean-field calculations. Furthermore, the  $C_6$  coefficients are scaled by a global factor  $s_6$  which depends only on the density functional used and is estimated

to be approximately 1 by a least-squares optimisation for several systems. Summarising, the dispersive energy correction is given by

$$E_{\text{dispersion}} = -s_6 \sum_{A=1}^{N_{\text{at}}-1} \sum_{B=A+1}^{N_{\text{at}}} \frac{C_6^{AB}}{|\vec{r}_A - \vec{r}_B|^6} f_{\text{damp}}(|\vec{r}_A - \vec{r}_B|). \quad (2.24)$$

In DFT-D1 [45] the scaling factor in  $R_0$  is given by  $c = 1.22$  and the damping parameter in  $f_{\text{damp}}(|\vec{r}_A - \vec{r}_B|)$  is  $d = 23$ . Furthermore, the dispersion coefficients  $C_6^{AB}$  are a simple average of the form:

$$C_6^{AB} = 2 \frac{C_6^A C_6^B}{C_6^A + C_6^B}, \quad (2.25)$$

with the empirical  $C_6$  coefficients of a single atom  $A$ .

An improved Version DFT-D2 [46] of the initial approach produces better results for intermediate distances. Here, the scaling factor in  $R_0$  is decreased to  $c = 1.10$  and the damping parameter is reduced to  $d = 20$ . Moreover, the dispersion coefficients  $C_6^{AB}$  are given by a geometric mean:

$$C_6^{AB} = \sqrt{C_6^A C_6^B}. \quad (2.26)$$

The atomic  $C_6$  coefficients of a single atom  $A$  are assumed to be induced by polarising single atoms:

$$C_6^A = 0.05 N I_p^A \alpha^A, \quad (2.27)$$

with the atomic ionisation potential  $I_p$  and the static dipole polarizability  $\alpha$  (both in atomic units) of atom  $A$ . The calculation of the  $C_6$  coefficients yields the greatest improvement compared to DFT-D1.  $N$  depends on the position of the atom in the periodic table;  $N = 2, 10, 18, 36, 54$  for atoms in the first to fifth row and is the number of electrons of the next noble gas.

### Enhanced Approach DFT-D3

The refined approach DFT-D3 [47] offers a broader range of applicability as well as higher accuracy, since it includes higher multipole terms and important parameters are calculated. Furthermore, it gives a consistent description across the periodic table for the elements  $Z = 1 - 94$  and provides an asymptotically correct behaviour for finite systems with all density functionals. In contrast to DFT-D1 and DFT-D2, the atomic dispersion coefficients  $C_6$  depend on the system.

Here, the dispersion energy is the sum over two-body and three-body energies:

$$E_{\text{dispersion}} = E^{(2)} + E^{(3)}, \quad (2.28)$$

with the two-body term:

$$E^{(2)} = - \sum_{AB} \sum_{n=6,8} s_n \frac{C_n^{AB}}{|\vec{r}_A - \vec{r}_B|^n} f_{\text{damp},n}(|\vec{r}_A - \vec{r}_B|), \quad (2.29)$$

which is a sum over every atom pair in the system with the  $n$ -th order dispersion coefficient  $C_n^{AB}$ . Thus, not only the  $C_6$  coefficient but also the  $C_8$  coefficient are taken into account. The global scaling factor  $s_n$  varies for different  $n$ , namely  $s_6 < 1$  is functional dependent and  $s_8 = 1$  for all functionals. Furthermore, the damping function is adjusted:

$$f_{\text{damp},n}(|\vec{r}_A - \vec{r}_B|) = \frac{1}{1 + 6 \left( \frac{|\vec{r}_A - \vec{r}_B|}{s_n R_0^{AB}} \right)^{-\alpha_n}}, \quad (2.30)$$

where  $s_n$  is the order dependent scaling factor to the cut-off radius  $R_0^{AB}$ . This cut-off radius determines the inter-atomic distance region in which the dispersive energy decreases and eventually vanishes. The energy of the single atom  $A$  and the single atom  $B$  are subtracted from the energy of the atom pair  $AB$  derived from KS-DFT. Then the cut-off radius is the distance at which this energy equals a cut-off energy. Since the cut-off radius depends on the functional, the choice for the cut-off energy has practically no influence on the results. Moreover, the parameter  $\alpha_n$  is chosen in such a way, that the dispersive corrections for typical covalent bond distances is  $< 1\%$  of  $\max(|E_{\text{dispersion}}|)$ , thus  $\alpha_6 = 14$  and  $\alpha_{n+2} = \alpha_n + 2$ .

Furthermore, the dispersion coefficients are calculated ab initio by time dependent DFT (TD-DFT). The  $C_6^{AB}$  coefficients can be expressed by the averaged dipole polarizability  $\alpha(i\omega)$  at imaginary frequency  $\omega$  (Casimir-Polder formula):

$$C_6^{AB} = \frac{3}{\pi} \int_0^\infty \alpha^A(i\omega) \alpha^B(i\omega) d\omega. \quad (2.31)$$

Coefficients of higher order are calculated recursively but only the  $C_8$  term is of interest here:

$$C_8^{AB} = 3 C_6^{AB} \sqrt{Q^A Q^B} \quad \text{with} \quad Q^A = s_{42} \sqrt{Z^4} \frac{\langle r^4 \rangle^A}{\langle r^2 \rangle^A} \quad (2.32)$$

In order to achieve consistent dispersive energies for heavy atoms too, the charge dependent factor  $\sqrt{Z^4}$  is required.  $\langle r^4 \rangle$  and  $\langle r^2 \rangle$  are multipole-type expectation values derived from geometrically averaged atomic densities to obtain the pair coefficients. The dispersion coefficients (2.31) apply for pairs of free atoms and thus yield inconsistent treatment for the dispersion in and between molecules. Instead of using  $\alpha(i\omega)$  for single atoms, the dipole polarizability is computed for reference molecules like hybrids.

Now we consider the three-body energy of an atom triplet  $ABC$ . It is derived from third order perturbation theory, known as the Axilrod-Teller-Muto or triple dipole:

$$E^{ABC} = \frac{C_9^{ABC} (3 \cos \theta_a \cos \theta_b \cos \theta_c + 1)}{(r_{AB} r_{BC} r_{CA})^3}, \quad (2.33)$$

where  $\theta_a$ ,  $\theta_b$  and  $\theta_c$  are the inner angles of the triangle spanned by the intermolecular distances  $r$ . The triple-dipole constant  $C_9^{ABC}$  is approximated via a geometric mean:

$$C_9^{ABC} = \frac{3}{\pi} \int_0^\infty \alpha^A(i\omega) \alpha^B(i\omega) \alpha^C(i\omega) d\omega \approx -\sqrt{C_6^{AB} C_6^{AC} C_6^{BC}}. \quad (2.34)$$

Eventually, the three-body term is a sum over all atom triplets  $ABC$  in the system:

$$E^{(3)} = - \sum_{ABC} E^{ABC} f_{\text{damp},(3)}(\bar{r}_{ABC}) . \quad (2.35)$$

Here, the damping function  $f_{\text{damp},(3)}(\bar{r}_{ABC})$ , analogue to (2.30), implies the constants  $\alpha_{(3)} = 16$  and  $s_{(3)} = \frac{4}{3}$ , as well as the geometrically averaged radii  $\bar{r}_{ABC}$ . Since  $C_9^{ABC}$  is negative in the approximation, the correction  $E^{(3)}$  is repulsive in a densely packed system. For small molecules (less than 10 atoms), the three-body term is negligible, but can be essential in bigger molecules.

A drawback of all three approaches is that the dispersion correction does not depend on and does not affect the electronic structure.

### 2.1.4 Contracted Gaussian Type Orbitals

Numerical solutions of the KS equations are found by expanding the KS orbitals  $\phi_i$  in terms of basis functions. Therefore, the system is transformed into an eigenvalue problem, which may be solved using linear algebra. The choice of the basis set is essential: it shall describe molecular orbitals properly without causing great computational costs.

One choice for the basis set might be Slater-type atomic orbitals (STOs):

$$\phi(\vec{r}) = A |\vec{r}|^l Y_l^m(\Omega) \exp(-B |\vec{r} - \vec{r}_0|) , \quad (2.36)$$

where  $\vec{r}_0$  denotes the position of the atom,  $A$  is a normalisation factor,  $B$  is the orbital exponent and  $Y_l^m(\Omega)$  are spherical harmonics. This approach has the disadvantage, that integrals with two STOs from different atoms are quite expensive to evaluate. A better choice for the basis set are Gaussian-type orbitals (GTOs) that describe the wave function in terms of Gaussian functions:

$$\phi(\vec{r}) = A |\vec{r}|^l Y_l^m(\Omega) \exp(-B (\vec{r} - \vec{r}_0)^2) . \quad (2.37)$$

The product of two Gaussian functions is itself a Gaussian and therefore integrals with Gaussian functions are easy to solve. However, molecular orbitals are not well described by a single Gaussian. Consequently, instead of taking just one Gaussian, a sum of Gaussian functions is used [48]:

$$\phi(\vec{r}) = |\vec{r}|^l Y_l^m(\Omega) \sum_{i=1}^n A_i \exp(-B_i (\vec{r} - \vec{r}_0)^2) , \quad (2.38)$$

called contracted Gaussian-type orbitals (CGTOs). The accuracy increases with the number of Gaussians applied in the sum. If the number of basis functions is large enough then their explicit form becomes insignificant and convergence has been reached.

In our calculations, we use the following basis sets:

- Single molecules in vacuum: def2-TZVP [49, 50].

- Molecule on Au(111) cluster: def-SV(P) [35, 51], def-TZVP [52] and def-TZVPP [49] for the fullerene and in all calculations def-SV(P) [36] for the gold cluster.

We are interested in the electronic properties of the molecule on the gold surface. Moreover, we examine its electronic structure at larger distances to the molecule, i.e. the distance interval of an STM tip to the sample. The description for such larger distances to the molecule becomes better with increasing basis set size. Thus, we perform a convergence check of our results using three basis sets of different size for the fullerene on the surface.

## 2.2 Embedding Formalism

In order to describe the electronic structure of a single molecule with a given contact geometry, a microscopic description of the molecule and the contact with the surface is essential. Knowledge of the molecular states and comprehension of the hybridisation of the molecular orbitals with the surface states is needed. To model the real surface, the molecule is investigated on a finite surface cluster which is then embedded into a bigger, effectively infinite surface. The embedding formalism has been implemented during this study. It is based on an existing transport code that was developed in our group.

### 2.2.1 Embedding Green's Function Formalism

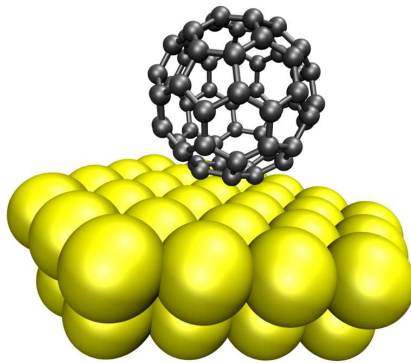


Figure 2.1: Example for an extended molecule, consisting of the molecule and a finite-size surface.

The molecule and a finite part of the surface are combined to a so called extended molecule (Fig. 2.1). This extended molecule contains the information about the hybridisation of the molecule and the contact of the molecule to the finite surface [53]. So far, the infinite reservoir of the surface is not included. With the KS orbitals  $|i\rangle$  and the corresponding energies  $\epsilon_i$  of the extended molecule, the Kohn-Sham Hamiltonian reads:

$$\hat{H} = \sum_i \epsilon_i |i\rangle \langle i|. \quad (2.39)$$

The retarded Green's function of this system is given by:

$$\hat{G}_{\text{eM}}^{-1}(E) = E - \hat{H} + i\eta \quad (\eta \rightarrow 0^+) . \quad (2.40)$$

The metallic reservoir is coupled to the extended molecule via a self-energy contribution. Hence, the Green's function of the whole system is given by the Green's function of the extended molecule  $\hat{G}_{\text{eM}}^{-1}(E)$  and the self-energy of the surface  $\hat{\Sigma}_{\text{s}}(E)$  [53, 54]:

$$\hat{G}^{-1}(E) = \hat{G}_{\text{eM}}^{-1}(E) - \hat{\Sigma}_{\text{s}}(E) . \quad (2.41)$$

Thus, the Green's function  $\hat{G}(E)$  describes the propagation of particles with energy  $E$  within the molecule in the presence of the reservoir.

## 2.2.2 Self-Energy

The self-energy contribution in the Green's function couples the surface reservoir to the extended molecule. An adequate model for the self-energy is found using absorbing boundary conditions. In this thesis, we give a brief summary of this model, for a detailed discussion see [54]. The surface space  $S$  between the extended molecule and the reservoir contains all atoms at which absorption can occur, i. e. the gold atoms of the lower layer of the finite surface in Figure 2.1. An imaginary self-energy that is independent of  $E$  is added to the self-energy  $\delta\epsilon$  for these atoms:

$$\hat{\Sigma}_{\text{s}} = (\delta\epsilon - i\eta') \sum_{n \in S} \sum_{\alpha} |n, \alpha\rangle \langle n, \alpha| . \quad (2.42)$$

It is summed over all atoms  $n$  of the surface space  $S$  and over all orbitals  $\alpha$  of atom  $n$ . Any wave packet is partially absorbed when reaching the surface space leading to a broadening, i. e. a finite lifetime, of the molecular states. Therefore, the local absorption rates  $\eta'$  are only unequal zero at the surface space. The constraint for  $\eta'$  is to be homogeneous on  $S$ , its value is found in such a way, that physical quantities do not change significantly under variation of  $\eta'$ . Furthermore, the extended molecule is required to fulfil charge neutrality which is achieved by adjusting the real part of the self energy in an iterative procedure. If the number of surface atoms in the extended molecule is large enough, the approximation for  $\hat{\Sigma}_{\text{s}}$  gives reasonable results [55]. One advantage of this model for the self-energy is, that it is less computationally intensive than using better approximations for the self-energy. In our calculations the value for  $\eta'$  is 0.2 Ry.

## 2.2.3 Local Density of States

The *Local Density of States* (LDOS)  $\rho(E)$  is of great interest when analysing the electronic structure of a molecule with a given contact geometry. It can be expressed by the imaginary part of the Green's function:

$$\rho(E) = -\frac{1}{\pi} \sum_{n \in \mathcal{M}} \sum_{\alpha} \text{Im} \langle n, \alpha | \hat{G}(E) | n, \alpha \rangle , \quad (2.43)$$

where the sum of  $n$  is carried out over all the atoms within a certain subspace  $\mathcal{M}$  (e.g. the atoms of the molecule) and  $\alpha$  are the orbitals of atom  $n$ .

### 2.2.4 Tunnel Current

The tunnel current  $I$  in the STM experiments can be expressed in terms of the LDOS of the tip and of the surface, the chemical potential of the tip and the surface follow the condition

$$\mu_{\text{tip}} - \mu_{\text{surface}} = |e|V, \quad (2.44)$$

with the applied Voltage  $V$ . Furthermore, the LDOS of the surface depends on the position  $\vec{r}$  of the tip (Fig. 2.2). Since the tip geometry is not well known, it is often modelled as a

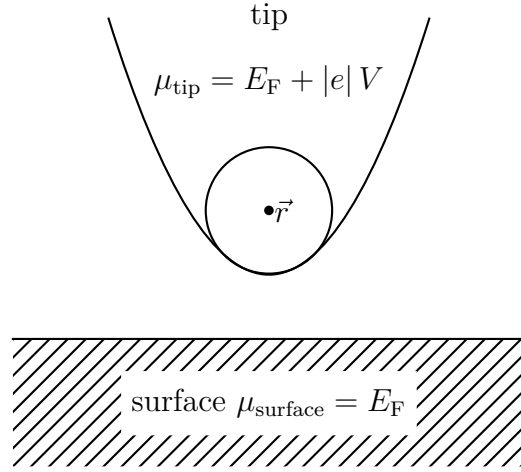


Figure 2.2: Sketch of the tunnelling geometry

locally spherical potential well leading to a geometry factor  $g$  entering the formula of the tunnel current. The detailed discussion of  $g$  should not be part of this thesis but can be found in [56, 57]. Under the assumption of perfect transmission ( $T = 1$ ) and no reflection (i. e. neglecting overlap matrix elements), the tunnel current is given by

$$I = \frac{2\pi |e|}{\hbar} g \int_{-\infty}^{\infty} \rho_{\text{tip}}(E) f(E, \mu_{\text{tip}}) \rho_{\text{surface}}(E, \vec{r}) (1 - f(E, \mu_{\text{surface}})) dE. \quad (2.45)$$

The Fermi distribution  $f(E, \mu) = (1 + \exp(\beta(E - \mu)))^{-1}$  depends on the energy and on the chemical potential of the tip or of the surface. For small temperatures, the Fermi distribution is approximated by the Heaviside step function which defines new integration limits.

$$I = \frac{2\pi |e|}{\hbar} g \int_{E_F}^{E_F + |e|V} \rho_{\text{tip}}(E) \rho_{\text{surface}}(E, \vec{r}) dE. \quad (2.46)$$

The Fermi energy for metals is inside an energy band which often leads to an approximately constant LDOS around the Fermi energy. Therefore, the LDOS of the metallic tip is approximately constant,  $\rho_{\text{tip}}(E) = \rho_{\text{tip}}(E_{\text{F}})$ , and the tunnel current can be rewritten [58]:

$$I = \frac{2\pi |e|}{\hbar} g \rho_{\text{tip}}(E_{\text{F}}) \int_{E_{\text{F}}}^{E_{\text{F}}+|e|V} \rho_{\text{surface}}(E, \vec{r}) dE. \quad (2.47)$$

The tunnel current in STM experiments is shown to be proportional to the LDOS of the surface at the position of the tip (2.47).

In this study, we aim to simulate STM images of  $\text{C}_{60}$  and  $\text{C}_{58}$  on a gold surface. Therefore, we calculate the spatially resolved density of states in a tip plane above the surface. Since the tunnel current is proportional to this calculated quantity, we are able to compare our simulated topographies with the experimental STM images. To this end, we model the real surface as an effectively infinite surface. The energy levels of the molecule experience a broadening in the presence of the real surface while the energy levels of the extended molecule are discrete levels. Therefore, it is important to include an infinite surface in our calculations using the embedding method described above.

As mentioned above, the embedding formalism, based on an existing transport code, has been implemented during this study. We have also developed this code further in order to calculate the spatially resolved density of states. Especially the integration of the surface LDOS over the energy in (2.47) has been added. Therefore, experimental STM images obtained at voltages that are not close to zero can be simulated due to this implementation. In this part of the implementation, we approximate the integral over the energy by a sum over infinitesimal energy steps. It is now possible to specify an energy window for the summation by defining a starting energy value and an end energy value. Furthermore, the width of the energy step can be regulated. Thus, not only STM images near zero bias can be simulated but also STM images that are obtained for non-zero voltages.



## Chapter 3

# Electronic Structure of C<sub>60</sub>

Motivated by the STM images of C<sub>60</sub> (Fig. 1.6), we aim to simulate the topography of C<sub>60</sub> on the Au(111) surface used in the experiment. To this end, we first analyse the electronic properties of C<sub>60</sub> in vacuum by using DFT. Afterwards, we examine the contact geometry as well as the electronic properties of C<sub>60</sub> on the Au(111) surface. In the end, we simulate the topography of C<sub>60</sub> on Au(111).

### 3.1 C<sub>60</sub> in Vacuum

To begin our study of icosahedral C<sub>60</sub>, we analyse the ground state properties of C<sub>60</sub> in vacuum with DFT calculations. To this end, we use the B-P86 functional, the def2-TZVP basis set as well as the RI and MARI-J approximations (Sec. 2.1).

We first determine the electron density of C<sub>60</sub> in vacuum as displayed in Figure 3.1. The electron density is fully delocalised over the entire molecule. This is explained by

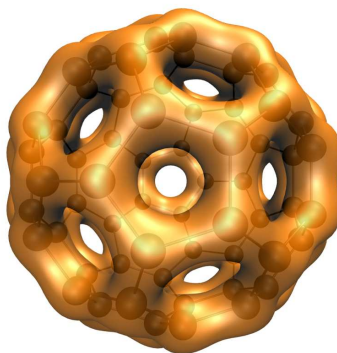


Figure 3.1: The ground state electron density of C<sub>60</sub> at a value of  $n(\vec{r}) = 0.185 a_0^{-3}$ .

the molecular orbitals of the molecule. The  $sp^2$  hybridised carbon atoms form  $\sigma$ -bonds

with each of their three neighbours. Since the  $\sigma$ -bonds are not planar, a pyramidalization angle occurs as explained in Section 1.1. The pyramidalization angle for C<sub>60</sub> is equal for all atoms,  $\Theta_p = 11.6^\circ$ . Thus, the curved  $\pi$ -conjugation is perfectly uniform over the entire molecule leading to a delocalised electron cloud.

In order to find the optimal atomic structure of the fullerene, the total energy of the molecule is minimised by performing an iterative relaxation procedure. The resulting Kohn-Sham energy spectrum, as illustrated in Table 3.1, presents a high degeneracy of the single-particle levels. This degeneracy is due to the I<sub>h</sub> symmetry group which has 120 symmetry operations and declares the possible degeneracies to be one, three, four and five [59]. In Table 3.1, HOMO stands for the highest occupied molecular orbital and LUMO

Orbital	Degeneracy	Energy [eV]
LUMO+4	5	-0.638
LUMO+3	5	-2.109
LUMO+2	3	-2.302
LUMO+1	3	-3.179
LUMO	3	-4.263
HOMO	5	-5.912
HOMO-1	4	-7.069
HOMO-2	5	-7.181
HOMO-3	5	-8.735
HOMO-4	4	-8.736

Table 3.1: Kohn-Sham energy spectrum of C<sub>60</sub>: numerical values for the ground state energy levels of C<sub>60</sub> around the Fermi energy as well as their degeneracy.

denotes the lowest unoccupied molecular orbital. Furthermore, the molecular orbital just above the LUMO is denoted by LUMO+1, HOMO-1 corresponds to the molecular orbital just below the HOMO and so forth. The energy gap between the HOMO and LUMO, the HOMO-LUMO gap, is found to be approximately 1.6 eV and is therefore smaller than the experimental value of 2.2 eV [23]. This difference in the value of the HOMO-LUMO gap is caused by the use of GGA functionals which underestimate the gap [60]. Furthermore, C<sub>60</sub> exhibits a closed-shell electronic structure. Thus, the ground state is a singlet with spin zero.

## 3.2 C<sub>60</sub> on Au(111)

We aim to simulate the topography of C<sub>60</sub> on a surface and compare this with the experimental results from the STM experiments as presented in Figure 1.6. Since C<sub>60</sub> is deposited on Au(111) surfaces in the STM experiments, we model the surface in our calculations as

Au(111) too. It has been shown, that the bond between  $C_{60}$  and two flat gold electrodes is stronger than the bond between  $C_{60}$  and two adatom electrodes [60]. Therefore, we neglect the possibility of adatoms on the surface.

We would like to understand how  $C_{60}$  adsorbs on Au(111) surfaces. Therefore, we examine the possible contact geometries and the corresponding optimal binding distance of the molecule to the surface. Since the interaction between  $C_{60}$  and the surface is determined by van-der-Waals interaction, it is essential to include this contribution. As before, our DFT calculations are performed using the Generalised Gradient Approximation (GGA); we use the B-P86 functional as well as the RI and MARI-J approximations. As mentioned in Section 2.1.2, the GGA energy functional does not include dispersive interactions. Thus, we include these by adding empirical corrections determined with different versions of DFT-D as described in Section 2.1.3. Furthermore, we use the basis sets def-SV(P), def-TZVP and def-TZVPP for the carbon atoms as well as the def-SV(P) basis set for the gold atoms.

### 3.2.1 Geometry Optimisation

We prepare the contact geometries for our calculations in two ways. Method A: we use the structure of  $C_{60}$  optimised in vacuum and add the surface without performing another optimisation of the whole geometry. Thereby we neglect the force on the carbon atoms of the molecule exerted by the presence of the surface. This force causes the carbon atoms to adjust their positions relative to each other as well as to the surface. Method B: we perform a relaxation procedure of the molecule on the surface while keeping the positions of the gold atoms of the surface fixed in order to account for the previously mentioned effects.

We model the Au(111) surface as a finite cluster. It consists of two layers with 45 gold atoms in total, 27 gold atoms in the upper layer and 18 gold atoms in the lower layer. Throughout this study, the geometry of the cluster is not optimised but constructed using the lattice constant for gold taken from [61]. The size of the cluster is chosen such, that it is small enough to be dealt with numerically, but still large enough so that boundary effects can be neglected for our purpose.

When contacting the fullerene with the Au(111) surface, we can vary two parameters:

- The orientation of  $C_{60}$  relative to the surface.
- The binding distance of the molecule to the surface.

There are several possible orientations of the molecule towards the surface. An example of a possible geometry is presented in Figure 2.1. Since it is not feasible for us to investigate all possibilities, we choose two possible orientations. Possible contact geometries of  $C_{60}$  between two flat gold electrodes have been studied in [62]. It was shown, that the bond between  $C_{60}$  and two flat gold electrodes is strongest when a hexagon is parallel to each electrode. Furthermore, it was shown, that carbon atoms prefer on-site positions when contacting gold electrodes [62]. We prepare the contact geometries in this study based on

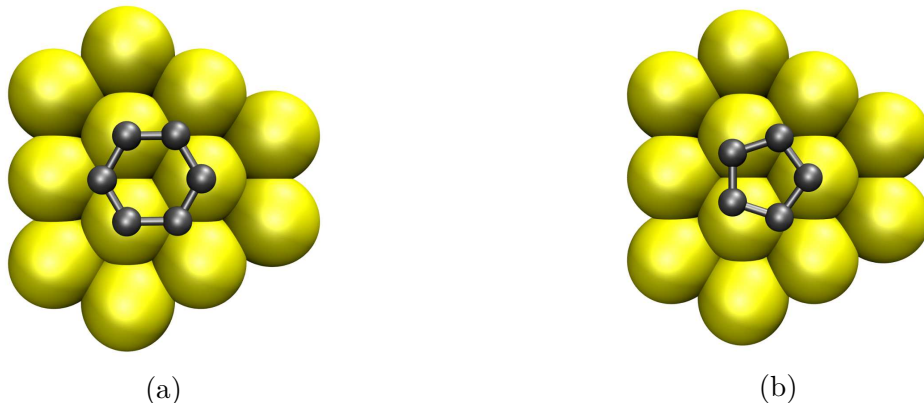


Figure 3.2: (a) A closer view of the arrangement of the hexagon on top of the Au(111) surface. (b) A detailed view of the contact geometry of a pentagon on the Au(111) surface.

the above mentioned findings: we rotate the molecule on the surface such that a polygon of the fullerene is parallel above the gold cluster. The possible polygons in case of  $C_{60}$  are a hexagon and a pentagon. Because of the icosahedral symmetry of  $C_{60}$  it does not matter which carbon atom of the selected polygon takes an on-site position. A detailed view of the two chosen contact geometries is displayed in Figure 3.2a and Figure 3.2b.

The remaining parameter which can be varied is the binding distance of the molecule to the surface. We define the binding distance as the interplanar distance between the nuclei of the upper layer of gold atoms and the nuclei of the polygon facing the surface. This parameter is easy to control and we are able to carry out a systematic study of the binding energy of the system as a function of the binding distance.

In order to investigate the possible contact geometries, we perform the following calculations:

- Method A: DFT calculations on the GGA level for several binding distances using the def-SV(P) basis set as well as the dispersive interaction computed by DFT-D2 (Sec. 2.1.3).
- Method B: Relaxation procedure on the GGA level for the optimised contact geometries found with method A, using all three basis sets mentioned above for the carbon atoms as well as the van-der-Waals interactions obtained with DFT-D3 (Sec. 2.1.3).

## Results and Discussion

The results of method A are presented in Figure 3.3. The curve for the hexagon facing the Au(111) surface has its minimum at approximately  $2.59 \text{ \AA}$  with the dissociation energy of  $-2.08 \text{ eV}$ . Whereas the minimal energy for the pentagon with  $-2.02 \text{ eV}$  at a binding distance

of  $2.54 \text{ \AA}$  is  $60 \text{ meV}$  higher than for the hexagon. Therefore, it is more likely that  $C_{60}$  binds with a hexagon parallel to the surface than with a pentagon.

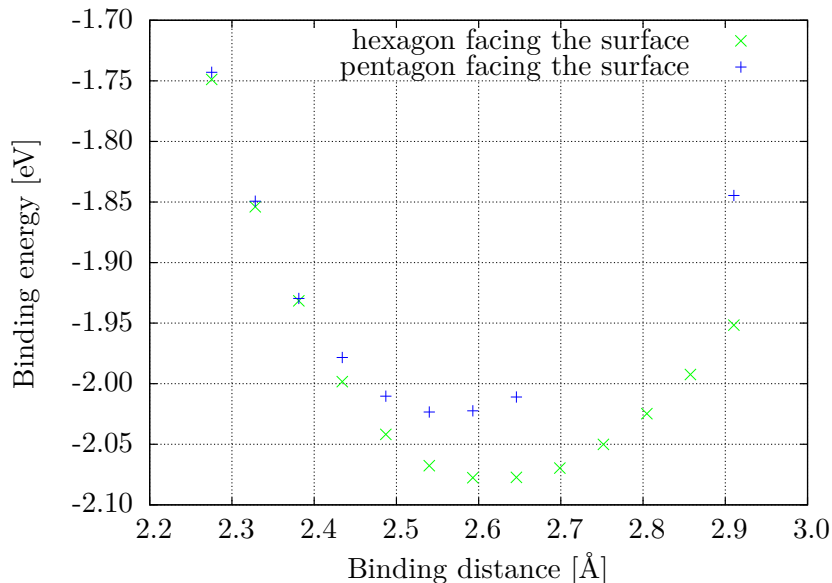


Figure 3.3: Binding energy of  $C_{60}$  obtained using the def-SV(P) basis set and including van-der-Waals interactions DFT-D2, on a flat Au(111) surface without relaxation as a function of the binding distance.

The results of method B are presented in the following: The great stability of  $C_{60}$  is reflected in the relaxation procedure. Its interatomic distances of the carbon atoms change by less than 1%. The molecule as a whole is drawn closer to the Au(111) surface leading to a smaller binding distance. Furthermore, the polygon facing the surface stays nearly in a plane parallel to the surface and the atoms of this polygon maintain their on-site positions. One exceptional case appears for the pentagon facing the surface while using the def-SV(P) basis set. There, the pentagon does not remain parallel to the surface. Furthermore, with the def-TZVP basis set, the relaxation did not converge until now.

Some coordinates of the system before and after the relaxation procedure are found in Appendix A. The binding energies and the binding distances of the two geometries obtained with method B as well as with method A are shown in Table 3.2. The binding distance for the hexagon is for all three basis sets very close on the one hand. On the other hand, the binding distance for the pentagon differs by  $0.09 \text{ \AA}$  for the def-SV(P) and the def-TZVPP basis set due to the different behaviour of the molecule during the relaxation procedure. Furthermore, the binding energy increases with increasing basis set. According to the binding energies,  $C_{60}$  prefers to bind with a hexagon facing the surface which is in agreement with the results of method A.

Polygon	Basis Set	Method B		Method A	
		Distance [ $\text{\AA}$ ]	Energy [eV]	Distance [ $\text{\AA}$ ]	Energy [eV]
hexagon	def-SV(P)	2.49	-2.76	2.59	-2.08
	def-TZVP	2.50	-2.80		
	def-TZVPP	2.49	-2.86		
pentagon	def-SV(P)	2.44	-2.65	2.54	-2.02
	def-TZVPP	2.53	-2.73		

Table 3.2: Binding energies and binding distances for  $C_{60}$  on a flat gold surface obtained for method A and B using the B-P86 functional and the dispersive correction DFT-D.

### 3.2.2 Local Density of States

We now analyse the electronic structure of  $C_{60}$  in the presence of the Au(111) surface. The analysis in this chapter follows partly an earlier one given by C. Seiler in his diploma thesis [60]. We perform a DFT calculation of the extended molecule consisting of  $C_{60}$  and the finite Au(111) cluster. In order to include an infinite gold reservoir to the extended molecule, the embedding Green's function formalism as presented in Section 2.2.1 is used.

The local density of states on the molecule is presented for two contact geometries of  $C_{60}$  on the Au(111) surface optimised with method B from Section 3.2.1. Therefore, we use the structure for the hexagon and for the pentagon facing the surface obtained using the def-SV(P) basis set. Our results of the local density of states as a function of the energy  $E$  for the two chosen contact geometries are shown in Figure 3.4.

We now examine the resonances in Figure 3.4. We refer to the resonances closest to the Fermi energy  $E_F$  as HOMO and LUMO. Recall, that the Kohn-Sham spectrum of  $C_{60}$  in vacuum (Tab. 3.1) shows a fivefold degeneracy of the HOMO and a threefold degeneracy of the LUMO. Thus, we also plotted the contributions of those degenerate orbitals to the local density of states. We find that each resonance actually is a superposition of several resonances: the HOMO is a superposition of 5 resonances and the LUMO is a superposition of three resonances. Eventually, the HOMO resonance can be associated with the HOMO states of  $C_{60}$  in vacuum and the LUMO resonance corresponds to the LUMO states of  $C_{60}$  in vacuum as seen in Figure 3.4. The separation of these two resonances is approximately 1.6 eV for both contact geometries. This resembles the HOMO-LUMO gap for  $C_{60}$  in vacuum which was found to be 1.6 eV as well; the experimental value of 2.0 eV for HOMO-LUMO gap of  $C_{60}$  on Au(111) is similar [23].

The icosahedral symmetry of  $C_{60}$  in vacuum is broken on the surface. On the one hand, the contact geometry with a hexagon facing the surface follows a  $C_{3v}$  symmetry which is a subgroup of  $I_h$ . Thus, the fivefold degenerate HOMO of  $C_{60}$  in vacuum splits into one non-degenerate orbital (HOMO(3)) and two doublets (HOMO(1) and HOMO(2), HOMO(4)

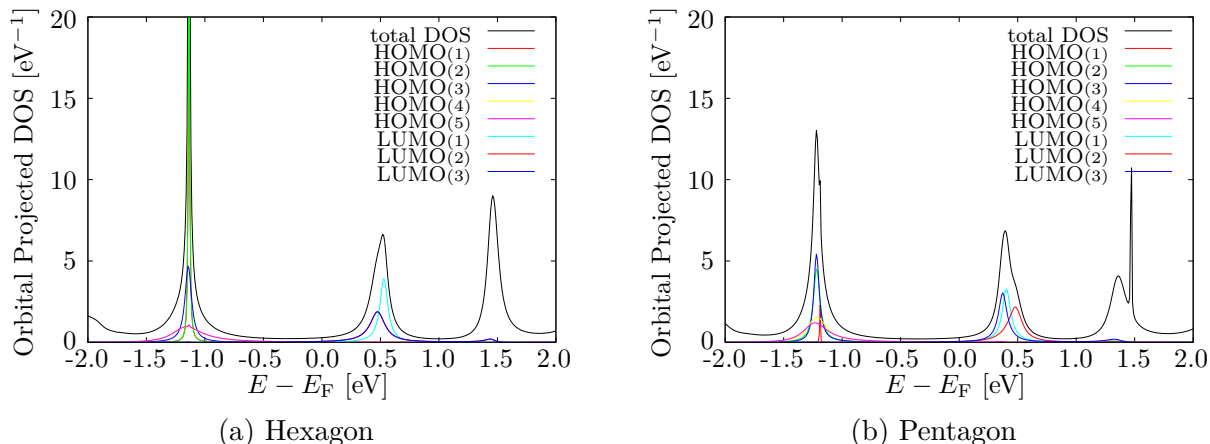


Figure 3.4: The local density of states as a function of the energy  $E$  for  $C_{60}$  for two contact geometries obtained with the def-SV(P) basis set: (a) a hexagon facing the surface at a binding distance of  $2.49\text{\AA}$  and (b) a pentagon facing the surface at a binding distance of  $2.44\text{\AA}$ . The energy axis is normalised to the Fermi energy of the extended molecule. The (x) in the key denotes the contribution to the HOMO and LUMO state.

and HOMO(5)). Furthermore, the threefold degenerate LUMO of  $C_{60}$  in vacuum splits into one non-degenerate orbital (LUMO(1)) and one doublet (LUMO(2) and LUMO(3)). This is also displayed in Figure 3.4a where the curves of the doublets are equal. On the other hand, the symmetry for the contact geometry with a pentagon facing the surface is even more reduced to a  $C_s$  symmetry which is also a subgroup of  $I_h$ . The fivefold degenerate HOMO of  $C_{60}$  in vacuum splits into five non-degenerate orbitals as well as the threefold degenerate LUMO into three non-degenerate orbitals (Fig. 3.4b).

The extended molecule is embedded onto an effectively infinite surface via a self-energy as explained in Section 2.2.2. Due to the real part of the self-energy, the energy levels are slightly shifted along the energy axis. The LUMO is shifted downwards relative to the Fermi energy for both contact geometries suggesting that electron transport through  $C_{60}$  would be via the LUMO orbital when contacted between two gold electrodes [60]. The LUMO+1 is a superposition of three resonances which results for the hexagonal face into one resonance. For the pentagonal face, one of the three resonances is shifted relative to the other two resulting into two peaks for the LUMO+1 displayed in Figure 3.4b.

Furthermore, the energy levels experience a broadening, i.e. a finite life-time, due to the imaginary part of the self energy. The broadening of the energy levels is related to the hybridisation of the molecule to the surface. Different orbitals are distributed differently over the surface of the molecule. When the molecule is contacted to the surface, the orbitals with a higher density on the face towards the surface hybridise more strongly than

other orbitals.<sup>1</sup> The LUMO is broader than the HOMO for both contact geometries, thus the LUMO is stronger hybridised than the HOMO. Furthermore, the contributions to the resonances show different width. For example, the HOMO(1) and HOMO(2) in Figure 3.4a are weakly hybridised while the HOMO(5) is strongly hybridised. We determine the HOMO orbitals of  $C_{60}$  in vacuum under the constraint of  $C_{3v}$  symmetry. Two such orbitals are displayed in Figure 3.5. As mentioned above, the density is distributed differently over the faces which explains the different hybridisation of the orbitals.



Figure 3.5: Two HOMO orbitals of  $C_{60}$  plotted at isosurface values of  $\pm 0.02a_0^{-3/2}$  in  $C_{3v}$  symmetry. The density is distributed differently over the faces which explains the different hybridisation of the molecule on the surface for different orientations of the molecule towards the surface.

### 3.2.3 Simulated Topography

We now analyse the spatially resolved density of states in order to simulate the surface topography of  $C_{60}$  on the Au(111) surface. We calculate the local density of states in a tip-plane (Fig. 3.6) above the molecule for different distances  $z \approx 0.5 \text{ \AA}$ ,  $1.5 \text{ \AA}$ ,  $3.0 \text{ \AA}$ ,  $4.5 \text{ \AA}$ . The tunnel current in the STM experiments is proportional to the spatially resolved density of states as depicted in Section 2.2.4. Since the applied bias in the experiments is approximately zero, we perform our calculations of the spatially resolved density at the Fermi energy  $E_F$ . Finally, we are able to compare our simulated topographies with the experimental STM image presented in Figure 1.6.

Here, we present the simulated topographies for the two relaxed geometries using the def-SV(P) and the def-TZVPP basis set. The whole catalogue of the simulated topographies is found in Appendix B. Note, that the colour scales in the pictures have a different scaling factor according to the distance  $z$ .

<sup>1</sup>It is assumed here, that effects of matrix elements, like symmetry induced extinction of overlap matrices, can be ignored.

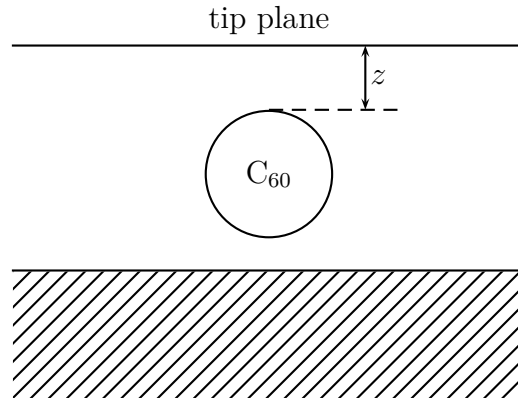


Figure 3.6: Sketch of the geometry for calculating the spatially resolved density of states.

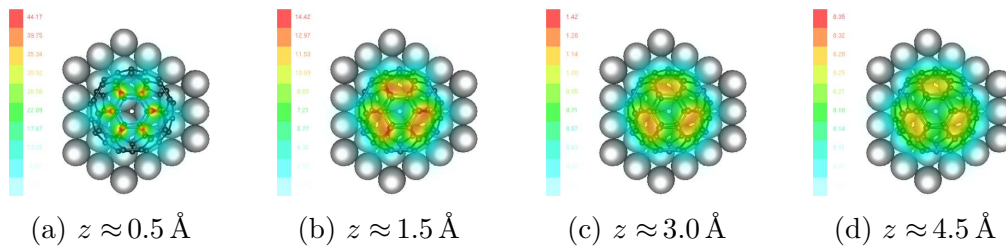


Figure 3.7: Simulated topography for the relaxed contact geometry with a hexagon facing the surface at different distances  $z$  at the Fermi energy using the def-SV(P) basis set. The scaling factors for the colour scale are  $10^{-2}$  for  $z \approx 0.5 \text{ \AA}$ ,  $10^{-3}$  for  $z \approx 1.5 \text{ \AA}$ ,  $10^{-5}$  for  $z \approx 3.0 \text{ \AA}$  and  $10^{-10}$  for  $z \approx 4.5 \text{ \AA}$ .

Our simulated topographies in Figure 3.7 display the sixfold symmetry of the topmost hexagon for small distances  $z \approx 0.5 \text{ \AA}$  (Fig. 3.7a). However, for larger distances  $z$ , the sixfold symmetry becomes a threefold symmetry. The topographies for the contact geometry with a pentagon displayed in Figure 3.8 for the def-SV(P) basis set and Figure 3.9 for the def-TZVPP basis set show different features. Figure 3.9 displays the fivefold symmetry of the topmost pentagon for small distances  $z$ , while Figure 3.8 does not. This difference arises because the orientation of the molecule on the Au(111) surface is different for the basis sets after the relaxation procedure. The pentagon facing the surface stays in the plane parallel above the Au(111) surface for the def-TZVPP basis set. For the def-SV(P) basis set, the pentagon leaves the plane parallel to the surface during relaxation. Therefore, the topmost pentagon is not parallel to the tip plane either, leading to a reduced symmetry in the spatially resolved density of states. For larger distances  $z$ , the fivefold symmetry of the pentagon fades into a ring like structure.

The experimental STM image (Fig. 1.6b) of  $C_{60}$  displays a sixfold symmetry of the

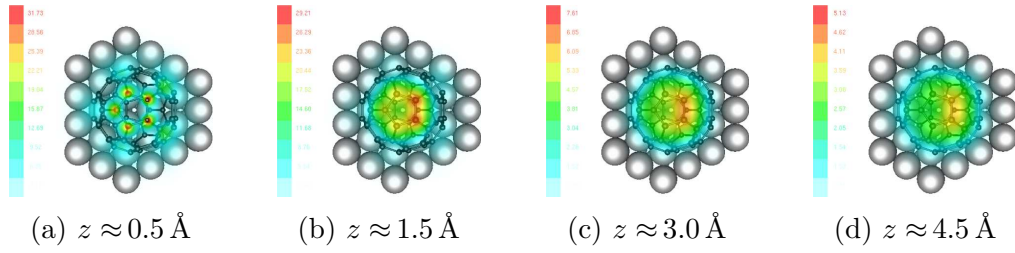


Figure 3.8: Simulated topography for the relaxed contact geometry with a pentagon facing the surface at different distances  $z$  at the Fermi energy using the def-SV(P) basis set. The scaling factors for the colour scale are analogue Figure 3.7.

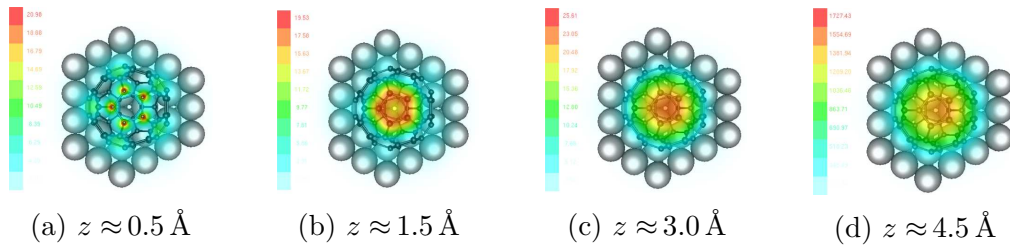


Figure 3.9: Similar to Figure 3.8, now with the def-TZVPP basis set.

topmost polygon. Comparison with our simulated topographies for  $z \approx 0.5 \text{ \AA}$  reveals, that  $C_{60}$  binds with a hexagon to the Au(111) surface as already predicted in Section 3.2.1. However, the distance from the molecule to the tip in the STM experiments is in the range of  $z \approx 1.5 \text{ \AA}$ - $3.0 \text{ \AA}$ . The simulated and the experimental images do not match for such distances  $z$ .

### 3.2.4 Comparison with Literature

There have been several theoretical and experimental works on  $C_{60}$  on metal surfaces. We draw a comparison of experimental as well as theoretical data to three other works.

Property	Karlsruhe [23]	Study [63]	Study [64]
Surface	Au(111)	Au(111)	Ag(100)
Temperature	4.2 K	7 K	7 K
STM mode	<i>constant current mode</i>	<i>constant current mode</i>	<i>constant current mode</i>
Topmost feature	Hexagonal ring	Hexagonal ring (38%), hexagon-hexagon bond (6:6 bond, 35%), pentagon-hexagon bond (5:6 bond, 13%), apex atom (8%) and pentagonal ring (6%)	6:6 bond (47%), apex atom (27%), hexagonal ring (16%), 5:6 bond (10%)
HOMO-LUMO gap	2.0 eV	2.7 eV $\pm$ 0.2 eV	2.1 $\pm$ 0.2 eV

Table 3.3: Comparison of experimental STM data: STM experiments done in Karlsruhe [23] as presented in Section 1.2 of our study compared to a study done in 2003 [64] and 2004 [63].

Property	Our study	Study [63]	Study [58]	Study [64]
Method	DFT and embedding formalism	Ab-initio pseudopotential density functional calculations	Tight-binding parametrized from DFT and non-equilibrium Green's function formalism	Ab-initio pseudopotential density functional calculations
Approximation	GGA	LDA	LDA	LDA
Basis set	CGTOs	CGTOs	STOs	CGTOs
Surface	Au(111)	Au(111)	Au(111)	Ag(100)
Surface model	Two layers of 45 atoms in total	Four layers of 144 atoms in total	Not specified	Four layers of 200 atoms in total
Relaxation procedure	C <sub>60</sub> on a fixed surfaces	C <sub>60</sub> and the top surface layer keeping the other surface layers fixed	Not relaxed	C <sub>60</sub> and the top surface layer keeping the other surface layers fixed
Orientation	Hexagon and pentagon facing the surfaces	6:6 bond directly above a surface atom	5 different orientations with the topmost features: hexagon, 6:6 bond, 5:6 bond, apex atom and pentagon	6:6 bond directly above a surface atom
Distance C <sub>60</sub> -surface	2.44 Å- 2.59 Å	Not specified	2.4 Å	Not specified
$z$	0.5 Å, 1.5 Å, 3.0Å and 4.5Å	Not specified	>3 Å	Not specified
LDOS features at $E_F$	Sixfold symmetry for the hexagon for small $z$ fades into a threefold symmetry for larger $z$	Not specified	Threefold symmetry for the hexagon as a topmost feature	“Nodal structure”
HOMO-LUMO gap	1.6 eV	1.7 eV	2.0 eV	1.6 eV

Table 3.4: Comparison of our theoretical data with a study done in 2003 [64], 2004 [63] and 2006 [58].

## Chapter 4

# Electronic Structure of $C_{58}$

In the previous chapter, we studied  $C_{60}$  in vacuum as well as on the Au(111) surface. We perform an analogue study of  $C_{58}$  in the present chapter. Thus, we determine the electronic properties of two isomers of  $C_{58}$  in vacuum. These two isomers exhibit  $C_{3v}$  (Fig. 1.3a) and  $C_s$  symmetry (Fig. 1.3b). Afterwards, we investigate possible contact geometries as well as electronic properties of the two isomers on the Au(111) surface. In the end, we simulate the topography of  $C_{58}$  on the Au(111) surface and compare the results with STM images presented in Figure 1.7.

### 4.1 $C_{58}$ in Vacuum

We first determine the ground state properties of the two chosen isomers of  $C_{58}$  in vacuum using DFT. To this end, we use the B-P86 functional, the RI and MARI-J approximations as well as the def2-TZVP basis set.

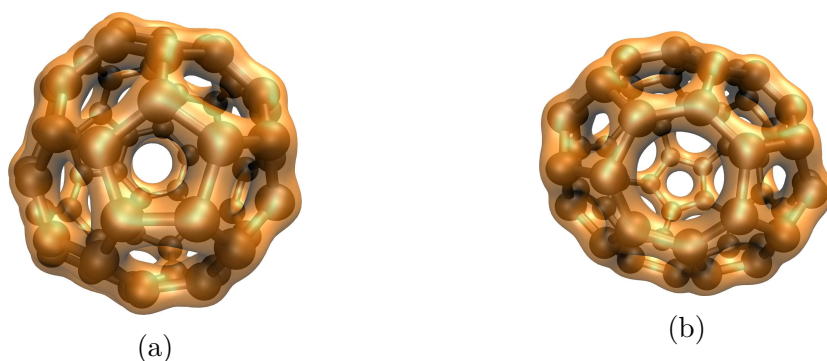


Figure 4.1: The ground state electron density of two isomers of  $C_{58}$  at a value of  $n(\vec{r}) = 0.15a_0^{-3}$ : (a)  $C_{3v}$  symmetry and (b)  $C_s$  symmetry.

We determine the electron density of the two isomers in vacuum as presented in Fig-

ure 4.1. The electron density is fully delocalised over the two isomers of C<sub>58</sub>. Since the pyramidalization angle (Sec. 1.1) is not equal for all carbon atoms, we expect the  $\pi$ -conjugation to be slightly non-uniform over the molecule.

In order to find the optimal atomic structure of the isomers, the total energy of the molecule is minimised by performing an iterative relaxation procedure. We find, that the ground state energy of the isomer with C<sub>s</sub> symmetry is approximately 340 meV higher in energy than the isomer with C<sub>3v</sub> symmetry. The corresponding Kohn-Sham spectra are presented in Table 4.1 and in Table 4.2. Both isomers display much lesser degeneracies than icosahedral C<sub>60</sub> (Tab. 3.1) due to their lower symmetry. While the I<sub>h</sub> symmetry group of C<sub>60</sub> has 120 symmetry operations, the C<sub>3v</sub> symmetry group of C<sub>58</sub> has 6 operations and the C<sub>s</sub> symmetry group has only two operations [59].

Orbital	C <sub>3v</sub> symmetry				C <sub>1</sub> symmetry	
	$\alpha$ spin		$\beta$ spin		Closed shell	
	Deg.	Energy [eV]	Deg.	Energy [eV]	Deg.	Energy [eV]
LUMO+4	2	-2.515	1	-2.716	2	-3.160
LUMO+3	1	-2.776	1	-3.115	2	-3.812
LUMO+2	1	-3.198	2	-3.788	2	-3.869
LUMO+1	2	-3.869	1	-4.180	2	-4.254
LUMO	1	-4.272	2	-5.122	2	-5.242
HOMO	2	-5.484	1	-5.494	2	-5.346
HOMO-1	1	-5.546	2	-5.788	2	-5.537
HOMO-2	2	-5.881	2	-6.583	2	-5.776
HOMO-3	2	-6.683	1	-6.895	2	-5.882
HOMO-4	1	-6.966	1	-6.978	2	-6.628

Table 4.1: Kohn-Sham energy spectrum of C<sub>58</sub> with C<sub>3v</sub> symmetry: numerical values for the ground state energy levels of the isomer around the Fermi energy as well as their degeneracy Deg.). The calculations are performed under the constraint of C<sub>3v</sub> and C<sub>1</sub> symmetry.

We find, that C<sub>58</sub> with C<sub>s</sub> symmetry exhibits a closed shell structure. Thus, the ground state of this isomer is a singlet. Its HOMO-LUMO gap is 0.6 eV. For the isomer with C<sub>3v</sub> symmetry, we find an open shell structure, leading to a triplet state with spin one. For this isomer, we also perform a calculation under the constraint of C<sub>1</sub> symmetry and find a closed shell structure. The HOMO-LUMO gap under the constraint of C<sub>3v</sub> symmetry is found to be 372 meV. Thus the HOMO-LUMO gap of the isomer with C<sub>s</sub> symmetry is twice as big as for the isomer with C<sub>3v</sub> symmetry.

We compare our results with the work of Chen et. al. [22]. In their work, they optimised all 1205 classical isomers as well as the non-classical isomer with a heptagon and

Orbital	Degeneracy	Energy [eV]
LUMO+4	1	-3.247
LUMO+3	1	-3.726
LUMO+2	1	-4.132
LUMO+1	1	-4.166
LUMO	1	-4.778
HOMO	1	-5.368
HOMO-1	1	-5.801
HOMO-2	1	-5.835
HOMO-3	1	-5.962
HOMO-4	1	-6.406

Table 4.2: Kohn-Sham energy spectrum of  $C_{58}$  with  $C_s$  symmetry: numerical values for the ground state energy levels of the isomer around the Fermi energy as well as their degeneracy.

$C_s$  symmetry. In that study, they used a hybrid functional and found that the two isomers with  $C_{3v}$  symmetry and  $C_s$  symmetry have essentially the same stability. They showed, that the  $C_{3v}$  symmetry favours a triplet, while the  $C_s$  symmetry prefers a singlet state. Furthermore, they determined the total energy for the  $C_{3v}$  symmetry in the triplet state to be approximately 400 meV lower than for the  $C_s$  symmetry in a singlet state. They find that the HOMO-LUMO gap for the  $C_{3v}$  symmetry is 1.5 times as big as the HOMO-LUMO gap for the  $C_s$  symmetry. Our results are in agreement with this work, except for the HOMO-LUMO gap. We find, that the HOMO-LUMO gap for the isomer with  $C_{3v}$  symmetry is smaller than the HOMO-LUMO gap for the isomer with  $C_s$  symmetry.

Study	Symmetry	Functional	State	$E_{\text{rel}}$	$\Delta E_{\text{gap}}$
Our study	$C_{3v}$	GGA-functional (B-P86)	Triplet	0.00 eV	372 meV
Study [22]	$C_{3v}$	Hybrid-functional (B3LYP)	Triplet	0.00 eV	2.28 eV
Our study	$C_s$	GGA-functional (B-P86)	Singlet	340 meV	0.6 eV
Study [22]	$C_s$	Hybrid-functional (B3LYP)	Singlet	400 meV	1.55 eV

Table 4.3: Comparison between our study and the study of Chen et. al. [22]: The symmetry of the isomer of  $C_{58}$ , the functional used, the electronic ground state, the relative ground state energy  $E_{\text{rel}}$  with respect to the  $C_{3v}$  isomer as well as the HOMO-LUMO gap  $\Delta E_{\text{gap}}$ .

## 4.2 $C_{58}$ on Au(111)

Motivated by the STM experiments on  $C_{58}$  (Sec. 1.2), we aim at simulating the topography of  $C_{58}$  on the Au(111) surface. Therefore, we examine possible contact geometries of the two isomers of  $C_{58}$  on the Au(111) surface as well as the corresponding optimal binding distance of the molecule to the surface in an analogue procedure to  $C_{60}$  in Section 3.2. As before, our DFT calculations are performed using the B-P86 functional as well as the RI and MARI-J approximations. The van-der-Waals interactions are added by different versions of DFT-D (Sec. 2.1.3). Furthermore, we use three different basis sets for the carbon atoms, namely def-SV(P), def-TZVP and def-TZVPP, as well as the def-SV(P) basis set for the gold atoms.

### 4.2.1 Geometry Optimisation of $C_{58}$ with $C_{3v}$ Symmetry

We begin our study of  $C_{58}$  on the Au(111) surface with the classical non-IPR fullerene with  $C_{3v}$  symmetry as illustrated in Figure 1.3a. The Au(111) cluster is modelled as a finite cluster of two layers and 45 gold atoms in total as explained in Section 3.2.1. We use the structure of this isomer optimised in vacuum and add the surface without performing an optimisation procedure of the whole system. Since the isomer is a classical one, it is constructed of hexagons and pentagons. However, due to the reduced  $C_{3v}$  symmetry of the fullerene compared to the  $I_h$  symmetry of  $C_{60}$ , the hexagonal faces of the isomer are not equal to one another. The pentagonal faces are not equal to another as well. Thus, there are many more possible orientations of the fullerene towards the surface compared to  $C_{60}$ . We prepare our contact geometries by rotating the molecule on the surface such that a polygon of the fullerene is parallel to the Au(111) plane. Furthermore, we allow for the carbon atoms of this polygon to take on-site positions to the underlying gold atoms. A closer view of the arrangement of a hexagon or a pentagon of the fullerene on top of the Au(111) cluster is shown in Figure 3.2. Note, that the carbon atoms of a polygon are also not equivalent due to the reduced symmetry. The possible contact geometries are labelled and colour coded in Figure 4.2. Furthermore, we mark the carbon atom that takes an on-site position when the corresponding polygon is facing the surface. For example, **H1a** implies that the hexagon **H1** is parallel on top of the Au(111) surface while the carbon atom **a** takes an on-site position.

We carry out a systematic study of the binding energy of the chosen contact geometries as a function of the binding distance. The latter is defined as the interplanar distance between the nuclei of the upper layer of gold atoms and the nuclei of the polygon facing the surface. Thus, we perform a DFT calculation for several binding distances using the def-SV(P) basis set as well as the dispersive interaction computed by DFT-D2 (Sec. 2.1.3). Our results are presented in Figure 4.3a for the hexagons and in Figure 4.3b for the pentagons.

For the hexagons, the minimal binding energy with -3.12 eV is found for the contact geometry **H1b**. In this configuration, the symmetric axis of the isomer (black dot in Fig-

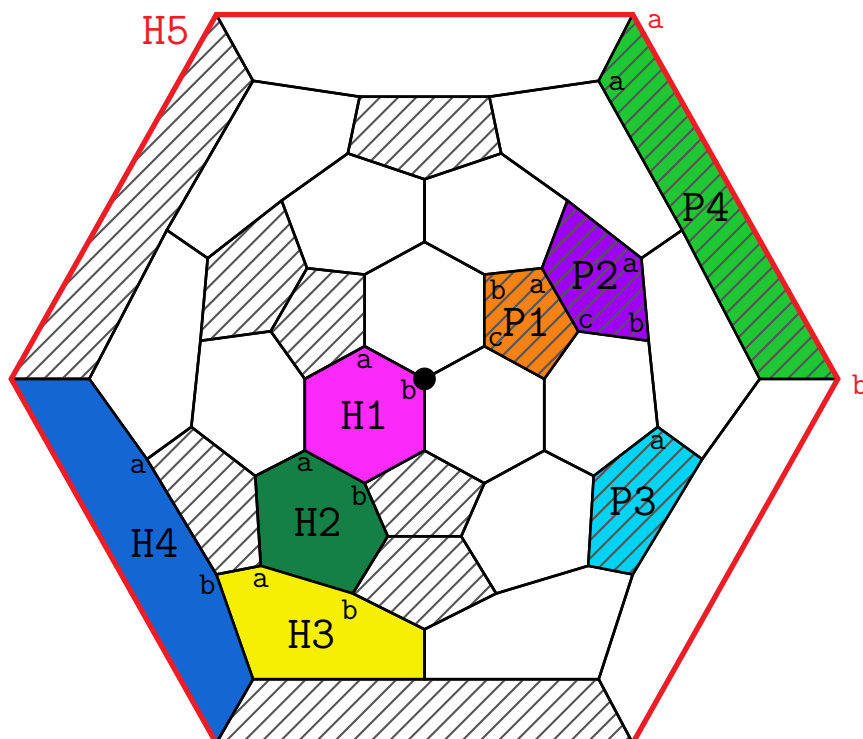


Figure 4.2: Schlegel Graph of  $C_{58}$  with  $C_{3v}$  symmetry: The investigated contact geometries are labelled and colour coded. The black dot denotes the carbon atom through which the symmetric axis goes.

ure 4.2) takes an on-site position. Whereas the configuration H1a, where the symmetric axis does not exhibit an on-site position, is 90 meV higher in energy. For the pentagons, the minimal binding energy -2.81 eV is found for the configuration P1 with all three investigated on-site positions. Therefore, the binding energy for the pentagon is 310 meV higher than for the hexagon. Thus, it is more likely, that  $C_{58}$  with  $C_{3v}$  symmetry binds with a hexagon, i.e. H1a, parallel to the surface than with a pentagon. Furthermore, the binding energy decreases with increasing distance of the investigated polygon to the symmetric axis. All binding distances as well as the corresponding binding energies for the investigated contact geometries are listed in Table 4.4.

As said in Section 3.2.1, the presence of the gold surface causes the carbon atoms to adjust their positions relative to each other and to the surface. Therefore, a relaxation procedure of the fullerene on the surface is done by keeping the positions of the gold atoms fixed. The DFT calculations are performed using all three basis sets mentioned above for the carbon atoms. Furthermore, the van-der-Waals interactions are included by DFT-D3 (Sec. 2.1.3).

During the relaxation procedure, the molecule as a whole is drawn closer to the sur-

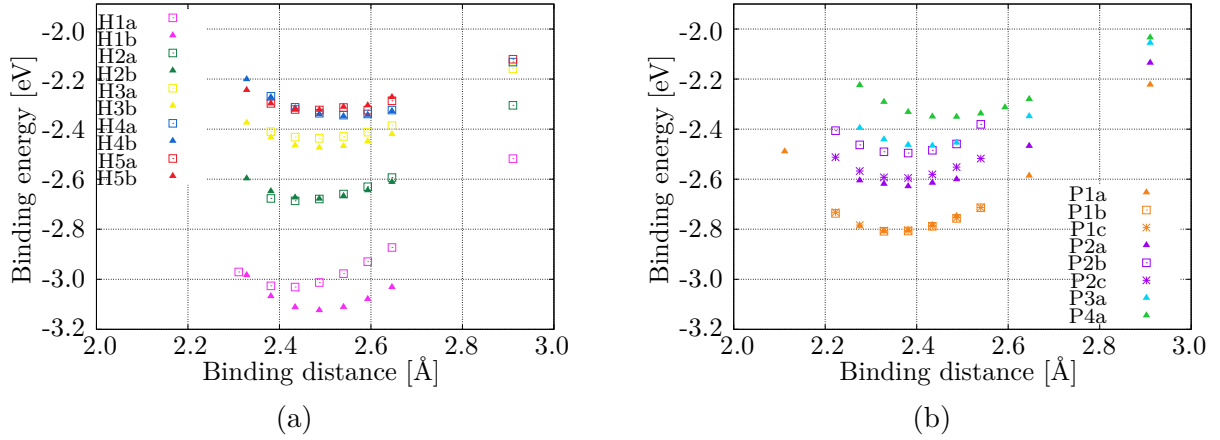


Figure 4.3: Binding energy with van-der-Waals interactions of  $C_{58}$  with  $C_{3v}$  symmetry for the examined contact geometries on a flat Au(111) surface as a function of the binding distance.

face. Considering the hexagonal faces, they stay nearly in a plane parallel to the surface. Furthermore, the carbon atoms maintain their on-site positions. However, the reactive carbon atoms are pulled closer to the surface for the configurations H1, H2 and H3. On the one hand, for the configurations P3 and P4 the pentagonal face stays nearly in a plane and the carbon atom maintains its on-site position. On the other hand, the pentagonal face of configuration P1 and P2, which are faces of adjacent pentagons, does not stay in a plane parallel to the surface and the carbon atom does not always maintain its on-site position. Instead, the fullerene rotates on the Au(111) in such a way, that the carbon atoms of the reactive centres are pulled closer to the surface and take on-site positions. Some coordinates of the system before and after the relaxation procedure are found in Appendix A.

As just mentioned, the polygon is nearly parallel to the Au(111) surface after relaxation. Therefore, the binding distance has to be redefined as the interplanar distance between the nuclei of the upper layer of gold atoms and the nucleus of the carbon atoms which is closest to the surface. The binding energies and the corresponding binding distances for the investigated contact geometries after the relaxation procedure are shown in Table 4.4.

Comparing the values gained for a hexagon facing the surface, the minimal binding energy is found for H1a with all three basis sets. Also, H1b is just 20 meV to 70 meV higher in energy depending on the basis set. Not every calculation for a pentagon facing the surface is converged for the bigger basis sets def-TZVP and def-TZVPP up to this point. For this reason, we focus on the values obtained with the def-SV(P) basis set. Thus, the minimal binding energy -3.79 eV is found for the geometry P1a. The other two geometries for P1 are just 10 meV or 50 meV higher. Comparing the hexagonal faces with the pentagonal ones,

Geometry	After Relaxation						Before relaxation	
	def-SV(P)		def-TZVP		def-TZVPP		def-SV(P)	
	$D$ [Å]	$E$ [eV]	$D$ [Å]	$E$ [eV]	$D$ [Å]	$E$ [eV]	$D$ [Å]	$E$ [eV]
H1a	2.29	-4.03	2.28	-4.06	2.28	-4.09	2.43	-3.03
H1b	2.32	-4.01	2.33	-4.00	2.31	-4.02	2.49	-3.12
H2a	2.24	-3.68	2.24	-3.71	2.24	-3.75	2.43	-2.69
H2b	2.10	-3.98					2.49	-2.68
H3a	2.35	-3.30					2.49	-2.44
H3b	2.29	-3.32	2.32	-3.32	2.31	-3.36	2.49	-2.47
H4a	2.20	-3.39	2.42	-3.20	2.42	-3.24	2.54	-2.34
H4b	2.22	-3.40	2.41	-3.20			2.54	-2.35
H5a	2.38	-3.16	2.38	-3.17	2.38	-3.20	2.49	-2.32
H5b	2.38	-3.16	2.38	-3.17	2.38	-3.20	2.49	-2.32
P1a	2.06	-3.79					2.33	-2.81
P1b	2.15	-3.74					2.33	-2.81
P1c	2.12	-3.78					2.33	-2.81
P2a	2.13	-3.63					2.38	-2.63
P2c			2.05	-3.66			2.38	-2.60
P3a	2.23	-3.31	2.24	-3.32			2.43	-2.47
P4a	2.35	-3.09	2.36	-3.11	2.33	-3.16	2.49	-2.35

Table 4.4: The binding distances  $D$  and the corresponding binding energies  $E$  for the investigated contact geometries of C<sub>58</sub> with C<sub>3v</sub> symmetry on a flat Au(111) surface after relaxation obtained with three basis sets as well as before the relaxation procedure gained with the def-SV(P) basis set.

P1a is 240 meV higher in energy than H1a. Therefore, the here analysed isomer of C<sub>58</sub> with C<sub>3v</sub> symmetry prefers to bind with the hexagon H1 to the surface.

## 4.2.2 Geometry Optimisation of C<sub>58</sub> with C<sub>s</sub> Symmetry

We continue our study of C<sub>58</sub> on the Au(111) surface with a non-classical non-IPR isomer. This isomer contains a heptagon and exhibits C<sub>s</sub> symmetry (Fig. 1.3b). Analogue to Section 4.2.1, we use the structure of this isomer optimised in vacuum (Sec. 4.1) and add the surface without performing another relaxation procedure of the whole system. We then prepare the contact geometries by rotating the fullerene on the surface such that a polygon of the molecule is parallel above the Au(111) cluster. Furthermore, the carbon atoms of this polygon take on-site positions.

The symmetry C<sub>s</sub> of the isomer is even lower than the C<sub>3v</sub> symmetry of the isomer

above (Sec. 4.2.1). Thus, there are many possible inequivalent orientations of the molecule towards the surface. In this study, we focus on two configurations where the heptagon or the middle pentagon of a pentagon chain faces the surface. These two polygons are chosen, because they exhibit the most reactive carbon atoms which seem to play an important role in the binding to the surface according to Section 4.2.1. Both polygons are colour coded and labelled in Figure 4.4. The notation **Hept1** implies, that the heptagon **Hept** is parallel on top of the Au(111) cluster while the carbon atom 1 occupies an on-site position. A closer view of the arrangement of the pentagon on top of the Au(111) cluster is presented in Figure 3.2b and for the heptagon see Figure 4.5.

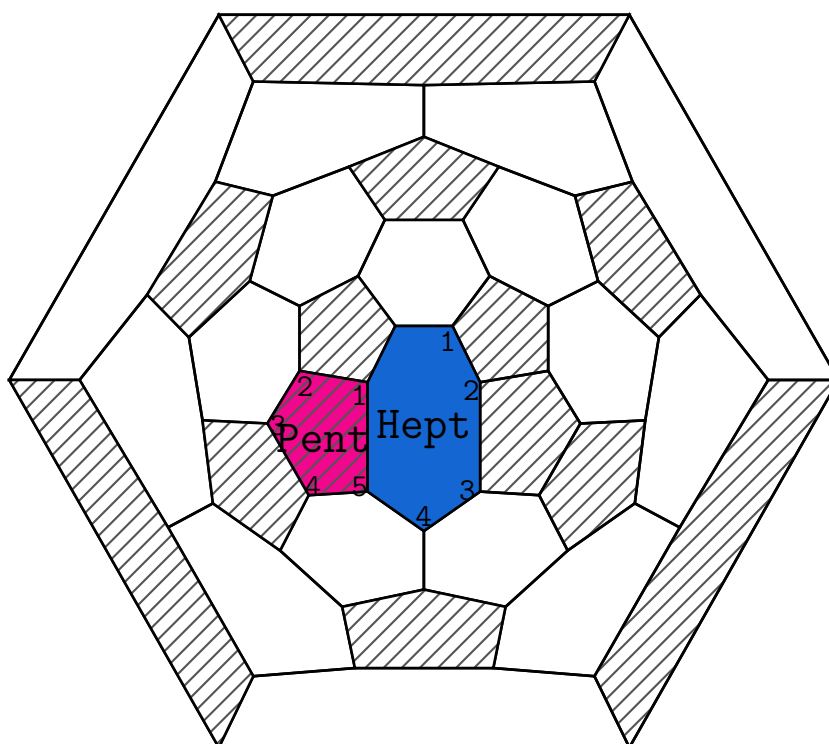


Figure 4.4: Schlegel Graph of  $C_{58}$  with  $C_s$  symmetry: The investigated binding geometries are labelled and colour coded.

We perform a systematic study of the binding energy as a function of the binding distance for the chosen contact geometries. The binding distance is again defined as the interplanar distance between the nuclei of the polygon facing the surface and the nuclei of the upper layer of gold atoms. For our DFT calculations on the GGA level we use the def-SV(P) basis set as well as the dispersive interactions computed by DFT-D2 (Sec. 2.1.3). The results are presented in Figure 4.6.

For the heptagon, the binding energies and the binding distances of the four configurations are very close. They only differ by  $0.05 \text{ \AA}$  in the binding distance and by  $60 \text{ meV}$

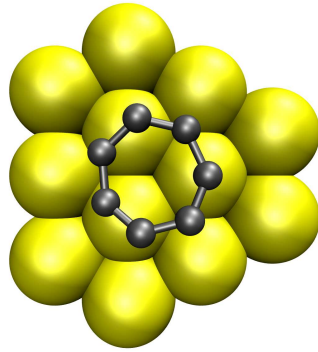


Figure 4.5: A detailed view of the contact geometry of the heptagon on the Au(111) surface.

in the binding energy. The minimal binding energy for the heptagon is found for **Hept1**, namely  $-2.83$  eV at a binding distance of  $2.54$  Å. For the pentagon, the minimal binding distance is in between  $2.38$  Å and  $2.43$  Å. The minimal binding energy with  $-2.34$  eV is found for **Pent2** at a binding distance of  $2.38$  Å which is  $420$  meV higher than the minimal binding energy for **Hept1**. Thus,  $C_{58}$  with  $C_s$  symmetry prefers to bind with the heptagon rather than with the pentagon to the Au(111) surface. All binding distances as well as the corresponding binding energies for the heptagon and the pentagon are listed in Table 4.5.

The effect of the gold surface on the geometry of the fullerene is included by performing a relaxation procedure of the molecule on the surface by keeping the positions of the gold atoms fixed. In this study, the DFT calculations are performed using all three basis sets mentioned above for the carbon atoms. Further, we include the dispersive interactions by using DFT-D3 (Sec. 2.1.3).

The fullerene as a whole is drawn closer to the surface during the relaxation procedure. Furthermore, the contact geometries with the pentagon **Pent** facing the surface display an absolutely different behaviour during relaxation than the heptagon **Hept**. We start by analysing the heptagonal face. While it is nearly in a plane parallel above the Au(111) cluster in the beginning, it bends towards the surface during the relaxation procedure in order to bring some of the reactive carbon atoms closer to the Au(111) surface. For the pentagonal face, we find a different behaviour for **Pent5** compared to the other four geometries. On the one hand, **Pent5** stays in a plane parallel above the surface and the carbon atom maintains its on-site position. On the other hand, the contact geometries **Pent1** to **Pent4** wander around the surface significantly. The pentagonal face leaves the plane parallel to the Au(111) cluster completely while the bond between **Pent** and **Hept** is rotated onto the surface. Most calculations of the relaxation procedure for the bigger basis sets def-TZVP and def-TZVPP are not converged up to this point. Again, some coordinate files of the system before and after the relaxation are found in Appendix A.

Since the polygon on top of the gold surface is not parallel to it anymore, we redefine the binding distance according to Section 4.2.1. The computed binding energies as well as

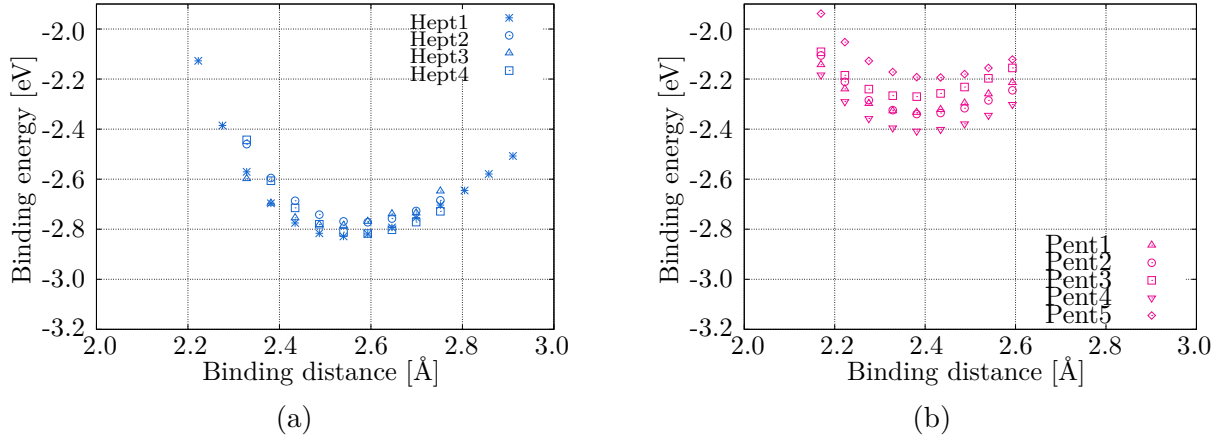


Figure 4.6: Binding energy with van-der-Waals interactions of  $C_{58}$  with  $C_s$  symmetry for the analysed contact geometries on a flat Au(111) surface as a function of the binding distance.

Geometry	After Relaxation						Before relaxation	
	def-SV(P)		def-TZVP		def-TZVPP		def-SV(P)	
	$D$ [Å]	$E$ [eV]	$D$ [Å]	$E$ [eV]	$D$ [Å]	$E$ [eV]	$D$ [Å]	$E$ [eV]
Hept1	2.13	-3.95	2.18	-3.94			2.54	-2.83
Hept2	2.26	-4.14	2.25	-4.16			2.59	-2.77
Hept3	2.16	-3.97	2.14	-3.98	2.15	-4.04	2.54	-2.78
Hept4	2.27	-4.16	2.25	-4.18	2.15	-4.22	2.59	-2.82
Pent1	2.19	-3.78					2.38	-2.33
Pent2	2.18	-3.57					2.38	-2.34
Pent3	2.10	-3.88					2.38	-2.27
Pent4	2.17	-3.83					2.38	-2.41
Pent5	2.18	-3.05	2.23	-3.09	2.24	-3.12	2.43	-2.19

Table 4.5: The binding distances  $D$  and the corresponding binding energies  $E$  for the investigated contact geometries of  $C_{58}$  with  $C_s$  symmetry on a flat Au(111) surface after relaxation obtained with three basis sets as well as before the relaxation procedure gained with the def-SV(P) basis set.

the corresponding binding distances are listed in Table 4.5.

Comparing the values gained for the heptagon, the minimal binding energy is found for Hept4 with -4.16 eV. The configuration Hept2 is just 20 meV higher in energy than Hept4. Whereas the other two heptagonal geometries are 190 meV and 210 meV higher in

energy and thus less favourable. As mentioned above, most of the contact geometries for the analysed pentagon are not yet converged with the def-TZVP and def-TZVPP basis sets. Therefore, we focus on the values obtained using the def-SV(P) basis set. For the configurations **Pent1** to **Pent4**, the fullerene rotates on the surface in such a way that the bond between the heptagon **Hept** and the pentagon **Pent** faces the surface. We find that the binding energies for these configurations are at least 280 meV higher compared to the binding energy of **Hept4**. The geometry **Pent5** is over 1 eV higher in energy than **Hept4** and thus less favourable. There are many more possible contact geometries for  $C_{58}$  with  $C_s$  symmetry which are unfeasible for us to investigate in this study. Nevertheless, the fullerene shows a dominant behaviour for the heptagonal face to be on top of the Au(111) surface.

### 4.2.3 Summary regarding Geometry Optimisation

We performed a geometry optimisation for two isomers of  $C_{58}$  with  $C_{3v}$  and  $C_s$  symmetry. In Section 4.2.1 and Section 4.2.2 we analysed different contact geometries of these isomers on the Au(111) surface. Here we compare the isomers with each other.

Isomer	Geometry	Binding distance [ $\text{\AA}$ ]	Binding energy [eV]
$C_s$	<b>Hept4</b>	2.27	-4.16
$C_{3v}$	<b>H1a</b>	2.29	-4.03
$C_s$	<b>Pent3</b>	2.10	-3.88
$C_{3v}$	<b>P1a</b>	2.06	-3.79

Table 4.6: The minimal binding energies and the corresponding binding distances for relaxed structures of the two investigated isomers of  $C_{58}$ : the hexagonal and pentagonal face of the isomer with  $C_{3v}$  symmetry as well as the heptagonal and the pentagonal face of the isomer with  $C_s$  symmetry. The values are obtained using the B-P86 functional as well as the def-SV(P) basis set. The dispersive interactions are included by DFT-D3.

On the one hand, we used the structures of these isomers optimised in vacuum and added the Au(111) surface without performing another relaxation procedure. Comparing Figure 4.3 and Figure 4.6, we find that the hexagonal face **H1** of the isomer with  $C_{3v}$  symmetry binds better to the surface than the heptagonal face **Hept** of the isomer with  $C_s$  symmetry. The contact geometry **H1b** is 290 meV lower in energy than **Hept1**. The pentagonal faces of the isomer with  $C_{3v}$  symmetry are lower in energy than the pentagonal face **Pent** of the isomer with  $C_s$  symmetry, the configuration **P1** is 400 meV lower in energy than **Pent4**.

On the other hand, we performed a relaxation procedure of the fullerene on the surface keeping the positions of the gold atoms fixed. Thus, we accounted for the force exerted

on the molecule due to the presence of the surface. We summarise the minimal binding energies after relaxation for the two isomers obtained with the def-SV(P) basis set in Table 4.6. The heptagonal face of the isomer with  $C_s$  symmetry is 130 meV lower in energy than the hexagonal face of the isomer with  $C_{3v}$  symmetry. This result is the other way round than for the contact geometries before relaxation. Furthermore, the pentagonal face of the first isomer is 90 meV lower in energy than the pentagonal face of the latter one. However, they are both lower in energy than the hexagon or the heptagon. For further clarification, we display these four configurations in Figure 4.7.

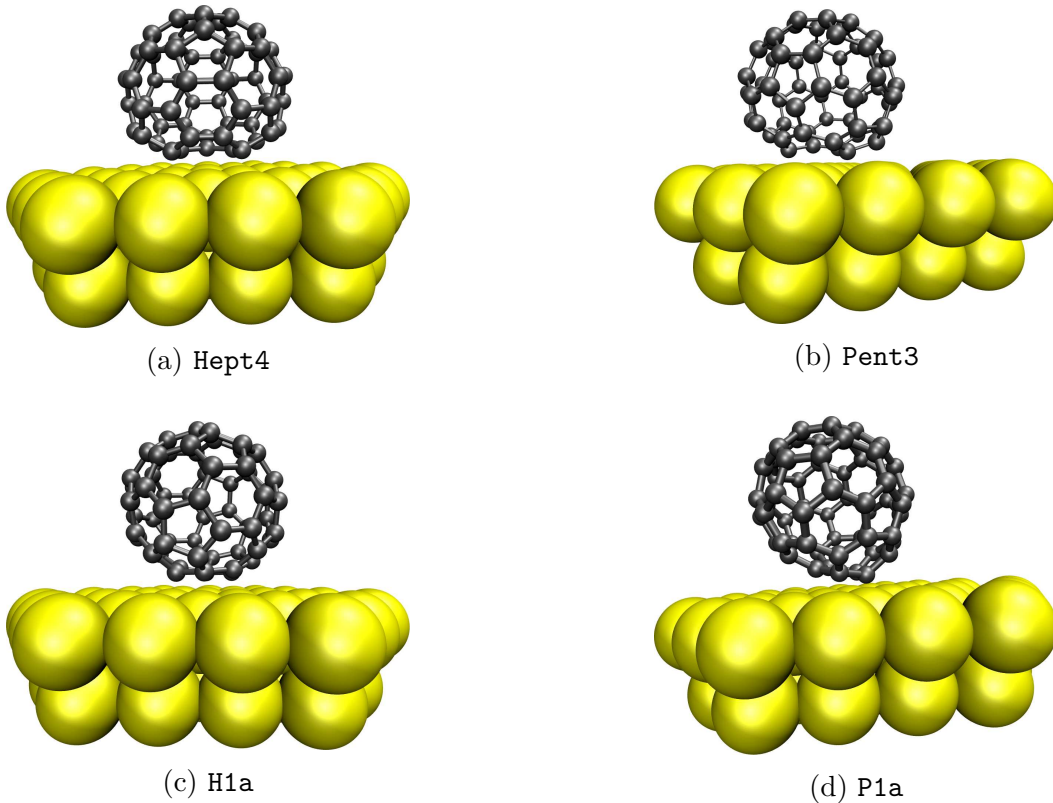


Figure 4.7: The optimised structures for  $C_{58}$  with  $C_{3v}$  and  $C_s$  symmetry with the minimal binding energy for the hexagons, the pentagons and the heptagon facing the surface.

#### 4.2.4 Local Density of States

We continue our study of  $C_{58}$  by analysing the electronic structure of the two investigated isomers in the presence of the Au(111) surface. Thus, we define an extended molecule consisting of the isomer and the finite gold cluster. An infinite gold reservoir is included to the extended molecule by the embedding Green's function formalism presented in Section 2.2.1.

The local density of states of  $C_{58}$  on Au(111) is presented for the four contact geometries mentioned in Section 4.2.3. These are the two optimised structures with the minimal binding energy for each isomer obtained using the def-SV(P) basis set. Our results are presented in Figure 4.8 for the isomer with  $C_{3v}$  symmetry and in Figure 4.9 for the isomer with  $C_s$  symmetry. As explained in Section 3.2.2, the energy levels of the extended molecule experience a shift along the energy axis as well as a level broadening.

### Discussion of the LDOS of $C_{58}$ with $C_{3v}$ Symmetry

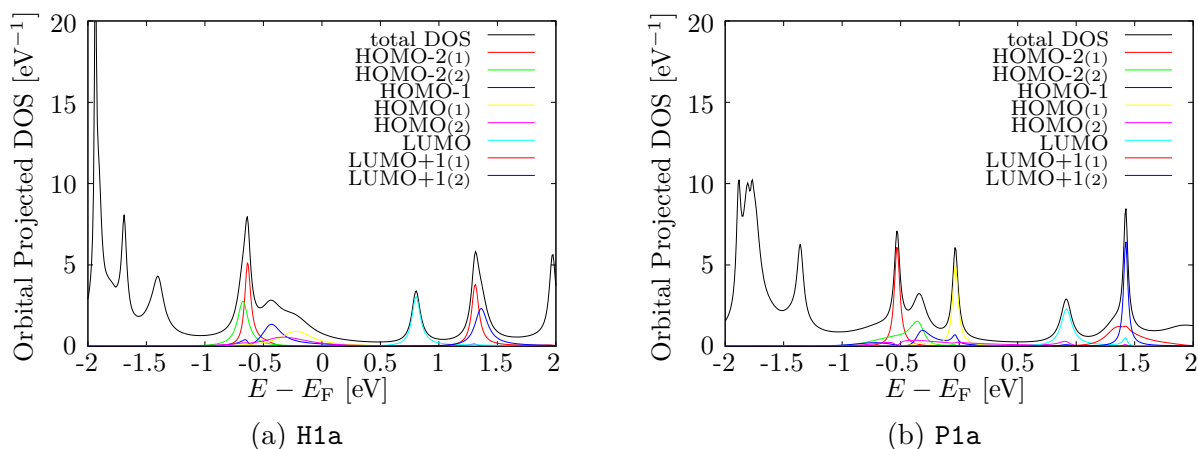


Figure 4.8: The local density of states as a function of the energy  $E$  for  $C_{58}$  with  $C_{3v}$  symmetry for two contact geometries obtained with the def-SV(P) basis set: (a) **H1a** at a binding distance of 2.29Å and (b) **P1a** at a binding distance of 2.06Å. The energy axis is normalised to the Fermi energy of the extended molecule. The (x) in the key denotes the contribution to the degenerate states in vacuum.

We examine the resonances for the isomer with  $C_{3v}$  symmetry in the LDOS (Fig. 4.8). The  $C_{3v}$  symmetry of the isomer in vacuum is broken when contacting the fullerene to the surface. The symmetry of both investigated geometries **H1a** and **P1a** reduces to a  $C_1$  symmetry. Thus, the degenerate orbitals of the isomer in vacuum split into non-degenerate orbitals on the surface. Besides the local density of states, the density of states projected onto some orbitals is shown. Therefore, we find that the resonances of the LDOS are superpositions of several resonances. The LUMO of the LDOS can be associated with the LUMO in vacuum as well as the LUMO+1 with the LUMO+1 in vacuum for both contact geometries. Therefore, we refer to the resonance just above the Fermi energy as LUMO. Furthermore, the resonance just below the Fermi energy is referred to as HOMO. For the contact geometry **H1a** the HOMO-LUMO gap is 1.2 eV whereas for **P1a** it is 300 meV smaller.

We find that all the LUMO and LUMO+1 are clearly above the Fermi energy and thus completely empty. For the HOMO orbitals we first focus on the geometry **H1a**. The curves

for the HOMO-2 are clearly below the Fermi energy and therefore completely filled. The HOMO-1 and HOMO curves have a tail that leaks over the Fermi energy. Therefore, they are only partially filled. This means, that there is a charge exchange of the fullerene with the surface. Furthermore, both HOMO orbitals exhibit a great broadening. Thus they hybridise strongly with the surface.

We now investigate the HOMO resonances of the contact geometry **P1a**. The HOMO(1) and also the HOMO resonance of the total DOS is right at the Fermi energy. Therefore, this energy level is half filled indicating a charge transfer between the fullerene and the surface. The HOMO-1 orbital has a little tail that leaks over the Fermi energy, thus this energy level is partially filled. Furthermore, the orbital HOMO(2) exhibits a great width and is thus delocalised over the molecule. The two HOMO-2 orbitals are clearly below the Fermi energy which means they are completely filled.

In Section 4.1 we found, that the isomer exhibits a spin 1 in vacuum. Within a Löwdin analysis, we find, that the number of electrons with  $\alpha$  spin  $n_\alpha$  and the number of electrons with  $\beta$  spin  $n_\beta$  are nearly equal for both contact geometries (Tab. 4.7). Therefore, the molecule does not keep its spin on the Au(111) surface. Furthermore, the Löwdin analysis gives us the total number of electrons of the molecule. In vacuum,  $C_{58}$  has 348 electrons. On the Au(111) surface it loses approximately 0.1 electrons for **H1a** and approximately 0.2 electrons for **P1a**. Thus, the molecule charges partially positive. This also explains why the HOMO is moved towards the Fermi energy.

	H1a	P1a
$n_\alpha$	173.95	173.88
$n_\beta$	173.96	173.96
$n = n_\alpha + n_\beta$	347.91	347.84
$n = n_\alpha - n_\beta$	-0.01	-0.08

Table 4.7

### Discussion of the LDOS of $C_{58}$ with $C_s$ Symmetry

We now continue with the analysis of the LDOS of the isomer with  $C_s$  symmetry. The  $C_s$  symmetry of the isomer in vacuum is conserved for the contact geometry **Hept4**. However, for **Pent3**, the symmetry is reduced to  $C_1$ . Again, we find that the resonances of the total DOS are superpositions of several resonances, namely the contributions of the orbital projected DOS. The Fermi energy is in between the HOMO and LUMO states of the total DOS for both contact geometries. While the HOMO-LUMO gap for **Hept4** is 1.5 eV, it is 200 meV bigger for **Pent3**.

First we focus on the contact geometry **Hept4**. The LUMO orbitals are all clearly above the Fermi energy and thus fully empty. Furthermore, the HOMO-2 to HOMO-4 resonances

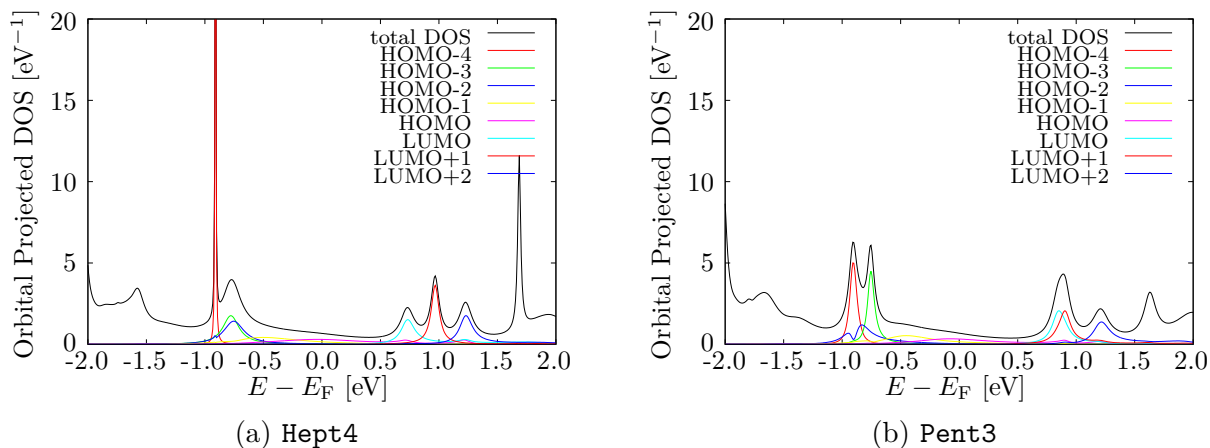


Figure 4.9: The local density of states as a function of the energy  $E$  for  $C_{58}$  with  $C_s$  symmetry for two contact geometries obtained with the def-SV(P) basis set: (a) **Hept4** at a binding distance of  $2.27\text{\AA}$  and (b) **Pent3** at a binding distance of  $2.20\text{\AA}$ . The energy axis is normalised to the Fermi energy of the extended molecule.

are all well below the Fermi energy. Therefore, they are completely filled. On the one hand, the HOMO-4 orbital exhibits quite a small broadening, thus it hybridises weakly with the surface. On the other hand, the HOMO-2 and HOMO-3 display a greater broadening. Therefore, their hybridisation with the surface is much better than for the HOMO-4. However, the HOMO and HOMO-1 resonances show a great broadening indicating that these orbitals are delocalised over the molecule.

The LUMO orbitals for the geometry **Pent3** are also well above the Fermi energy. Instead of three resonances for LUMO to LUMO+2 of the total DOS as for the geometry **H1a**, the contributions LUMO and LUMO+1 combine to the LUMO state of the LDOS. Again, the HOMO-2 to HOMO-4 are clearly below the Fermi energy and thus completely filled. Also, the HOMO and HOMO-1 are delocalised over the molecule due to their great broadening.

Comparing both isomers of  $C_{58}$ , we find that the HOMO-LUMO gap for the  $C_{3v}$  symmetry is smaller than for the  $C_s$  symmetry. In the STM experiments (Sec. 1.2), the HOMO-LUMO gap was found to be  $1.2\text{ eV}$ . Caution with the values determined with DFT is needed since they are obtained using approximations. Therefore, the actual values for the HOMO-LUMO gaps of the four discussed contact geometries should not be compared directly to the experimental value. Nevertheless, we observe that all four HOMO-LUMO gaps are close to the experimental value.

### 4.2.5 Simulated Topography

In order to simulate the surface topography of  $C_{58}$  on Au(111), we analyse the spatially resolved density of states analogously to  $C_{60}$  in Section 3.2.3. Thus, we calculate the local density of states in a plane above the molecule (Fig. 3.6) and choose different distances  $z \approx 0.5\text{\AA}$ ,  $1.5\text{\AA}$ ,  $3.0\text{\AA}$  and  $4.5\text{\AA}$ . As derived in Section 2.2.4, the tunnel current in the STM experiments is proportional to the spatially resolved density of states. Since the applied bias in the experiments is non-zero, we integrate over an equivalent energy window as depicted in (2.47). However, we start by calculating the spatially resolved density of states at the Fermi energy  $E_F$  for all investigated contact geometries of  $C_{58}$  before and after the relaxation procedure. We compare these results with the experimental STM image of the smallest applied voltage (Fig. 1.7d). For the contact geometries that are in agreement with the experimental STM image, we determine the topographies for the different voltages applied in the experiments. The whole catalogue of simulated topographies is found in Appendix B.

The simulated topographies for the different contact geometries of the two isomers exhibit different features. For example the topography of **H1b** on Page 93 exhibits a “butterfly” structure, **H5b** on Page 108 shows a threefold symmetry, **P1a** on Page 109 displays a “banana” structure, **Pent3** on Page 136 exhibits a ring like structure and **Hept4** on Page 128 shows a centric maximum. These features also depend on the distance  $z$  as can be seen in Figure 4.11. While for small distances  $z \approx 0.5\text{\AA}$  the LDOS displays two maxima, for larger distances  $z \approx 3.0\text{\AA}$  there is only one maximum. It is simple to exclude several binding geometries by comparing them with Figure 1.7d due to the different features. We find, that none of the topographies of the contact geometries for the isomer with  $C_{3v}$  symmetry before and after relaxation is similar to this experimental STM image see Page 90 to Page 120. The simulated images obtained for the contact geometry **Hept4** of the isomer with  $C_s$  symmetry before relaxation resembles the experimental image the most. Especially with the def-TZVPP basis set, the centric maximum is well reconstructed for all four distances  $z$ . These images are displayed in Figure 4.10.

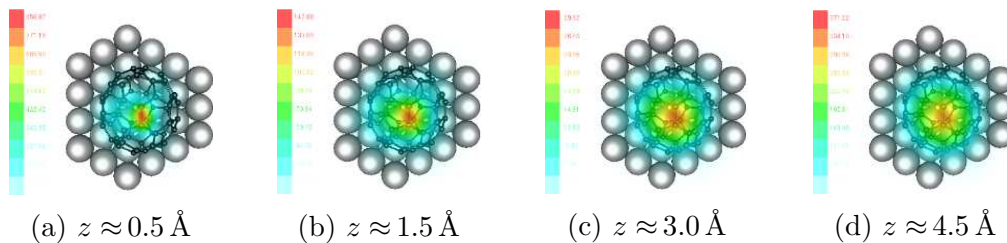


Figure 4.10: Simulated topography for the not relaxed contact geometry **Hept4** of the isomer  $C_s$  at different distances  $z$  at the Fermi energy using the def-TZVPP basis set. The scaling factors for the colour scale are  $10^{-2}$  for  $z \approx 0.5\text{\AA}$ ,  $10^{-3}$  for  $z \approx 1.5\text{\AA}$ ,  $10^{-5}$  for  $z \approx 3.0\text{\AA}$  and  $10^{-10}$  for  $z \approx 4.5\text{\AA}$ .

For the contact geometries of the isomer with  $C_s$  symmetry after the relaxation procedure, we find that the topography images for **Hept2** and **Hept4** are alike, see Page 123 and Page 127. They are just rotated by  $120^\circ$  relative to each other due to the construction and symmetry of the gold cluster used in our calculations. Moreover, they resemble the experimental STM image (Fig. 1.7d) well with the def-TZVP basis set. The binding energy of **Hept2** is determined to be 20 meV higher in energy than **Hept4** (Sec. 4.2.2). Furthermore, these contact geometries exhibit the greatest binding energy of all investigated configurations for both isomers. The topography for the relaxed contact geometry **Hept4** is shown in Figure 4.11.

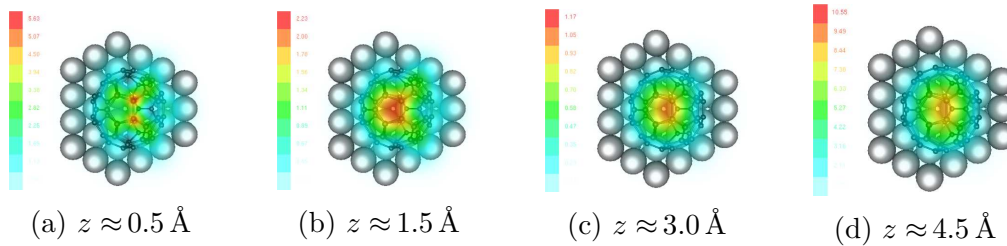


Figure 4.11: Simulated topography for the relaxed contact geometry **Hept4** at different distances  $z$  at the Fermi energy using the def-TZVP basis set. The scaling factors for the colour scales are analogue Figure 4.10.

In order to simulate the experimental STM images at different voltages, we calculate the spatially resolved density of states by integrating over an equivalent energy window as depicted in (2.47). Some of the features in the experimental images are found in the simulated images. For a direct comparison of the experimental STM images and our simulated topographies of the binding geometry **Hept4** see Figure 4.12. All simulated images for **Hept4** at different bias as well as different distances  $z$  are found on Page 132 and Page 131. The experimental image for bias -2.0 V (Fig. 4.12a) displays a centric maximum. The simulated image for -2.0 V at  $z \approx 3.0 \text{ \AA}$  (Fig. 4.12e) resemble such a centric maximum. The ring like structures of the experimental images at bias -1.8 V (Fig. 4.12b) and bias -1.2 V (Fig. 4.12c) are found at  $z \approx 1.5 \text{ \AA}$  see Figure 4.12f and Figure 4.12g. Figure 4.12d at bias -0.5 V shows a centric maximum with a dark shadow. A similar feature in the simulated topography is found for  $z \approx 3.0 \text{ \AA}$  in Figure 4.12h. Figure 4.12l at bias 0.6 V resembles the ring like structure of the experimental image (Fig. 4.12i). The centric maximum at bias 1.4 V (Fig. 4.12j) is found for  $z \approx 3.0 \text{ \AA}$  (Fig. 4.12m). Also, Figure 4.12n matches the centric maximum of the experimental image at bias +2.0 V (Fig. 4.12k).

Thus, we give evidence for the presence of  $C_{58}$  on the surface in the experiments due to the similarities in the simulated topographies and the experimental STM images shown in Figure 4.12. We identify the isomer of  $C_{58}$  with  $C_s$  symmetry to be found in the experiment. Furthermore, its binding geometry is identified:  $C_{58}$  with  $C_s$  symmetry binds with the heptagon to the Au(111) surface.

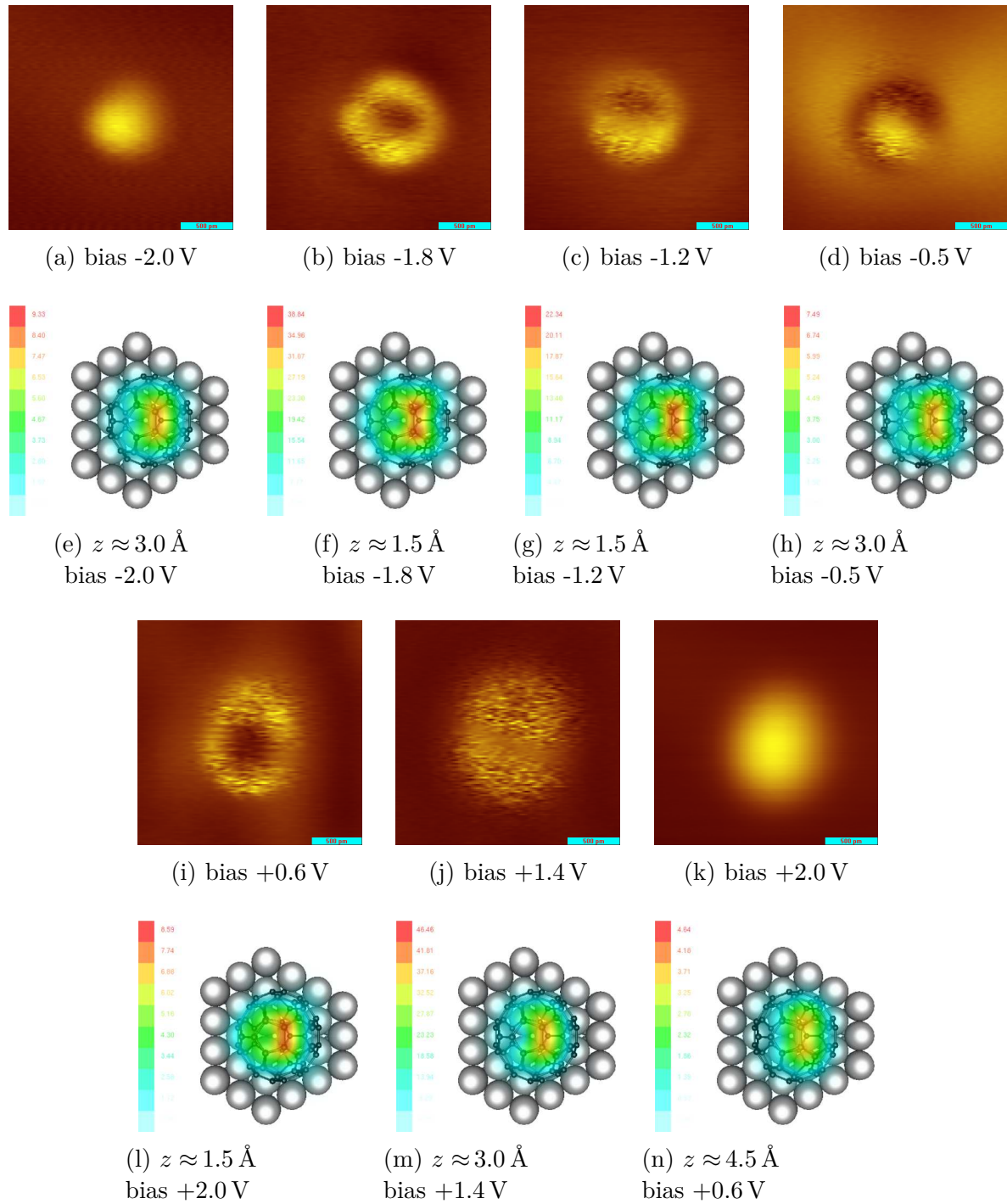


Figure 4.12: Direct comparison of the experimental images with the simulated topography for the relaxed contact geometry  $\text{Hept}_4$  for different voltages at different distances  $z$  the def-TZVP basis set. The scaling factors for the colour scale are found in Table B.1.

## Chapter 5

# Summary and Outlook

In this study we have analysed spherical carbon molecules called fullerenes. Specifically, we have examined the molecules  $C_{60}$  and  $C_{58}$ . This choice was motivated by recent STM experiments on these fullerenes. We developed a catalogue of simulated topographies of  $C_{60}$  and  $C_{58}$  on the Au(111) surface. Our aim is to give evidence for the presence of  $C_{58}$  on the surface in the experiments and identify its binding geometry.

In order to obtain numerical results that may be compared directly with the experimental data, we have used ab-initio simulations. In particular, we have performed DFT calculations on the GGA level and have accounted for the van-der-Waals interactions using DFT-D. The surface is modelled as a finite gold cluster in these calculations. An effectively infinite surface is included via an embedding Green's function formalism. This embedding formalism, based on an existing transport code, has been implemented during this study. The physical reason for treating an infinite surface goes as follows: The local density of states of a finite system only displays discrete states. These discrete levels experience a level broadening on an infinite surface. Therefore the embedding formalism is necessary. Moreover, we developed the code further in order to calculate the spatially resolved density of states. This representation of the density of states is proportional to the tunnel current in the STM experiments. Therefore, the simulated topographies can be compared to the experimental STM images.

Our analysis of  $C_{60}$  and  $C_{58}$  has been divided into two parts. Initially, we have examined the electronic properties of the molecules in vacuum. Afterwards, we have investigated several binding geometries of the fullerene towards the surface. The binding geometries have been prepared using the optimised structure of the molecule in vacuum and adding the gold surface. Furthermore, a relaxation of the molecule on the surface has been performed keeping the positions of the gold atoms fixed.

Our analysis has been started by investigating the buckminsterfullerene  $C_{60}$ . It is a classical IPR-fullerene that exhibits icosahedral  $I_h$  symmetry. This high symmetry causes a great degeneracy of the energy levels in vacuum. Our DFT calculations obtained an HOMO-LUMO gap of approximately 1.6 eV. This value is smaller than the experimental one of 2.2 eV due to the GGA-functional used in our calculations which tends to underes-

timate the HOMO-LUMO gap.

In our study, two contact geometries for  $C_{60}$  have been prepared. One with a hexagon and one with a pentagon facing the surface. For both binding geometries, we have performed a systematic study of the binding distance in order to find the optimal binding geometry. Our findings indicate that  $C_{60}$  prefers to bind with the hexagon to the surface than with the pentagon. We have calculated the local density of states for both contact geometries at the Fermi energy in order to simulate the experimental STM images. These images of  $C_{60}$  display a sixfold symmetry. In accordance, our numerical results show such a sixfold symmetry when a hexagon is the topmost feature. Therefore, we have proven our method to be adequate.

We have continued our study by applying the same method to  $C_{58}$  on the Au(111) surface, performing an investigation of two isomers of  $C_{58}$ . In particular, we have examined a classical isomer with  $C_{3v}$  symmetry as well as a non-classical isomer with  $C_s$  symmetry which also contains a heptagon. We began this part of our study by investigating the electronic ground state properties of both isomers in vacuum. While the isomer with  $C_s$  symmetry exhibits a singlet ground state, the isomer with  $C_{3v}$  symmetry exhibits a triplet state. Furthermore, according to the ground state energies, the isomer with  $C_{3v}$  symmetry is found to be more stable than the other isomer.

Due to the reduced symmetry of both isomers of  $C_{58}$  compared to the icosahedral symmetry of  $C_{60}$ , more binding geometries are possible. We have prepared the contact geometries such, that a polygon of the isomer is parallel to the gold surface. On the one hand our findings indicate that the isomer with  $C_{3v}$  symmetry prefers to bind with a hexagon rather than with a pentagon to the surface. On the other hand we find that the isomer with  $C_s$  symmetry prefers to bind with the heptagon to the surface. Furthermore, the bond between the surface and the heptagon of the isomer with  $C_s$  symmetry is stronger than the bond between the surface and the hexagon of the isomer with  $C_{3v}$  symmetry.

Finally, we have calculated the spatially resolved density of states for the investigated binding geometries of both isomers of  $C_{58}$  in order to develop a catalogue of simulated topography images. The experimental STM images show a ring like structure and a centric maximum depending on the applied voltage. Since these images are obtained at different voltages, we have integrated the density of states over an equivalent energy window. The simulated topographies for the different contact geometries reveal several characteristics. The best resemblance with the experimental images shows the isomer with  $C_s$  symmetry when the heptagon faces the surface. This agrees with the fact that this geometry exhibits the highest binding energy.

In conclusion, we give evidence for the presence of  $C_{58}$  in the experiments. Especially, we identify the isomer with  $C_s$  symmetry to be on the Au(111) surface as well as its binding geometry using our catalogue of simulated topography images. This knowledge of the binding of  $C_{58}$  on a gold surface is a great step towards possible applications.

This study focused on single  $C_{58}$  molecules on the Au(111) surface. However, the resolution of STM images is much better for an oligomer of  $C_{58}$  than for a single molecule.

Therefore, we suggest a theoretical analysis of  $C_{58}$  dimers or trimers on Au(111) as a natural next step.



## Acknowledgements

At the end of this thesis, I would like to thank Prof. Ferdinand Evers for his supervision and his support. I want to express my thanks to Prof. Wulf Wulfhekel for taking over the position as the coreferent. Furthermore, I express my gratitude to Prof. Artur Böttcher who shared his experimental data as well as his knowledge on C<sub>60</sub> and C<sub>58</sub> with me and provided me with the initial coordinate files of C<sub>58</sub>. For scientific support and discussions I would like to mention Dr. Alexej Bagrets. In addition, I acknowledge the help of Christian Seiler who shared his experience on TURBOMOLE with me. I am deeply grateful for the patience and caring support of Dr. Stefan Kremer. Last but not least, I am indebted to my friends and family for their motivating support.



# Appendix A

## Atomic Coordinate Files

This appendix contains some of the TURBOMOLE coordinate files used in this study. Each line contains the x-, y- and z-coordinate of the atom in units of  $a_0$  as well as the element type.

### Single $C_{60}$ with $I_h$ Symmetry

```

Scoord
-1.89733626785315      1.37849548852228      -6.32502243809897      c
 0.72471796623203      2.23045255376744      -6.32502243809897      c
 2.34523660324224      0.00000000000000      -6.32502243809897      c
 0.72471796623203      -2.23045255376744      -6.32502243809897      c
-1.89733626785315      -1.37849548852228      -6.32502243809897      c
-3.72831465791049      2.70877915675773      -4.92627941342829      c
-5.62565092576363      1.33028366823545      -3.47684348096423      c
-6.07355126115272      2.70877915675773      -1.13160687772200      c
-4.45303262414251      4.93923171052517      -1.13160687772200      c
-3.00359669167846      4.93923171052517      -3.47684348096423      c
 1.42408947856737      4.38289674365128      -4.92627941342829      c
-0.47324678928578      5.76139223217356      -3.47684348096423      c
 0.69937151233534      6.61334929741872      -1.13160687772200      c
 3.32142574642051      5.76139223217356      -1.13160687772200      c
 3.76932608180960      4.38289674365128      -3.47684348096423      c
 4.60845035868623      0.00000000000000      -4.92627941342829      c
 5.33316832491826      2.23045255376744      -3.47684348096423      c
 6.50578662653938      1.37849548852228      -1.13160687772200      c
 6.50578662653938      -1.37849548852228      -1.13160687772200      c
 5.33316832491826      -2.23045255376744      -3.47684348096423      c
 1.42408947856737      -4.38289674365128      -4.92627941342829      c
 3.76932608180960      -4.38289674365128      -3.47684348096423      c
 3.32142574642051      -5.76139223217356      -1.13160687772200      c
 0.69937151233534      -6.61334929741872      -1.13160687772200      c
-0.47324678928578      -5.76139223217356      -3.47684348096423      c
-3.72831465791049      -2.70877915675773      -4.92627941342829      c
-3.00359669167846      -4.93923171052517      -3.47684348096423      c
-4.45303262414251      -4.93923171052517      -1.13160687772200      c
-6.07355126115272      -2.70877915675773      -1.13160687772200      c
-5.62565092576363      -1.33028366823545      -3.47684348096423      c
 5.62565092576363      1.33028366823544      3.47684348096424      c
 6.07355126115272      2.70877915675772      1.13160687772200      c
 4.45303262414251      4.93923171052517      1.13160687772200      c
 3.00359669167846      4.93923171052517      3.47684348096424      c
 3.72831465791048      2.70877915675772      4.92627941342829      c
 0.47324678928578      5.76139223217356      3.47684348096424      c
-0.69937151233534      6.61334929741872      1.13160687772200      c
-3.32142574642051      5.76139223217356      1.13160687772200      c
-3.76932608180960      4.38289674365128      3.47684348096424      c
-1.42408947856737      4.38289674365128      4.92627941342829      c
-5.33316832491826      2.23045255376744      3.47684348096424      c
-6.50578662653938      1.37849548852228      1.13160687772200      c
-6.50578662653938      -1.37849548852228      1.13160687772200      c
-5.33316832491826      -2.23045255376744      3.47684348096424      c
-4.60845035868623      0.00000000000000      4.92627941342829      c
-3.76932608180960      -4.38289674365128      3.47684348096424      c

```

-3.32142574642051	-5.76139223217356	1.13160687772200	c
-0.69937151233534	-6.61334929741872	1.13160687772200	c
0.47324678928578	-5.76139223217356	3.47684348096424	c
-1.42408947856737	-4.38289674365128	4.92627941342829	c
3.00359669167846	-4.93923171052517	3.47684348096424	c
4.45303262414251	-4.93923171052517	1.13160687772200	c
6.07355126115272	-2.70877915675772	1.13160687772200	c
5.62565092576363	-1.33028366823544	3.47684348096424	c
3.72831465791048	-2.70877915675772	4.92627941342829	c
1.89733626785315	1.37849548852228	6.32502243809897	c
-0.72471796623202	2.23045255376744	6.32502243809897	c
-2.34523660324223	0.00000000000000	6.32502243809897	c
-0.72471796623202	-2.23045255376744	6.32502243809897	c
1.89733626785315	-1.37849548852228	6.32502243809897	c

Send

## Single $C_{58}$ with $C_{3v}$ Symmetry

-24.02390610054034	-17.12262432540065	12.92384065174707	c
-21.33747067569407	-17.11147493808594	12.21935055159043	c
-25.31534530238329	-19.39237502094290	13.12415167807917	c
-23.99801684525024	-21.78722562160952	12.63263377290013	c
-21.45538961949711	-21.78080055095359	11.99522896929810	c
-20.08533778845213	-19.37272186364239	11.78263471965319	c
-27.90143624139716	-19.61044947791199	12.15169833703676	c
-25.23956726317653	-14.93224214972584	11.73803717039435	c
-20.88960545644212	-14.93280906772489	10.57037506501132	c
-18.30256965409649	-19.58985145727972	9.67105414584676	c
-20.51354985040357	-23.47569639545599	10.01460645327294	c
-25.75432880631674	-23.48268838411098	11.32626573041545	c
-23.30845558573533	-13.53951359871873	10.30203387879286	c
-28.20813887888488	-22.15043108633621	11.06340475152116	c
-18.53236041637935	-22.14079348035230	8.59995707296911	c
-29.04150833749294	-17.54403337136345	11.01276007693909	c
-27.67712568643849	-15.14653715336791	10.80073274529323	c
-19.25102346651233	-15.15069455202763	8.55384774237946	c
-17.92859274738780	-17.53288398404874	8.08557347516160	c
-24.87900741577876	-25.04152390884065	9.42841324225204	c
-22.19899706158842	-25.03831137351268	8.74924547938643	c
-23.92469545070605	-12.36996176667220	8.06686518119285	c
-29.69308609107129	-22.50758942573966	8.96316253769580	c
-18.29198718478084	-22.50588867174250	6.01802353261496	c
-26.53554180901190	-12.56668231234362	7.08817574216086	c
-22.18066671295237	-12.59805177495790	5.85418423088862	c
-26.35431702198126	-12.87338494983135	4.37604003469085	c
-23.62403993854156	-12.86488117984555	3.67929781385459	c
-27.55259269931316	-14.82188211257684	3.09027001283843	c
-25.61354416988522	-16.07155835515621	1.43524740093609	c
-23.22266199521196	-14.88159747514376	1.87801035819656	c
-30.94030568898811	-20.30756964408094	7.77263473968429	c
-30.78969447390633	-20.66850743681142	5.06541232153941	c
-29.44723265214860	-23.09869592608569	4.58428791300968	c
-28.76919872528110	-24.17735190561738	6.87803813717851	c
-29.83746120816349	-18.83717332720357	3.44497170757931	c
-27.89822370606920	-20.08684956978294	1.78994909567697	c
-27.65350410314461	-22.66878311013709	2.56643778171336	c
-17.85697210684076	-20.30171149142406	4.35827660405385	c
-19.33813986570015	-20.74107294069021	2.05318801990396	c
-20.63713797419715	-23.02386275021068	2.25519980023321	c
-20.07758990913174	-24.20456396957193	4.70352966547718	c
-23.24137028918071	-22.67105078213330	1.40671252831708	c
-23.44924022216685	-20.05037784517719	0.59923232499912	c
-21.04172845285470	-18.80542591925659	1.06448302955536	c
-30.52192020568692	-17.88871951478774	8.68688449949059	c
-29.90813698537877	-15.81398861091975	6.94852494172744	c
-28.31868788870024	-14.01704752658779	8.34446602806252	c
-19.92527794005281	-14.07997542448269	6.05449525722071	c
-19.24006305186397	-15.78942216429412	4.13491091242693	c
-17.80783921358950	-17.90119171076690	5.34112344174557	c
-26.32918365735658	-25.33480948701744	7.04943634555890	c
-24.66131090414237	-25.31723502904680	4.97716208635348	c
-22.02986652520425	-25.32120345504017	5.99704756665000	c
-29.47765725143112	-16.28868794879355	4.34788310740454	c
-25.77549374494805	-18.70243581609528	0.87267577320907	c
-25.23540986451680	-23.89861722274960	2.67282939286900	c
-20.92135286438910	-16.31684487607985	2.00273231798824	c

Send

## Single $C_{58}$ with $C_s$ Symmetry

Scoord

1.84970225277717	-0.17759651183670	-5.18707292413621	c
6.14102584114285	0.35997403213208	-3.50149343208491	c
5.85142522995989	-2.35227505893774	-4.15222080866468	c
3.28897477150654	-2.65907218275864	-5.38993508146404	c
-0.94928529214777	-0.23202063974580	-4.77131416089730	c
-2.51824975179385	2.00286459885468	-4.02715869807357	c
3.69018263943641	1.73057388390948	-4.18171944188208	c
-1.61902331896247	4.38121788574886	-2.77238019350272	c
3.24934720337272	3.65265266789910	-2.20156935752279	c
6.90850053099429	1.15560564926983	-0.89172421797725	c
7.36184595757042	-0.82535701755477	1.06693967421793	c
6.89992117194196	-3.57517387469517	0.45720046896969	c
6.07543342865241	-4.33964389915164	-2.12329687912019	c
3.83246015993210	-6.08140496490910	-2.38988061954160	c
2.13837689789501	-5.03814356578496	-4.42233833794685	c
-0.61178011004483	-5.14498871133983	-4.10968306146907	c
-2.17921389109347	-2.82124852502110	-4.53558965689102	c
-5.21921717468252	1.58818297981398	-3.13103141697034	c
-6.03661844298390	-0.95725993866779	-2.25193057310534	c
-4.57387551909374	-3.16714409351003	-3.05778561149268	c
-4.25279206169670	-5.40469384670605	-1.33766191603241	c
-1.77796822863032	-6.64012155024256	-1.99471987693495	c
-0.11978977319992	-7.64120425023715	0.04272671986197	c
2.70238471788630	-7.30602343193033	-0.13779886830317	c
3.68050723891924	-6.67855859057836	2.45384786710142	c
5.74123526821061	-4.79718451892076	2.75240578266942	c
5.27122245246232	3.37102670323615	-0.20892817991770	c
2.19244197773804	-0.40243619026116	7.38270853993557	c
3.12468193538095	2.02385946208628	6.33183154235749	c
1.26483185042073	4.01846595542142	5.52641114110275	c
-1.48797077484803	3.62655554267602	5.88821820809844	c
-2.42578542614829	1.15280885380784	6.92220104930474	c
-1.12387713858949	-3.55886553358908	6.97721099247953	c
1.35098448901016	-4.79425544259232	6.32007744251045	c
3.40239616585042	-2.84759131471043	6.58496042893469	c
5.56464031150557	-2.83591280392994	4.80083169138133	c
6.53660232361547	-0.37921144956662	3.75772147039027	c
5.26829337613388	2.01990993335954	4.46342099561156	c
2.21963514442595	5.17987306554823	3.11888047452397	c
0.40545975292277	5.79981679477943	1.08292676179122	c
-2.38931370154254	5.79692551298426	1.57682572256628	c
-3.33361011529865	4.51368772486094	3.90655634240834	c
-5.42115336594523	2.57537618883177	3.72841180983922	c
-4.82483122000791	0.47725046886953	5.55768611738385	c
-5.30586114220446	-2.19263095040439	4.83964667704983	c
-3.44565200917818	-4.22066670841703	5.55309408159152	c
1.47428915380421	-6.67663106938158	4.24685831997328	c
-0.86738453855124	-7.29717951114510	2.76200559412005	c
-3.30535870167917	-6.08010105351128	3.40925587363897	c
-5.04515445170658	-5.18246199107724	1.35037977647784	c
-6.31911368191206	-2.80254023105234	2.25735408862962	c
-6.88140185063956	-0.73311945910883	0.45461154344068	c
-6.61273941088830	1.99417185620253	1.24536766578657	c
-5.81009690782892	3.46906572253907	-1.05613043770265	c
-3.64567957651074	5.245427683350540	-0.90313816702485	c
4.68608748837298	3.94864055520472	2.46403349381774	c
0.85908863849843	4.84571269963970	-1.56688576031622	c
-0.60216140132756	-0.84856286098267	7.64853638969157	c

Send

Icosahedral C<sub>60</sub> on Au(111) with hexagon before Relaxation

4.88577551345951	2.89303314516468	2.56586777630683	c
4.91404240373711	0.32732107472422	1.58579349639573	c
2.69540702574835	0.00000000000000	0.00000000000000	c
1.29594806323072	2.36341652102672	0.00000000000000	c
2.64967023652294	4.15140933531849	1.58579349639574	c
5.69751245552047	3.37369007916984	5.03564388011854	c
4.30472640062087	5.13142414088090	6.62143737651426	c
4.31552339195065	4.15140933531851	9.18730515282111	c
5.71498235446829	1.78799281429175	9.18730515282111	c
6.56909856783509	1.30733588028661	6.62143737651427	c
5.75298764186903	-1.66164822039602	3.11219907315365	c
6.59630686390604	-1.16229034883880	5.67806684946049	c
5.77045754081685	-3.24734548527409	7.26386034585623	c
4.41673536752463	-5.03533829956588	5.67806684946048	c
4.40593837619486	-4.05532349400347	3.11219907315365	c
1.39880471531764	-2.30403220525641	0.00000000000000	c
2.27039082763224	-4.37038640413963	1.58579349639573	c
0.06255244097322	-5.67772228442626	2.56586777630683	c
-2.17355283596335	-4.41934609427243	1.58579349639574	c
-1.34770351287417	-2.33429095783713	0.00000000000000	c
-1.34770351287418	2.33429095783712	0.00000000000001	c
-2.69475277854835	-0.05938431577033	0.00000000000000	c

Scoord

-4.92006106415518	0.21897706882109	1.58579349639573	c
-4.94832795443278	2.78468913926156	2.56586777630684	c
-2.74048956777378	4.09202501954818	1.58579349639574	c
1.30904397827344	5.84331630829524	3.11219907315366	c
-1.43746424991838	5.81305755571452	3.11219907315366	c
-2.29158046328517	6.29371448971967	5.67806684946049	c
-0.07294508529638	6.62103556444391	7.26386034585624	c
2.15236320031044	6.34267417985245	5.67806684946049	c
-2.15236320031045	-6.34267417985247	6.62143737651426	c
0.07294508529637	-6.62103556444391	5.03564388011851	c
2.29158046328516	-6.29371448971970	6.62143737651426	c
1.43746424991837	-5.81305755571454	9.18730515282110	c
-1.30904397827345	-5.84331630829525	9.18730515282109	c
2.74048956777376	-4.09202501954819	10.71371072957901	c
4.94832795443276	-2.78468913926158	9.73363644966791	c
4.92006106415517	-0.21897706882112	10.71371072957902	c
2.69475277854833	0.05938431577031	12.29950422597475	c
1.34770351287417	-2.33429095783714	12.29950422597475	c
1.34770351287415	2.33429095783711	12.29950422597475	c
2.17355283596334	4.41934609427240	10.71371072957901	c
-0.06255244097324	5.67772228442623	9.73363644966792	c
-2.27039082763225	4.37038640413960	10.71371072957902	c
-1.39880471531765	2.30403220525638	12.29950422597475	c
-4.40593837619487	4.05532349400345	9.18730515282110	c
-4.41673536752464	5.03533829956586	6.62143737651427	c
-5.77045754081686	3.24734548527407	5.03564388011852	c
-6.59630686390605	1.162290348883878	6.62143737651426	c
-5.75298764186905	1.66164822039599	9.18730515282110	c
-6.56909856783509	-1.30733588028663	5.67806684946048	c
-5.71498235446830	-1.78799281429178	3.11219907315364	c
-4.31552339195066	-4.15140933531852	3.11219907315365	c
-4.30472640062089	-5.13142414088091	5.67806684946049	c
-5.69751245552047	-3.37369007916986	7.26386034585622	c
-2.64967023652294	-4.15140933531852	10.71371072957901	c
-1.29594806323073	-2.36341652102674	12.29950422597475	c
-2.69540702574836	-0.00000000000003	12.29950422597475	c
-4.91404240373713	-0.32732107472425	10.71371072957902	c
-4.88577551345952	-2.89303314516470	9.73363644966792	c
-11.01183702550682	-8.17416909121969	-4.90000000000000	au
-11.01183702550682	-2.72472303040656	-4.90000000000000	au
-11.01183702550682	2.72472303040657	-4.90000000000000	au
-11.01183702550682	8.17416909121969	-4.90000000000000	au
-6.29247830028962	-10.89889212162625	-4.90000000000000	au
-6.29247830028962	-5.44944606081312	-4.90000000000000	au
-6.29247830028962	0.00000000000000	-4.90000000000000	au
-6.29247830028962	5.44944606081313	-4.90000000000000	au
-6.29247830028961	10.89889212162625	-4.90000000000000	au
-1.57311957507240	-13.62361515203282	-4.90000000000000	au
-1.57311957507240	-8.17416909121969	-4.90000000000000	au
-1.57311957507240	-2.72472303040656	-4.90000000000000	au
-1.57311957507241	2.72472303040657	-4.90000000000000	au
-1.57311957507241	8.17416909121969	-4.90000000000000	au
-1.57311957507240	13.62361515203282	-4.90000000000000	au
3.14623915014480	-10.89889212162625	-4.90000000000000	au
3.14623915014480	-5.44944606081312	-4.90000000000000	au
3.14623915014480	0.00000000000000	-4.90000000000000	au
3.14623915014480	5.44944606081314	-4.90000000000000	au
3.14623915014480	10.89889212162626	-4.90000000000000	au
7.86559787536201	-8.17416909121969	-4.90000000000000	au
7.86559787536201	-2.72472303040656	-4.90000000000000	au
7.86559787536200	2.72472303040657	-4.90000000000000	au
7.86559787536201	8.17416909121969	-4.90000000000000	au
12.58495660057921	-5.44944606081312	-4.90000000000000	au
12.58495660057922	0.00000000000000	-4.90000000000000	au
12.58495660057921	5.44944606081312	-4.90000000000000	au
-7.86559787536202	-8.17416909121969	-9.34945407660398	au
-7.86559787536201	-2.72472303040657	-9.34945407660398	au
-7.86559787536202	2.72472303040657	-9.34945407660398	au
-7.86559787536202	8.17416909121969	-9.34945407660398	au
-3.14623915014481	-10.89889212162624	-9.34945407660398	au
-3.14623915014482	-5.44944606081312	-9.34945407660398	au
-3.14623915014481	-0.00000000000001	-9.34945407660398	au
-3.14623915014481	5.44944606081314	-9.34945407660398	au
-3.14623915014482	10.89889212162626	-9.34945407660398	au
1.57311957507240	-8.17416909121969	-9.34945407660398	au
1.57311957507239	-2.72472303040655	-9.34945407660398	au
1.57311957507240	2.72472303040657	-9.34945407660398	au
1.57311957507240	8.17416909121970	-9.34945407660398	au
6.29247830028961	-5.44944606081313	-9.34945407660398	au
6.29247830028961	-0.00000000000001	-9.34945407660398	au
6.29247830028961	5.44944606081312	-9.34945407660398	au
11.01183702550681	-2.72472303040656	-9.34945407660398	au
11.01183702550681	2.72472303040658	-9.34945407660398	au

Send

Icosahedral C<sub>60</sub> on Au(111) with pentagon before Relaxation

Scoord			
2.33646122912845	0.00000000000000	0.00000000000000	c
0.72200622649885	-2.22210667703361	0.00000000000000	c
-1.89023684106311	-1.37333745303485	0.00000000000000	c
-1.89023684106310	1.37333745303485	0.00000000000000	c
0.72200622649889	2.22210667703359	0.00000000000000	c
4.58542205418303	-0.00000000000001	1.38993422925074	c
5.30742828068190	2.22210667703359	2.83394668224848	c
6.47565889524614	1.37333745303483	5.17040791137695	c
6.47565889524613	-1.37333745303489	5.17040791137695	c
5.30742828068191	-2.22210667703363	2.83394668224848	c
1.41697334112422	-4.36099552459429	1.38993422925074	c
3.75343457025268	-4.36099552459430	2.83394668224848	c
3.30721018218731	-5.73433297762915	5.17040791137695	c
0.69496711462532	-6.58310220162791	5.17040791137695	c
-0.47326349993889	-5.73433297762913	2.83394668224848	c
-3.70968436821576	-2.69524345898543	1.38993422925074	c
-2.98767814171690	-4.91735013601903	2.83394668224848	c
-4.43169059471466	-4.91735013601902	5.17040791137695	c
-6.04614559734422	-2.69524345898543	5.17040791137695	c
-5.59992120927885	-1.32190600595057	2.83394668224848	c
-3.70968436821574	2.69524345898546	1.38993422925074	c
-5.59992120927885	1.32190600595061	2.83394668224848	c
-6.04614559734422	2.69524345898546	5.17040791137695	c
-4.43169059471461	4.91735013601907	5.17040791137695	c
-2.98767814171687	4.91735013601906	2.83394668224848	c
1.41697334112426	4.36099552459428	1.38993422925074	c
-0.47326349993884	5.73433297762915	2.83394668224848	c
0.69496711462538	6.58310220162789	5.17040791137695	c
3.30721018218737	5.73433297762912	5.17040791137695	c
3.75343457025272	4.36099552459425	2.83394668224848	c
-3.75343457025272	-4.36099552459425	9.75582996555998	c
-3.30721018218737	-5.73433297762911	7.41936873643151	c
-0.69496711462538	-6.58310220162789	7.41936873643151	c
0.47326349993885	-5.73433297762914	9.75582996555998	c
-1.41697334112426	-4.36099552459426	11.19984241855772	c
2.98767814171687	-4.91735013601906	9.75582996555998	c
4.43169059471461	-4.91735013601907	7.41936873643151	c
6.04614559734422	-2.69524345898546	7.41936873643151	c
5.59992120927885	-1.32190600595061	9.75582996555998	c
3.70968436821574	-2.69524345898546	11.19984241855772	c
5.59992120927885	1.32190600595057	9.75582996555998	c
6.04614559734422	2.69524345898543	7.41936873643151	c
4.43169059471466	4.91735013601902	7.41936873643151	c
2.98767814171690	4.91735013601903	9.75582996555998	c
3.70968436821576	2.69524345898543	11.19984241855772	c
0.47326349993889	5.73433297762913	9.75582996555998	c
-0.69496711462532	6.58310220162791	7.41936873643151	c
-3.30721018218731	5.73433297762915	7.41936873643151	c
-3.75343457025268	4.36099552459430	9.75582996555998	c
-1.41697334112422	4.36099552459429	11.19984241855772	c
-5.30742828068190	2.22210667703364	9.75582996555998	c
-6.47565889524613	1.37333745303489	7.41936873643151	c
-6.47565889524613	-1.37333745303483	7.41936873643151	c
-5.30742828068190	-2.22210667703359	9.75582996555998	c
-4.58542205418302	0.00000000000001	11.19984241855772	c
-0.72200622649889	-2.22210667703359	12.58977664780846	c
1.89023684106310	-1.37333745303485	12.58977664780846	c
1.89023684106311	1.37333745303485	12.58977664780846	c
-0.72200622649885	2.22210667703361	12.58977664780846	c
-2.33646122912845	0.00000000000000	12.58977664780846	c
-11.0118370250682	-8.17416909121969	-4.80000000000000	au
-11.0118370250682	-2.72472303040656	-4.80000000000000	au
-11.0118370250682	2.72472303040657	-4.80000000000000	au
-11.0118370250682	8.17416909121969	-4.80000000000000	au
-6.29247830028962	-10.89889212162625	-4.80000000000000	au
-6.29247830028962	-5.44944606081312	-4.80000000000000	au
-6.29247830028962	0.00000000000000	-4.80000000000000	au
-6.29247830028962	5.44944606081313	-4.80000000000000	au
-6.29247830028961	10.89889212162625	-4.80000000000000	au
-1.57311957507240	-13.62361515203282	-4.80000000000000	au
-1.57311957507240	-8.17416909121969	-4.80000000000000	au
-1.57311957507240	-2.72472303040656	-4.80000000000000	au
-1.57311957507241	2.72472303040657	-4.80000000000000	au
-1.57311957507241	8.17416909121969	-4.80000000000000	au
-1.57311957507240	13.62361515203282	-4.80000000000000	au
3.14623915014480	-10.89889212162625	-4.80000000000000	au
3.14623915014480	-5.44944606081312	-4.80000000000000	au
3.14623915014480	0.00000000000000	-4.80000000000000	au
3.14623915014480	5.44944606081314	-4.80000000000000	au
3.14623915014480	10.89889212162626	-4.80000000000000	au
7.86559787536201	-8.17416909121969	-4.80000000000000	au
7.86559787536201	-2.72472303040656	-4.80000000000000	au
7.86559787536200	2.72472303040657	-4.80000000000000	au

7.86559787536201	8.17416909121969	-4.80000000000000	au
12.58495660057921	-5.44944606081312	-4.80000000000000	au
12.58495660057922	0.00000000000000	-4.80000000000000	au
12.58495660057921	5.44944606081312	-4.80000000000000	au
-7.86559787536202	-8.17416909121969	-9.24945407660398	au
-7.86559787536201	-2.72472303040657	-9.24945407660398	au
-7.86559787536202	2.72472303040657	-9.24945407660398	au
-7.86559787536202	8.17416909121969	-9.24945407660398	au
-3.14623915014481	-10.89889212162624	-9.24945407660398	au
-3.14623915014482	-5.44944606081312	-9.24945407660398	au
-3.14623915014481	-0.00000000000001	-9.24945407660398	au
-3.14623915014481	5.44944606081314	-9.24945407660398	au
-3.14623915014482	10.89889212162626	-9.24945407660398	au
1.57311957507240	-8.17416909121969	-9.24945407660398	au
1.57311957507239	-2.72472303040655	-9.24945407660398	au
1.57311957507240	2.72472303040657	-9.24945407660398	au
1.57311957507240	8.17416909121970	-9.24945407660398	au
6.29247830028961	-5.44944606081313	-9.24945407660398	au
6.29247830028961	-0.00000000000001	-9.24945407660398	au
6.29247830028961	5.44944606081312	-9.24945407660398	au
11.01183702550681	-2.72472303040656	-9.24945407660398	au
11.01183702550681	2.72472303040658	-9.24945407660398	au

Send

## Icosahedral $C_{60}$ on Au(111) with pentagon after Relaxation (def-SV(P))

Scoord			
2.79706912851805	0.00016203930376	0.00338939258074	c
1.16152147515985	-2.21929884251238	0.02347279695754	c
-1.45975018884270	-1.39363302154776	-0.19193602714806	c
-1.46012041516841	1.39419163622242	-0.19204140820915	c
1.16180815941509	2.22006067401445	0.02355457665027	c
5.01371718868324	0.00018167579243	1.49483641980121	c
5.67186731466917	2.23505398511035	2.95770686602800	c
6.73673442337782	1.37977150024790	5.35280841317595	c
6.73677203723118	-1.37958757603307	5.35260492076265	c
5.67185436938632	-2.23488598559261	2.95769681032956	c
1.81409738334492	-4.40153507389556	1.36813946509835	c
4.09910105343992	-4.39041370451890	2.89962216201850	c
3.54548245980692	-5.77367104319680	5.21759931006934	c
0.92301033953325	-6.63261116978848	5.10252692947891	c
-0.15188837976142	-5.78431110745266	2.71472422795402	c
-3.34988117035091	-2.72165656966105	1.14018355467333	c
-2.68467185039216	-4.95633672847966	2.60002597495760	c
-4.23476116976330	-4.94899017035110	4.87819630843313	c
-5.85507791376670	-2.71588813500259	4.80650990833876	c
-5.30841329293759	-1.33469432021794	2.48486590107770	c
-3.34960680685044	2.72212634345078	1.14020368955934	c
-5.30845628369466	1.33506156964932	2.48487216290530	c
-5.85496001478340	2.71615576707034	4.80667843451929	c
-4.23471377074901	4.94942682333164	4.87842733851279	c
-2.68458191513013	4.95659941185318	2.60024037270756	c
1.81411341123119	4.40176284828889	1.36805353990804	c
-0.15178351118955	5.78468416045964	2.71514257873874	c
0.92342195221898	6.63290368599639	5.10246464630900	c
3.54531234870149	5.77383839004665	5.21770148319507	c
4.09925120961269	4.39071626045128	2.89984636156885	c
-3.74045165233430	-4.38115560401118	9.50979836669811	c
-3.19445945636360	-5.76749752272330	7.18813517495968	c
-0.57714632939954	-6.62133124976135	7.30366014537734	c
0.49350192781594	-5.75938776290255	9.69327840350275	c
-1.46375750327534	-4.38229656928335	11.06180704060791	c
3.02200915798045	-4.93575557571865	9.80431045334942	c
4.57374252835033	-4.93815127191185	7.52482687456774	c
6.19508310512524	-2.70944929406100	7.59367466980887	c
5.64122754095523	-1.32981528861162	9.91616794656871	c
3.68290864932864	-2.70724922749160	11.28379219419294	c
5.64107834243420	1.32985784294813	9.916274445520460	c
6.19514888680600	2.70952725235221	7.59358627437085	c
4.57404376324201	4.93829510393057	7.52512067728815	c
3.02177390849153	4.93579513660210	9.80442263918818	c
3.68320117792945	2.70727933674972	11.28380023288052	c
0.49383865293695	5.75933643556180	9.69332616486776	c
-0.57736966238634	6.621627698885869	7.30419745674636	c
-3.19421663501032	5.76764286069921	7.18823573289144	c
-3.74034338828098	4.38132897146909	9.51004292886059	c
-1.46385875781922	4.38245090286709	11.06197414411726	c
-5.30299750269813	2.22951268973081	9.44163009670148	c
-6.37527780989594	1.37826509607585	7.04843223135245	c
-6.37542622878057	-1.37799296631241	7.04848669828992	c
-5.30293667141127	-2.22930668546480	9.44142805260536	c
-4.64270495925848	0.00006387085757	10.92212935362116	c

```

-0.82527120452332      -2.22974645206849      12.48941725163815      c
 1.79335699511975      -1.37755477719226      12.60334153930384      c
 1.79317084920702      1.37749589473880      12.60356602535147      c
-0.82510448060636      2.22955739649387      12.48943231288119      c
-2.44393647940337      0.00004333940431      12.42035302337902      c
-11.01183702550682     -8.17416909121969     -4.80000000000000      au
-11.01183702550682     -2.72472303040656     -4.80000000000000      au
-11.01183702550682     2.72472303040657     -4.80000000000000      au
-11.01183702550682     8.17416909121969     -4.80000000000000      au
-6.29247830028962     -10.89889212162625    -4.80000000000000      au
-6.29247830028962     -5.44944606081312    -4.80000000000000      au
-6.29247830028962     0.00000000000000      -4.80000000000000      au
-6.29247830028962     5.44944606081313     -4.80000000000000      au
-6.29247830028961     10.89889212162625    -4.80000000000000      au
-1.57311957507240     -13.62361515203282    -4.80000000000000      au
-1.57311957507240     -8.17416909121969     -4.80000000000000      au
-1.57311957507240     -2.72472303040656     -4.80000000000000      au
-1.57311957507241     2.72472303040657     -4.80000000000000      au
-1.57311957507241     8.17416909121969     -4.80000000000000      au
-1.57311957507240     13.62361515203282    -4.80000000000000      au
 3.14623915014480     -10.89889212162625    -4.80000000000000      au
 3.14623915014480     -5.44944606081312    -4.80000000000000      au
 3.14623915014480     0.00000000000000      -4.80000000000000      au
 3.14623915014480     5.44944606081314     -4.80000000000000      au
 3.14623915014480     10.89889212162626     -4.80000000000000      au
 7.86559787536201     -8.17416909121969     -4.80000000000000      au
 7.86559787536201     -2.72472303040656     -4.80000000000000      au
 7.86559787536200     2.72472303040657     -4.80000000000000      au
 7.86559787536201     8.17416909121969     -4.80000000000000      au
12.58495660057921     -5.44944606081312    -4.80000000000000      au
12.58495660057922     0.00000000000000      -4.80000000000000      au
12.58495660057921     5.44944606081312     -4.80000000000000      au
-7.86559787536202     -8.17416909121969     -9.24945407660398      au
-7.86559787536201     -2.72472303040657     -9.24945407660398      au
-7.86559787536202     2.72472303040657     -9.24945407660398      au
-7.86559787536202     8.17416909121969     -9.24945407660398      au
-3.14623915014481     -10.89889212162624    -9.24945407660398      au
-3.14623915014482     -5.44944606081312    -9.24945407660398      au
-3.14623915014481     -0.00000000000000      -9.24945407660398      au
-3.14623915014481     5.44944606081314     -9.24945407660398      au
-3.14623915014482     10.89889212162626     -9.24945407660398      au
 1.57311957507240     -8.17416909121969     -9.24945407660398      au
 1.57311957507239     -2.72472303040655     -9.24945407660398      au
 1.57311957507240     2.72472303040657     -9.24945407660398      au
 1.57311957507240     8.17416909121970     -9.24945407660398      au
 6.29247830028961     -5.44944606081313     -9.24945407660398      au
 6.29247830028961     -0.00000000000000      -9.24945407660398      au
 6.29247830028961     5.44944606081312     -9.24945407660398      au
11.01183702550681     -2.72472303040656     -9.24945407660398      au
11.01183702550681     2.72472303040658     -9.24945407660398      au
Send

```

## Icosahedral C<sub>60</sub> on Au(111) with pentagon after Relaxation (def-TZVPP)

```

$coord
 2.36040704923014      -0.00002690839546      -0.02001745569257      c
 0.72467219568570      -2.21416273360449      0.07305918854428      c
-1.88527340513634      -1.38068528722188      0.01688157805571      c
-1.88542906648759      1.38071033707972      0.01691700390591      c
 0.72474734802842      2.21421753656262      0.07313785357623      c
 4.60820785563354      0.00002089568509      1.39388520661768      c
 5.32573569914124      2.22584860399271      2.82274508463834      c
 6.48842361852810      1.37438846658071      5.16126191608790      c
 6.48842490478336      -1.37438137019773      5.16126501286108      c
 5.32572476079489      -2.22587346488664      2.82274883778010      c
 1.42416920260413      -4.37706222269202      1.39853855429781      c
 3.76364475112553      -4.36747760979728      2.83067564712511      c
 3.31367765135339      -5.74332674243776      5.16132821083001      c
 0.69867053186198      -6.59485966103417      5.16017501604252      c
-0.47251084931723      -5.74835634138764      2.82676664967149      c
-3.71509500891158      -2.70629593588850      1.39390697059100      c
-2.99317086482325      -4.93123332431090      2.82149601592227      c
-4.43703678682269      -4.92518940584516      5.15624723095626      c
-6.05223013062580      -2.70067530406491      5.15540639299740      c
-5.60620382205796      -1.32544630537356      2.81982442218414      c
-3.71496594294829      2.70627938747939      1.39378693402619      c
-5.60619954450443      1.32542659463374      2.81984264183459      c
-6.05223016543615      2.70068677259568      5.15540484407192      c
-4.43703032361968      4.92520066367940      5.15625282436690      c
-2.99322926919539      4.93119176693489      2.82149222911177      c
 1.42413324952484      4.37705597987496      1.39851508023944      c
-0.47244718963225      5.74836253909662      2.82675470223888      c

```

0.69866498046673	6.59486205191273	5.16018529843154	c
3.31367481599879	5.74333427793424	5.16133563831857	c
3.76364651191682	4.36747860187507	2.83067854476866	c
-3.75084050272173	-4.35894202535470	9.73971343930828	c
-3.30704220925042	-5.73800219197895	7.40575828626800	c
-0.69596459607549	-6.58630651489512	7.40755396792051	c
0.47217944853677	-5.73104483271947	9.74289240941577	c
-1.41737110262239	-4.36009058227471	11.18761526300497	c
2.98679948608963	-4.91358640216866	9.74413062947725	c
4.43404680721872	-4.91616689320991	7.41008874346518	c
6.04953726562476	-2.69585544135965	7.40946556220119	c
5.59859474510372	-1.32128241978902	9.74524301326668	c
3.70777767422955	-2.69338517913882	11.18944239171285	c
5.59859333605158	1.32128322724814	9.74524529447649	c
6.04953827746375	2.69585281598861	7.40946601636380	c
4.43404693919300	4.91616921442425	7.41009115981178	c
2.98679930780138	4.91358833956858	9.74413002458190	c
3.70778013593220	2.69338192998229	11.18944195084468	c
0.47217862228421	5.73104571003202	9.74289004417478	c
-0.69594827400943	6.58631068593790	7.40754905654254	c
-3.30705406174036	5.73798888241927	7.40574912303346	c
-3.75083619126469	4.35894362695846	9.73970997540317	c
-1.41737488242441	4.36008978748797	11.18761318696291	c
-5.30543918980030	2.22104359347769	9.74014020467260	c
-6.47434591930862	1.37324145684475	7.40295588331854	c
-6.47435268652577	-1.37324327012933	7.40295574116995	c
-5.30543833178135	-2.22104360357783	9.74014496622129	c
-4.58538401251121	0.00000017097454	11.18591542886722	c
-0.72351568484671	-2.22122340552708	12.57876538006383	c
1.88772499868787	-1.37262730931238	12.57976134155214	c
1.88772393530678	1.37262753008105	12.57976142089807	c
-0.72351548739670	2.22122276409225	12.57876438679044	c
-2.33794085130686	0.00000110735513	12.58005072998227	c
-11.01183702550682	-8.17416909121969	-4.80000000000000	au
-11.01183702550682	-2.72472303040656	-4.80000000000000	au
-11.01183702550682	2.72472303040657	-4.80000000000000	au
-11.01183702550682	8.17416909121969	-4.80000000000000	au
-6.29247830028962	-10.89889212162625	-4.80000000000000	au
-6.29247830028962	-5.44944606081312	-4.80000000000000	au
-6.29247830028962	0.00000000000000	-4.80000000000000	au
-6.29247830028962	5.44944606081313	-4.80000000000000	au
-6.29247830028961	10.89889212162625	-4.80000000000000	au
-1.57311957507240	-13.62361515203282	-4.80000000000000	au
-1.57311957507240	-8.17416909121969	-4.80000000000000	au
-1.57311957507240	-2.72472303040656	-4.80000000000000	au
-1.57311957507241	2.72472303040657	-4.80000000000000	au
-1.57311957507241	8.17416909121969	-4.80000000000000	au
-1.57311957507240	13.62361515203282	-4.80000000000000	au
3.14623915014480	-10.89889212162625	-4.80000000000000	au
3.14623915014480	-5.44944606081312	-4.80000000000000	au
3.14623915014480	0.00000000000000	-4.80000000000000	au
3.14623915014480	5.44944606081314	-4.80000000000000	au
3.14623915014480	10.89889212162626	-4.80000000000000	au
7.86559787536201	-8.17416909121969	-4.80000000000000	au
7.86559787536201	-2.72472303040656	-4.80000000000000	au
7.86559787536200	2.72472303040657	-4.80000000000000	au
7.86559787536201	8.17416909121969	-4.80000000000000	au
12.58495660057921	-5.44944606081312	-4.80000000000000	au
12.58495660057922	0.00000000000000	-4.80000000000000	au
12.58495660057921	5.44944606081312	-4.80000000000000	au
-7.86559787536202	-8.17416909121969	-9.24945407660398	au
-7.86559787536201	-2.72472303040657	-9.24945407660398	au
-7.86559787536202	2.72472303040657	-9.24945407660398	au
-7.86559787536202	8.17416909121969	-9.24945407660398	au
-3.14623915014481	-10.89889212162624	-9.24945407660398	au
-3.14623915014482	-5.44944606081312	-9.24945407660398	au
-3.14623915014481	-0.00000000000001	-9.24945407660398	au
-3.14623915014481	5.44944606081314	-9.24945407660398	au
-3.14623915014482	10.89889212162626	-9.24945407660398	au
1.57311957507240	-8.17416909121969	-9.24945407660398	au
1.57311957507239	-2.72472303040655	-9.24945407660398	au
1.57311957507240	2.72472303040657	-9.24945407660398	au
1.57311957507240	8.17416909121970	-9.24945407660398	au
6.29247830028961	-5.44944606081313	-9.24945407660398	au
6.29247830028961	-0.00000000000001	-9.24945407660398	au
6.29247830028961	5.44944606081312	-9.24945407660398	au
11.01183702550681	-2.72472303040656	-9.24945407660398	au
11.01183702550681	2.72472303040658	-9.24945407660398	au

Send

## $C_{58}$ on Au(111) with $C_{3v}$ Symmetry H1a before Relaxation

Scoord			
0.18669836297791	-1.37128098915170	11.92696575793372	c
0.18669836297791	1.37128098915170	11.92696575793372	c

2.26807755606390	-2.69974932548581	10.94597390449364	c
4.41653351894419	-1.32846833633412	9.93336754998531	c
4.41653351894419	1.32846833633412	9.93336754998531	c
2.26807755606390	2.69974932548581	10.94597390449364	c
1.87616713666372	-4.93303467451524	9.41381383913171	c
-2.36001564903205	-2.22923388876001	11.41040380037234	c
-2.36001564903205	2.22923388876001	11.41040380037234	c
1.87616713666372	4.93303467451524	9.41381383913171	c
5.36882172667891	2.70380078575524	7.76766223395256	c
5.36882172667891	-2.70380078575524	7.76766223395256	c
-3.95380671420652	0.00000000000000	11.11189208383195	c
3.81216853783700	-4.95673842486999	7.45164676112532	c
3.81216853783700	4.95673842486999	7.45164676112532	c
-0.58843171149434	-5.73391742458153	8.86816620119067	c
-2.74271328208944	-4.35891816275048	9.88351827052529	c
-2.74271328208944	4.35891816275048	9.88351827052529	c
-0.58843171149434	5.73391742458153	8.86816620119067	c
6.2409800265265	-1.37499926183105	5.64937423564796	c
6.2409800265265	1.37499926183105	5.64937423564796	c
-5.91833751324224	0.00000000000000	9.36372036604750	c
3.24754067306722	-5.85024534964913	5.04367534000781	c
3.24754067306722	5.85024534964913	5.04367534000781	c
-6.32645293245813	-2.24350589963737	7.78314480658701	c
-6.32645293245813	2.24350589963737	7.78314480658701	c
-7.00551146516316	-1.37964277563949	5.33200853376753	c
-7.00551146516316	1.37964277563949	5.33200853376753	c
-5.77120395158509	-2.24440831070847	3.13968448026377	c
-5.01608188180712	0.00000000000000	1.71187045908069	c
-5.77120395158509	2.24440831070847	3.13968448026377	c
0.66849728337783	-6.70812719826474	4.48629760077830	c
0.08169374864402	-5.90314707073404	1.99167987020737	c
2.24325054948687	-4.52350429509459	0.97289885259237	c
4.18351256176713	-4.46462129862741	2.82960699664827	c
-2.14457124092971	-4.55915554159431	1.43038655108761	c
-1.38399101143501	-2.31823097492560	0.00000000000000	c
1.37185789097465	-2.31474723088590	-0.22697042790810	c
0.66849728337783	6.70812719826474	4.48629760077830	c
0.08169374864402	5.90314707073404	1.99167987020737	c
2.24325054948687	4.52350429509459	0.97289885259237	c
4.18351256176713	4.46462129862741	2.82960699664827	c
1.37185789097465	2.31474723088590	-0.22697042790810	c
-1.38399101143501	2.31823097492560	0.00000000000000	c
-2.14457124092971	4.55915554159431	1.43038655108761	c
-1.23042161334846	-6.54946441669251	6.33774048948110	c
-3.70599780391517	-5.53372456416053	5.70656898757703	c
-4.69942025365029	-4.33532925682562	7.97274261549216	c
-4.69942025365029	4.33532925682562	7.97274261549216	c
-3.70599780391517	5.53372456416053	5.70656898757703	c
-1.23042161334846	6.54946441669251	6.33774048948110	c
5.56196015709992	-2.21413515986692	3.13636747470367	c
4.96397110170106	0.00000000000000	1.62025502122190	c
5.56196015709992	2.21413515986692	3.13636747470367	c
-4.14655120462230	-4.42043920516361	3.26422145736560	c
-2.75491042789504	0.00000000000000	0.23067806005385	c
2.77917666881577	0.00000000000000	0.00000000000000	c
-4.14655120462230	4.42043920516361	3.26422145736560	c
-11.01183702550682	-8.17416909121969	-4.60000000000000	au
-11.01183702550682	-2.72472303040656	-4.60000000000000	au
-11.01183702550682	2.72472303040657	-4.60000000000000	au
-11.01183702550682	8.17416909121969	-4.60000000000000	au
-6.29247830028962	-10.89889212162625	-4.60000000000000	au
-6.29247830028962	-5.44944606081312	-4.60000000000000	au
-6.29247830028962	0.00000000000000	-4.60000000000000	au
-6.29247830028962	5.44944606081313	-4.60000000000000	au
-6.29247830028961	10.89889212162625	-4.60000000000000	au
-1.57311957507240	-13.62361515203282	-4.60000000000000	au
-1.57311957507240	-8.17416909121969	-4.60000000000000	au
-1.57311957507240	-2.72472303040656	-4.60000000000000	au
-1.57311957507241	2.72472303040657	-4.60000000000000	au
-1.57311957507241	8.17416909121969	-4.60000000000000	au
-1.57311957507240	13.62361515203282	-4.60000000000000	au
3.14623915014480	-10.89889212162625	-4.60000000000000	au
3.14623915014480	-5.44944606081312	-4.60000000000000	au
3.14623915014480	0.00000000000000	-4.60000000000000	au
3.14623915014480	5.44944606081314	-4.60000000000000	au
3.14623915014480	10.89889212162626	-4.60000000000000	au
7.86559787536201	-8.17416909121969	-4.60000000000000	au
7.86559787536201	-2.72472303040656	-4.60000000000000	au
7.86559787536200	2.72472303040657	-4.60000000000000	au
7.86559787536201	8.17416909121969	-4.60000000000000	au
12.58495660057921	-5.44944606081312	-4.60000000000000	au
12.58495660057922	0.00000000000000	-4.60000000000000	au
12.58495660057921	5.44944606081312	-4.60000000000000	au
-7.86559787536202	-8.17416909121969	-9.04945407660398	au
-7.86559787536201	-2.72472303040657	-9.04945407660398	au
-7.86559787536202	2.72472303040657	-9.04945407660398	au
-7.86559787536202	8.17416909121969	-9.04945407660398	au
-3.14623915014481	-10.89889212162624	-9.04945407660398	au

-3.14623915014482	-5.44944606081312	-9.04945407660398	au
-3.14623915014481	-0.000000000000001	-9.04945407660398	au
-3.14623915014481	5.44944606081314	-9.04945407660398	au
-3.14623915014482	10.89889212162626	-9.04945407660398	au
1.57311957507240	-8.17416909121969	-9.04945407660398	au
1.57311957507239	-2.72472303040655	-9.04945407660398	au
1.57311957507240	2.72472303040657	-9.04945407660398	au
1.57311957507240	8.17416909121970	-9.04945407660398	au
6.29247830028961	-5.44944606081313	-9.04945407660398	au
6.29247830028961	-0.000000000000001	-9.04945407660398	au
6.29247830028961	5.44944606081312	-9.04945407660398	au
11.01183702550681	-2.72472303040656	-9.04945407660398	au
11.01183702550681	2.72472303040658	-9.04945407660398	au

Send

## C<sub>58</sub> on Au(111) with C<sub>3v</sub> Symmetry H1a after Relaxation (def-SV(P))

Scoord			
0.17875857986114	-1.37943771933723	11.83591852783328	c
0.17875847200821	1.37943697079738	11.83591878343976	c
2.27796122195741	-2.71084701597810	10.88259622552166	c
4.44744799222519	-1.33078154254038	9.89306713391122	c
4.44744812025919	1.33078096494378	9.893067442299703	c
2.27796156472210	2.71084660560169	10.88259667199283	c
1.90139320944535	-4.94940046665307	9.32024279244048	c
-2.37478538210005	-2.23488340307508	11.26870769392413	c
-2.37478549108481	2.23488298166970	11.26870805889085	c
1.90139341240421	4.94940047472641	9.32024293977097	c
5.41661100888733	2.71611304848102	7.71580486884973	c
5.41661095183134	-2.71611320234940	7.71580493328126	c
-3.96611941350829	-0.00000037671187	10.94766348415658	c
3.86246070258916	-4.97495893798066	7.38141418075768	c
3.86246068940532	4.97495889711736	7.38141334108996	c
-0.57180886043723	-5.75247582632399	8.73489487416588	c
-2.74417805550267	-4.37561094781073	9.72735205900461	c
-2.74417850090007	4.37561075456305	9.72735231474864	c
-0.57180886507827	5.75247599155061	8.73489455481772	c
6.32731949264424	-1.38205303629167	5.59906266615221	c
6.32731927263936	1.38205291418356	5.59906230425474	c
-5.92558752178115	-0.00000025981690	9.16050048137048	c
3.31934807271280	-5.88759762506312	4.94299073456574	c
3.31934806465617	5.88759757106637	4.94299031453321	c
-6.32862764155504	-2.25066644689642	7.57842056722980	c
-6.32862820420078	2.25066587994660	7.57842084989019	c
-7.00722299649613	-1.38156021252795	5.10509580263522	c
-7.00722302227769	1.38155961884674	5.10509526533523	c
-5.74275186660252	-2.26203161128210	2.92274533225389	c
-4.99492252950979	-0.00000018118708	1.47367415452808	c
-5.74275195386534	2.26203102543693	2.92274507675617	c
0.74303147830131	-6.76517765482067	4.35534695594145	c
0.17141960014161	-5.96147605578853	1.82378501101224	c
2.34238272756597	-4.60392076235513	0.84065931335150	c
4.29212586824187	-4.50945076175945	2.74501750170518	c
-2.07366710152179	-4.60347464466065	1.25685559167009	c
-1.35860909517998	-2.37032212444707	-0.26565692492516	c
1.43470920141785	-2.31366495987819	-0.22399116143748	c
0.74303148239245	6.76517784098609	4.35534661093592	c
0.17141922619850	5.96147663784680	1.82378345627868	c
2.34238347524828	4.60392118134857	0.84065749605416	c
4.29212632391985	4.50945046951856	2.74501690702887	c
1.43470880964440	2.31366439636881	-0.22399109573539	c
-1.35860858379525	2.37032136785909	-0.26565629508109	c
-2.07366718938619	4.60347446140261	1.25685482030538	c
-1.18225795769966	-6.58025419926334	6.18597917392466	c
-3.66983514148950	-5.55261722996613	5.52885383142381	c
-4.69384354275491	-4.35283985665083	7.78808055618585	c
-4.69384404637849	4.35283969986706	7.78808050079426	c
-3.66983538913949	5.55261762081819	5.52885384970050	c
-1.18225818341102	6.58025422350680	6.18597846719533	c
5.66816699278669	-2.24323148036351	3.07320390094184	c
5.08301053547944	-0.00000014038676	1.57496958635615	c
5.66816676497246	2.24323123400465	3.07320365145643	c
-4.10577732686127	-4.45118523172204	3.06941938151570	c
-2.70809795636898	-0.00000006936192	0.13627111034866	c
2.86736153084549	-0.00000005514753	-0.00332250007852	c
-4.10577762076118	4.45118487023410	3.06941909645047	c
-11.01183702550682	-8.17416909121969	-4.60000000000000	au
-11.01183702550682	-2.72472303040656	-4.60000000000000	au
-11.01183702550682	2.72472303040657	-4.60000000000000	au
-11.01183702550682	8.17416909121969	-4.60000000000000	au
-6.29247830028962	-10.89889212162625	-4.60000000000000	au
-6.29247830028962	-5.44944606081312	-4.60000000000000	au

-6.29247830028962	0.00000000000000	-4.60000000000000	au
-6.29247830028962	5.44944606081313	-4.60000000000000	au
-6.29247830028961	10.89889212162625	-4.60000000000000	au
-1.57311957507240	-13.62361515203282	-4.60000000000000	au
-1.57311957507240	-8.17416909121969	-4.60000000000000	au
-1.57311957507240	-2.72472303040656	-4.60000000000000	au
-1.57311957507241	2.72472303040657	-4.60000000000000	au
-1.57311957507241	8.17416909121969	-4.60000000000000	au
-1.57311957507240	13.62361515203282	-4.60000000000000	au
3.14623915014480	-10.89889212162625	-4.60000000000000	au
3.14623915014480	-5.44944606081312	-4.60000000000000	au
3.14623915014480	0.00000000000000	-4.60000000000000	au
3.14623915014480	5.44944606081314	-4.60000000000000	au
3.14623915014480	10.89889212162626	-4.60000000000000	au
7.86559787536201	-8.17416909121969	-4.60000000000000	au
7.86559787536201	-2.72472303040656	-4.60000000000000	au
7.86559787536200	2.72472303040657	-4.60000000000000	au
7.86559787536201	8.17416909121969	-4.60000000000000	au
12.58495660057921	-5.44944606081312	-4.60000000000000	au
12.58495660057922	0.00000000000000	-4.60000000000000	au
12.58495660057921	5.44944606081312	-4.60000000000000	au
-7.86559787536202	-8.17416909121969	-9.04945407660398	au
-7.86559787536201	-2.72472303040657	-9.04945407660398	au
-7.86559787536202	2.72472303040657	-9.04945407660398	au
-7.86559787536202	8.17416909121969	-9.04945407660398	au
-3.14623915014481	-10.89889212162624	-9.04945407660398	au
-3.14623915014482	-5.44944606081312	-9.04945407660398	au
-3.14623915014481	-0.00000000000001	-9.04945407660398	au
-3.14623915014481	5.44944606081314	-9.04945407660398	au
-3.14623915014482	10.89889212162626	-9.04945407660398	au
1.57311957507240	-8.17416909121969	-9.04945407660398	au
1.57311957507239	-2.72472303040655	-9.04945407660398	au
1.57311957507240	2.72472303040657	-9.04945407660398	au
1.57311957507240	8.17416909121970	-9.04945407660398	au
6.29247830028961	-5.44944606081313	-9.04945407660398	au
6.29247830028961	-0.00000000000001	-9.04945407660398	au
6.29247830028961	5.44944606081312	-9.04945407660398	au
11.01183702550681	-2.72472303040656	-9.04945407660398	au
11.01183702550681	2.72472303040658	-9.04945407660398	au

Send

## C<sub>58</sub> on Au(111) with C<sub>3v</sub> Symmetry P1a before Relaxation

Scoord			
-0.54624587698427	1.39369210540994	12.20497226555856	c
0.16886069735764	3.63229436825163	10.79113751532482	c
1.05185865049507	-0.72875094735546	12.22966820828944	c
3.41657199172228	-0.68099187528613	10.84132527886153	c
4.10935228156300	1.48771916742352	9.47163174897726	c
2.45974551467769	3.67856235819586	9.44613992817144	c
-0.00290971899105	-3.24681749217438	12.04131679335155	c
-3.25549478928424	1.07294161448491	11.99105371403348	c
-2.09297607706595	4.71214325678922	9.69264196380762	c
2.56960864530475	4.80631142334993	6.95519957732263	c
5.25130505687933	1.24474969787883	6.99664055935046	c
3.84130540480182	-3.16917757534119	9.78434602515354	c
-4.22821067672128	3.14291935261554	10.45229483067679	c
1.73458565169881	-4.77627205489024	10.54443953968079	c
4.31946523725366	3.31555299191700	5.43388299558743	c
-2.61996766640123	-3.55695105709852	11.78013318304831	c
-4.27404739529908	-1.36016732427429	11.75457224034727	c
-2.00092389992450	5.75572222707972	7.26038759061034	c
0.37020143788165	5.80361079941505	5.86828012450110	c
4.89679367887941	-3.40513834451370	7.36697989128334	c
5.61383928778771	-1.16046603935413	5.94931148247306	c
-6.22913350061766	2.73555146405715	8.79523572750535	c
0.80852281713718	-6.61116178437438	8.90399053946814	c
3.85935553788779	2.93930422624630	2.87219965330990	c
-7.30517714433724	0.18814724064878	8.56949734874534	c
-6.13521574977433	3.85064779550136	6.25637069683722	c
-7.88593403426417	-0.20559522710327	5.97659601632538	c
-7.16646688864768	2.04665756710365	4.55413999561243	c
-7.05801870257240	-2.36254644498396	4.65760516286113	c
-5.83371981031523	-1.46322762861779	2.34707518610739	c
-5.88758671146887	1.30142728676071	2.34354809615006	c
-1.93438183392304	-6.94480745562099	8.65249370544452	c
-2.44430437976209	-7.43262503480750	6.06068699535676	c
-0.06517150802247	-7.38457473784215	4.66387823927514	c
1.93444474061904	-6.86667047217532	6.38107334919924	c
-4.27345250067344	-6.06072956665228	4.70063581966108	c
-3.04496277678694	-5.16697659490021	2.39017060496524	c
-0.40306975820082	-5.98256115396949	2.42830182424201	c
1.56382597246420	4.00614194443963	1.73619907515006	c
0.63411595347721	2.20420249724153	-0.02564726463129	c
2.29378167960037	0.00000000000000	0.00000000000000	c

4.26269115244337	0.42177837303278	1.77790537081285	c
0.80404313539383	-2.20375985069082	0.04172307129193	c
-1.83603315249609	-1.38248811492170	0.00000000000000	c
-1.89590761597529	1.38204546837096	0.00000000000000	c
-3.60781796964950	-5.37205954657206	9.98852631693113	c
-5.76707429405056	-4.24095838243973	8.71698997448126	c
-6.27135109773191	-1.83462048279207	9.94736601704971	c
-4.01052893362484	5.24276041964234	5.47750228708080	c
-2.88130336326816	4.79279066627694	3.01154218593419	c
-0.19235089918967	5.31987447686901	3.23581811125000	c
3.86826535195348	-5.22106839008484	5.59925543220951	c
3.77558866639950	-4.04822942873707	3.11441294407517	c
5.02291025830626	-1.60651526907813	3.31641095649726	c
-6.05247100219352	-4.48719316210957	6.02320635287698	c
-3.74698438731573	-2.80650587600534	1.27564339107035	c
1.57038065638652	-4.33323779027286	1.54776655315264	c
-3.74726502172796	2.72912886504475	1.46559153213761	c
-11.01183702550682	-8.17416909121969	-4.40000000000000	au
-11.01183702550682	-2.72472303040656	-4.40000000000000	au
-11.01183702550682	2.72472303040657	-4.40000000000000	au
-11.01183702550682	8.17416909121969	-4.40000000000000	au
-6.29247830028962	-10.89889212162625	-4.40000000000000	au
-6.29247830028962	-5.44944606081312	-4.40000000000000	au
-6.29247830028962	0.00000000000000	-4.40000000000000	au
-6.29247830028962	5.44944606081313	-4.40000000000000	au
-6.29247830028962	10.89889212162625	-4.40000000000000	au
-1.57311957507240	-13.62361515203282	-4.40000000000000	au
-1.57311957507240	-8.17416909121969	-4.40000000000000	au
-1.57311957507240	-2.72472303040656	-4.40000000000000	au
-1.57311957507241	2.72472303040657	-4.40000000000000	au
-1.57311957507241	8.17416909121969	-4.40000000000000	au
-1.57311957507240	13.62361515203282	-4.40000000000000	au
3.14623915014480	-10.89889212162625	-4.40000000000000	au
3.14623915014480	-5.44944606081312	-4.40000000000000	au
3.14623915014480	0.00000000000000	-4.40000000000000	au
3.14623915014480	5.44944606081314	-4.40000000000000	au
3.14623915014480	10.89889212162626	-4.40000000000000	au
7.86559787536201	-8.17416909121969	-4.40000000000000	au
7.86559787536201	-2.72472303040656	-4.40000000000000	au
7.86559787536200	2.72472303040657	-4.40000000000000	au
7.86559787536201	8.17416909121969	-4.40000000000000	au
12.58495660057921	-5.44944606081312	-4.40000000000000	au
12.58495660057922	0.00000000000000	-4.40000000000000	au
12.58495660057921	5.44944606081312	-4.40000000000000	au
-7.86559787536202	-8.17416909121969	-8.84945407660398	au
-7.86559787536201	-2.72472303040657	-8.84945407660398	au
-7.86559787536202	2.72472303040657	-8.84945407660398	au
-7.86559787536202	8.17416909121969	-8.84945407660398	au
-3.14623915014481	-10.89889212162624	-8.84945407660398	au
-3.14623915014482	-5.44944606081312	-8.84945407660398	au
-3.14623915014481	-0.00000000000001	-8.84945407660398	au
-3.14623915014481	5.44944606081314	-8.84945407660398	au
-3.14623915014482	10.89889212162626	-8.84945407660398	au
1.57311957507240	-8.17416909121969	-8.84945407660398	au
1.57311957507239	-2.72472303040655	-8.84945407660398	au
1.57311957507240	2.72472303040657	-8.84945407660398	au
1.57311957507240	8.17416909121970	-8.84945407660398	au
6.29247830028961	-5.44944606081313	-8.84945407660398	au
6.29247830028961	-0.00000000000001	-8.84945407660398	au
6.29247830028961	5.44944606081312	-8.84945407660398	au
11.01183702550681	-2.72472303040656	-8.84945407660398	au
11.01183702550681	2.72472303040658	-8.84945407660398	au

Send

## $C_{58}$ on Au(111) with $C_{3v}$ Symmetry P1a after Relaxation (def-SV(P))

Scoord			
-0.12304052186557	0.94834322632723	12.17452699572156	c
0.37795066775375	3.25606022428318	10.74962140871285	c
1.50456347744579	-1.15105952004414	11.91990484158909	c
3.67255348823590	-1.00818367807353	10.22998400142843	c
4.17108600691479	1.23123066482822	8.87116768118338	c
2.49091579116535	3.40682626186864	9.13994105379003	c
0.46856616166310	-3.69393970260603	11.77576901889765	c
-2.83999409247801	0.57670168014842	12.28826133342340	c
-2.04095714901727	4.32115375495001	9.97465754679927	c
2.25662539488534	4.60760357922244	6.67473346304513	c
4.97115066414390	1.08882302847364	6.24929978553266	c
3.99291869214934	-3.47116236915283	9.03772036325145	c
-4.03975476083252	2.67724992878735	10.95030631132999	c
2.02356714991196	-5.14905732994507	10.01319876430508	c
3.82217596861246	3.20059559526040	4.90196330764485	c

```
-2.16987699535386      -4.05174375064722      11.83913809363050      c
-3.85048480431465      -1.88578616692176      12.09752245145093      c
-2.28589607091392      5.44829557170602      7.57771410934633      c
-0.10470816128030      5.58698947351530      5.89144752630016      c
4.73057081839920      -3.61794814053301      6.48890509249342      c
5.22290601312350      -1.30401828063155      5.06961496229273      c
-6.25081136263777      2.28012018690844      9.54738446473919      c
0.91700462307196      -6.97122034721054      8.44187740031326      c
3.00512929955238      2.88148155733818      2.38529962103723      c
-7.32268854810209      -0.29206668010300      9.38319026022610      c
-6.51833365594264      3.477308761777995      7.05947264815715      c
-8.26274033435342      -0.61364376828666      6.87925730385027      c
-7.77286979825101      1.68969105151407      5.45303055084393      c
-7.56109942917971      -2.74514557862139      5.37942357213541      c
-6.67320493461468      -1.76981305100021      2.96339449735548      c
-6.74141094345226      1.01681172771955      3.07607354591528      c
-1.83811384069671      -7.36755604748786      8.54149211020163      c
-2.66940077150318      -7.81656452397749      6.00707678554425      c
-4.50617701510637      -7.69480644776040      4.32200079723025      c
1.70456358386562      -7.14235351628492      5.78085211977101      c
-4.71136635659497      -6.42400819223510      4.93148136802901      c
-3.83278517394272      -5.45966674364232      2.50222590827812      c
-1.16525265488266      -6.20601091594553      2.17998301266331      c
0.59800919866659      3.95826203733647      1.56798827966998      c
-0.53619824513996      2.19212550318149      -0.21252822788534      c
1.21509913008173      0.00261605456906      -0.49831084676543      c
3.31212149594625      0.40914487992690      1.19972512462028      c
-0.33528248374572      -2.29420264308748      -0.18085874782469      c
-2.91999722810351      -1.50230145087253      0.30492997539493      c
-3.00769719865134      1.22120788299439      0.39154715407206      c
-3.35304752547953      -5.84976090495693      10.12568317625105      c
-5.68362819945636      -4.71316718472996      9.17579231113658      c
-6.06721882422749      -2.34598365124487      10.54478764363319      c
-4.52898017192577      4.96327885493240      6.05511645009462      c
-3.71207927138717      4.60190725544146      3.45911988996973      c
-0.98892012497714      5.17271852986305      3.32930332268223      c
3.51596771722907      -5.42923193863347      4.80316069047114      c
3.07183414635191      -4.17688662961997      2.40334828577978      c
4.29287956219094      -1.67524668669636      2.53141736847326      c
-6.33391064612875      -4.90280982570671      6.53017448915026      c
-4.71395526939998      -3.05858663418496      1.63843252897269      c
0.67257459258920      -4.48533320888087      1.14572889227306      c
-4.73993730787014      2.53196189239770      2.01570476465732      c
-11.01183702550682      -8.17416909121969      -4.40000000000000      au
-11.01183702550682      -2.72472303040656      -4.40000000000000      au
-11.01183702550682      2.72472303040657      -4.40000000000000      au
-11.01183702550682      8.17416909121969      -4.40000000000000      au
-6.29247830028962      -10.89889212162625      -4.40000000000000      au
-6.29247830028962      -5.44944606081312      -4.40000000000000      au
-6.29247830028962      0.00000000000000      -4.40000000000000      au
-6.29247830028962      5.44944606081313      -4.40000000000000      au
-6.29247830028961      10.89889212162625      -4.40000000000000      au
-1.57311957507240      -13.62361515203282      -4.40000000000000      au
-1.57311957507240      -8.17416909121969      -4.40000000000000      au
-1.57311957507240      -2.72472303040656      -4.40000000000000      au
-1.57311957507241      2.72472303040657      -4.40000000000000      au
-1.57311957507241      8.17416909121969      -4.40000000000000      au
-1.57311957507240      13.62361515203282      -4.40000000000000      au
3.14623915014480      -10.89889212162625      -4.40000000000000      au
3.14623915014480      -5.44944606081312      -4.40000000000000      au
3.14623915014480      0.00000000000000      -4.40000000000000      au
3.14623915014480      5.44944606081314      -4.40000000000000      au
3.14623915014480      10.89889212162626      -4.40000000000000      au
7.86559787536201      -8.17416909121969      -4.40000000000000      au
7.86559787536201      -2.72472303040656      -4.40000000000000      au
7.86559787536200      2.72472303040657      -4.40000000000000      au
7.86559787536201      8.17416909121969      -4.40000000000000      au
12.58495660057921      -5.44944606081312      -4.40000000000000      au
12.58495660057922      0.00000000000000      -4.40000000000000      au
12.58495660057921      5.44944606081312      -4.40000000000000      au
-7.86559787536202      -8.17416909121969      -8.84945407660398      au
-7.86559787536201      -2.72472303040657      -8.84945407660398      au
-7.86559787536202      2.72472303040657      -8.84945407660398      au
-7.86559787536202      8.17416909121969      -8.84945407660398      au
-3.14623915014481      -10.89889212162624      -8.84945407660398      au
-3.14623915014482      -5.44944606081312      -8.84945407660398      au
-3.14623915014481      -0.00000000000001      -8.84945407660398      au
-3.14623915014481      5.44944606081314      -8.84945407660398      au
-3.14623915014482      10.89889212162626      -8.84945407660398      au
1.57311957507240      -8.17416909121969      -8.84945407660398      au
1.57311957507239      -2.72472303040655      -8.84945407660398      au
1.57311957507240      2.72472303040657      -8.84945407660398      au
1.57311957507240      8.17416909121970      -8.84945407660398      au
6.29247830028961      -5.44944606081313      -8.84945407660398      au
6.29247830028961      -0.00000000000001      -8.84945407660398      au
6.29247830028961      5.44944606081312      -8.84945407660398      au
11.01183702550681      -2.72472303040656      -8.84945407660398      au
11.01183702550681      2.72472303040658      -8.84945407660398      au
```

Send

## $C_{58}$ on Au(111) with $C_{3s}$ Symmetry Hept4 before Relaxation

Scoord			
1.97065495379935	2.44342173947729	0.00000000000000	c
-1.17229439784586	5.19956611837025	1.67796133559295	c
1.15254489140021	6.08047151271425	2.46730946504756	c
3.10739071908570	4.50234690046377	1.32367139467074	c
3.24460771307506	0.00000000000000	0.00000000000000	c
1.97065495379935	-2.37826763730938	-0.56049339182283	c
-0.77845057041223	2.92484542174108	0.12705378323072	c
-0.77845057041223	-2.87599881061447	-0.54726067486813	c
-2.81450824020689	1.27794868298639	0.64553021565146	c
-3.16731961926733	4.75659859649514	3.44542775587108	c
-2.74121185978103	5.26940175560422	6.02560532885472	c
-0.24624080035129	6.09136666194729	6.86627774846283	c
1.71286390624160	6.46257299864486	5.09451730668437	c
4.19237527207635	5.34483424736985	5.53522159768842	c
5.01885605469629	4.14512745650556	3.15896693049347	c
6.29079514026409	1.83604650970497	3.20385157812748	c
5.54026441009825	-0.17406036187807	1.49736822954803	c
3.10739071908570	-4.68592662903149	0.25558795065285	c
5.01885605469629	-4.75922857850397	2.12388724657848	c
6.29079514026409	-2.52201555424733	2.69725216926491	c
7.03518594793086	-1.99264379885551	5.26490925931038	c
7.03518594793086	0.73179892861864	5.58160990628708	c
6.21277390439709	1.82157268963976	7.85559971062054	c
4.70676657164687	4.12391270630615	7.81284764914305	c
2.73030315149125	3.87877592002948	9.71582147624599	c
0.29881876016851	4.80445507966124	9.23381050312387	c
-4.36063875849200	2.41234217498150	2.69360910243304	c
-3.10993032781286	-1.21259852981425	10.43147615085640	c
-4.87467691518534	-0.98501121068084	8.47363797655052	c
-5.15577842010360	-3.02658919329145	6.65553507706536	c
-3.73524857999327	-5.24757215889495	6.89153689045498	c
-1.88576952668943	-5.46201171280048	8.90281521973050	c
0.96193179004477	-2.70228441280866	11.37288661721024	c
0.96193179004477	0.02141577528198	11.68950094829533	c
-1.56196682475791	0.94597117420901	11.12694017202829	c
-1.88576952668943	3.27416117431734	9.91834458929652	c
-3.73524857999327	3.52680424100090	7.91150719654412	c
-5.15577842010360	1.41918017838254	7.17232995115828	c
-5.45761291414697	-1.87105929394515	4.18155494712804	c
-4.36063875849200	-2.96590036417246	2.06841963723668	c
-3.16731961926733	-5.42010565794405	2.26244497962476	c
-2.74121185978103	-6.51109850372933	4.65619057984324	c
-0.24624080035129	-7.50398640041998	5.28589689945147	c
0.29881876016851	-6.79447576772472	7.88550214392749	c
2.73030315149125	-6.00404782339608	8.56700060292142	c
3.06546805231199	-3.92327864964785	10.33481209598826	c
3.06546805231199	1.44797465861505	10.95918910367808	c
5.22611974175968	0.19861412443133	9.82106198760509	c
5.22611974175968	-2.44615892238942	9.51362247838434	c
6.21277390439709	-3.57498624255251	7.22828107109174	c
4.70676657164687	-5.80612727551284	6.65853816227701	c
4.19237527207635	-6.47203108230712	4.16157962041151	c
1.71286390624160	-7.45887261576424	3.47623009202822	c
1.15254489140021	-6.48430805580065	1.00672680043873	c
-1.17229439784586	-5.44582453889070	0.44049648655208	c
-5.45761291414697	0.86196574944034	4.49925323849428	c
-2.81450824020689	-1.39194939622289	0.33517006730972	c
-1.56196682475791	-3.47314134517531	10.61324400222501	c
-11.01183702550682	-8.17416909121969	-4.90000000000000	au
-11.01183702550682	-2.72472303040656	-4.90000000000000	au
-11.01183702550682	2.72472303040657	-4.90000000000000	au
-11.01183702550682	8.17416909121969	-4.90000000000000	au
-6.29247830028962	-10.89889212162625	-4.90000000000000	au
-6.29247830028962	-5.44944606081312	-4.90000000000000	au
-6.29247830028962	0.00000000000000	-4.90000000000000	au
-6.29247830028962	5.44944606081313	-4.90000000000000	au
-6.29247830028961	10.89889212162625	-4.90000000000000	au
-1.57311957507240	-13.62361515203282	-4.90000000000000	au
-1.57311957507240	-8.17416909121969	-4.90000000000000	au
-1.57311957507240	-2.72472303040656	-4.90000000000000	au
-1.57311957507241	2.72472303040657	-4.90000000000000	au
-1.57311957507241	8.17416909121969	-4.90000000000000	au
-1.57311957507240	13.62361515203282	-4.90000000000000	au
3.14623915014480	-10.89889212162625	-4.90000000000000	au
3.14623915014480	-5.44944606081312	-4.90000000000000	au
3.14623915014480	0.00000000000000	-4.90000000000000	au
3.14623915014480	5.44944606081314	-4.90000000000000	au
3.14623915014480	10.89889212162626	-4.90000000000000	au
7.86559787536201	-8.17416909121969	-4.90000000000000	au
7.86559787536201	-2.72472303040656	-4.90000000000000	au

```

7.86559787536200      2.72472303040657      -4.90000000000000      au
7.86559787536201      8.17416909121969      -4.90000000000000      au
12.58495660057921     -5.44944606081312     -4.90000000000000      au
12.58495660057922     0.00000000000000      -4.90000000000000      au
12.58495660057921     5.44944606081312     -4.90000000000000      au
-7.86559787536202     -8.17416909121969     -9.34945407660398      au
-7.86559787536201     -2.72472303040657     -9.34945407660398      au
-7.86559787536202     2.72472303040657     -9.34945407660398      au
-7.86559787536202     8.17416909121969     -9.34945407660398      au
-3.14623915014481     -10.89889212162624    -9.34945407660398      au
-3.14623915014482     -5.44944606081312     -9.34945407660398      au
-3.14623915014481     -0.00000000000001     -9.34945407660398      au
-3.14623915014481     5.44944606081314     -9.34945407660398      au
-3.14623915014482     10.89889212162626     -9.34945407660398      au
1.57311957507240      -8.17416909121969     -9.34945407660398      au
1.57311957507239      -2.72472303040655     -9.34945407660398      au
1.57311957507240      2.72472303040657     -9.34945407660398      au
1.57311957507240      8.17416909121970     -9.34945407660398      au
6.29247830028961     -5.44944606081313     -9.34945407660398      au
6.29247830028961     -0.00000000000001     -9.34945407660398      au
6.29247830028961     5.44944606081312     -9.34945407660398      au
11.01183702550681     -2.72472303040656     -9.34945407660398      au
11.01183702550681     2.72472303040658     -9.34945407660398      au
Send

```

## C<sub>5s</sub> on Au(111) with C<sub>3s</sub> Symmetry Hept4 after Relaxation (def-SV(P))

```

$coord
1.32518703221002      2.41083350705241      -0.53710935290125      c
-1.66374336642238     5.38639189758399      0.78640285141843      c
0.74328494971961     6.38976217815938      1.26444906483941      c
2.62930831492534     4.70277916570623      0.14709688068629      c
2.65733841418244     0.00579832016956      -0.40261498220845      c
1.33767437355968     -2.40596568883271     -0.53891323997999      c
-1.43445463408912     2.94264710884062     -0.60880546256191      c
-1.41931497587509     -2.95220668409868     -0.61117947116475      c
-3.42042330703999     1.30848379909791     0.48189009504919      c
-3.45570275630357     5.11283243191444     2.80402721707154      c
-2.79635902658605     5.92237027066470     5.27594463939594      c
-0.23829294366998     6.84901497744128     5.78154471815621      c
1.54722421114947     7.03137301555693      3.784111785540427      c
4.09534034675657     5.97599299881597     4.13822818941951      c
4.74885609986972     4.53593385385902     1.87252089965515      c
6.05311244351474     2.24183568029429     2.07671247535162      c
5.15893512841326     0.01201850958562     0.73154202258093      c
2.65382171151073     -4.69180468078161     0.14304643671232      c
4.77301646404221     -4.51520868531667     1.86834022823562      c
6.06497395326340     -2.21421369600457     2.07472744922913      c
7.04186212268568     -1.36327561897052     4.49565647076023      c
7.03452127927839     1.39408675443783      4.49687679610491      c
6.37906357035620     2.73989749503663      6.69790932048196      c
4.83290899109067     5.01888406813311      6.51441958156241      c
3.03756696549913     4.98962311759843      8.60496348000139      c
0.53938323218420     5.84540909809638      8.22568980315107      c
-4.70468915029177     2.67674335614323      2.48358365644490      c
-2.68062071906879     -0.01278461315334     10.45263759690139      c
-4.64675454583369     -0.01737128813473      8.66152025663859      c
-5.07444872385377     -2.26075187517642      7.11013688393718      c
-3.58224134028800     -4.44383472326485      7.44113704117662      c
-1.53665681687091     -4.41794082874968      9.28346120274506      c
1.49533874546316     -1.37933731877118      11.17694744753467      c
1.48778769615261     1.37536599251336      11.17826936710795      c
-1.09793364350048     2.22426644926046      10.74568090174728      c
-1.56041289089532     4.39936002818154      9.28713908489887      c
-3.60584626592893     4.41570881643352      7.44470727085192      c
-5.08622322874422     2.22497884859353      7.11184064560296      c
-5.68069544783504     -1.38545711253641      4.56815477880212      c
-4.69061357584738     -2.70664185394945      2.48158887182889      c
-3.42867146193496     -5.13626570465129      2.79995103190852      c
-2.76477773182880     -5.94434050524317      5.27114894110834      c
-0.20167918023435     -6.85763668486396      5.77597744046396      c
0.57068222786353     -5.85198985479005      8.22079050112026      c
3.06445291632626     -4.98322736257264      8.60068630954982      c
3.52941585809176     -2.71282292794214      10.09819310418052      c
3.51486426558680     2.72045492823160      10.10066432982548      c
5.60150354156203     1.34117249587866      8.94431489441377      c
5.60878169333461     -1.32152661090206      8.94321575352362      c
6.39395320983686     -2.71432218280905      6.69558648851369      c
4.85988599757427     -5.00138000174813      6.51011006099164      c
4.12723965155702     -5.96020885884856      4.13304342814353      c
1.58472878929305     -7.02884552813786      3.77841638646706      c
0.77688157022056     -6.38912078913917      1.25958798231939      c

```

-1.63547767506888	-5.39875778358682	0.78179810761353	c
-5.68782127799200	1.34853616245286	4.56909961806913	c
-3.41336703547120	-1.32967048626467	0.48140721996711	c
-1.08592289913888	-2.24173086393499	10.74365149614127	c
-11.01183702550682	-8.17416909121969	-4.90000000000000	au
-11.01183702550682	-2.72472303040656	-4.90000000000000	au
-11.01183702550682	2.72472303040657	-4.90000000000000	au
-11.01183702550682	8.17416909121969	-4.90000000000000	au
-6.29247830028962	-10.89889212162625	-4.90000000000000	au
-6.29247830028962	-5.44944606081312	-4.90000000000000	au
-6.29247830028962	0.00000000000000	-4.90000000000000	au
-6.29247830028962	5.44944606081313	-4.90000000000000	au
-6.29247830028961	10.89889212162625	-4.90000000000000	au
-1.57311957507240	-13.62361515203282	-4.90000000000000	au
-1.57311957507240	-8.17416909121969	-4.90000000000000	au
-1.57311957507240	-2.72472303040656	-4.90000000000000	au
-1.57311957507241	2.72472303040657	-4.90000000000000	au
-1.57311957507241	8.17416909121969	-4.90000000000000	au
-1.57311957507240	13.62361515203282	-4.90000000000000	au
3.14623915014480	-10.89889212162625	-4.90000000000000	au
3.14623915014480	-5.44944606081312	-4.90000000000000	au
3.14623915014480	0.00000000000000	-4.90000000000000	au
3.14623915014480	5.44944606081314	-4.90000000000000	au
3.14623915014480	10.89889212162626	-4.90000000000000	au
7.86559787536201	-8.17416909121969	-4.90000000000000	au
7.86559787536201	-2.72472303040656	-4.90000000000000	au
7.86559787536200	2.72472303040657	-4.90000000000000	au
7.86559787536201	8.17416909121969	-4.90000000000000	au
12.58495660057921	-5.44944606081312	-4.90000000000000	au
12.58495660057922	0.00000000000000	-4.90000000000000	au
12.58495660057921	5.44944606081312	-4.90000000000000	au
-7.86559787536202	-8.17416909121969	-9.34945407660398	au
-7.86559787536201	-2.72472303040657	-9.34945407660398	au
-7.86559787536202	2.72472303040657	-9.34945407660398	au
-7.86559787536202	8.17416909121969	-9.34945407660398	au
-3.14623915014481	-10.89889212162624	-9.34945407660398	au
-3.14623915014482	-5.44944606081312	-9.34945407660398	au
-3.14623915014481	-0.00000000000001	-9.34945407660398	au
-3.14623915014481	5.44944606081314	-9.34945407660398	au
-3.14623915014482	10.89889212162626	-9.34945407660398	au
1.57311957507240	-8.17416909121969	-9.34945407660398	au
1.57311957507239	-2.72472303040655	-9.34945407660398	au
1.57311957507240	2.72472303040657	-9.34945407660398	au
1.57311957507240	8.17416909121970	-9.34945407660398	au
6.29247830028961	-5.44944606081313	-9.34945407660398	au
6.29247830028961	-0.00000000000001	-9.34945407660398	au
6.29247830028961	5.44944606081312	-9.34945407660398	au
11.01183702550681	-2.72472303040656	-9.34945407660398	au
11.01183702550681	2.72472303040658	-9.34945407660398	au

Send

## C<sub>58</sub> on Au(111) with C<sub>3s</sub> Symmetry Pent3 before Relaxation

Scored			
-1.94249824060354	-1.37873796100181	0.11507035967489	c
0.84277039799086	2.15660145504825	-0.06842495972190	c
2.30848888837392	0.00000000000000	0.00000000000000	c
0.62684368584797	-2.18853858940390	-0.04664539995297	c
-3.73732616805844	-2.92934771849419	1.51773479588682	c
-6.13458135134895	-1.97791081921031	2.48788985704163	c
-1.83560473160924	1.41067509535745	0.00000000000000	c
-6.87898667396255	0.68982641616711	2.85467503609568	c
-3.11445118084832	3.26480977089841	1.43295285269664	c
1.26357486737720	4.18240761836812	1.66919306319180	c
3.23611973997240	3.96627579407236	3.44801429393403	c
4.70642467303649	1.63696635759005	3.58857732130326	c
4.22097850435657	-0.36191533949594	1.89039169033755	c
3.90097823979945	-2.92680885480578	2.84457085973909	c
1.65786325612494	-4.02184455878637	1.60429464515043	c
-0.00333242852866	-5.55210798876612	2.96459653077019	c
-2.70748253205467	-5.14111804050595	2.77866398623607	c
-7.36164401419876	-3.33033012395898	4.47503006982909	c
-6.08378031099011	-5.12835475450502	5.98625042046137	c
-3.79232772586780	-6.09366765780655	5.10925866638288	c
-1.77292379945196	-6.62411564212851	6.86078593705589	c
0.59576680907681	-6.28555958667104	5.52005029068004	c
2.69156844174862	-5.21328147673202	6.74186583371746	c
4.31853522851410	-3.45162669028766	5.39271541009484	c
4.97942673736567	-1.41327433193072	7.12365479625101	c
5.12753182945213	1.07906307051456	6.24749728523877	c
-1.20778992923112	5.04707969143419	2.46258973173158	c
0.56611976122830	3.81823944489574	10.82454220764978	c
-0.62151802938972	5.48389363948126	9.14693396834056	c
-3.35576852488524	5.41945504941760	8.87808686633433	c
-4.81565210624847	3.76305400526762	10.33803300433836	c

-3.57538219329950	2.01796364392161	12.04922784493163	c
0.44496416110818	-0.34081673506770	12.36501350419016	c
2.81300918951650	-0.00235295213341	11.02464327163280	c
2.90130148462544	2.57691794710461	10.08607647622054	c
4.02003923491480	3.10357436446670	7.75003730422232	c
2.81298429874532	4.85341212991862	6.02004199082713	c
0.50948144061216	5.97191376942270	6.69026276122076	c
-3.91309859183968	5.71473127667033	6.20430186385370	c
-5.88375263691289	4.37874610490378	5.10929667637853	c
-7.58427630973797	2.91778758609666	6.67728885429002	c
-7.00610706357086	2.50235817932653	9.24536010361150	c
-7.11367519315456	-0.05247605899320	10.27903709568804	c
-4.95683452191893	-0.36229160933056	11.95549029610907	c
-3.61291824046410	-2.64137495948824	11.98712795574911	c
-0.86967805189877	-2.62876973513398	12.19100957910265	c
3.80020806426375	-1.961304673353797	9.54774213087158	c
2.41173824590605	-4.31488303107815	9.30801045115894	c
0.11231421525214	-4.64353884067998	10.60953955459291	c
-2.00031894210069	-5.88389117122195	9.39758652668506	c
-4.31486058856612	-4.68559469881920	10.27942432832755	c
-6.37286515811458	-4.39524541746259	8.65981241947242	c
-7.88263342018807	-2.09188002766891	8.74132608367146	c
-8.61560764778935	-1.56137699850007	6.18330041827712	c
-8.41256707696924	0.83373955988654	5.17031784072542	c
-1.53694632853151	6.05435382363167	4.85934274206588	c
-5.43571946891955	2.93303176982126	2.74684632929213	c
-0.94077242544060	2.0277717196277	12.26078237858222	c
-11.01183702550682	-8.17416909121969	-4.50000000000000	au
-11.01183702550682	-2.72472303040656	-4.50000000000000	au
-11.01183702550682	2.72472303040657	-4.50000000000000	au
-11.01183702550682	8.17416909121969	-4.50000000000000	au
-6.29247830028962	-10.89889212162625	-4.50000000000000	au
-6.29247830028962	-5.44944606081312	-4.50000000000000	au
-6.29247830028962	0.00000000000000	-4.50000000000000	au
-6.29247830028962	5.44944606081313	-4.50000000000000	au
-6.29247830028961	10.89889212162625	-4.50000000000000	au
-1.57311957507240	-13.62361515203282	-4.50000000000000	au
-1.57311957507240	-8.17416909121969	-4.50000000000000	au
-1.57311957507240	-2.72472303040656	-4.50000000000000	au
-1.57311957507241	2.72472303040657	-4.50000000000000	au
-1.57311957507241	8.17416909121969	-4.50000000000000	au
-1.57311957507240	13.62361515203282	-4.50000000000000	au
3.14623915014480	-10.89889212162625	-4.50000000000000	au
3.14623915014480	-5.44944606081312	-4.50000000000000	au
3.14623915014480	0.00000000000000	-4.50000000000000	au
3.14623915014480	5.44944606081314	-4.50000000000000	au
3.14623915014480	10.89889212162626	-4.50000000000000	au
7.86559787536201	-8.17416909121969	-4.50000000000000	au
7.86559787536201	-2.72472303040656	-4.50000000000000	au
7.86559787536200	2.72472303040657	-4.50000000000000	au
7.86559787536201	8.17416909121969	-4.50000000000000	au
12.58495660057921	-5.44944606081312	-4.50000000000000	au
12.58495660057922	0.00000000000000	-4.50000000000000	au
12.58495660057921	5.44944606081312	-4.50000000000000	au
-7.86559787536202	-8.17416909121969	-8.94945407660398	au
-7.86559787536201	-2.72472303040657	-8.94945407660398	au
-7.86559787536202	2.72472303040657	-8.94945407660398	au
-7.86559787536202	8.17416909121969	-8.94945407660398	au
-3.14623915014481	-10.89889212162624	-8.94945407660398	au
-3.14623915014482	-5.44944606081312	-8.94945407660398	au
-3.14623915014481	-0.00000000000001	-8.94945407660398	au
-3.14623915014481	5.44944606081314	-8.94945407660398	au
-3.14623915014482	10.89889212162626	-8.94945407660398	au
1.57311957507240	-8.17416909121969	-8.94945407660398	au
1.57311957507239	-2.72472303040655	-8.94945407660398	au
1.57311957507240	2.72472303040657	-8.94945407660398	au
1.57311957507240	8.17416909121970	-8.94945407660398	au
6.29247830028961	-5.44944606081313	-8.94945407660398	au
6.29247830028961	-0.00000000000001	-8.94945407660398	au
6.29247830028961	5.44944606081312	-8.94945407660398	au
11.01183702550681	-2.72472303040656	-8.94945407660398	au
11.01183702550681	2.72472303040658	-8.94945407660398	au

Send

## C<sub>58</sub> on Au(111) with C<sub>3s</sub> Symmetry Pent3 after Relaxation (def-SV(P))

Scoord			
-1.00653778139358	-3.30864057464864	0.24481945574918	c
2.44797521484612	-0.38304015799854	0.30455712802393	c
3.22468045180689	-2.65114489986478	1.49639914233335	c
1.22227366593985	-4.49852086942915	1.24740448713090	c
-3.50767251153511	-4.16788713511470	1.03729035662762	c

-5.78729591024331	-2.68341799733623	0.65216334093622	c
-0.22098210889695	-0.74067640476455	-0.52669320524094	c
-6.06043584930961	0.04972842653235	-0.20734244543902	c
-1.47850078590527	1.70913324361258	-0.09227092868175	c
2.58285234331376	1.96119657945568	1.72250256567649	c
3.64596359719896	1.98991727714877	4.17805069908511	c
4.38545859648243	-0.39067894505205	5.38796377476270	c
4.12989218769382	-2.71184466706139	4.06192672717522	c
2.89520802763950	-4.86505764722012	5.31808237781516	c
1.10066672262067	-5.97738082761304	3.51916230910027	c
-1.27064651294119	-6.82012761070734	4.32767162384496	c
-3.56474095669435	-6.11254800944766	2.95109171601675	c
-7.95441001523394	-3.26681295916244	2.12098439409931	c
-7.81977857748326	-4.78419180596424	4.35559539378969	c
-5.64696446477531	-6.25218963939447	4.73879290961170	c
-4.59395663247485	-6.54246423900257	7.25886062190442	c
-1.87731824491549	-6.89924634856244	7.00169108122145	c
-0.19439421006289	-5.79260972790526	8.74683807778461	c
2.18850569661285	-4.70069694455654	7.87514394748839	c
2.60216473794842	-2.35794923546454	9.27306162044391	c
3.63969031346073	-0.23641206583980	8.03507783212899	c
0.26959185402700	3.35298716887441	1.27704237151460	c
-1.53947869058503	4.26637521911499	9.65607082215723	c
-1.58691466969652	5.57995820809130	7.34472741790888	c
-3.96607508650701	5.79984458001304	5.95478703658895	c
-6.22101964793314	4.77788268035689	6.94019348594798	c
-6.15568026369070	3.41716488310395	9.33245261651528	c
-3.20087078115651	0.73248251838852	11.79574031001042	c
-0.48167649367867	0.37122494640428	11.53604784891853	c
0.55159448478450	2.56325673599724	10.22465626953401	c
2.55275469375516	2.26192155857703	8.49740935317553	c
2.52503992351290	3.62418946710432	6.10876579169406	c
0.46624017712668	5.21836338722561	5.53382039233175	c
-3.37234181423541	5.45074183376151	3.28837720771701	c
-5.05396055210884	4.03941209098540	1.77588758427971	c
-7.54255142124507	3.29085132320628	2.67760974359768	c
-8.07432274824976	3.54158954015665	5.29810008042094	c
-9.15841549079502	1.41322186241149	6.68567193907140	c
-7.91967687742400	1.30179653974231	9.14556944466714	c
-7.24778475952137	-1.04993887220655	10.21072815185507	c
-4.85813554573476	-1.33598819369168	11.55078925746879	c
0.50921431576160	-2.04730697080082	11.04254122187124	c
-1.20627897877396	-4.18436546891734	10.73999180538356	c
-3.83675995169116	-3.83535905930793	10.98559042400187	c
-5.57786166495705	-5.07708616620306	9.25273980374848	c
-7.71584189025003	-3.38157981576249	8.80923488651282	c
-8.89906011187509	-3.28740666116812	6.43164868822958	c
-9.75209282880710	-0.85817556461193	5.38663868870463	c
-9.34610502768113	-0.95675151890602	2.69197991776186	c
-8.2449038236800	1.02902973793124	1.34340450930272	c
-0.67727060564168	5.10832186263349	3.03227542284508	c
-4.10032124838353	1.99994918145611	0.23657217147588	c
-3.85648996743255	3.14617063154280	10.64481313661257	c
-11.01183702550682	-8.17416909121969	-4.50000000000000	au
-11.01183702550682	-2.72472303040656	-4.50000000000000	au
-11.01183702550682	2.72472303040657	-4.50000000000000	au
-11.01183702550682	8.17416909121969	-4.50000000000000	au
-6.29247830028962	13.62361515203282	-4.50000000000000	au
-6.29247830028962	-10.89889212162625	-4.50000000000000	au
-6.29247830028962	-5.44944606081312	-4.50000000000000	au
-6.29247830028962	0.00000000000000	-4.50000000000000	au
-6.29247830028962	5.44944606081313	-4.50000000000000	au
-6.29247830028961	10.89889212162625	-4.50000000000000	au
-1.57311957507240	-13.62361515203282	-4.50000000000000	au
-1.57311957507240	-8.17416909121969	-4.50000000000000	au
-1.57311957507240	-2.72472303040656	-4.50000000000000	au
-1.57311957507241	2.72472303040657	-4.50000000000000	au
-1.57311957507241	8.17416909121969	-4.50000000000000	au
-1.57311957507240	13.62361515203282	-4.50000000000000	au
3.14623915014480	-10.89889212162625	-4.50000000000000	au
3.14623915014480	-5.44944606081312	-4.50000000000000	au
3.14623915014480	0.00000000000000	-4.50000000000000	au
3.14623915014480	5.44944606081314	-4.50000000000000	au
3.14623915014480	10.89889212162626	-4.50000000000000	au
7.86559787536201	-8.17416909121969	-4.50000000000000	au
7.86559787536201	-2.72472303040656	-4.50000000000000	au
7.86559787536200	2.72472303040657	-4.50000000000000	au
7.86559787536201	8.17416909121969	-4.50000000000000	au
12.58495660057921	-5.44944606081312	-4.50000000000000	au
12.58495660057922	0.00000000000000	-4.50000000000000	au
12.58495660057921	5.44944606081312	-4.50000000000000	au
-7.86559787536202	-8.17416909121969	-8.94945407660398	au
-7.86559787536201	-2.72472303040657	-8.94945407660398	au
-7.86559787536202	2.72472303040657	-8.94945407660398	au
-7.86559787536202	8.17416909121969	-8.94945407660398	au
-3.14623915014481	-10.89889212162624	-8.94945407660398	au
-3.14623915014482	-5.44944606081312	-8.94945407660398	au
-3.14623915014481	-0.00000000000001	-8.94945407660398	au
-3.14623915014481	5.44944606081314	-8.94945407660398	au

---

```
-3.14623915014482    10.89889212162626    -8.94945407660398    au
1.57311957507240    -8.17416909121969    -8.94945407660398    au
1.57311957507239    -2.72472303040655    -8.94945407660398    au
1.57311957507240    2.72472303040657    -8.94945407660398    au
1.57311957507240    8.17416909121970    -8.94945407660398    au
6.29247830028961    -5.44944606081313    -8.94945407660398    au
6.29247830028961    -0.000000000000001    -8.94945407660398    au
6.29247830028961    5.44944606081312    -8.94945407660398    au
11.01183702550681    -2.72472303040656    -8.94945407660398    au
11.01183702550681    2.72472303040658    -8.94945407660398    au
Send
```



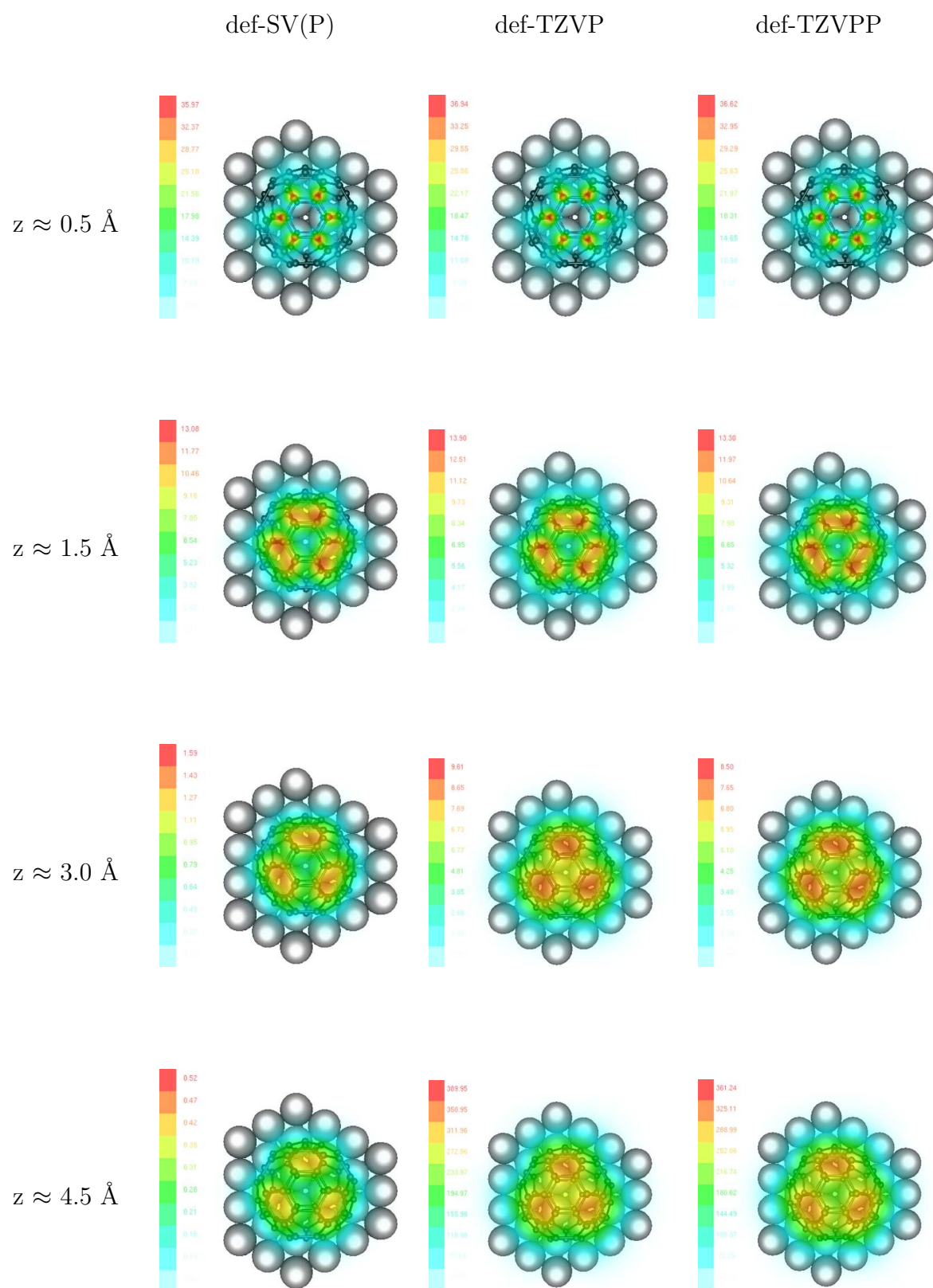
# Appendix B

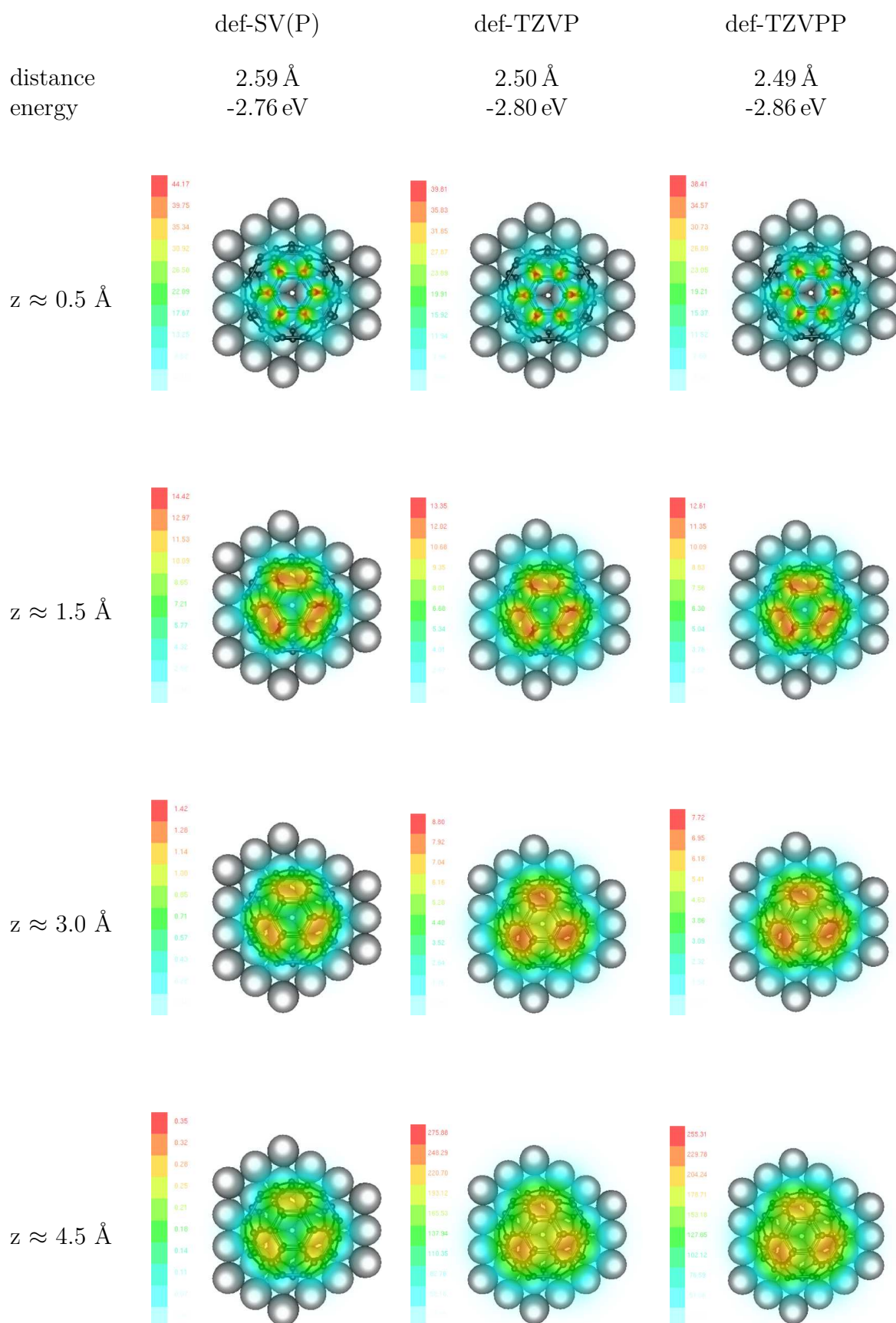
## Catalogue

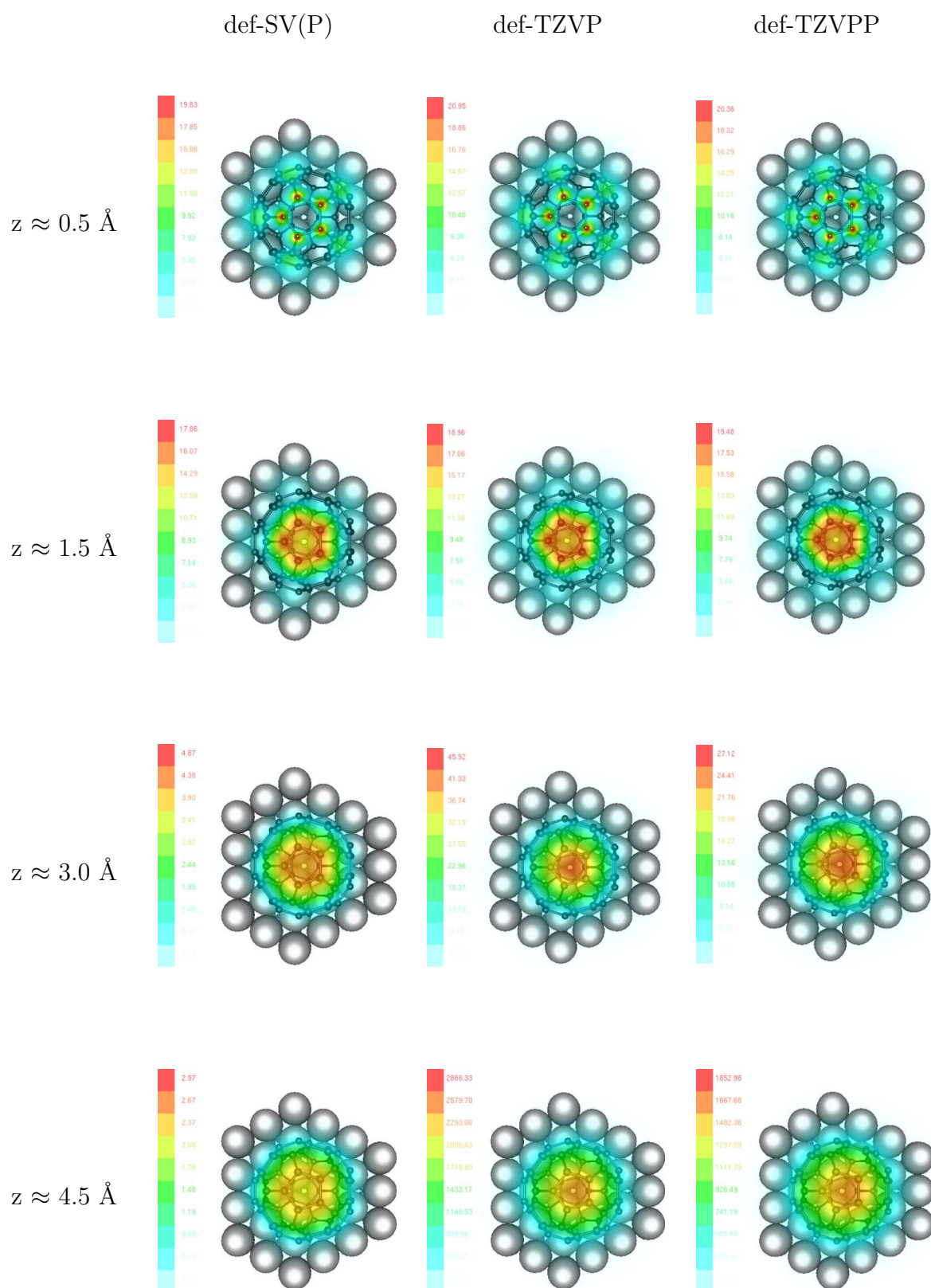
In this study, we prepared the following catalogue of topography images of icosahedral  $C_{60}$  and  $C_{58}$  with  $C_{3v}$  and  $C_s$  symmetry. The color scales in the images is multiplied with some scaling factors, which are listed below. Furthermore, for the contact geometries without relaxation, the binding distance as well as the corresponding binding energy obtained with the def-SV(P) basis set are given. For the geometries after the relaxation procedure, the binding energy and the binding distance are given for all three basis sets.

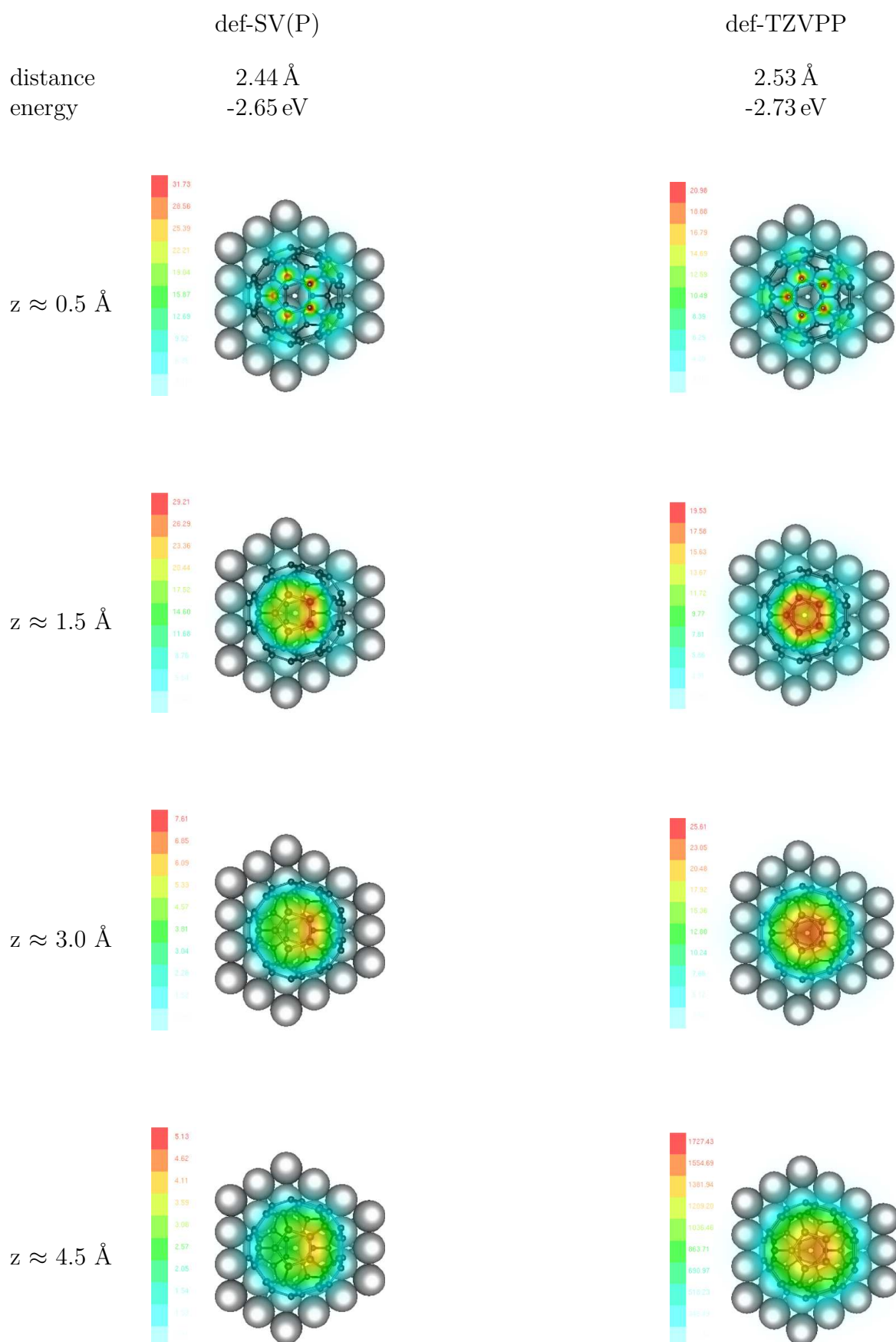
bias	$z \approx 0.5 \text{ \AA}$	$z \approx 1.5 \text{ \AA}$	$z \approx 3.0 \text{ \AA}$	$z \approx 4.5 \text{ \AA}$
-2.0	$10^{-2}$	$10^{-3}$	$10^{-7}$	$10^{-14}$
-1.8	$10^{-3}$	$10^{-4}$	$10^{-7}$	$10^{-14}$
-1.2	$10^{-3}$	$10^{-4}$	$10^{-8}$	$10^{-14}$
-0.5	$10^{-4}$	$10^{-5}$	$10^{-9}$	$10^{-16}$
0.0	$10^{-2}$	$10^{-3}$	$10^{-5}$	$10^{-10}$
+0.6	$10^{-4}$	$10^{-5}$	$10^{-9}$	$10^{-15}$
+1.4	$10^{-3}$	$10^{-4}$	$10^{-8}$	$10^{-14}$
+2.0	$10^{-3}$	$10^{-4}$	$10^{-7}$	$10^{-13}$

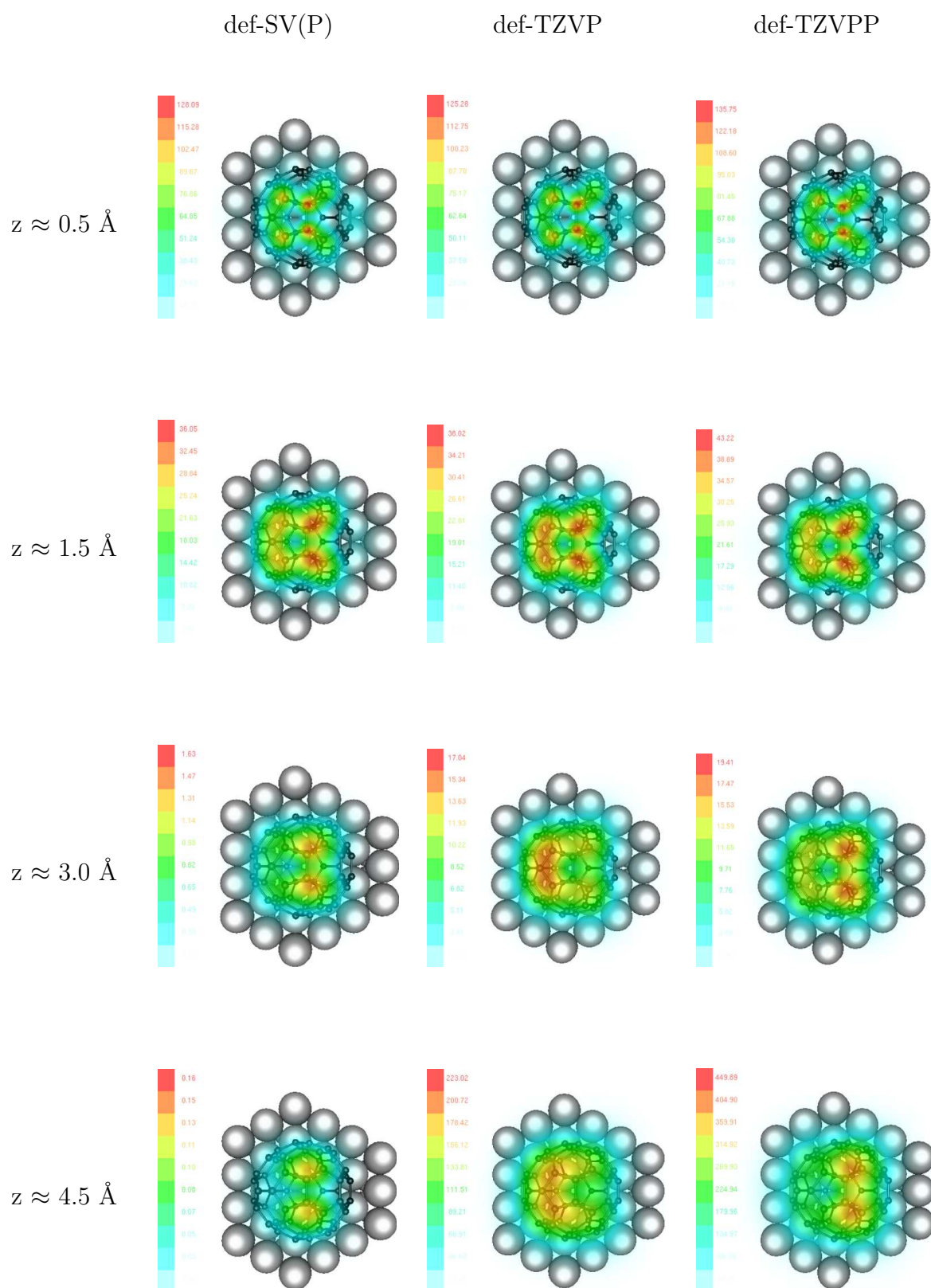
Table B.1: The scaling factors for the colour scale in the topography images.

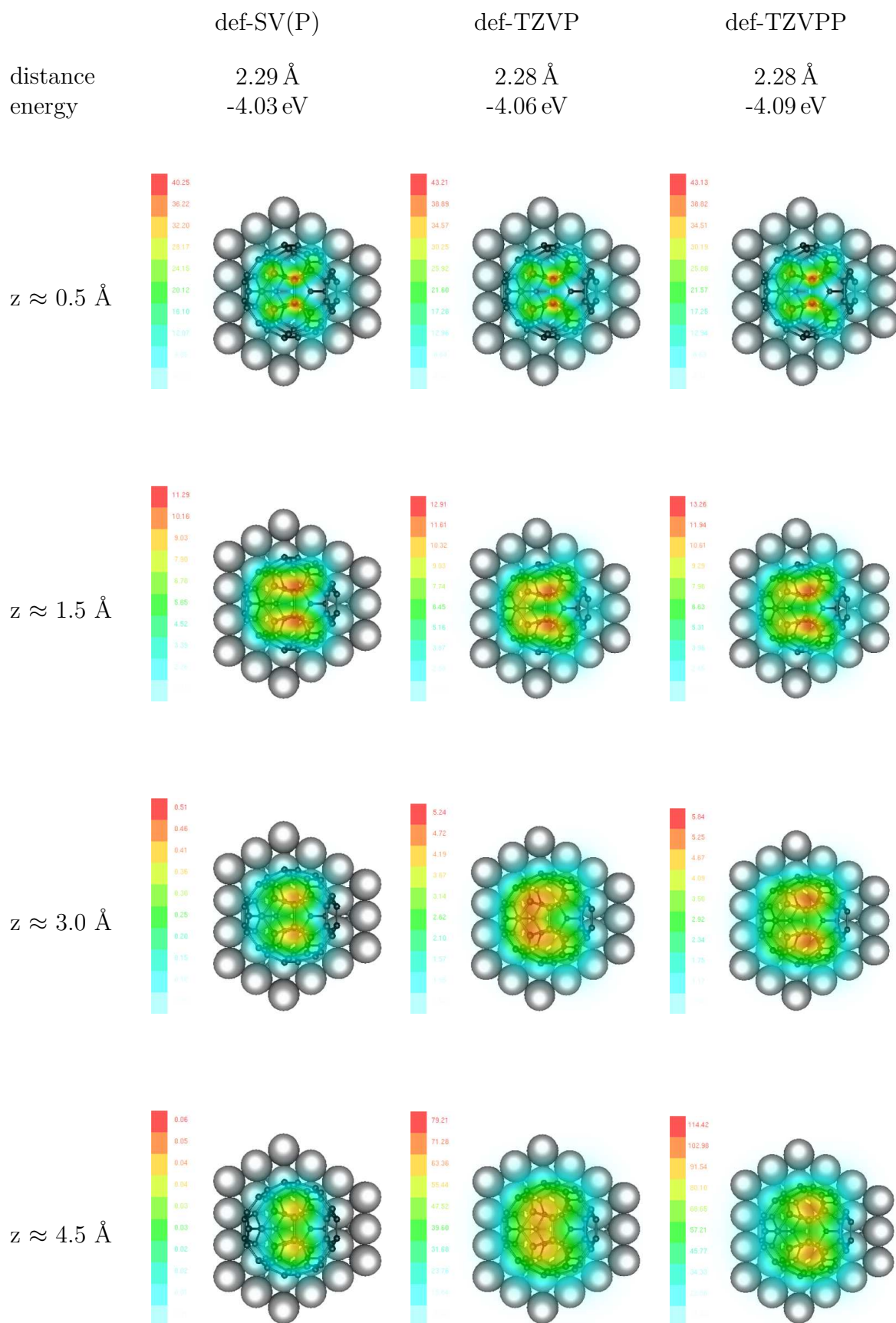
**C<sub>60</sub> without Relaxation: Hexagon, 2.59 Å, -2.08 eV**

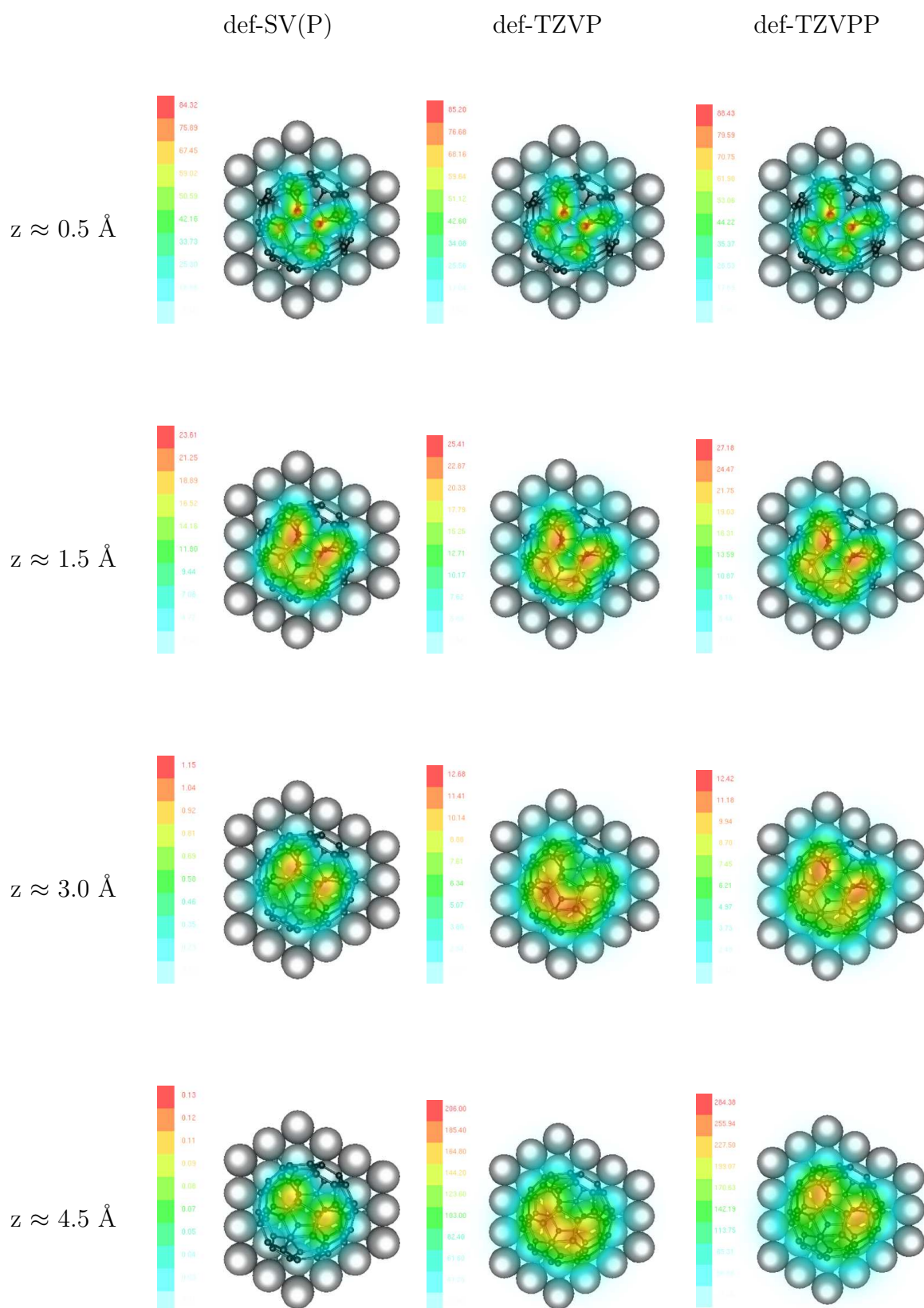
**C<sub>60</sub> after Relaxation: Hexagon**

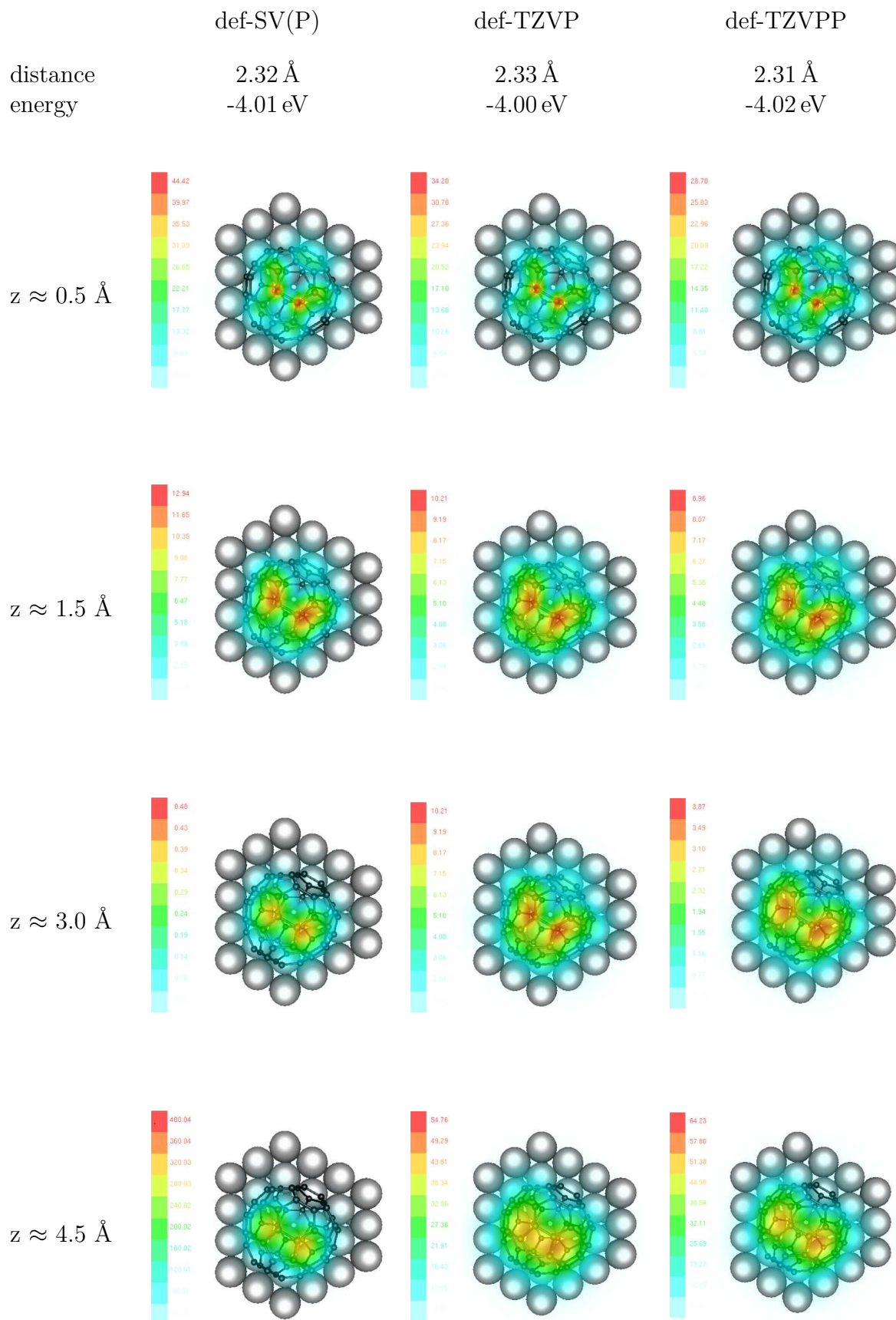
**C<sub>60</sub> without Relaxation: Pentagon, 2.54 Å, -2.02 eV**

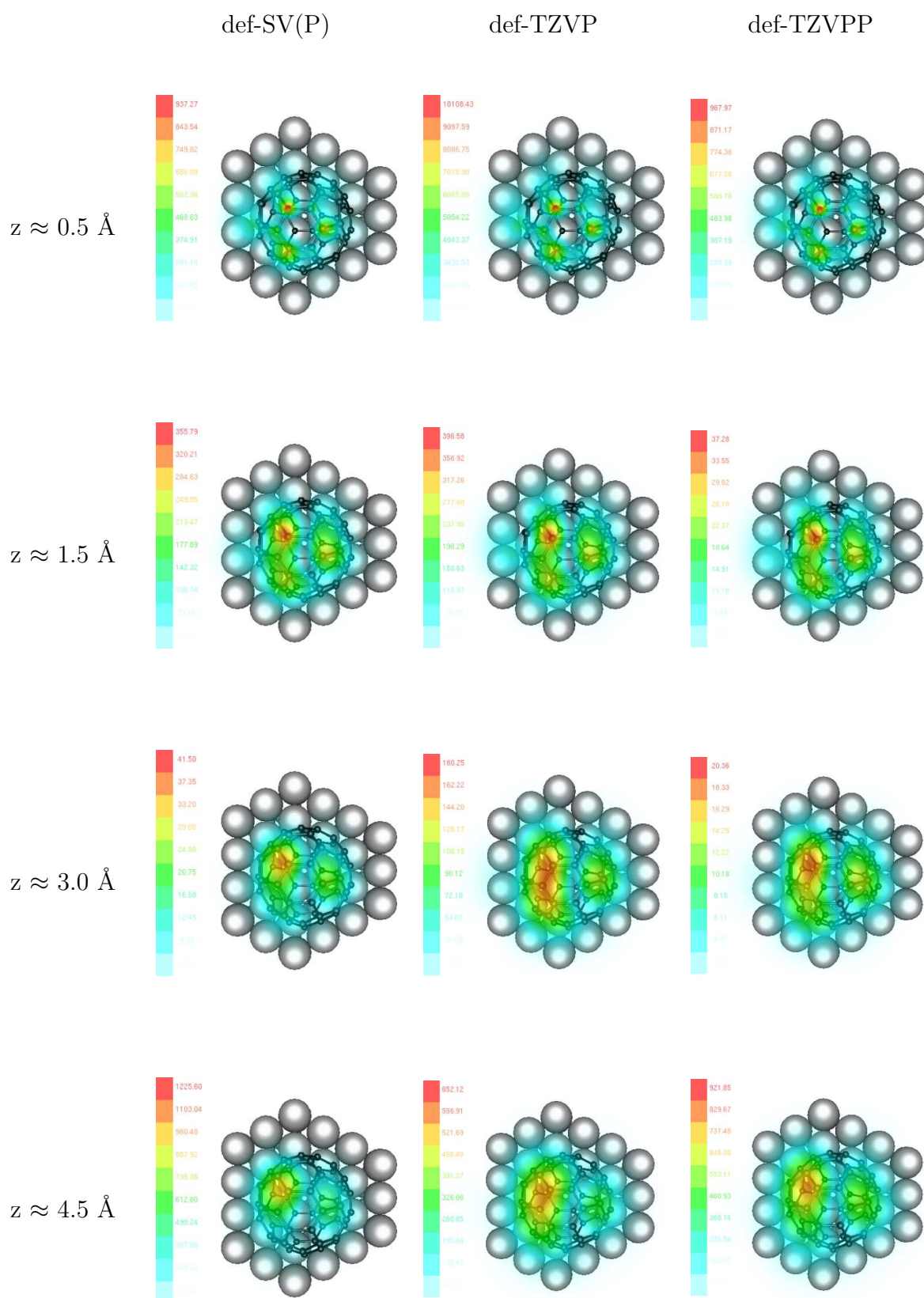
**C<sub>60</sub> after Relaxation: Pentagon**

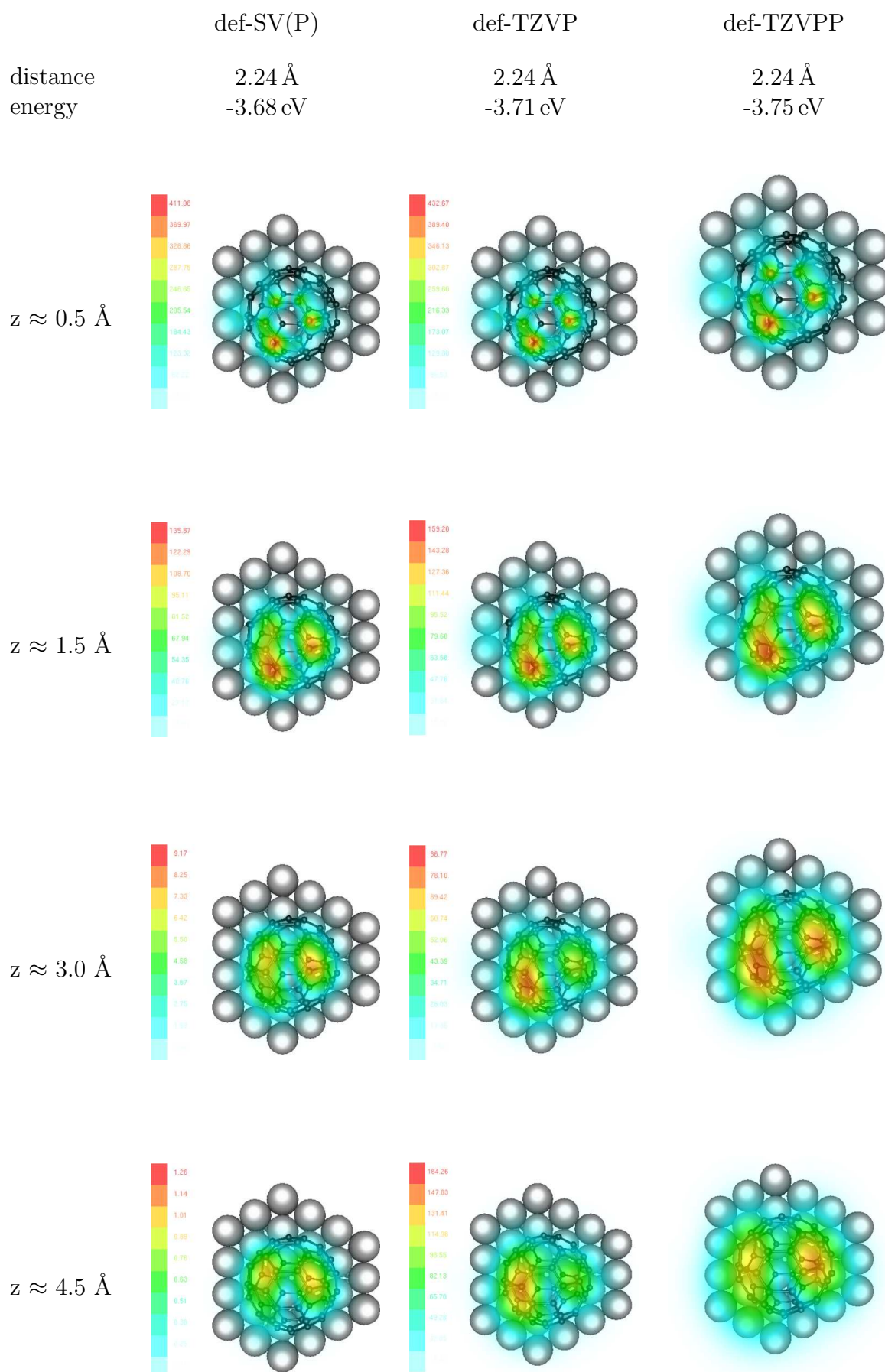
**C<sub>58</sub>: C<sub>3v</sub> Symmetry, H1a without Relaxation, 2.43 Å, -3.03 eV**

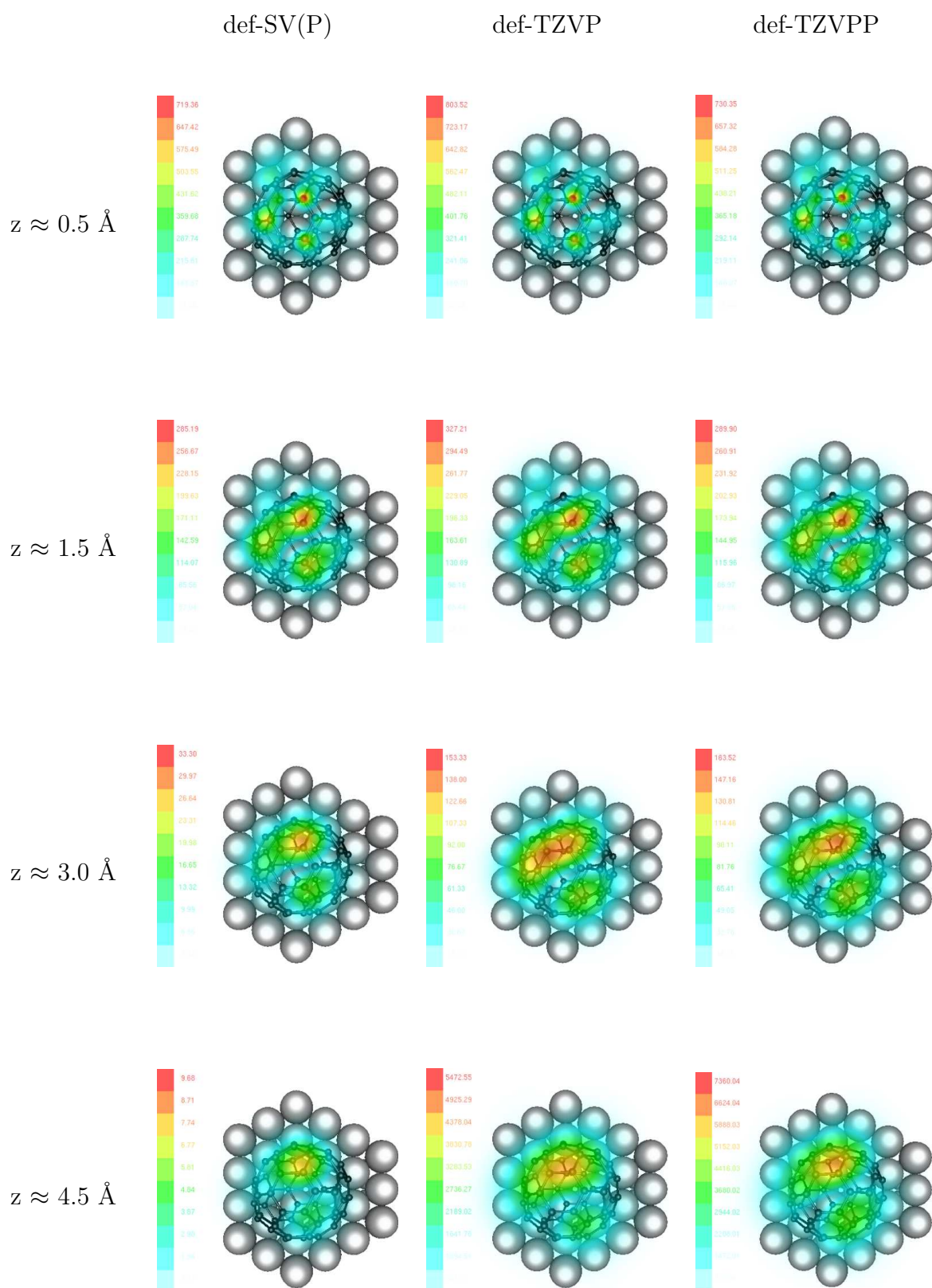
**C<sub>58</sub>: C<sub>3v</sub> Symmetry, H1a after Relaxation**

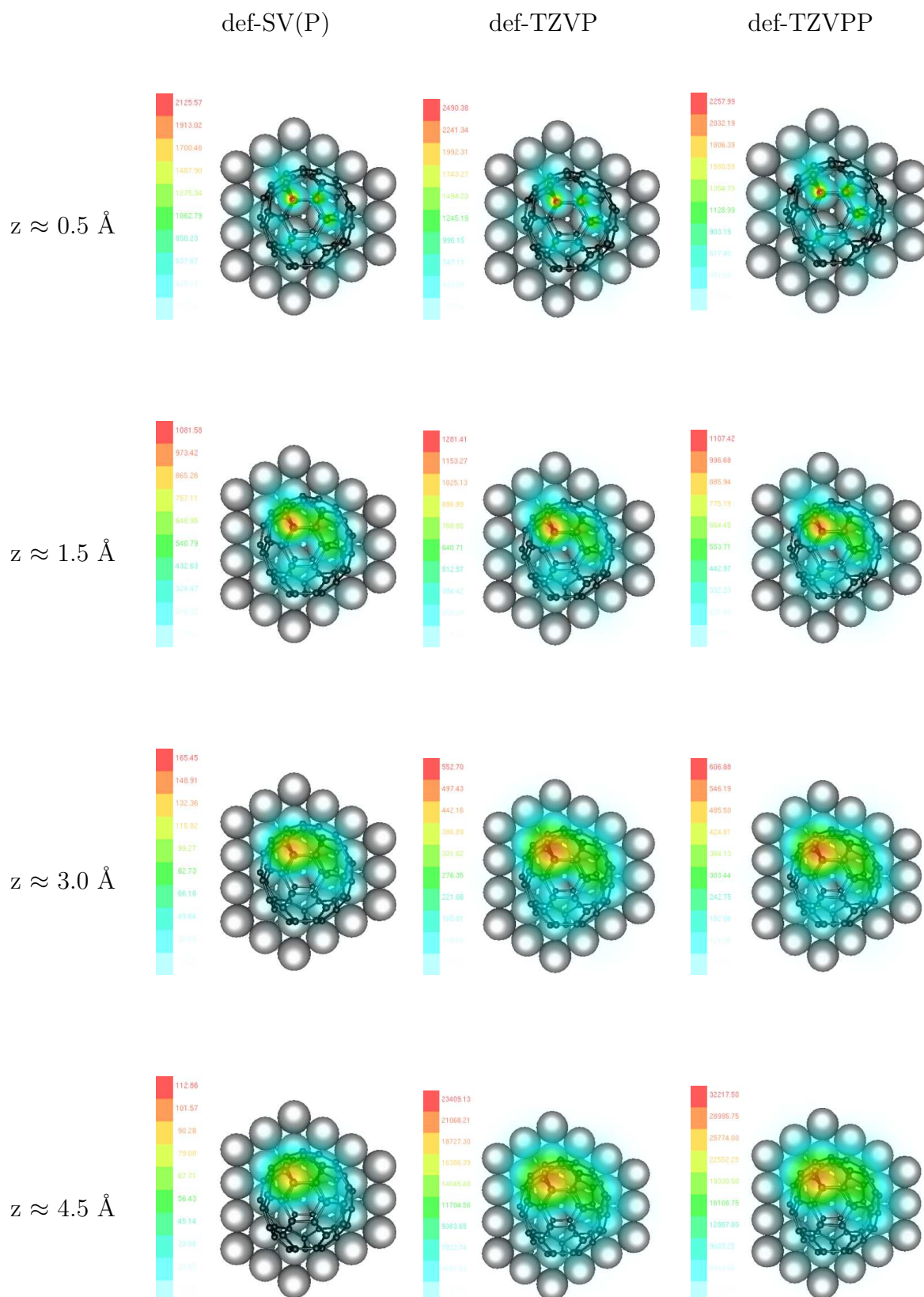
**C<sub>58</sub>: C<sub>3v</sub> Symmetry, H1b without Relaxation, 2.49 Å, -3.12 eV**

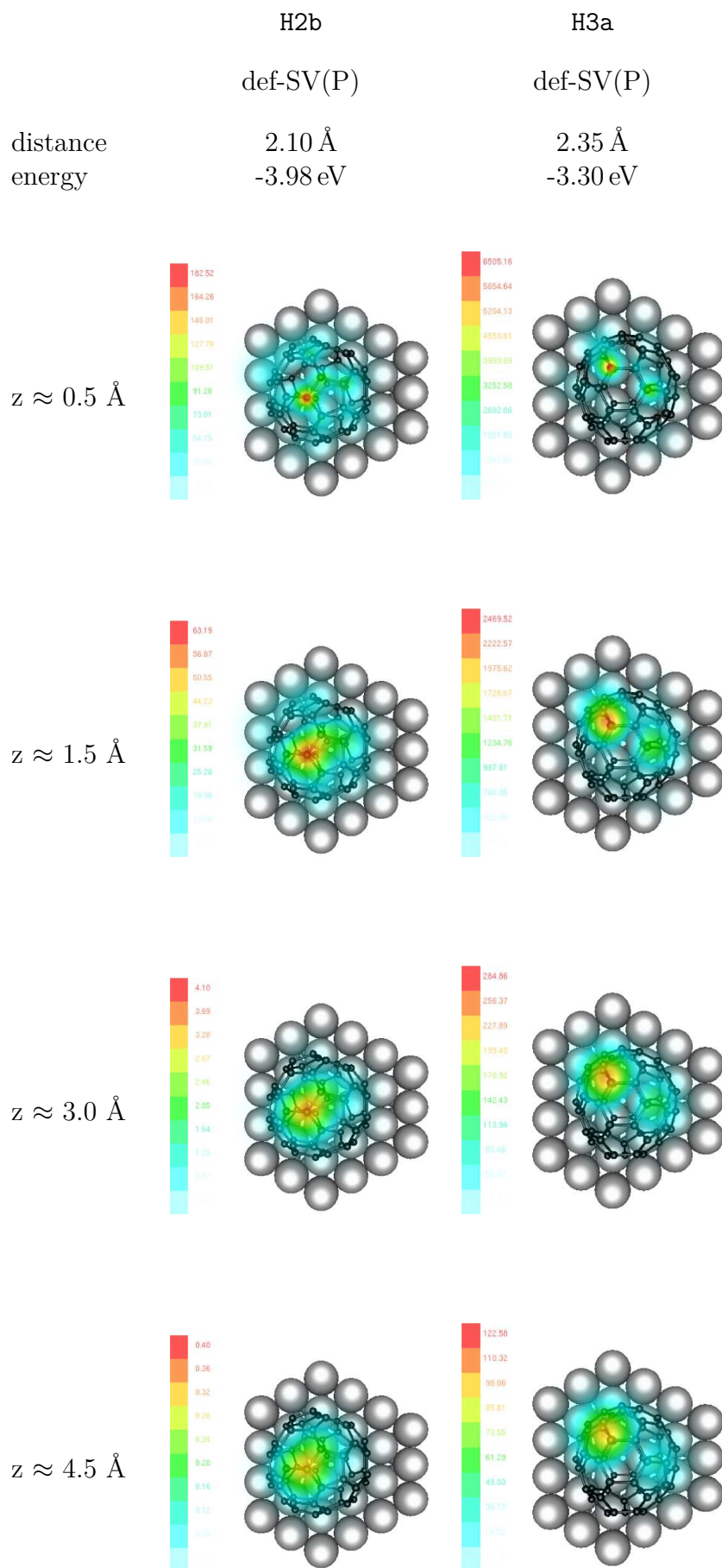
**C<sub>58</sub>: C<sub>3v</sub> Symmetry, H1b after Relaxation**

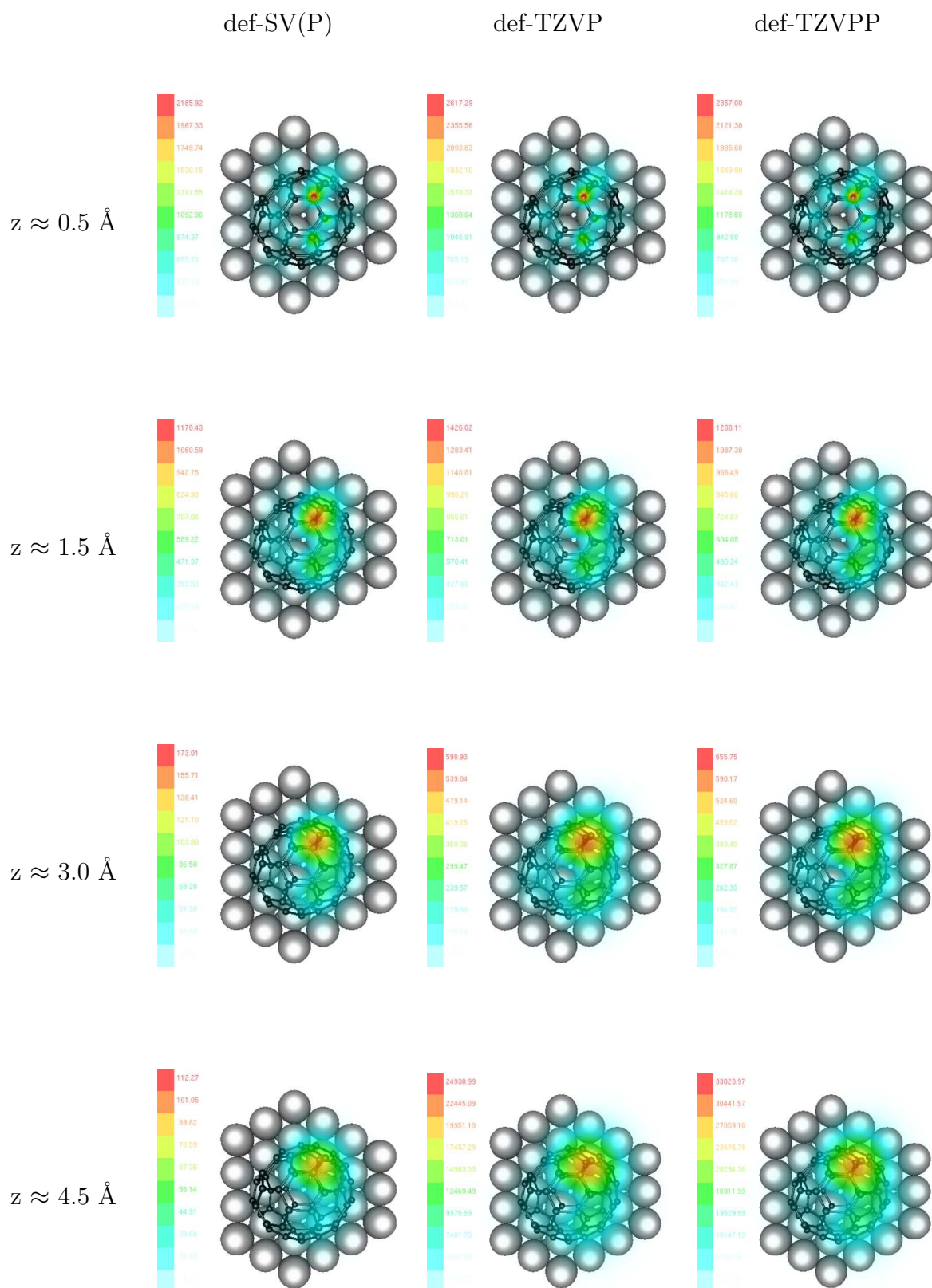
**C<sub>58</sub>: C<sub>3v</sub> Symmetry, H<sub>2</sub>a without Relaxation, 2.43 Å, -2.69 eV**

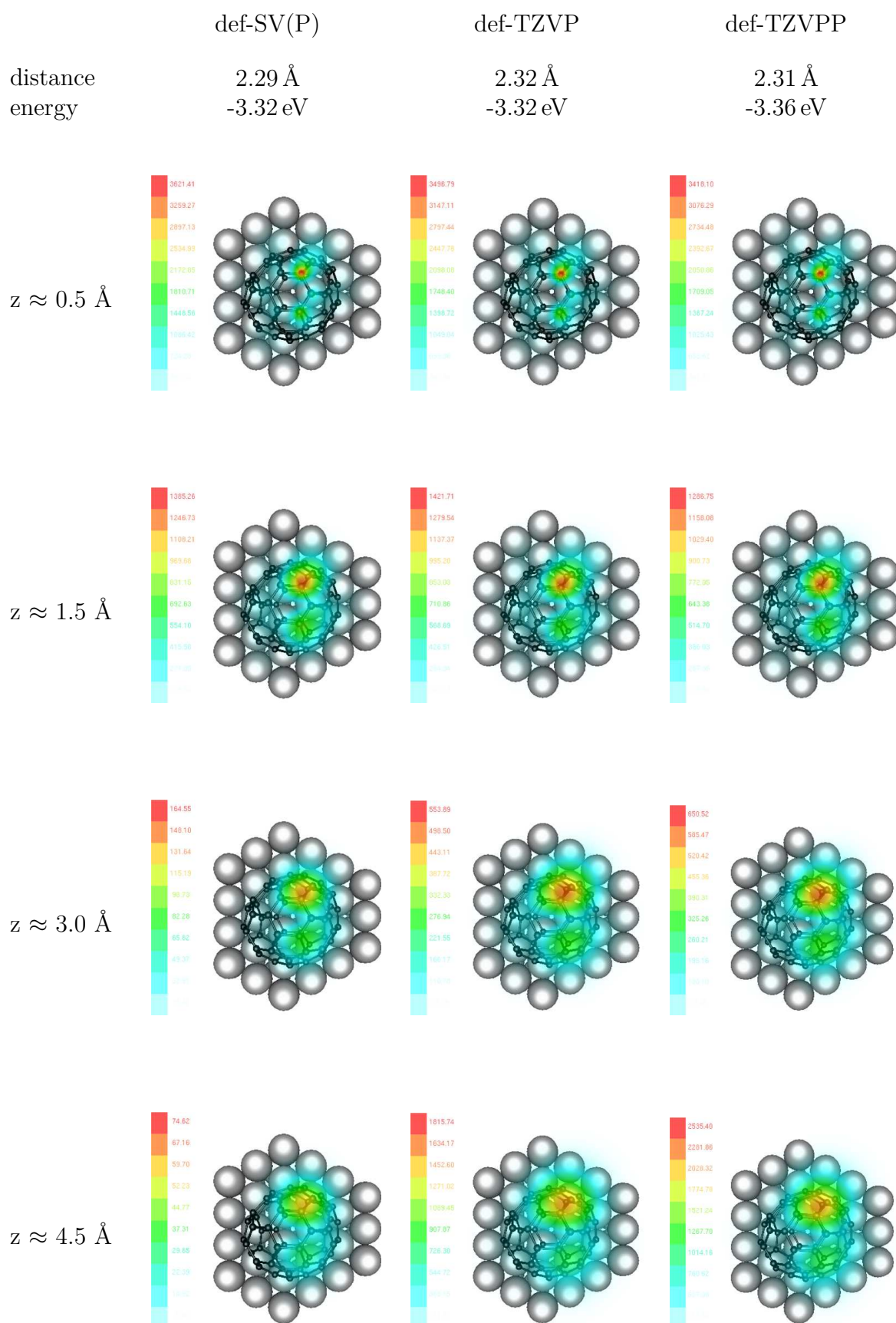
**C<sub>58</sub>: C<sub>3v</sub> Symmetry, H2a after Relaxation**

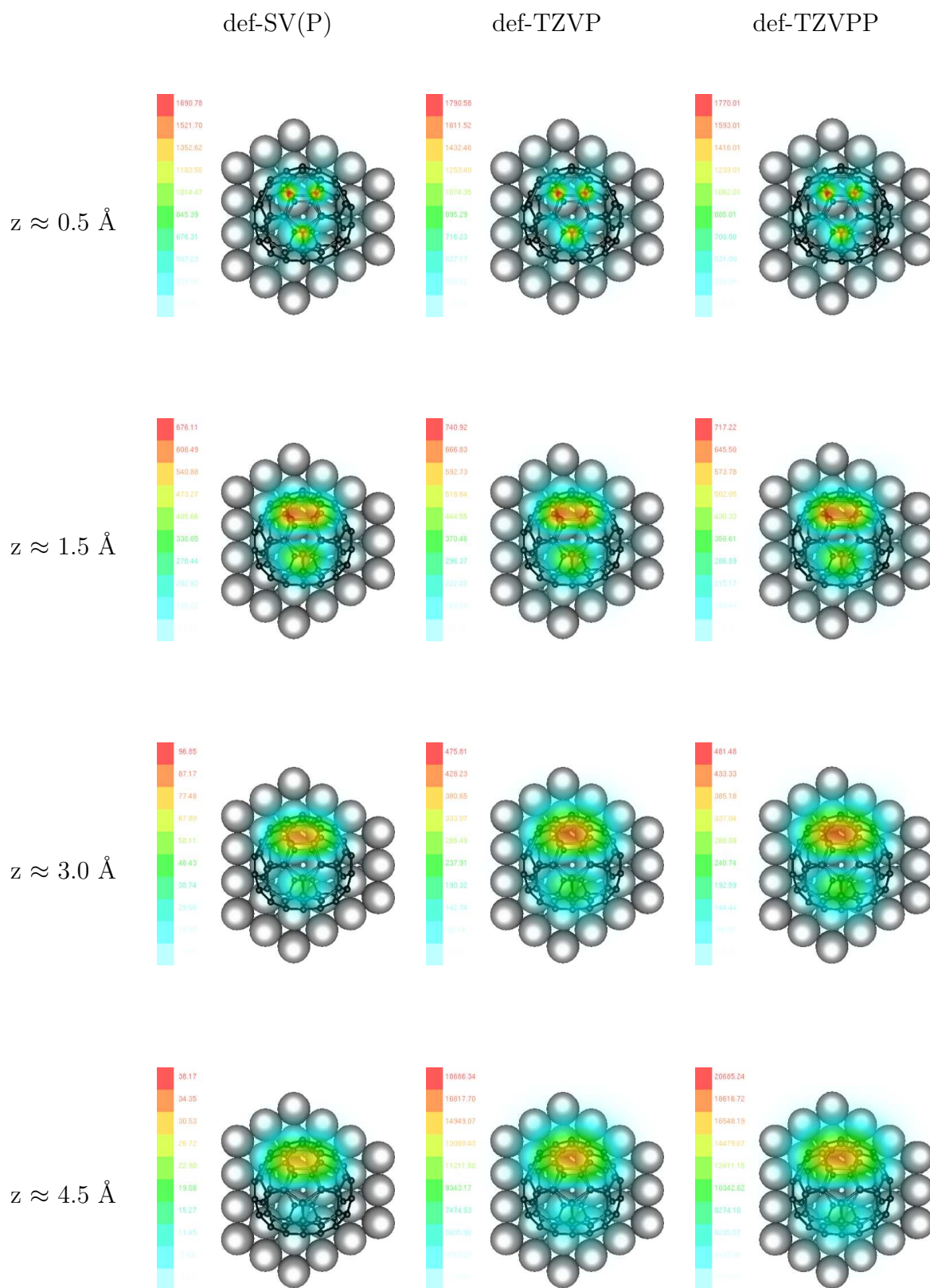
**C<sub>58</sub>: C<sub>3v</sub> Symmetry, H2b without Relaxation, 2.49 Å, -2.68 eV**

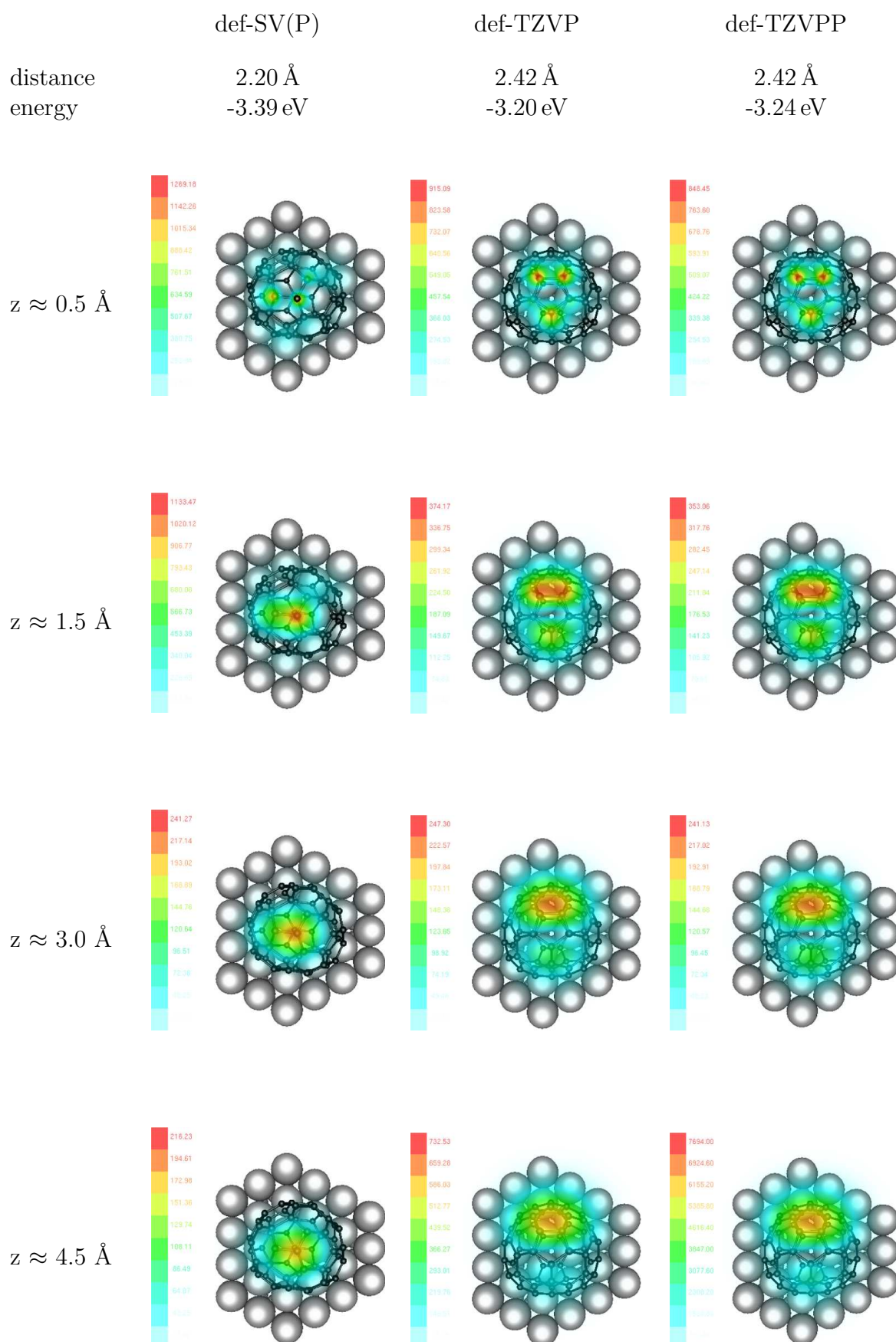
**C<sub>58</sub>: C<sub>3v</sub> Symmetry, H3a without Relaxation, 2.49 Å, -2.44 eV**

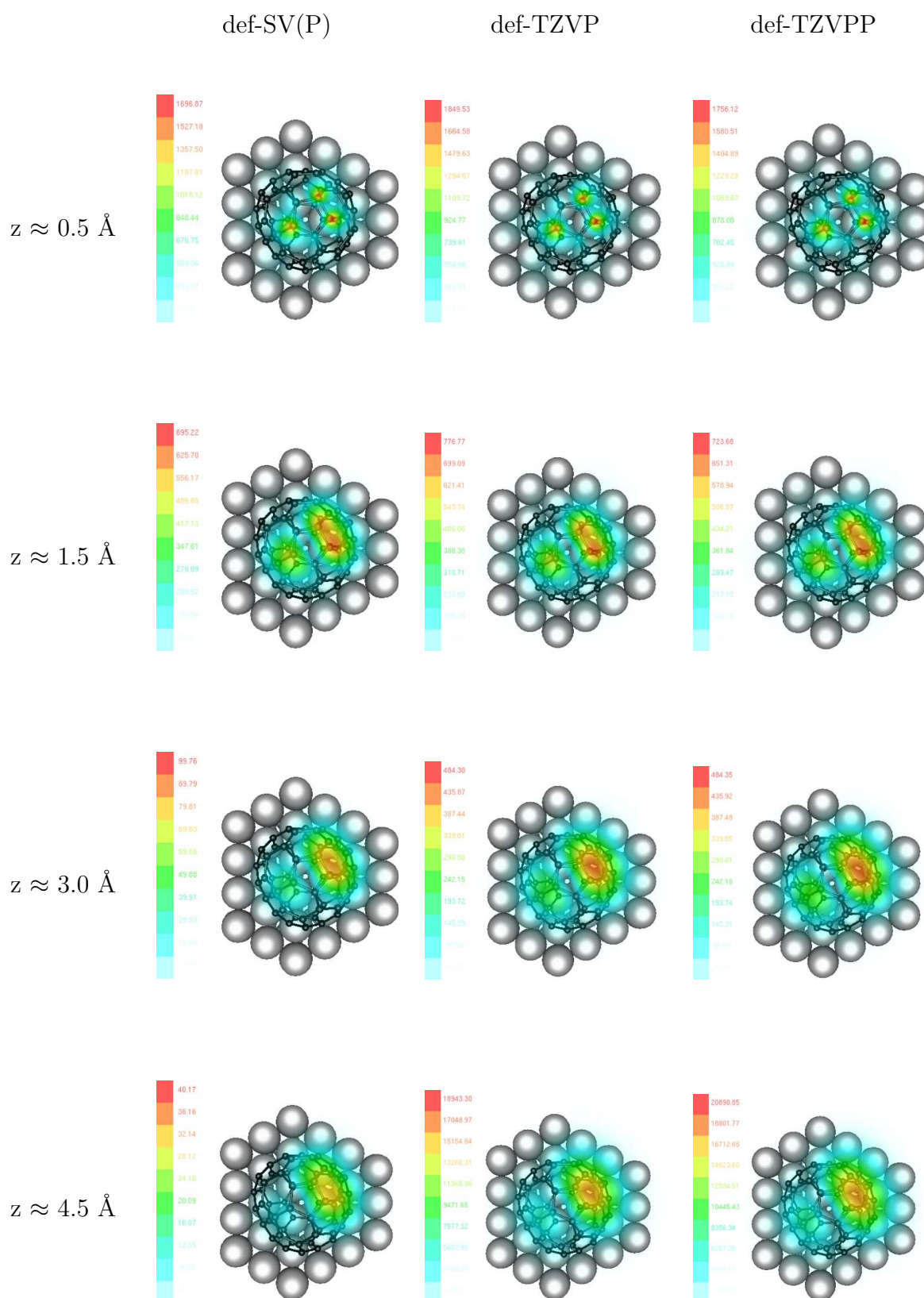
**C<sub>58</sub>: C<sub>3v</sub> Symmetry, H2b and H3a after Relaxation**

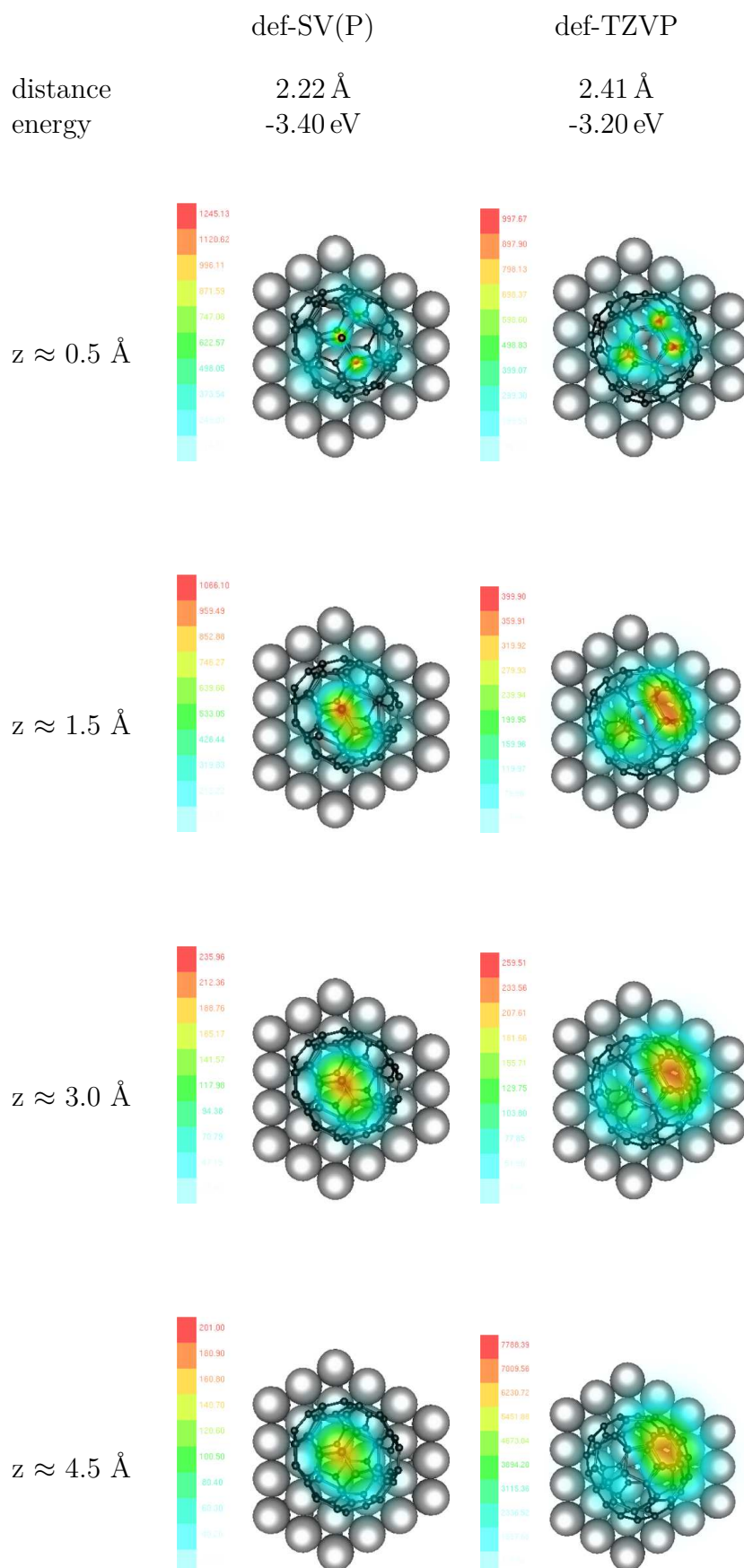
**C<sub>58</sub>: C<sub>3v</sub> Symmetry, H3b without Relaxation, 2.49 Å, -2.47 eV**

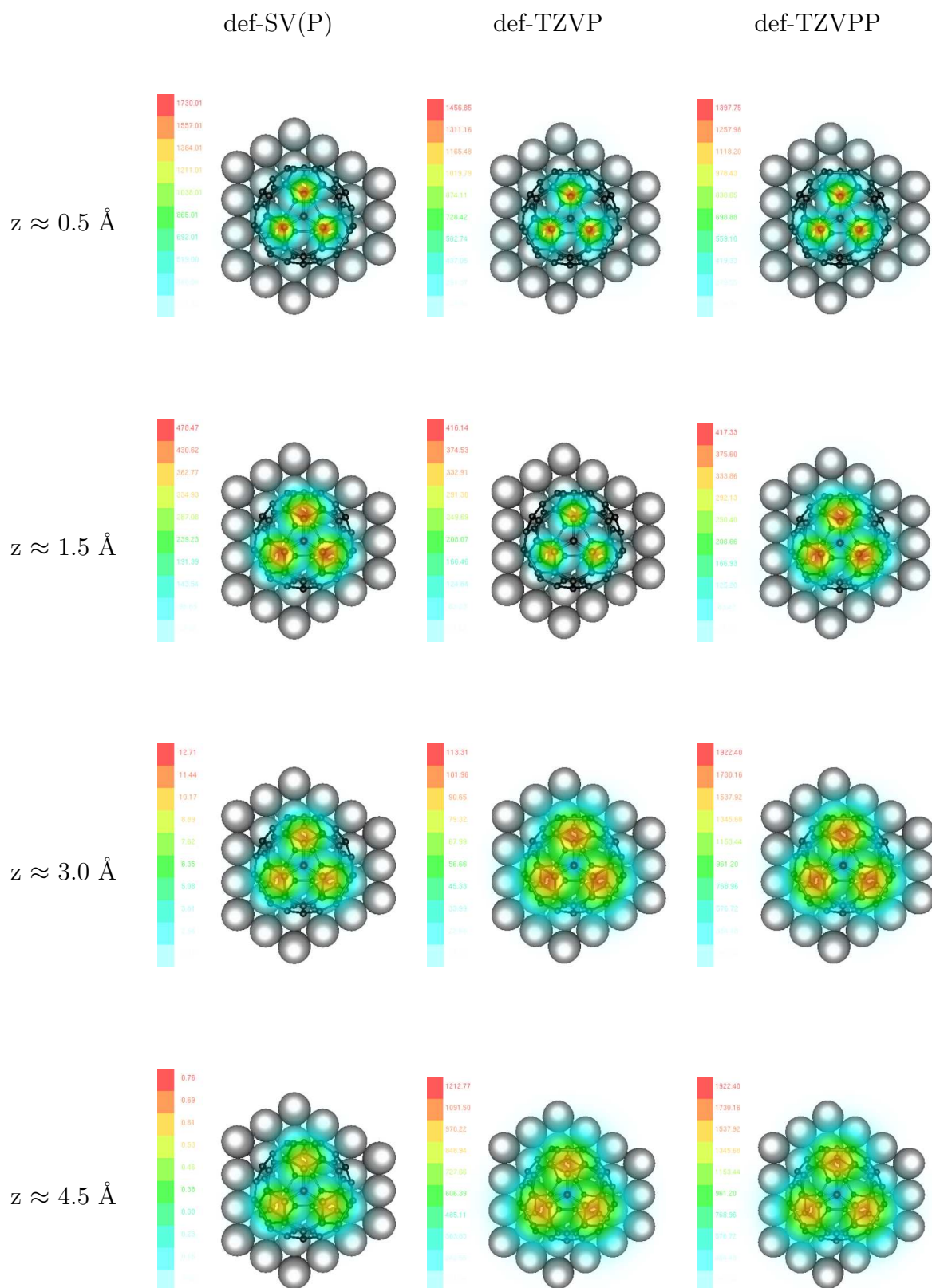
**C<sub>58</sub>: C<sub>3v</sub> Symmetry, H3b after Relaxation**

**C<sub>58</sub>: C<sub>3v</sub> Symmetry, H4a without Relaxation, 2.54 Å, -2.34 eV**

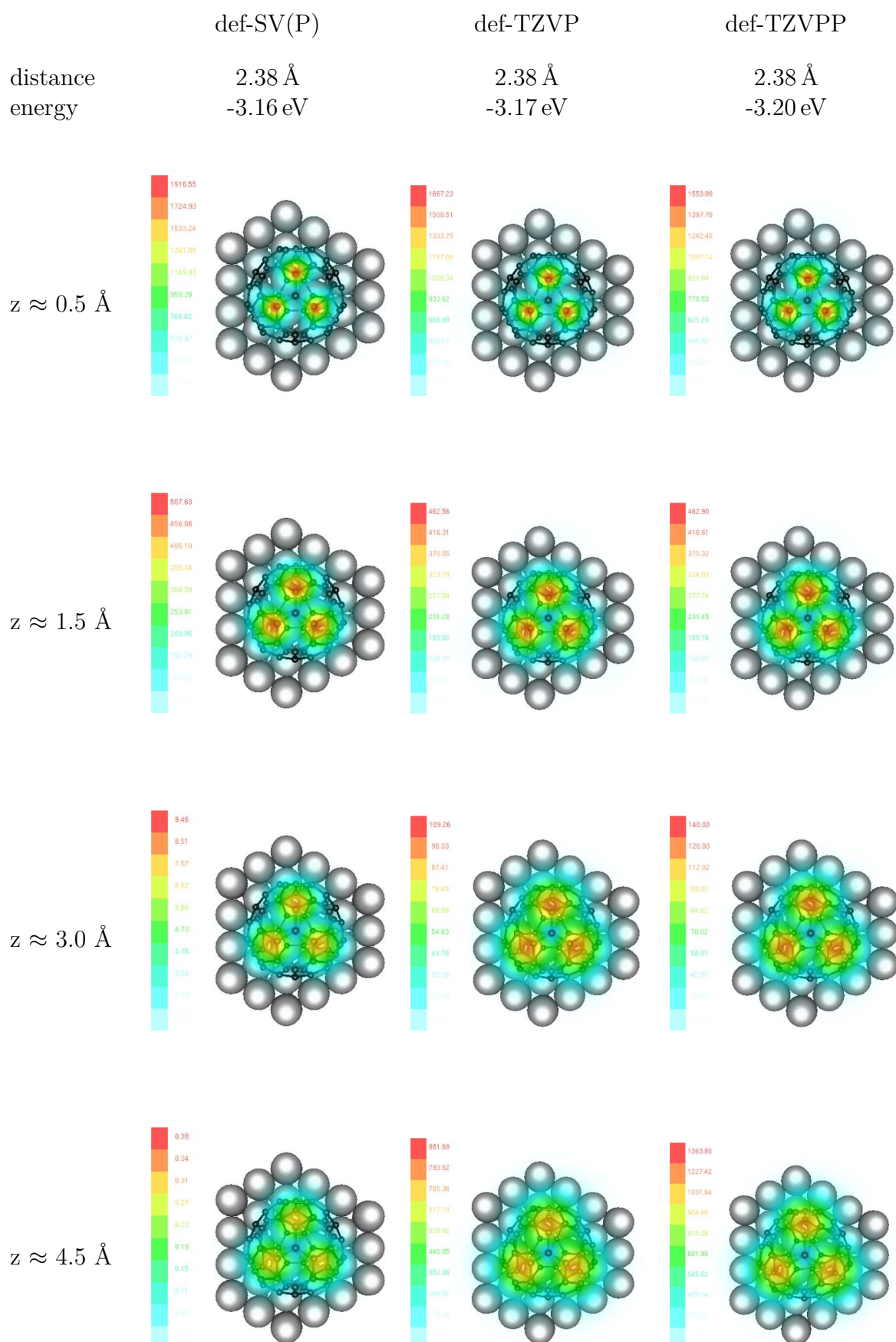
**C<sub>58</sub>: C<sub>3v</sub> Symmetry, H4a after Relaxation**

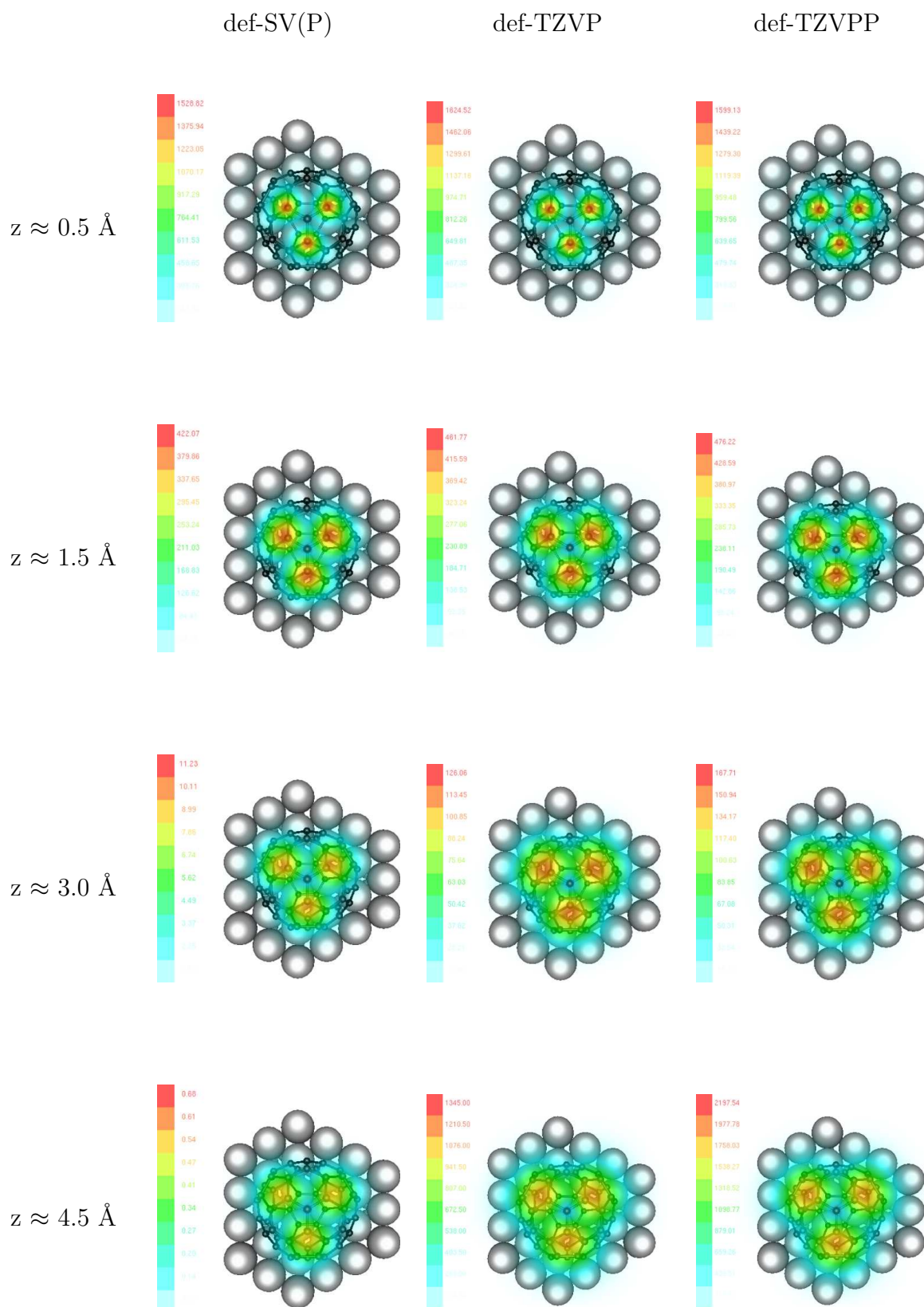
**C<sub>58</sub>: C<sub>3v</sub> Symmetry, H4b without Relaxation, 2.54 Å, -2.35 eV**

**C<sub>58</sub>: C<sub>3v</sub> Symmetry, H4b after Relaxation**

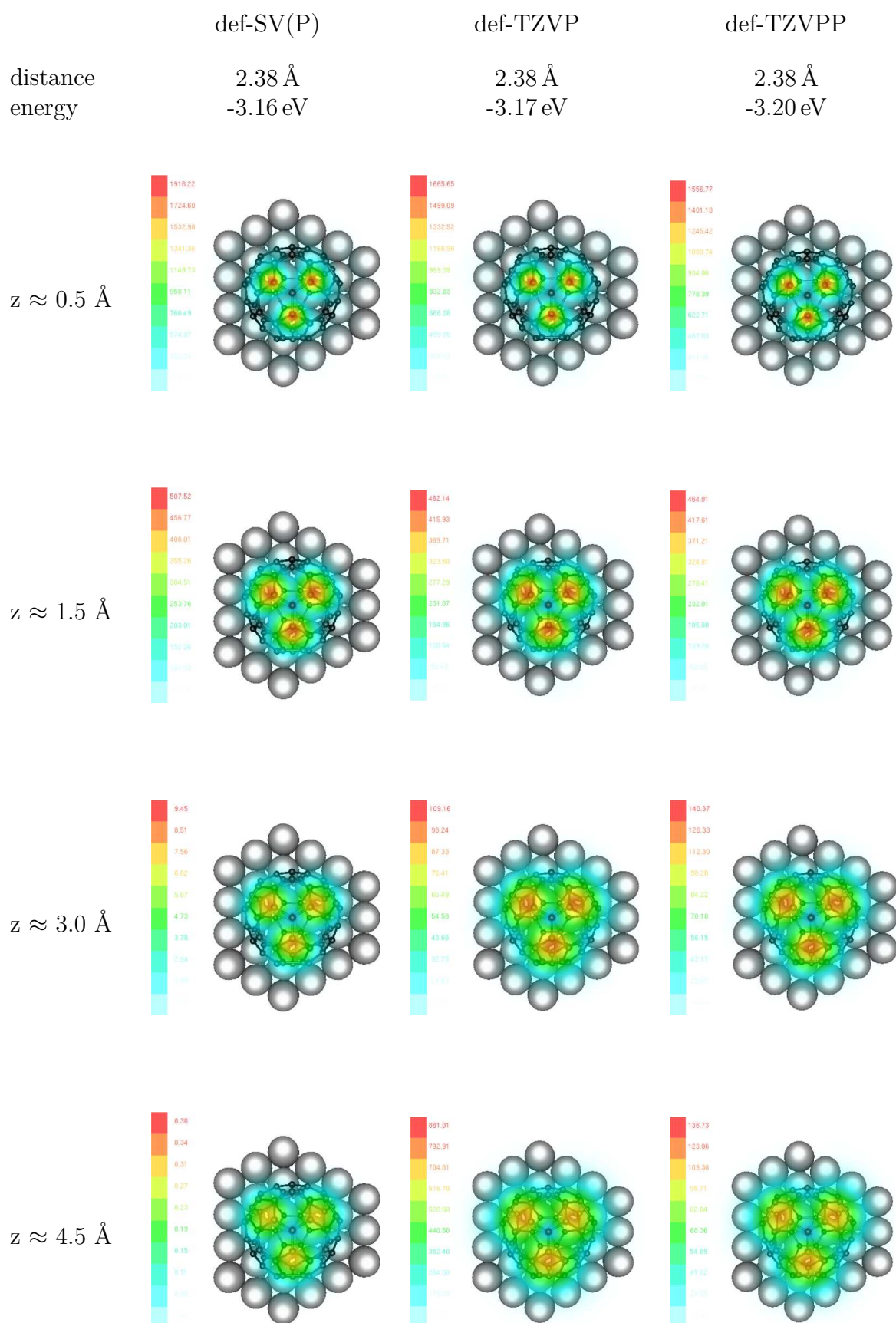
**C<sub>58</sub>: C<sub>3v</sub> Symmetry, H5a without Relaxation, 2.49 Å, -2.32 eV**

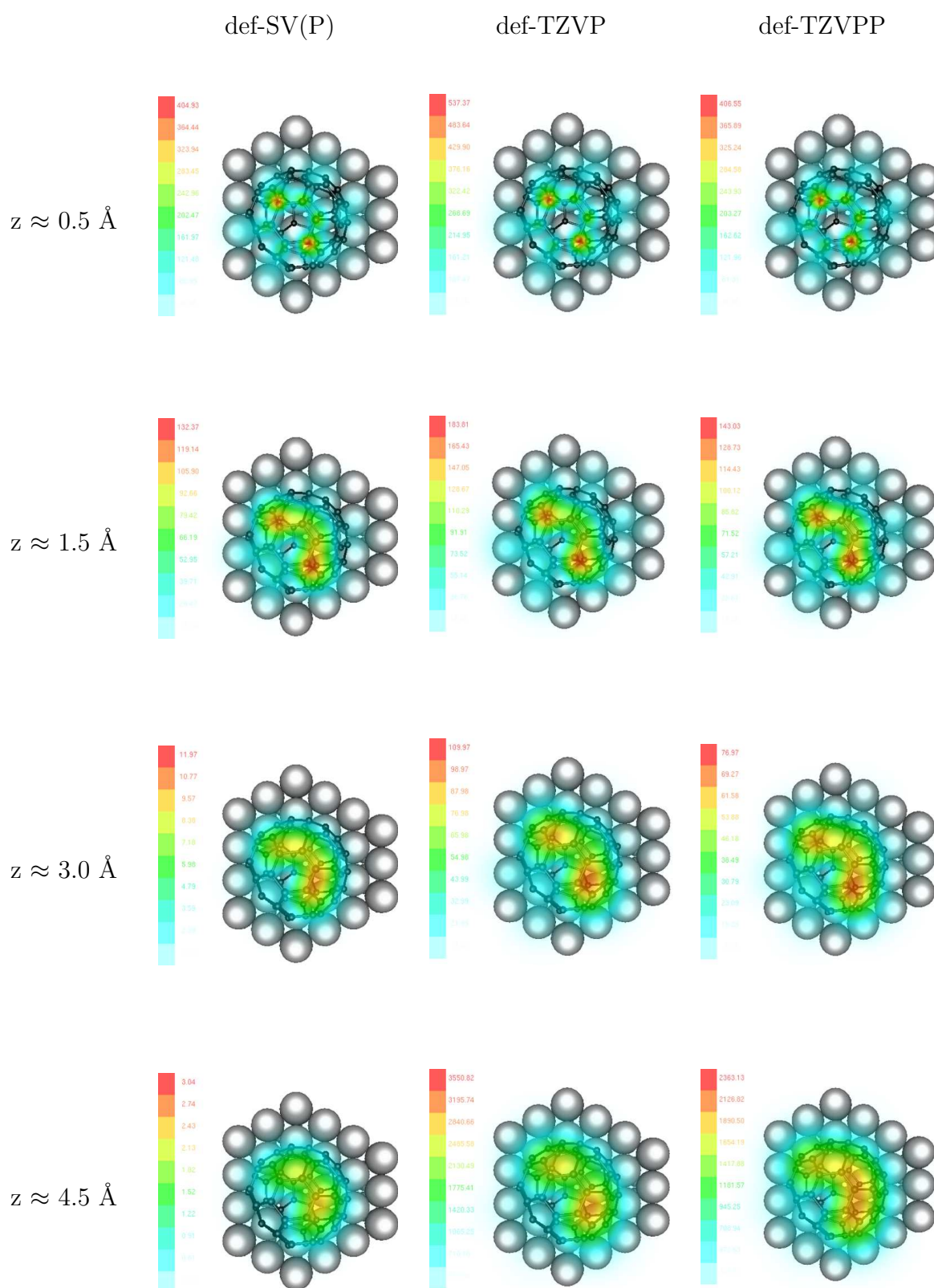
### $C_{58}$ : $C_{3v}$ Symmetry, H5a after Relaxation

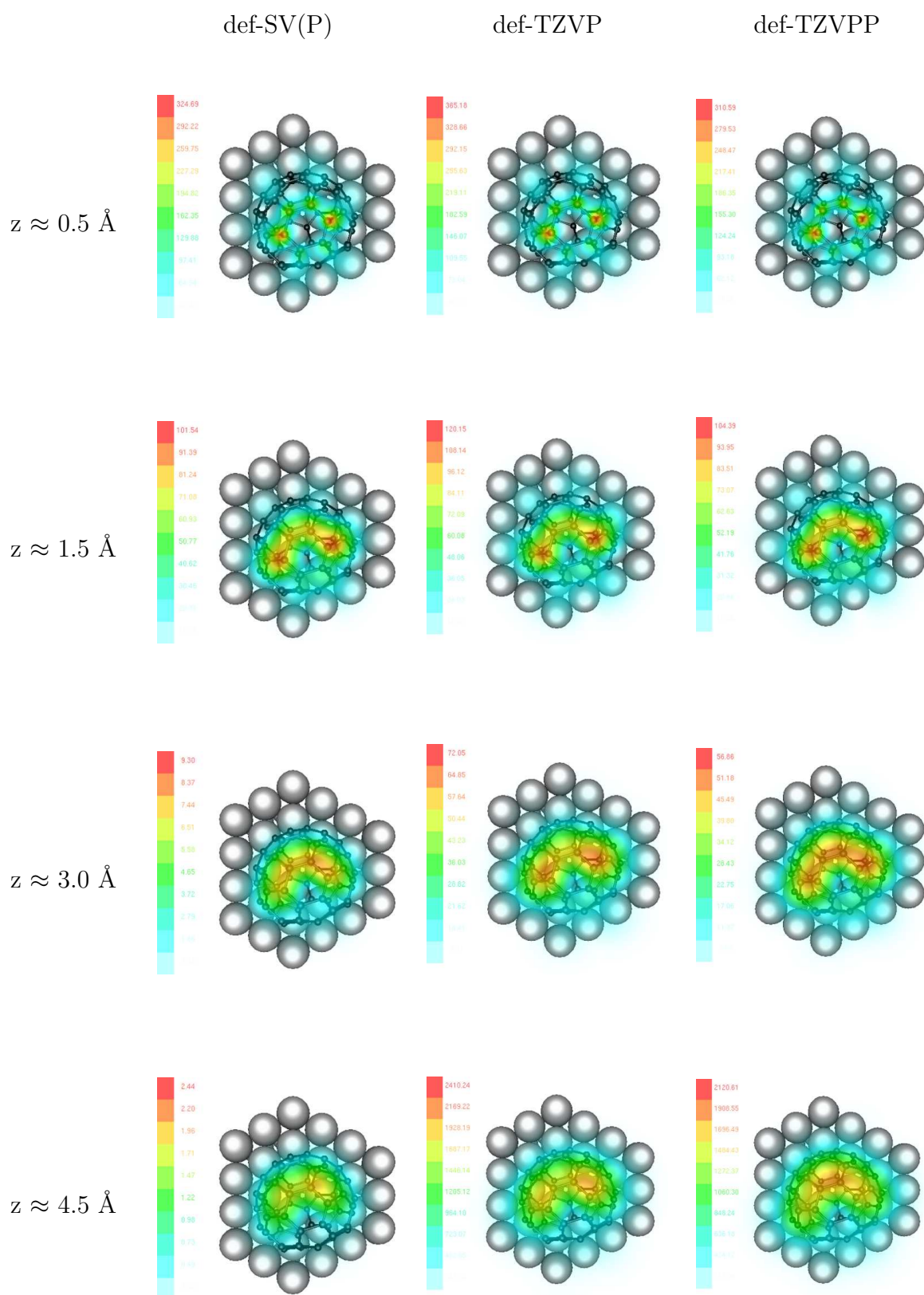


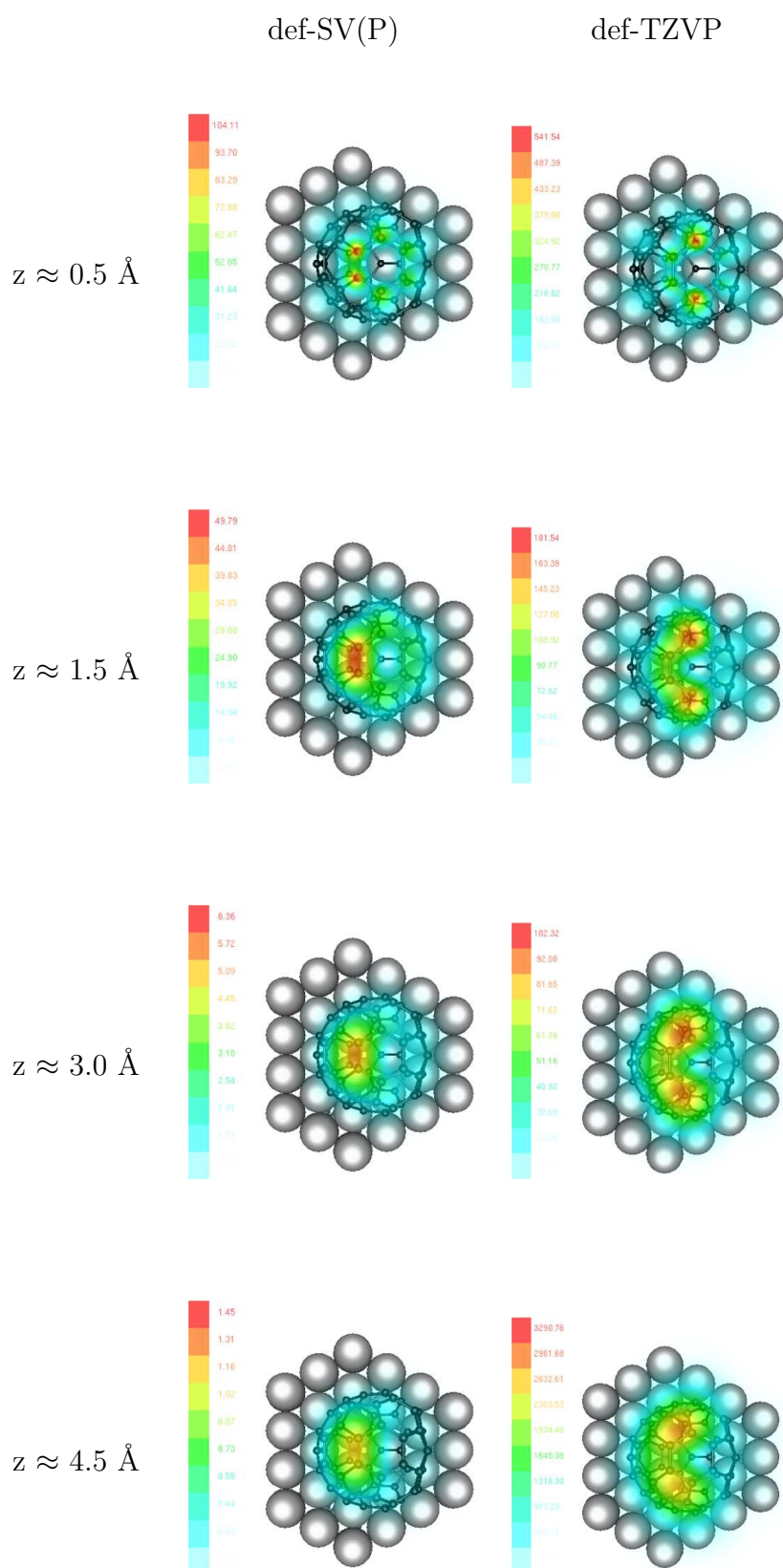
**C<sub>58</sub>: C<sub>3v</sub> Symmetry, H5b without Relaxation, 2.49 Å, -2.32 eV**

### $C_{58}$ : $C_{3v}$ Symmetry, H5b after Relaxation

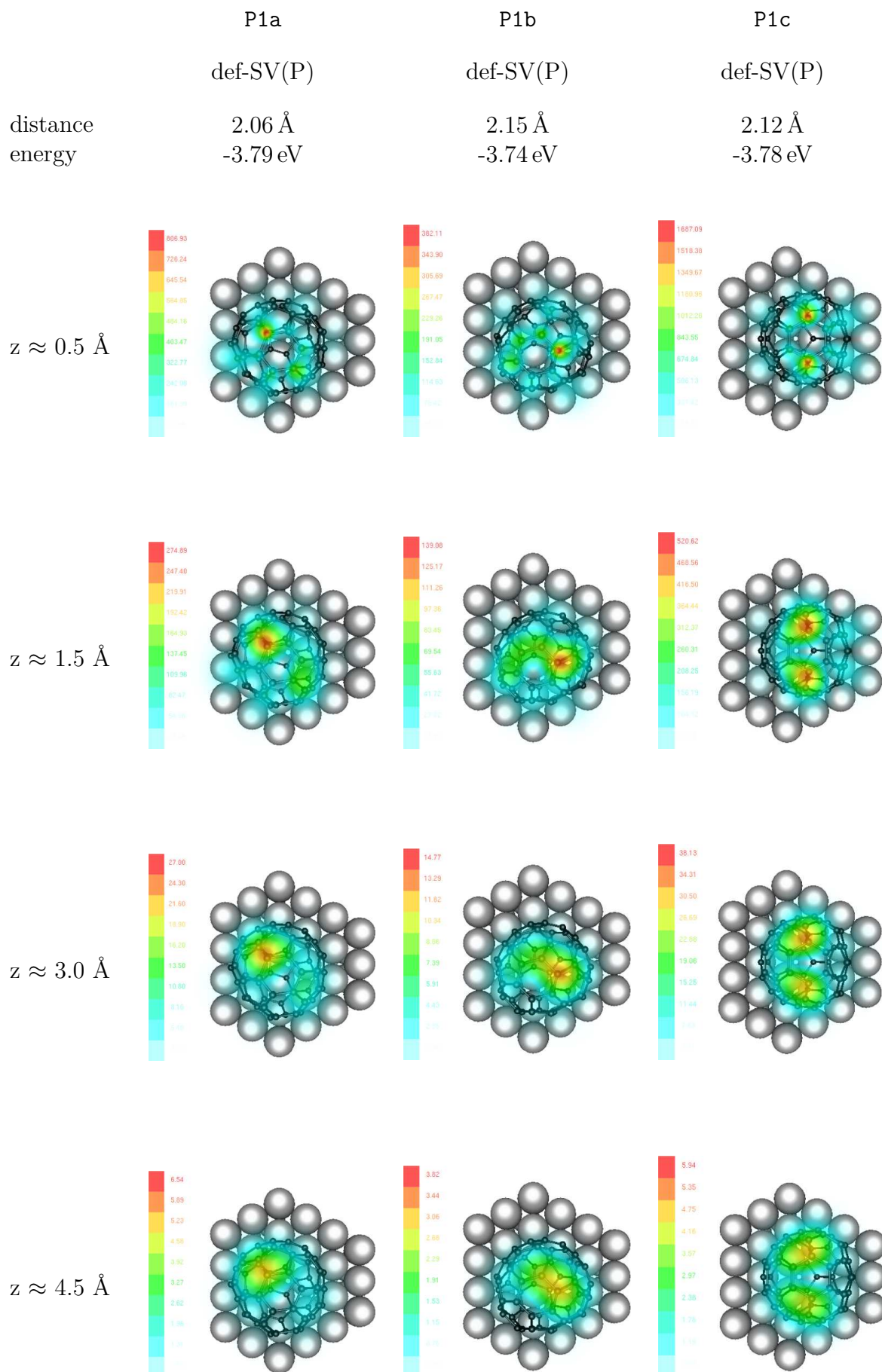


**C<sub>58</sub>: C<sub>3v</sub> Symmetry, P1a without Relaxation, 2.33 Å, -2.81 eV**

**C<sub>58</sub>: C<sub>3v</sub> Symmetry, P1b without Relaxation, 2.33 Å, -2.81 eV**

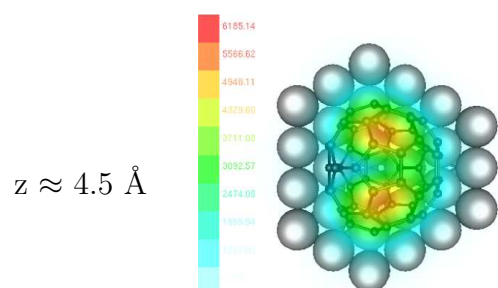
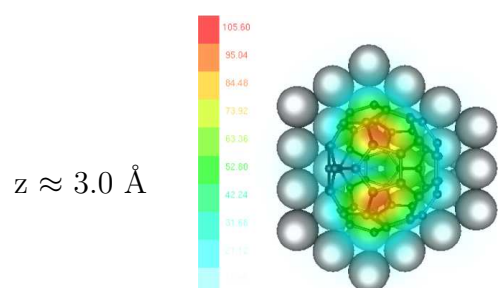
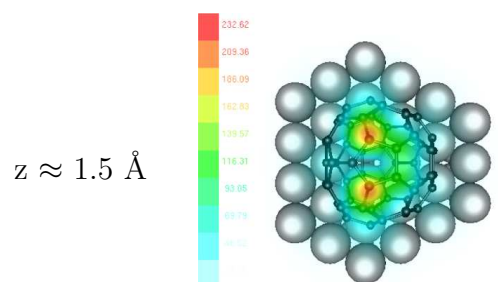
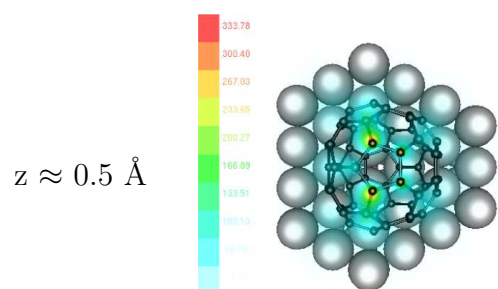
**C<sub>58</sub>: C<sub>3v</sub> Symmetry, P1c without Relaxation, 2.33 Å, -2.81 eV**

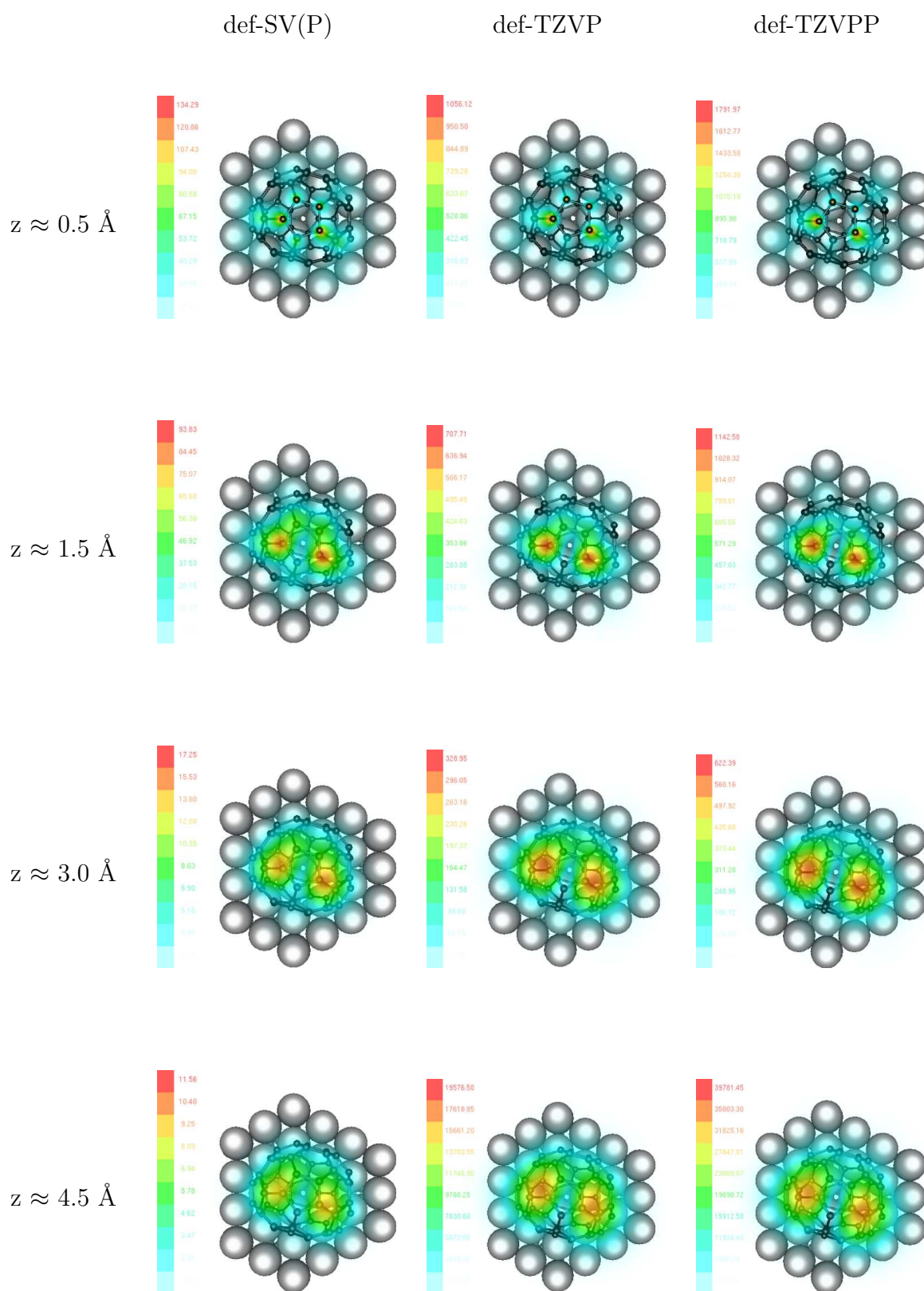
### $C_{58}$ : $C_{3v}$ Symmetry, P1a, P1b and P1c after Relaxation

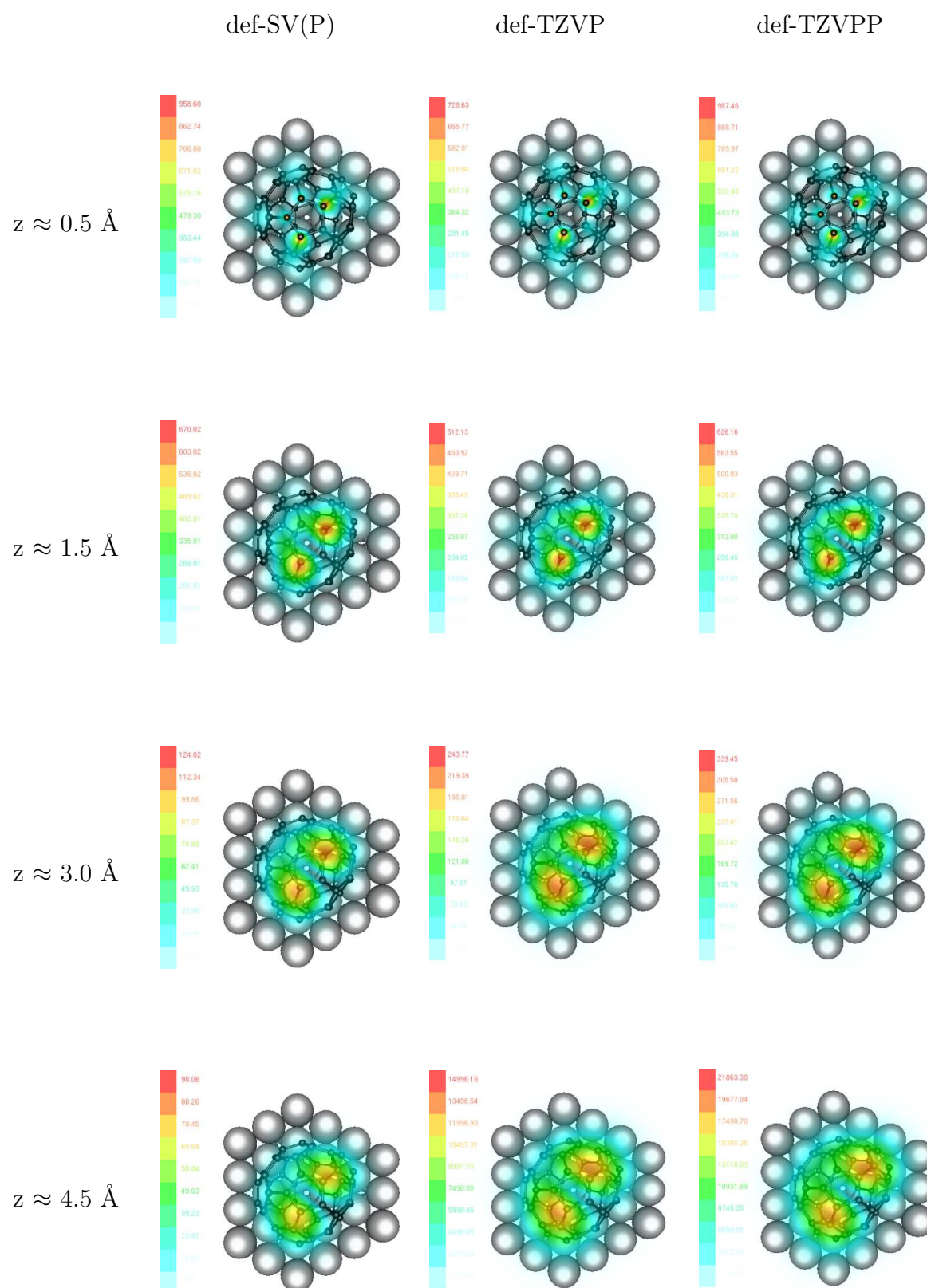


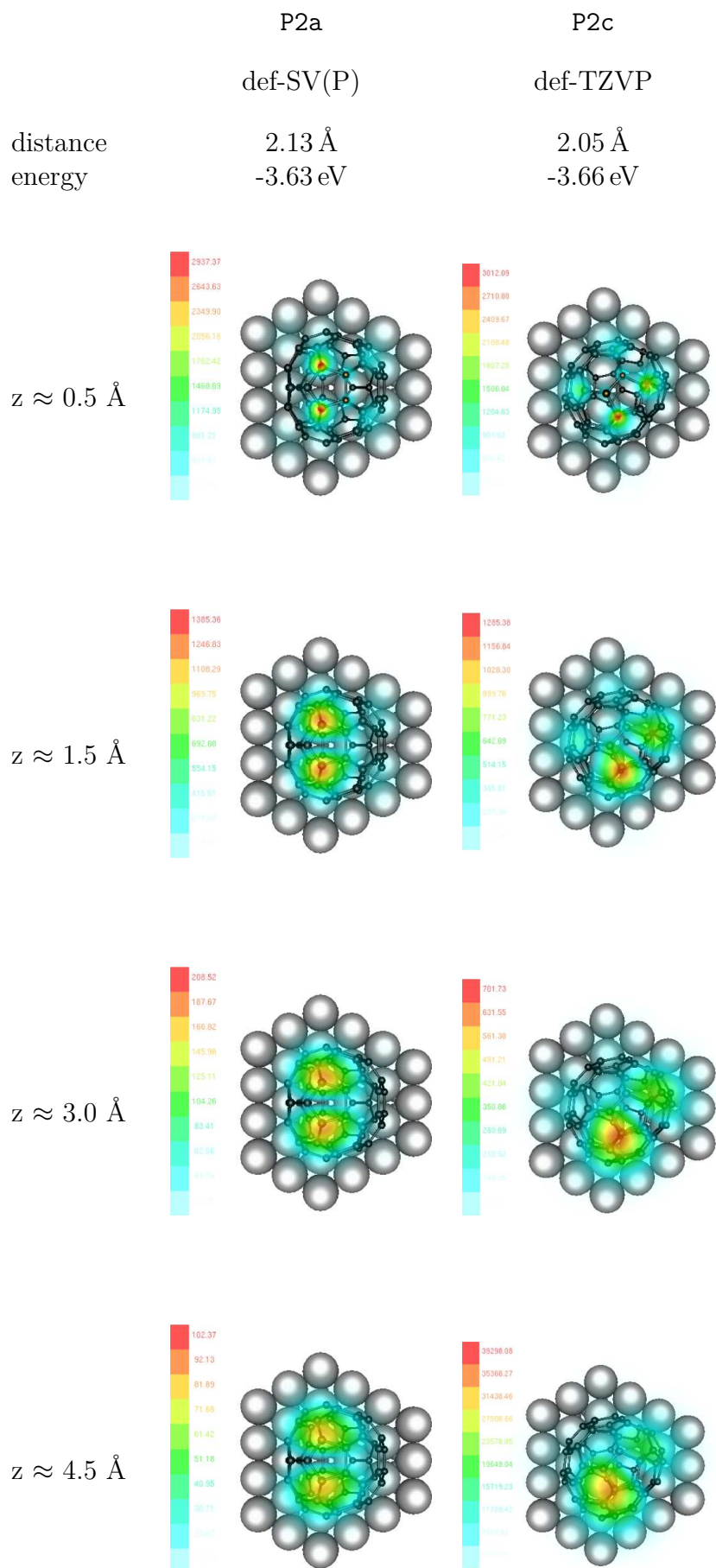
**C<sub>58</sub>: C<sub>3v</sub> Symmetry, P2a without Relaxation, 2.38 Å, -2.63 eV**

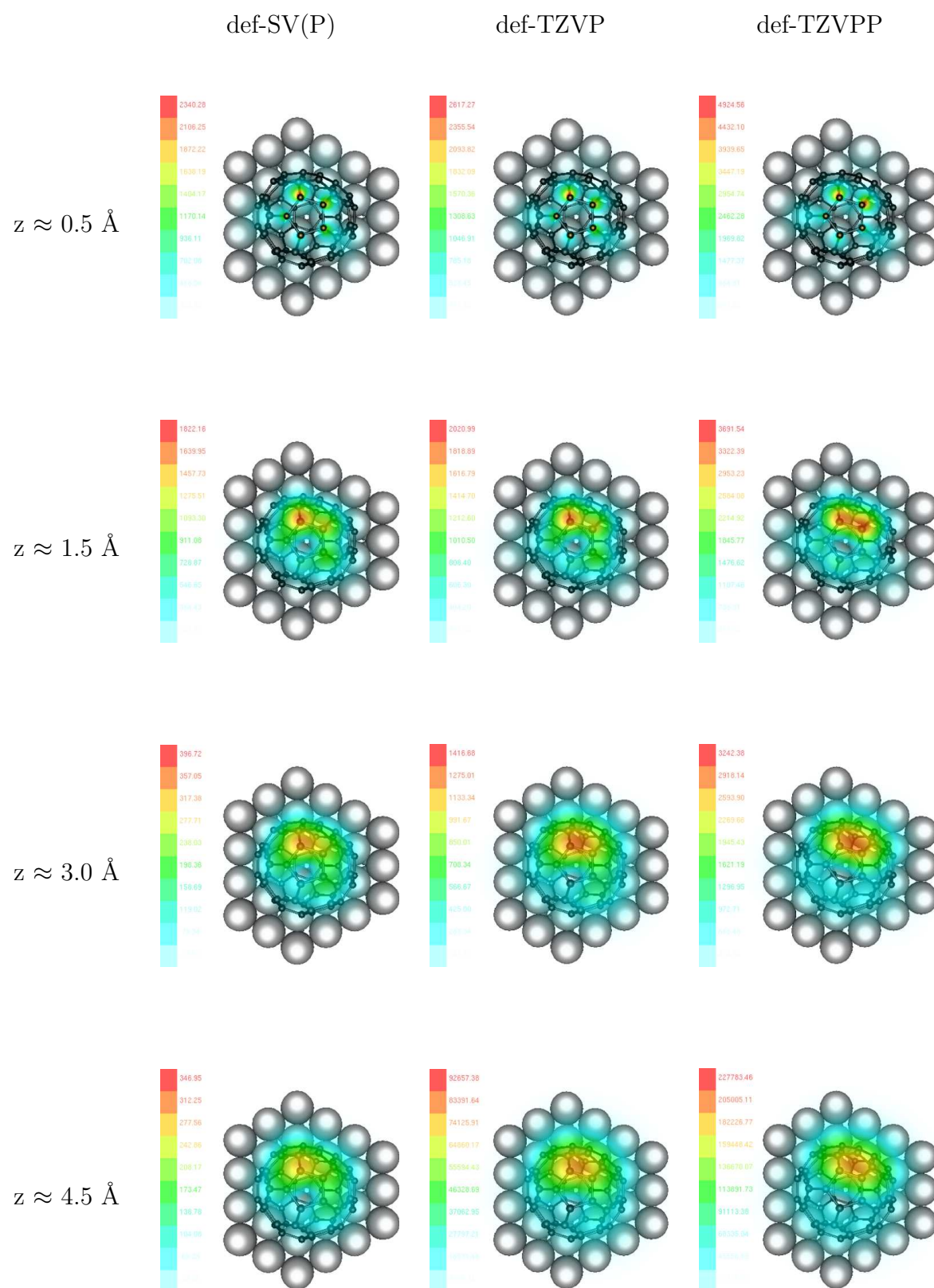
def-SV(P)

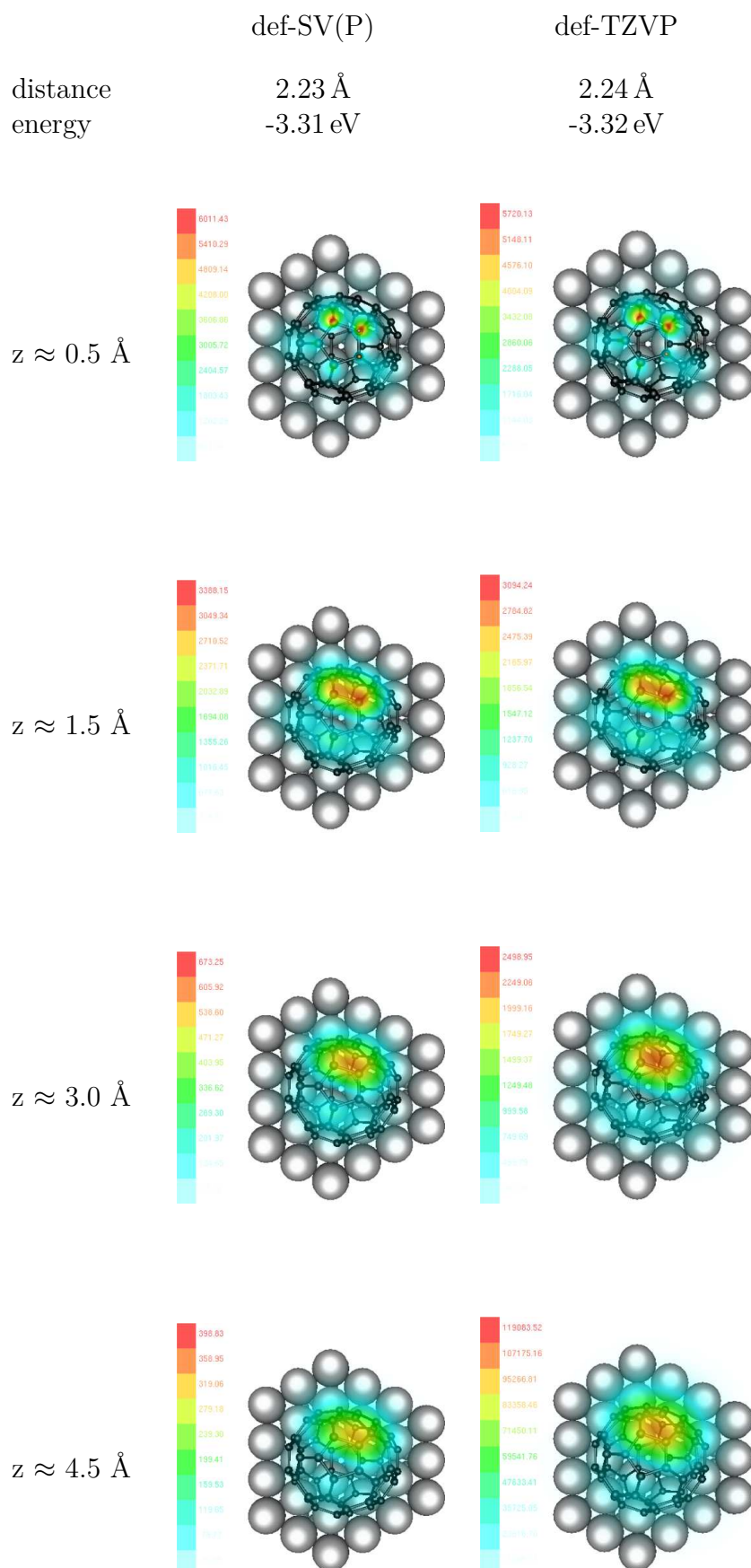


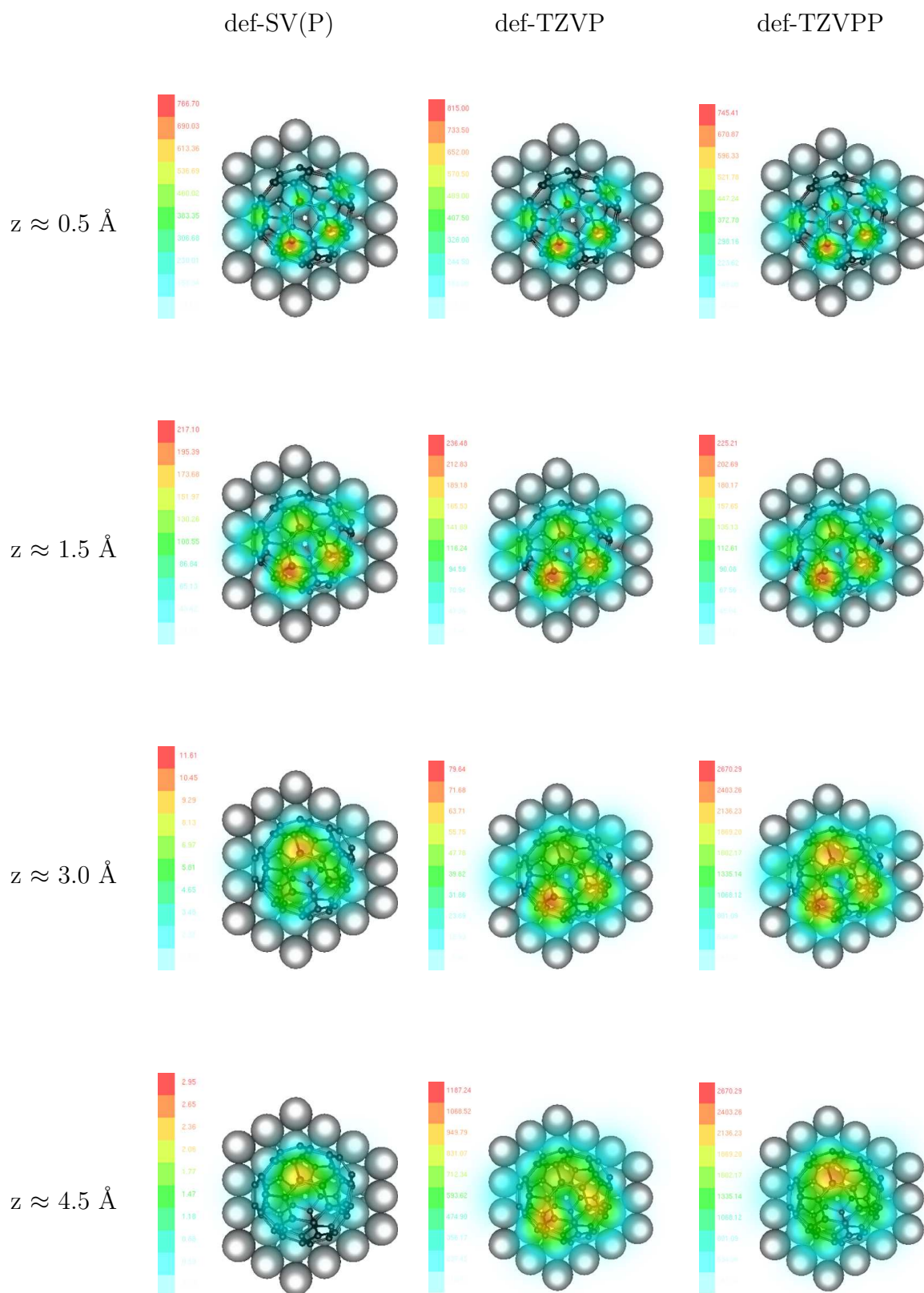
**C<sub>58</sub>: C<sub>3v</sub> Symmetry, P2b without Relaxation, 2.38 Å, -2.50 eV**

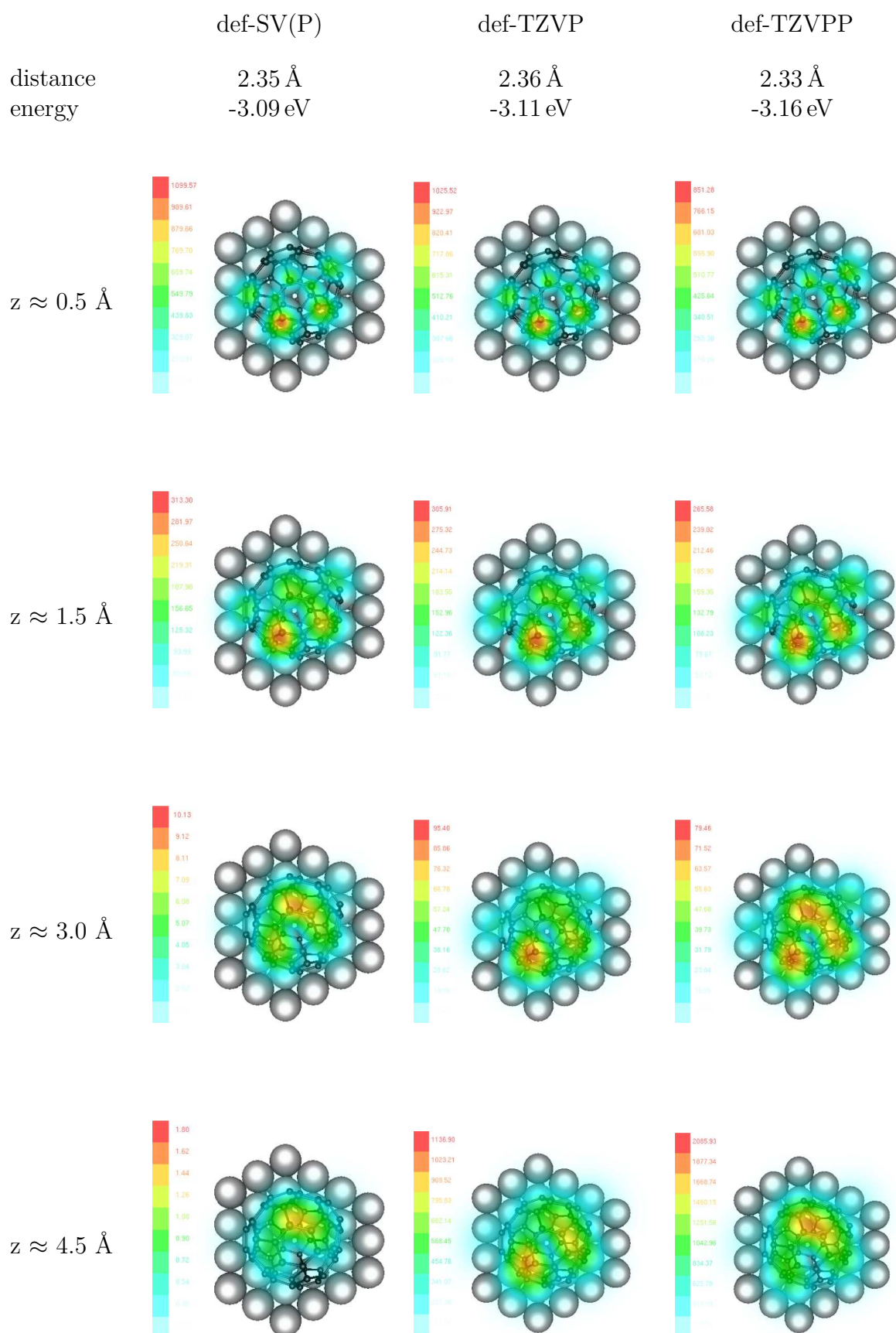
**C<sub>58</sub>: C<sub>3v</sub> Symmetry, P2c without Relaxation, 2.38 Å, -2.60 eV**

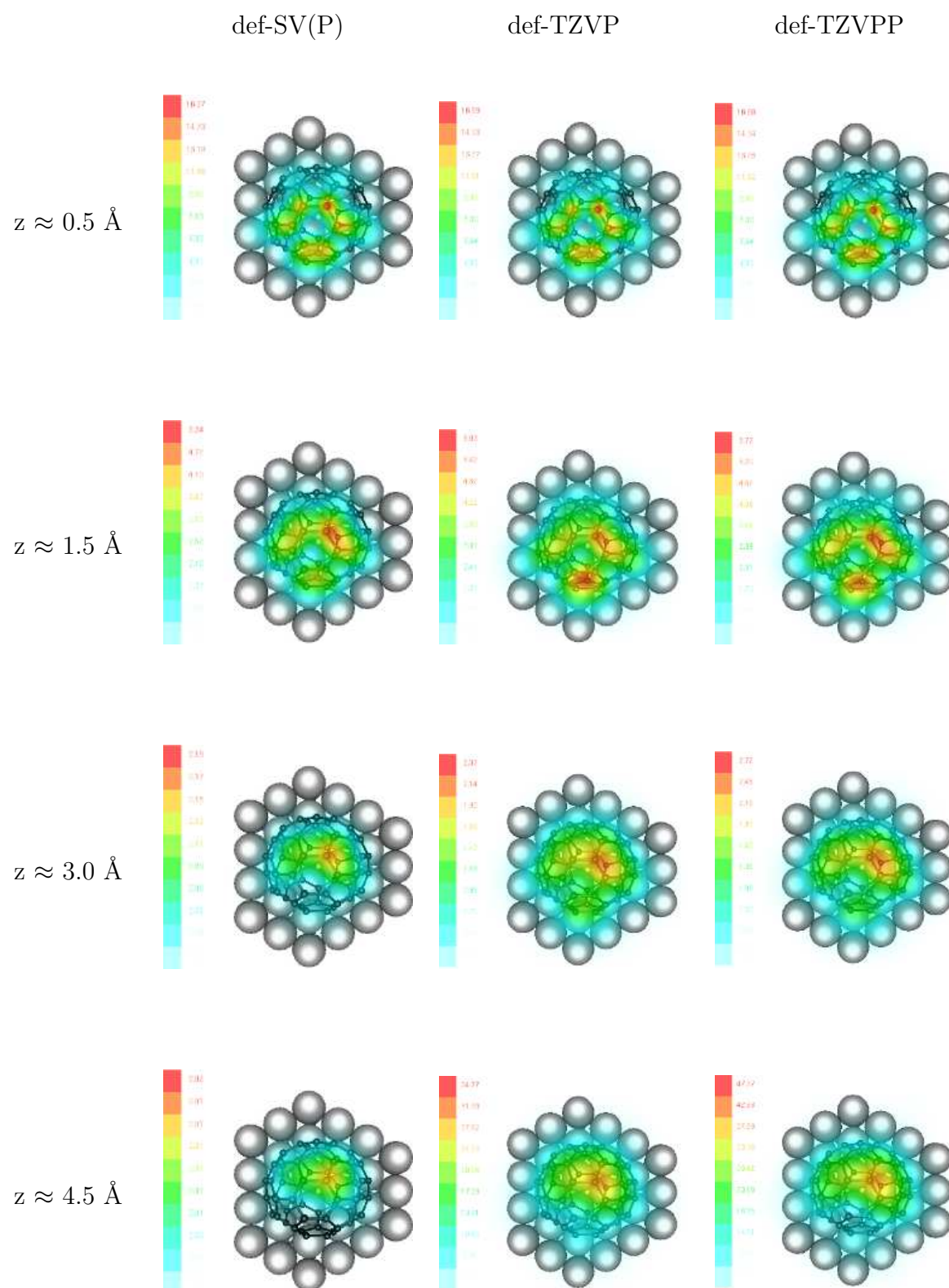
**C<sub>58</sub>: C<sub>3v</sub> Symmetry, P2a and P2c after Relaxation**

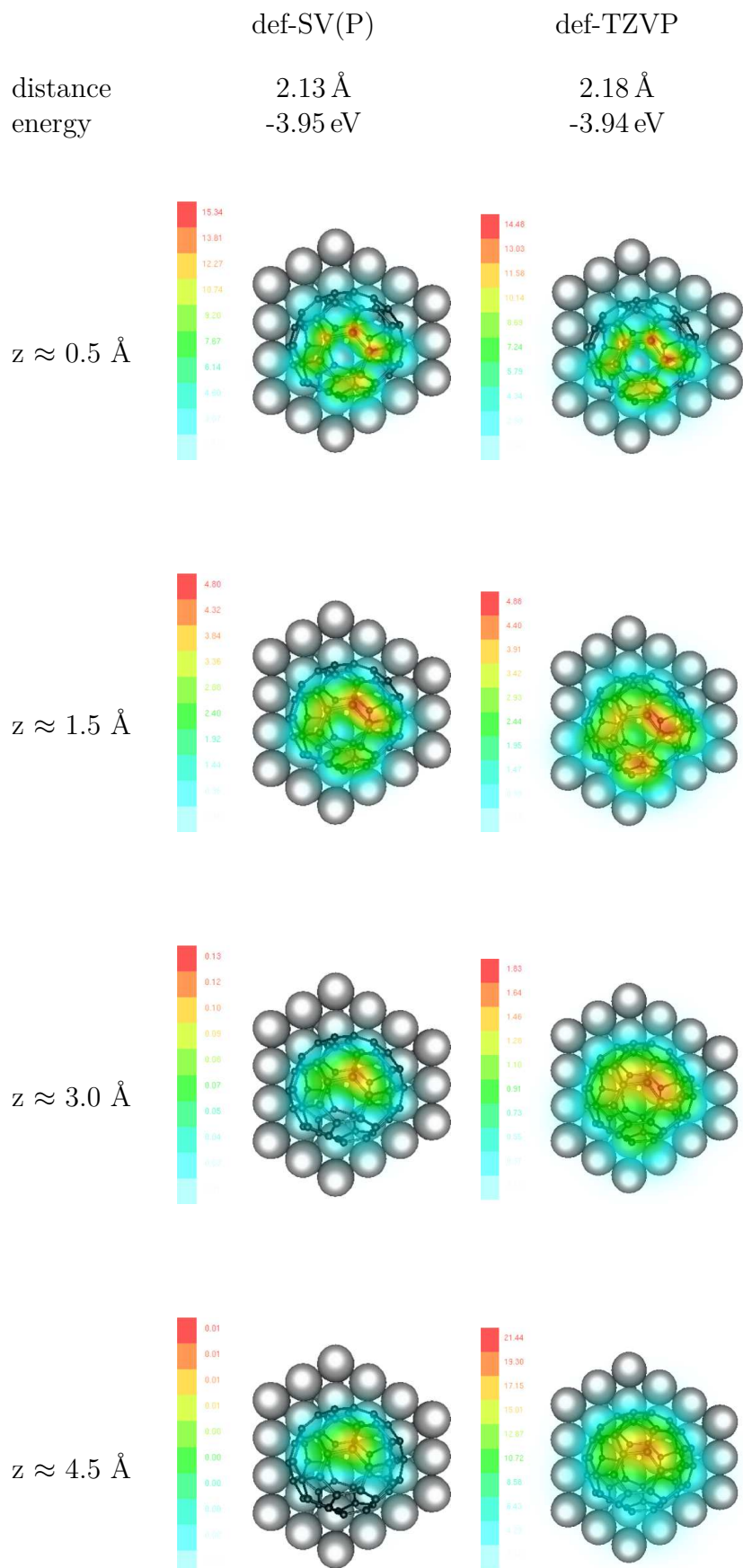
**C<sub>58</sub>: C<sub>3v</sub> Symmetry, P3a without Relaxation, 2.43 Å, -2.47 eV**

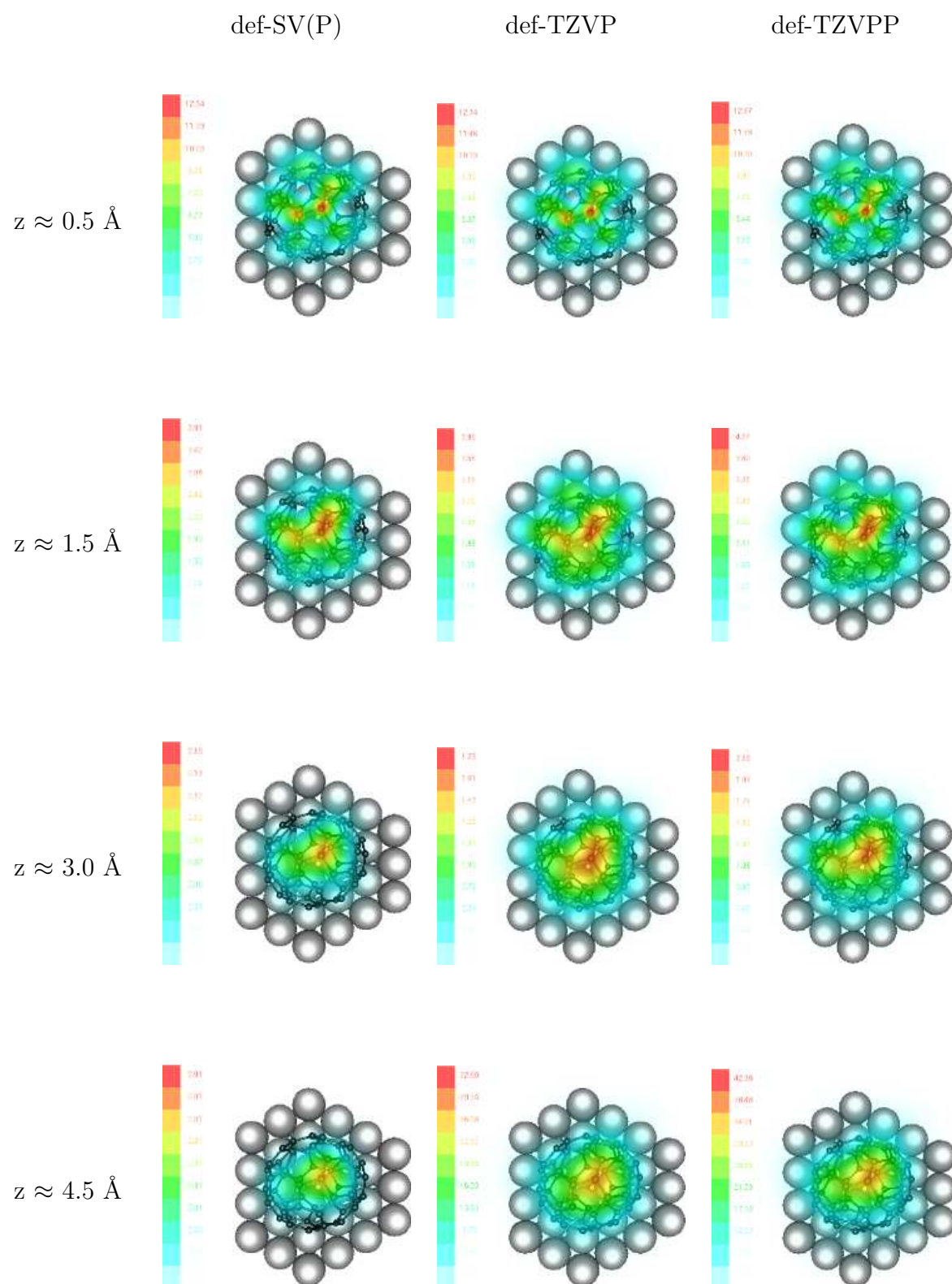
**C<sub>58</sub>: C<sub>3v</sub> Symmetry, P3a after Relaxation**

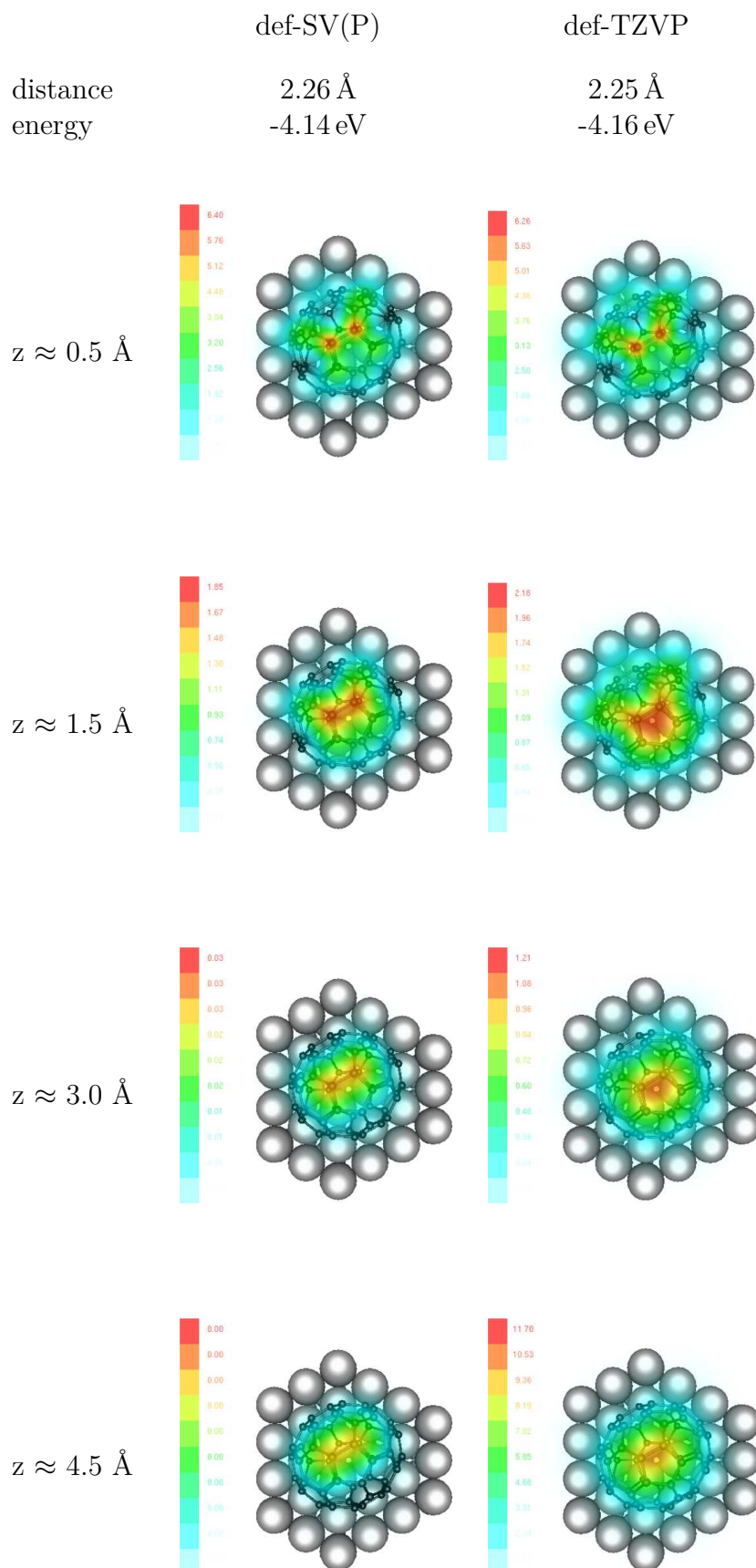
**C<sub>58</sub>: C<sub>3v</sub> Symmetry, P4a without Relaxation, 2.49 Å, -2.35 eV**

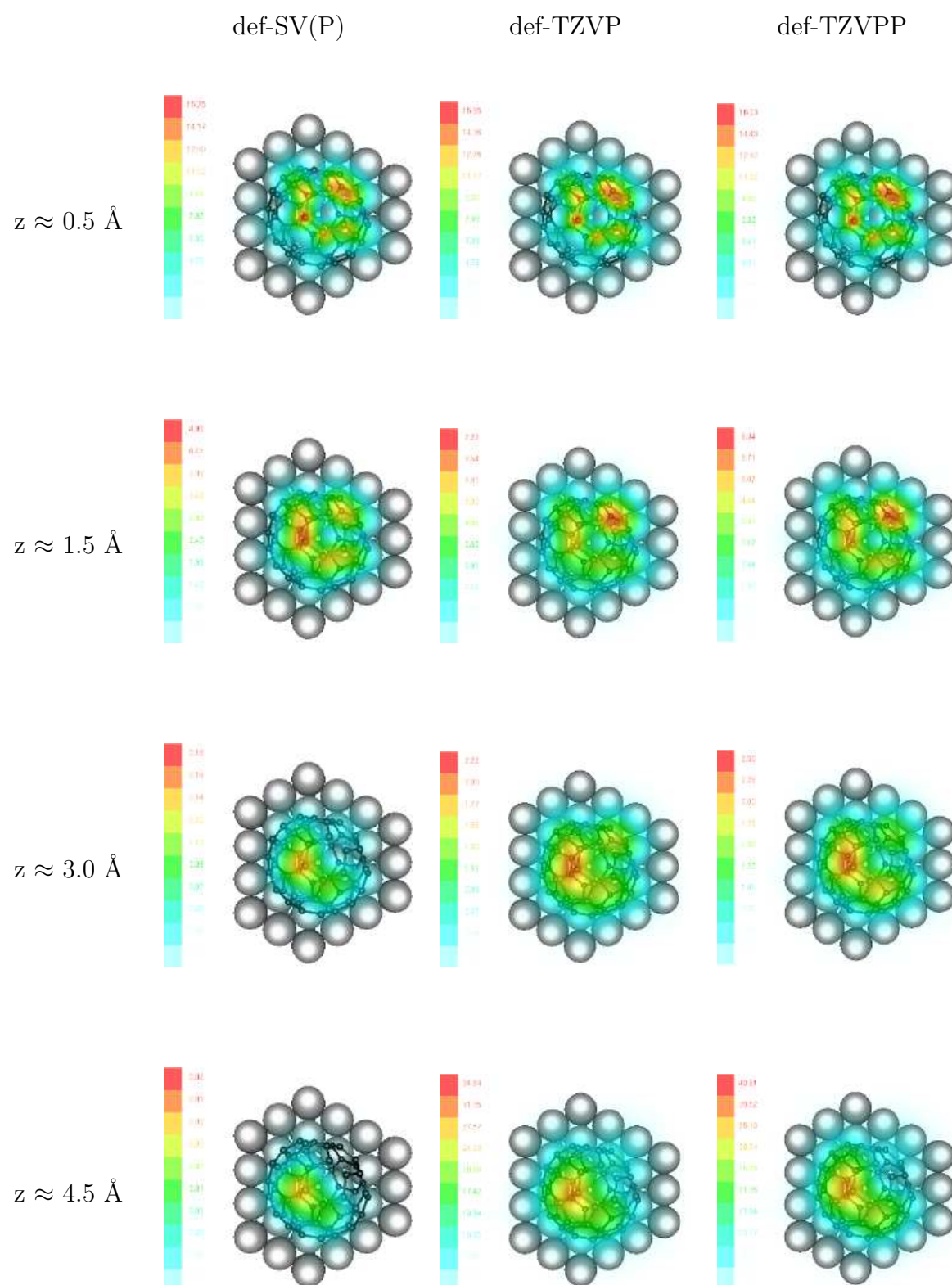
**C<sub>58</sub>: C<sub>3v</sub> Symmetry, P4a after Relaxation**

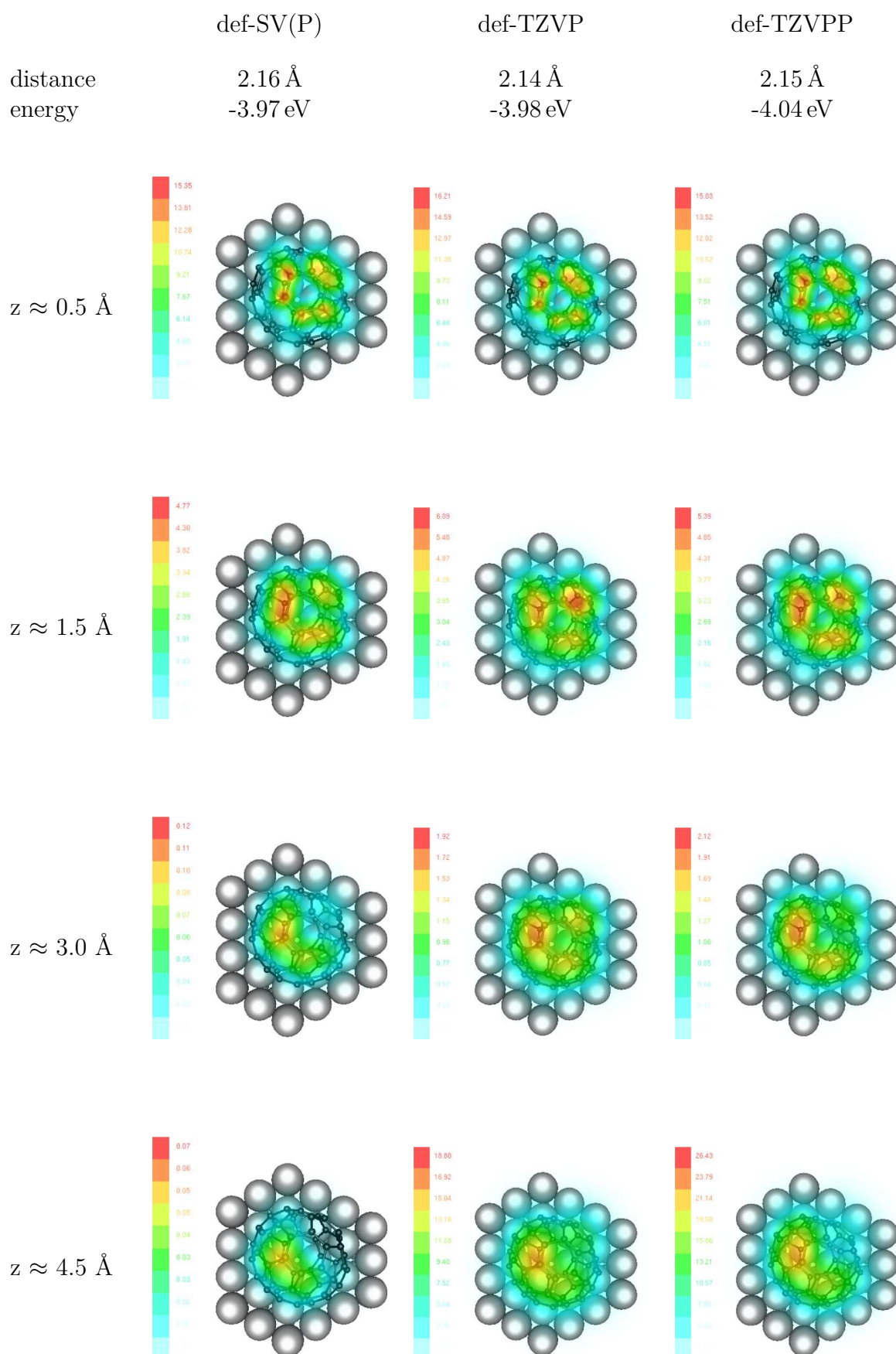
**C<sub>58</sub>: C<sub>s</sub> Symmetry, Hept1 without Relaxation, 2.54 Å, -2.83 eV**

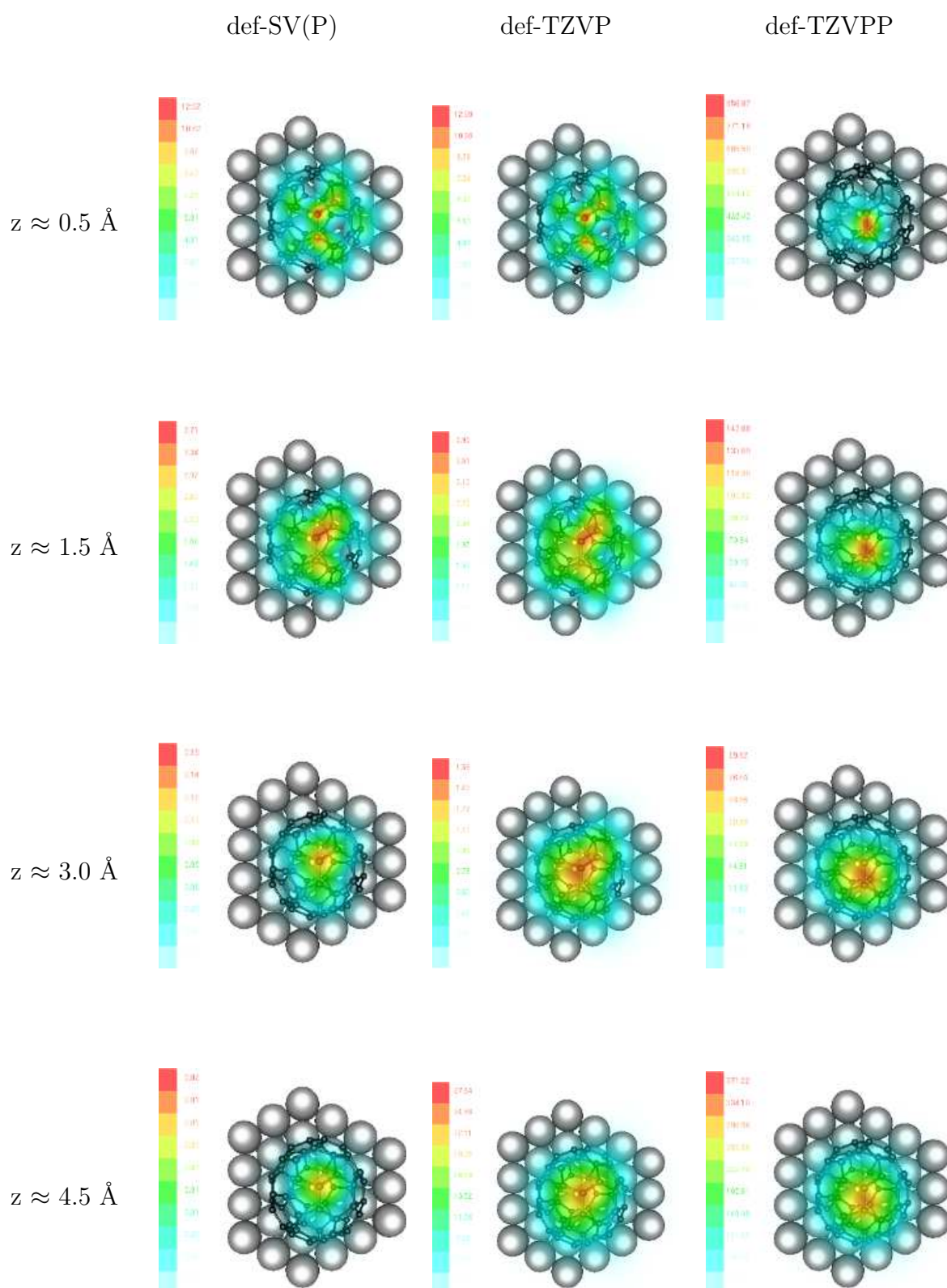
**C<sub>58</sub>: C<sub>s</sub> Symmetry, Hept1 after Relaxation**

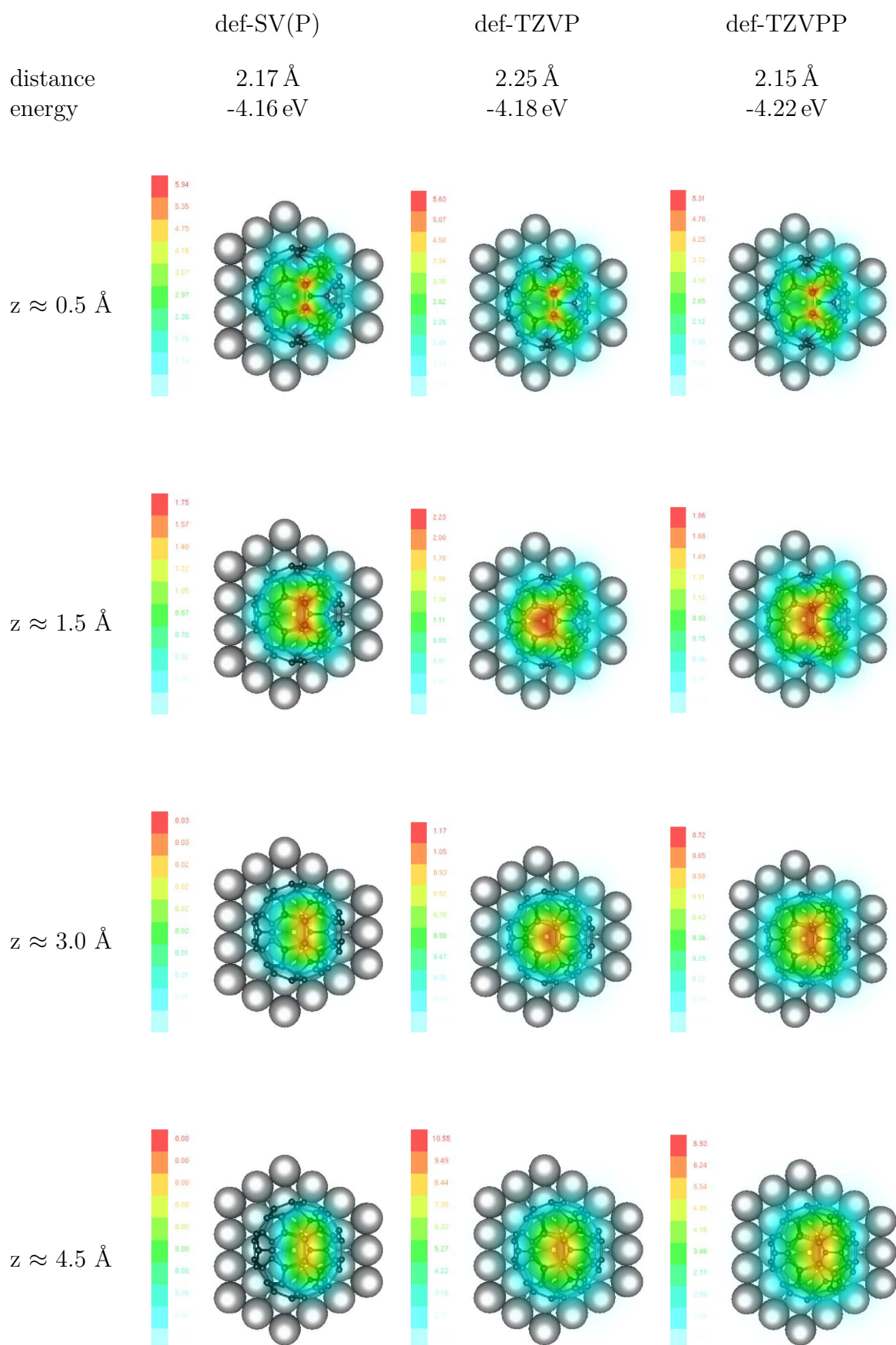
**C<sub>58</sub>: C<sub>s</sub> Symmetry, Hept2 without Relaxation, 2.59 Å, -2.77 eV**

**C<sub>58</sub>: C<sub>s</sub> Symmetry, Hept2 after Relaxation**

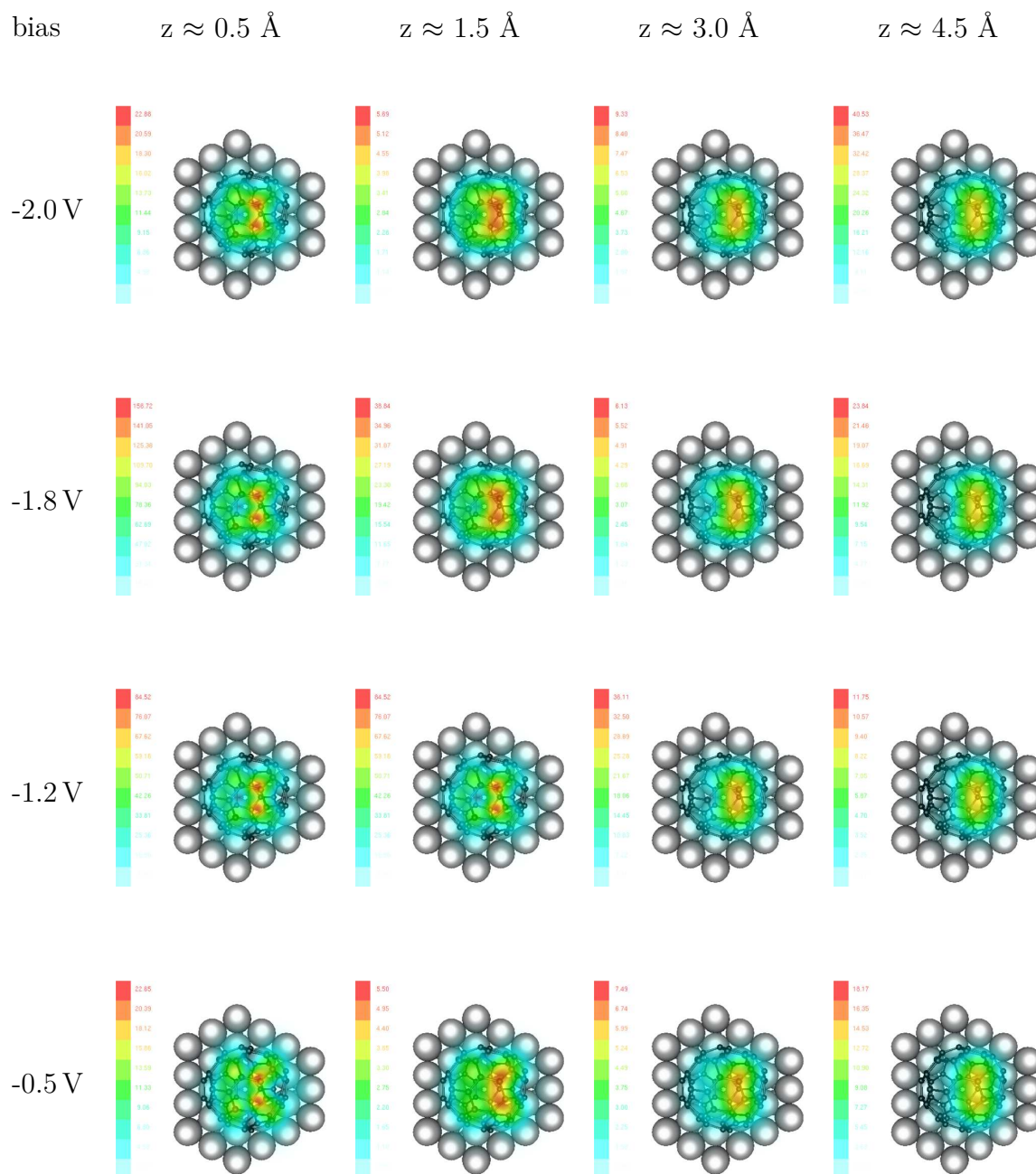
**C<sub>58</sub>: C<sub>s</sub> Symmetry, Hept3 without Relaxation, 2.54 Å, -2.78 eV**

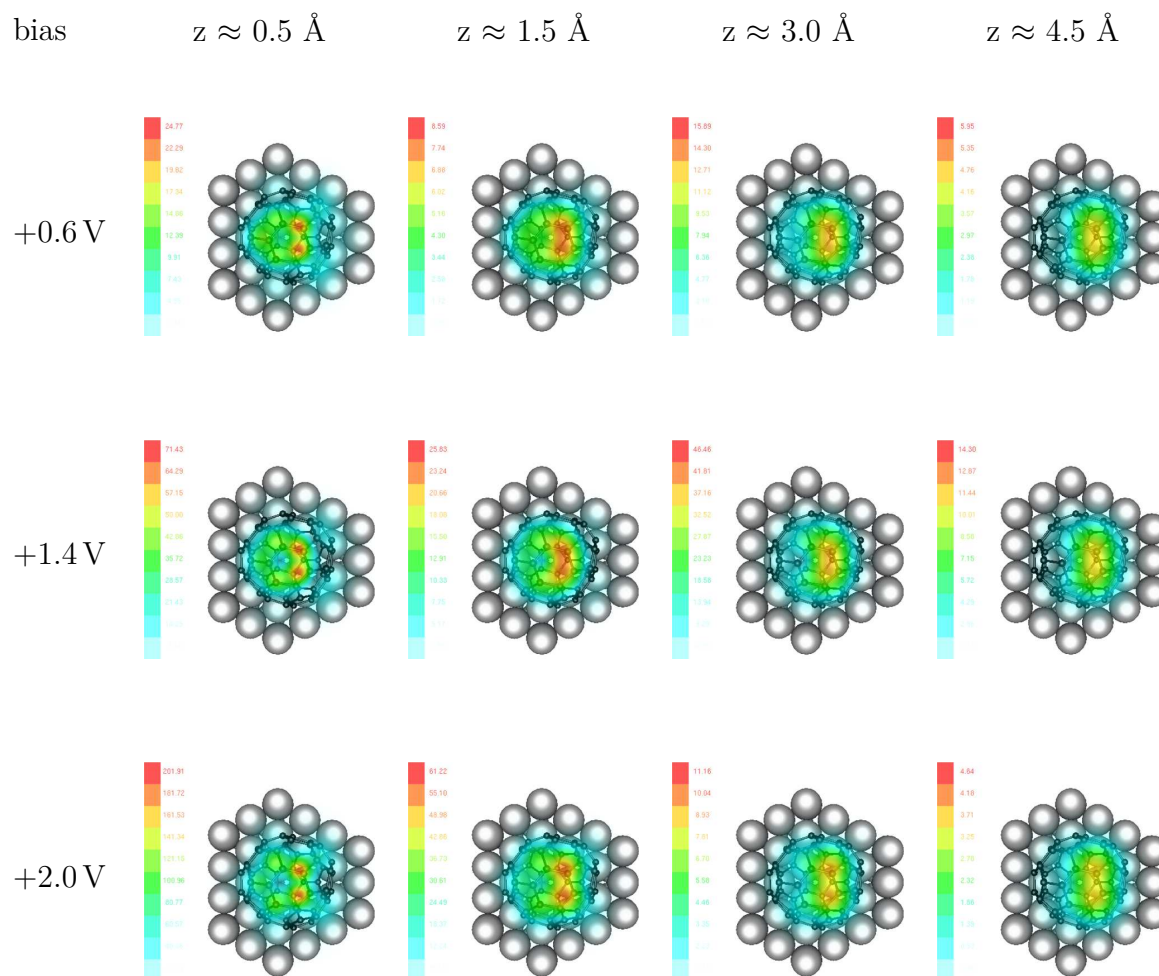
**C<sub>58</sub>: C<sub>s</sub> Symmetry, Hept3 after Relaxation**

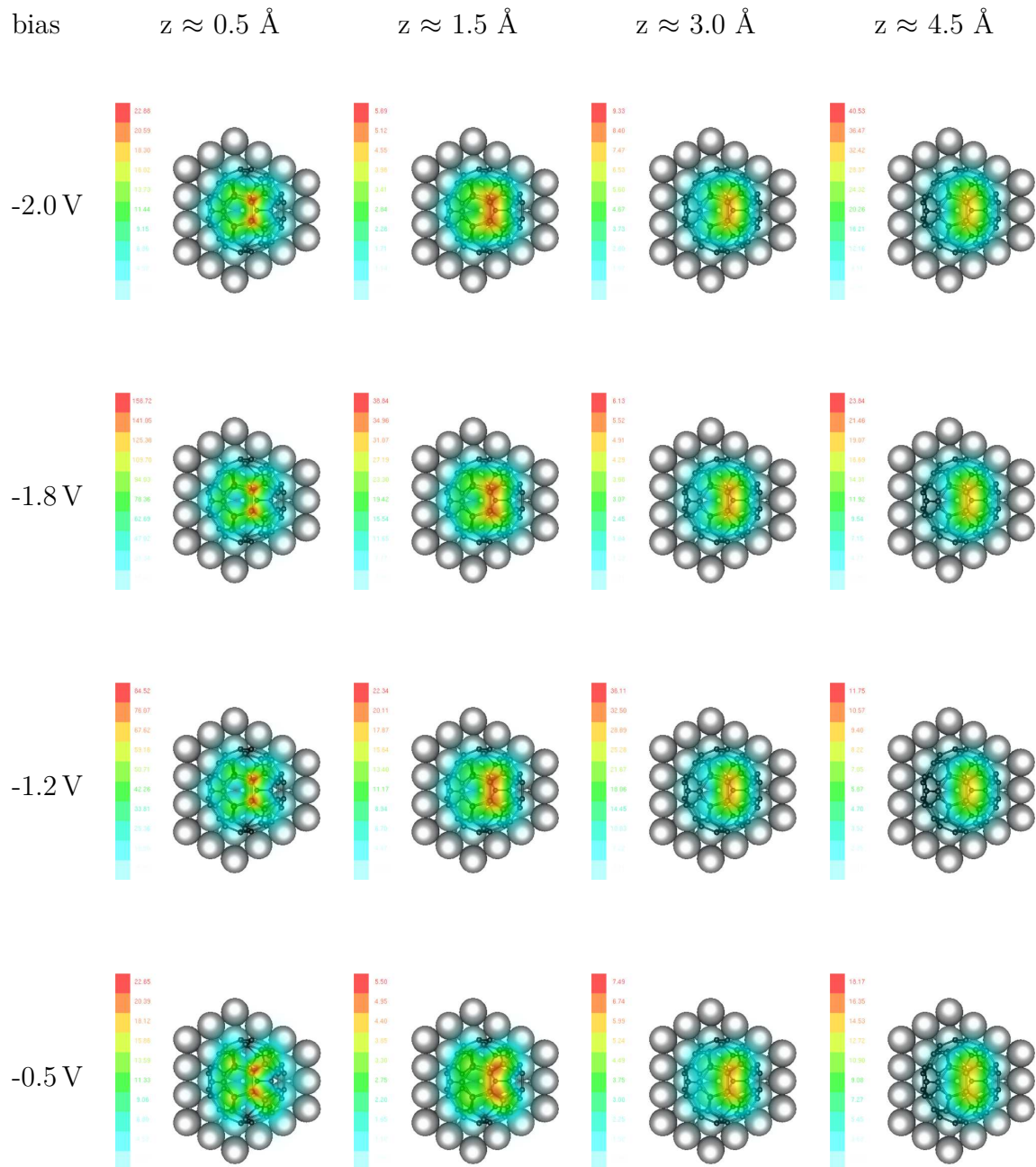
**C<sub>58</sub>: C<sub>s</sub> Symmetry, Hept4 without Relaxation, 2.59 Å, -2.82 eV**

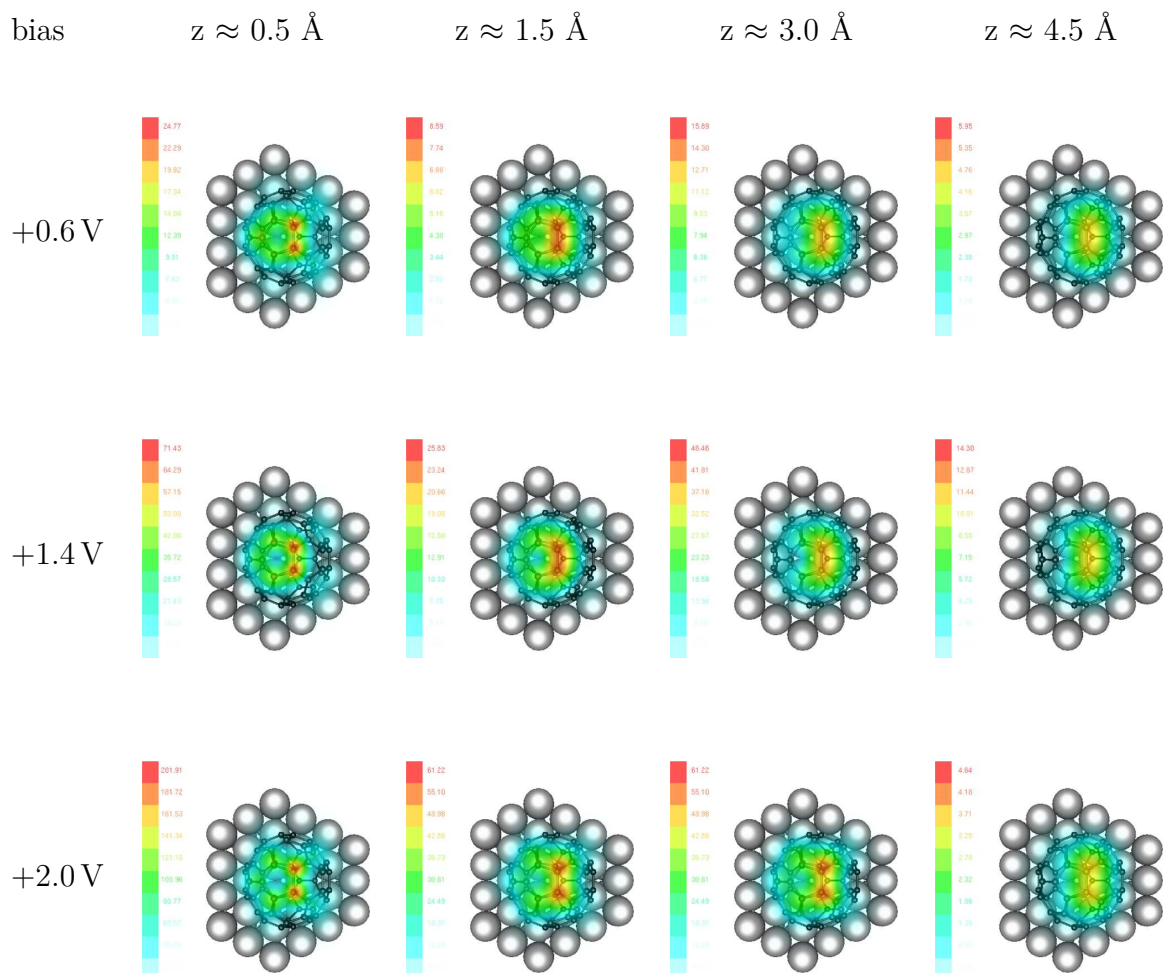
**C<sub>58</sub>: C<sub>s</sub> Symmetry, Hept4 after Relaxation**

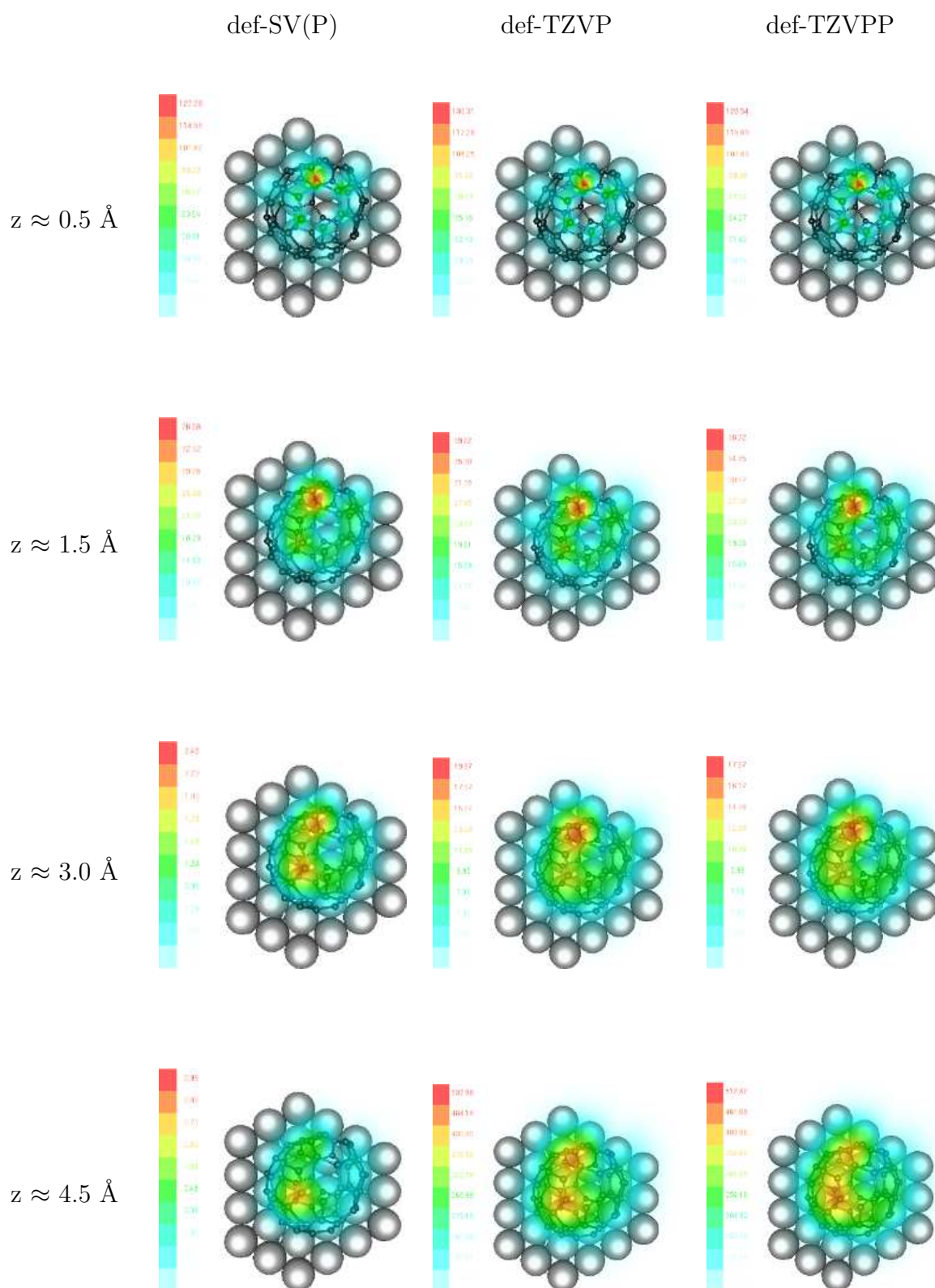
**C<sub>58</sub>: C<sub>s</sub> Symmetry, Hept4 after Relaxation, negative bias, def-SV(P)**

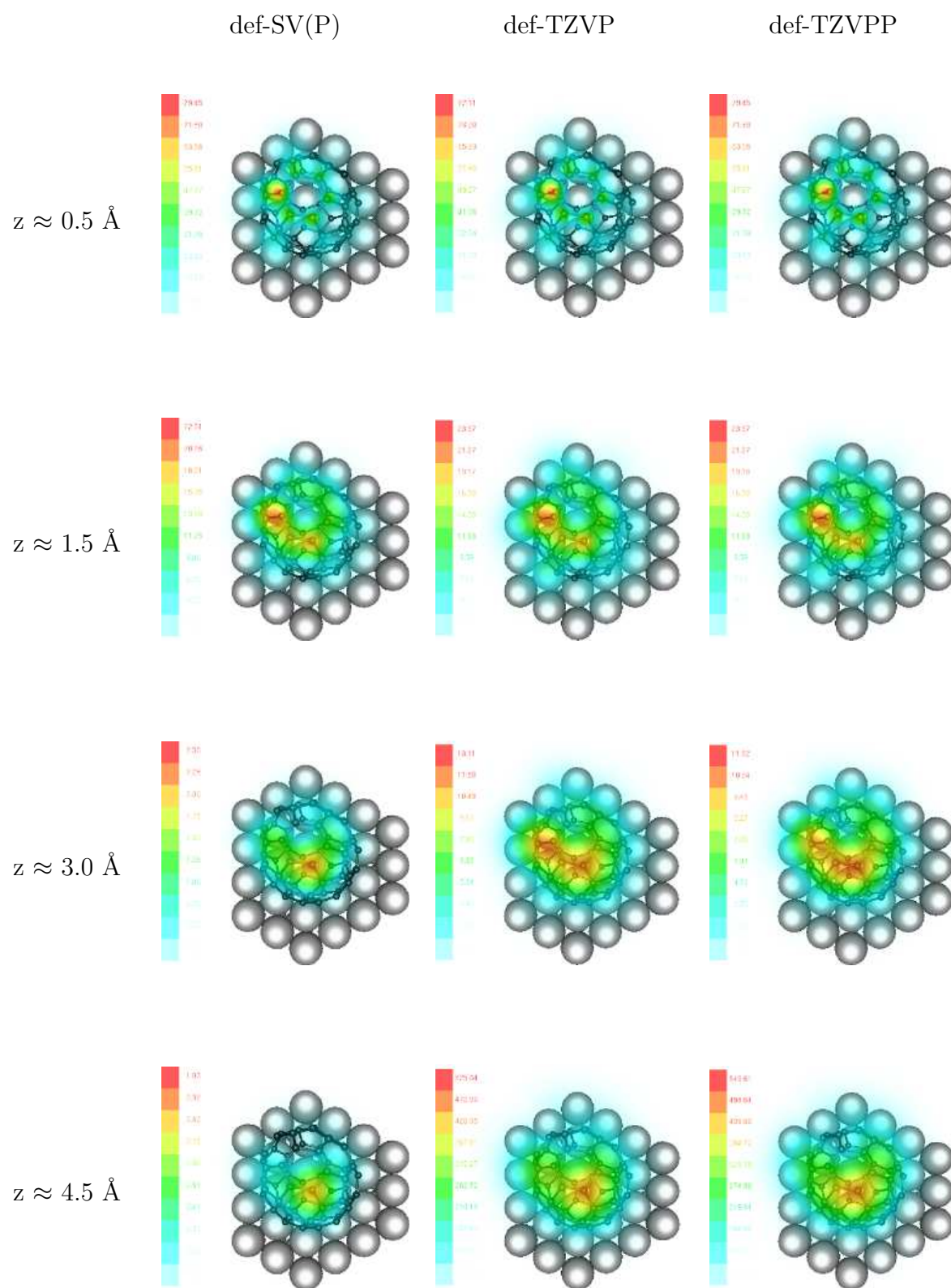


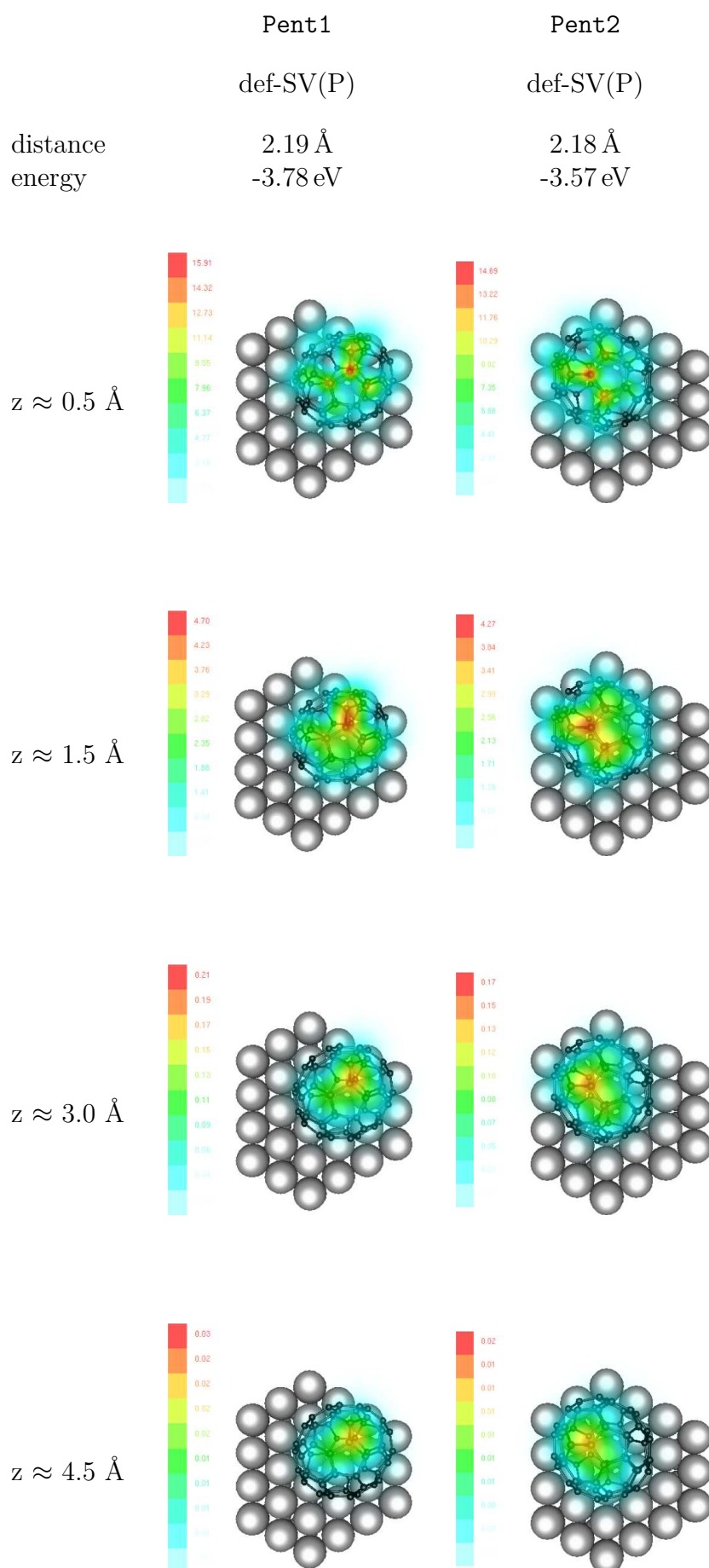
**C<sub>58</sub>: C<sub>s</sub> Symmetry, Hept4 after Relaxation, positive bias, def-SV(P)**

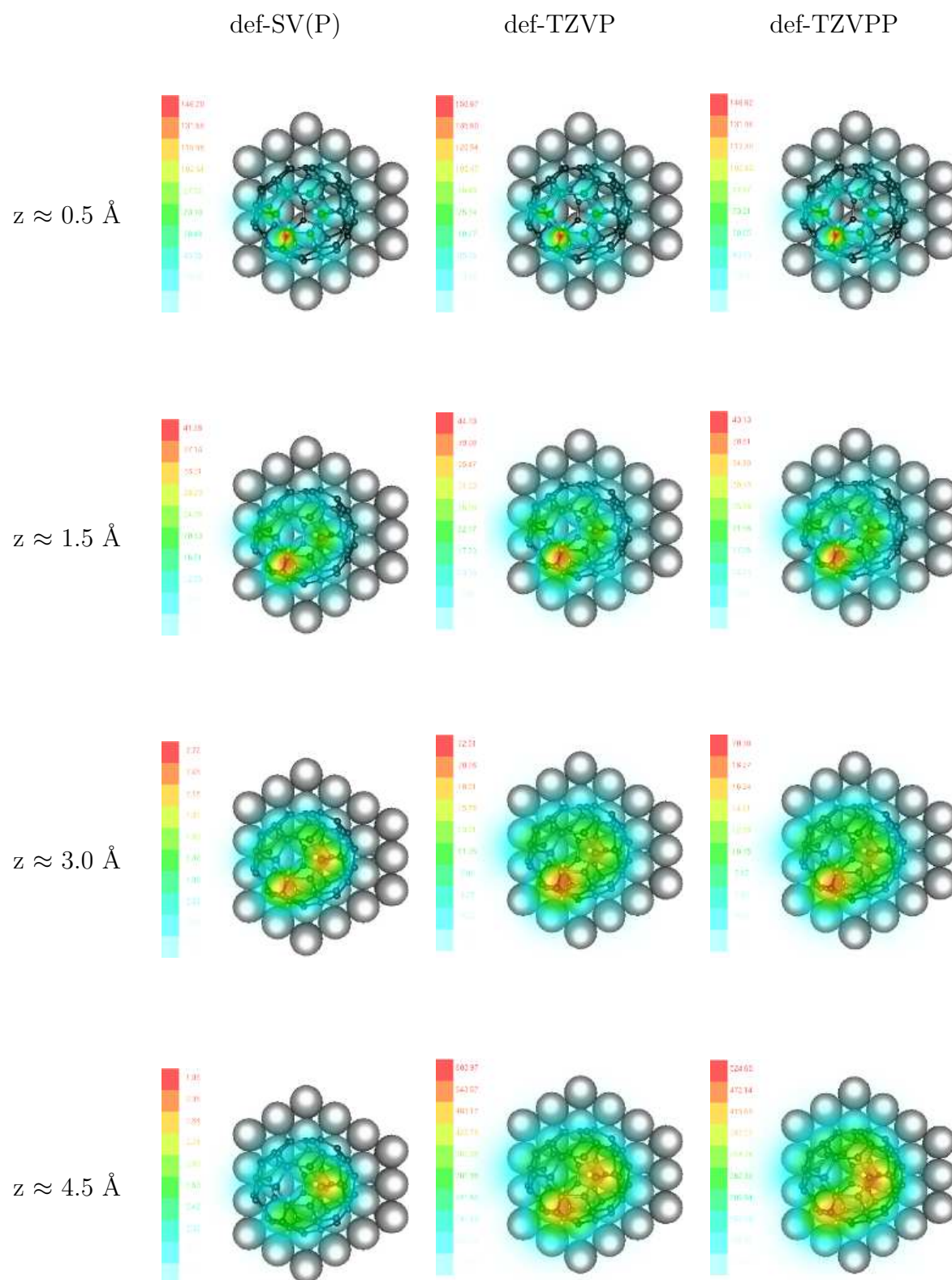
**C<sub>58</sub>: C<sub>s</sub> Symmetry, Hept4 after Relaxation, negative bias, def-TZVP**

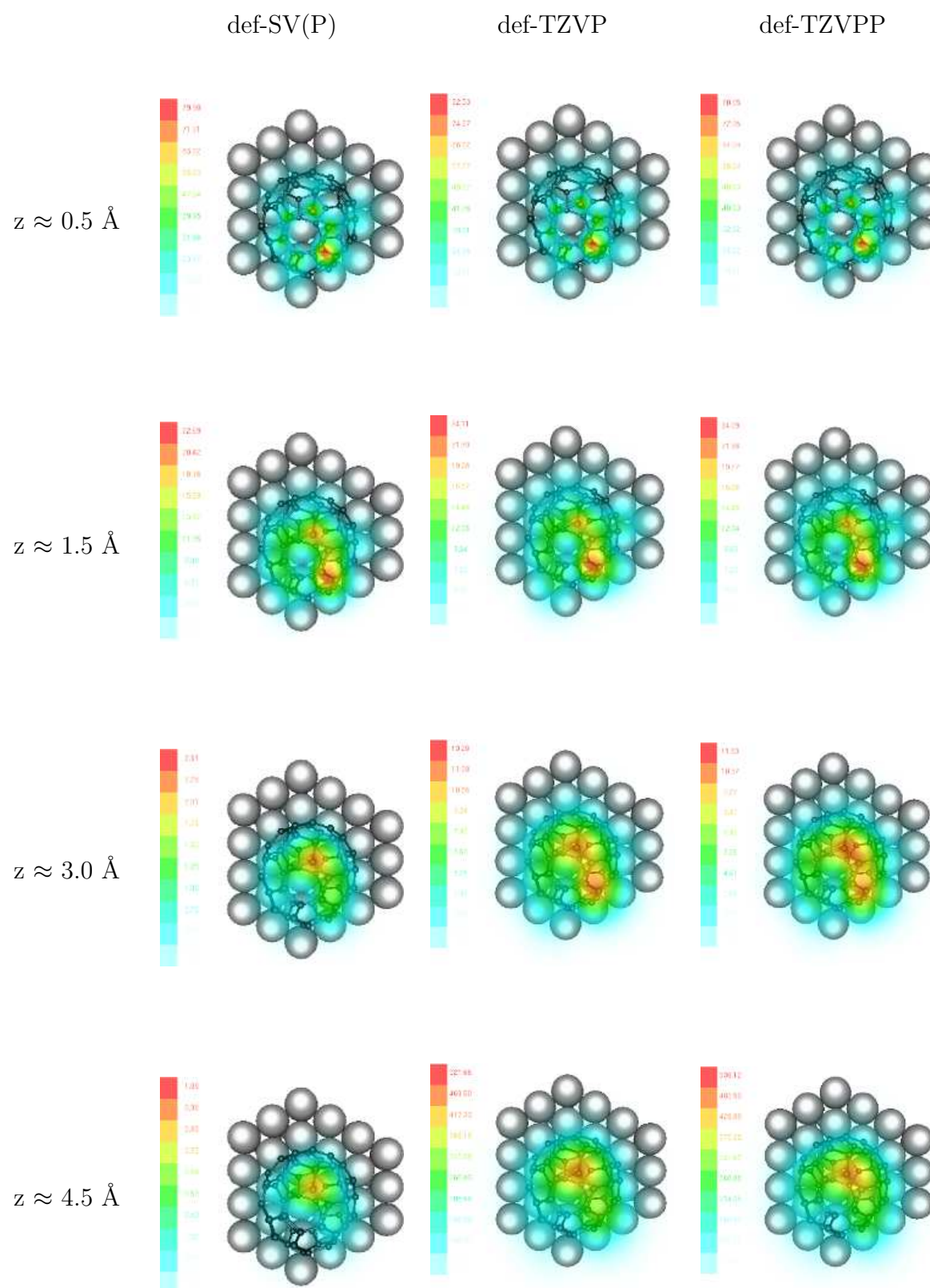
**C<sub>58</sub>: C<sub>s</sub> Symmetry, Hept4 after Relaxation, positive bias, def-TZVP**

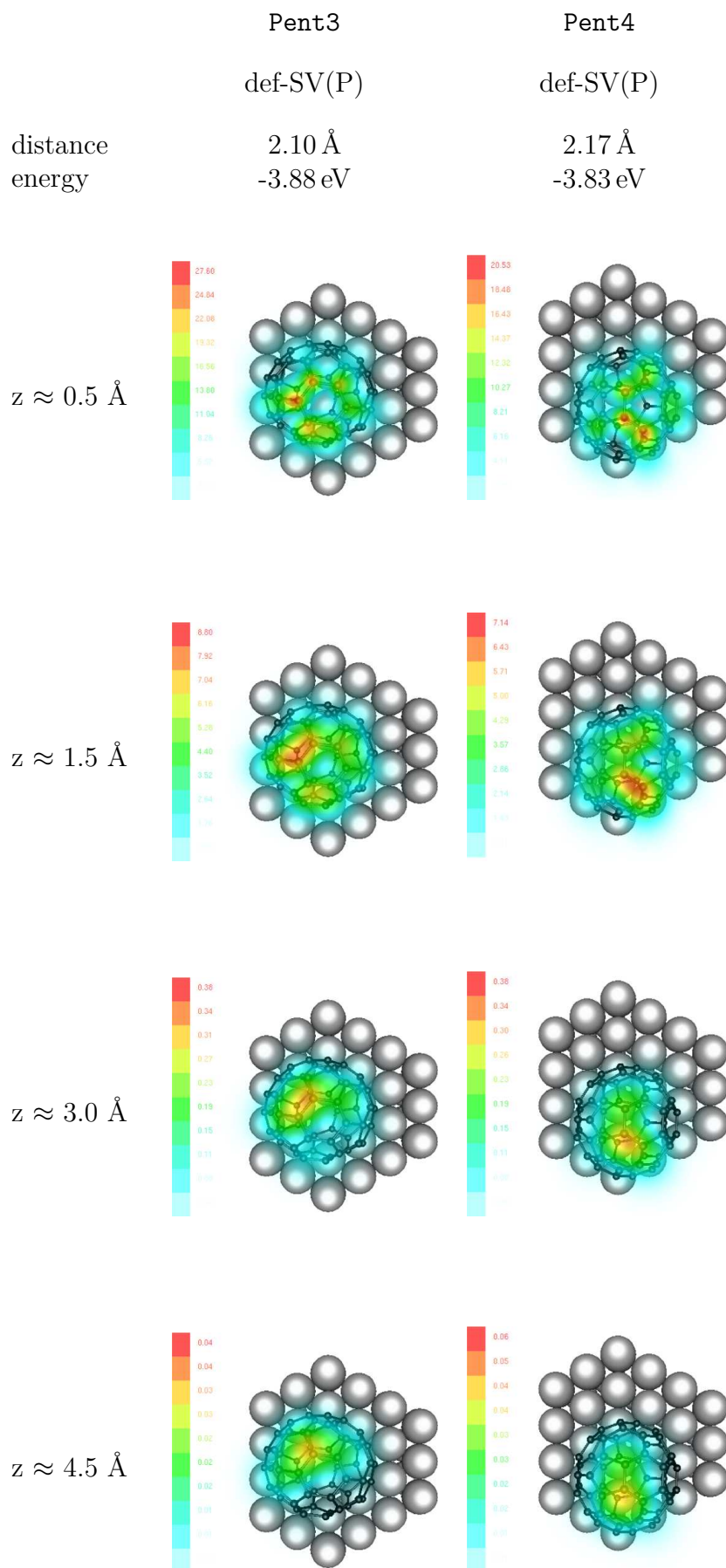
**C<sub>58</sub>: C<sub>s</sub> Symmetry, Pent1 without Relaxation, 2.38 Å, -2.33 eV**

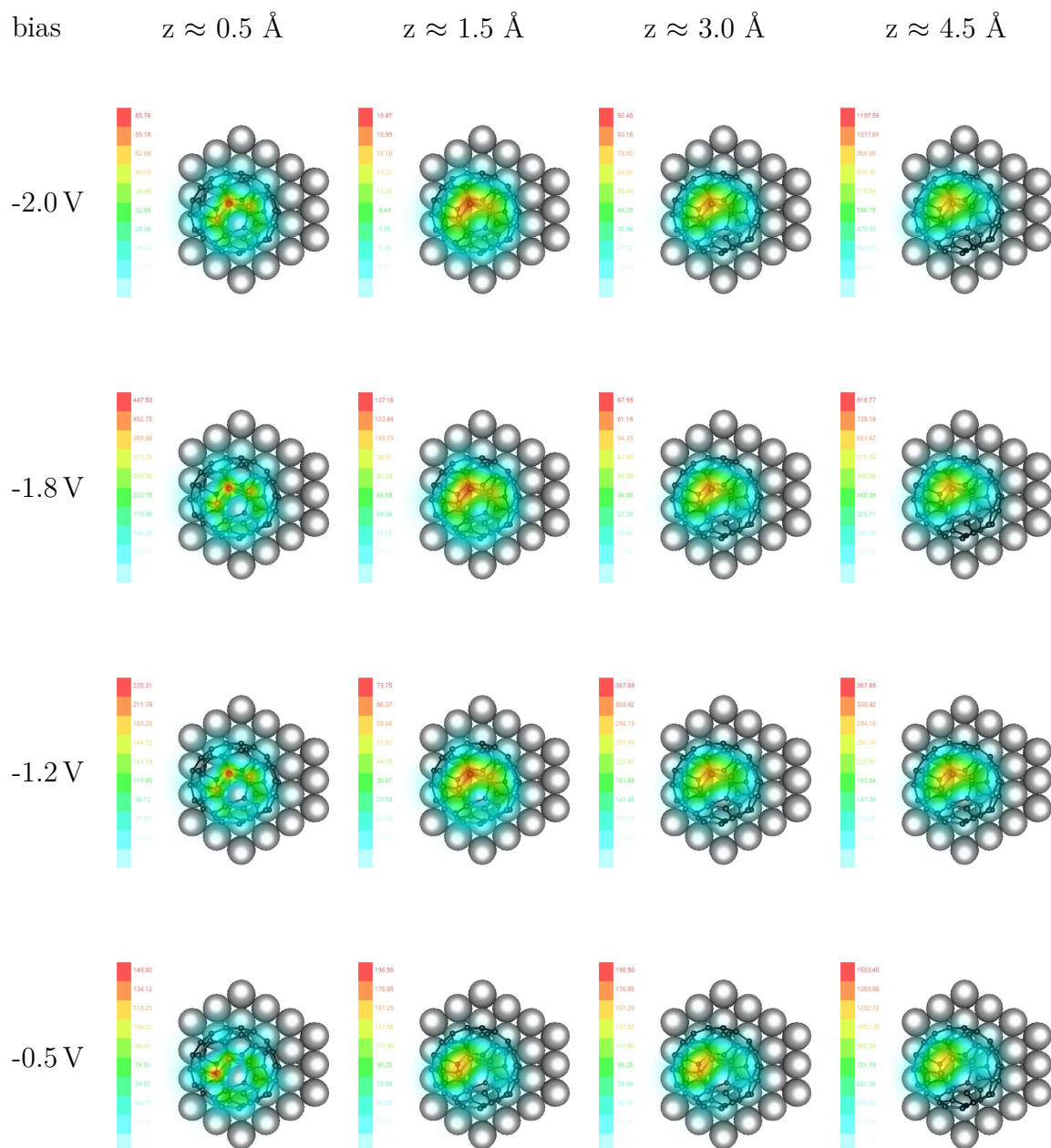
**C<sub>58</sub>: C<sub>s</sub> Symmetry, Pent2 without Relaxation, 2.38 Å, -2.34 eV**

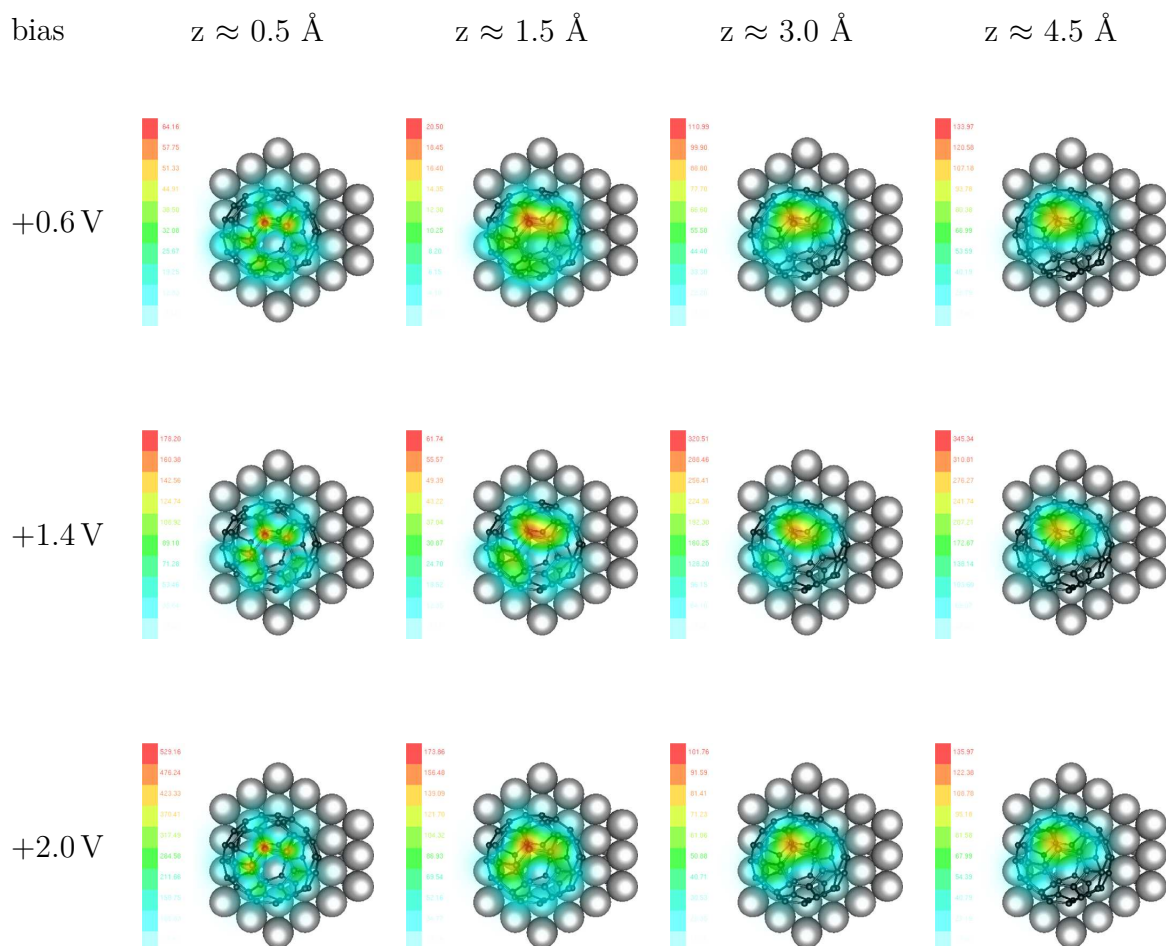
**C<sub>58</sub>: C<sub>s</sub> Symmetry, Pent1 and Pent2 after Relaxation**

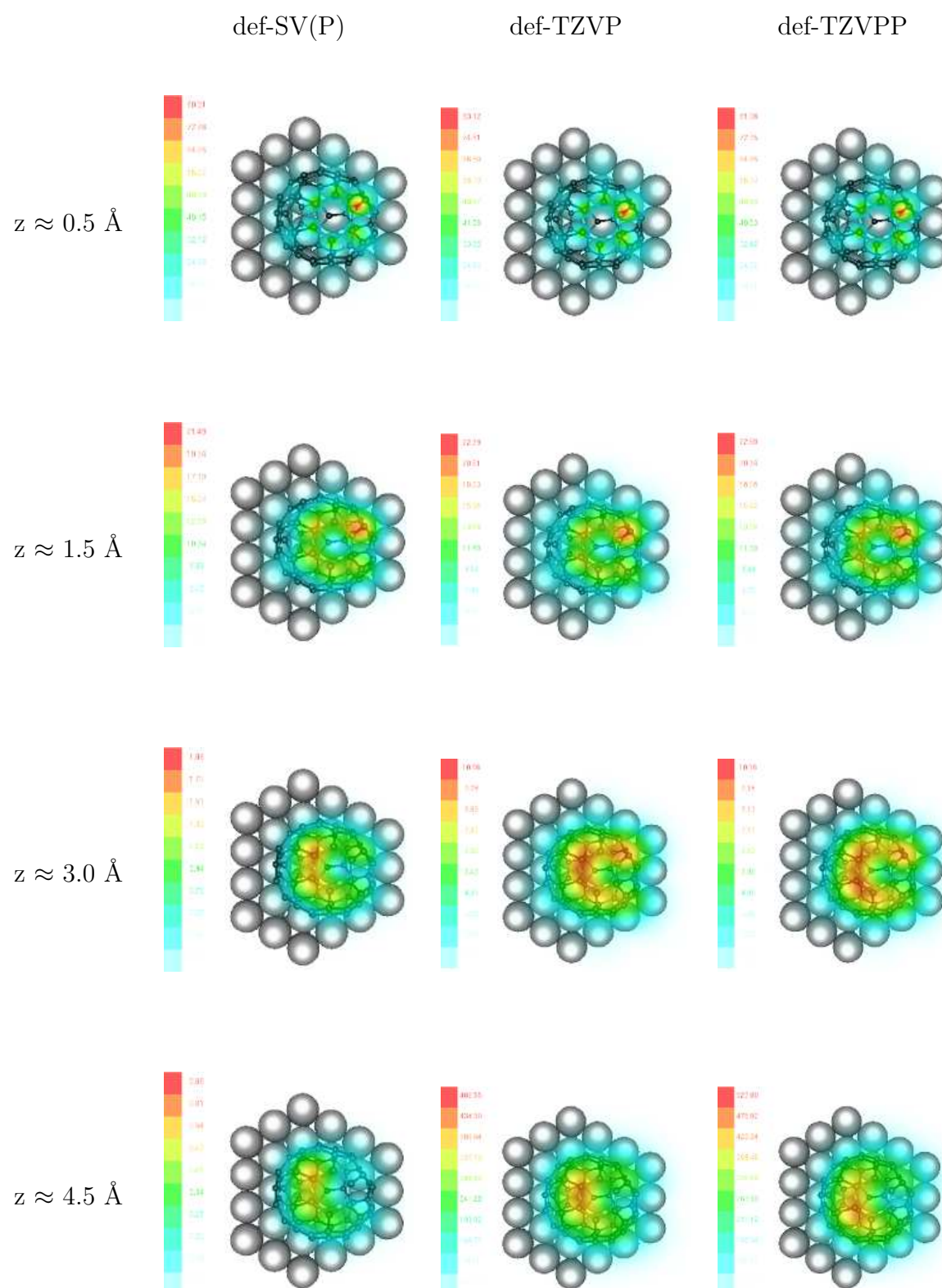
**C<sub>5s</sub>: C<sub>s</sub> Symmetry, Pent3 without Relaxation, 2.38 Å, -2.27 eV**

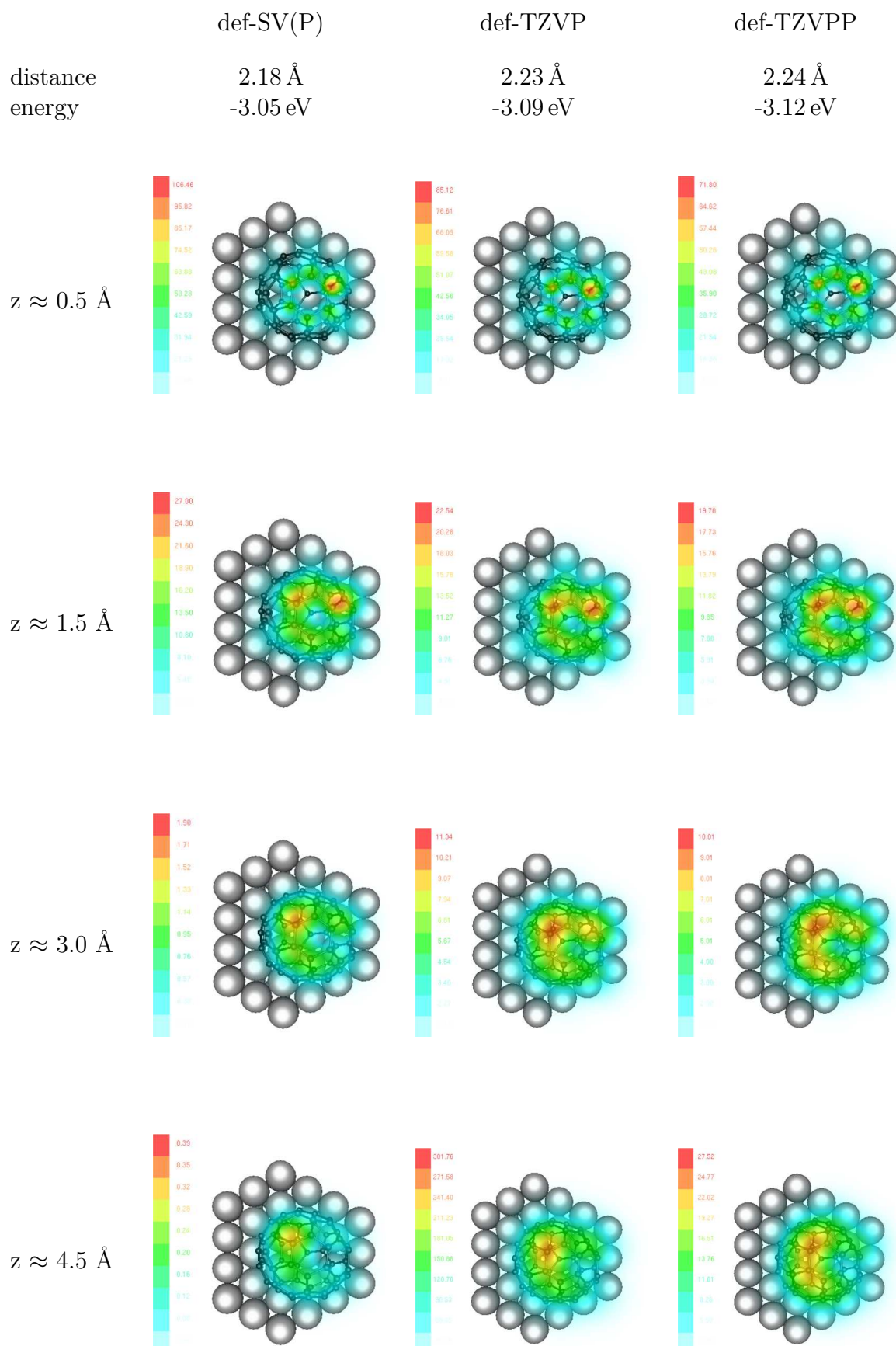
**C<sub>58</sub>: C<sub>s</sub> Symmetry, Pent4 without Relaxation, 2.38 Å, -2.41 eV**

**C<sub>58</sub>: C<sub>s</sub> Symmetry, Pent3 and Pent4 after Relaxation**

**C<sub>58</sub>: C<sub>s</sub> Symmetry, Pent3 after Relaxation, negative bias, def-SV(P)**

**C<sub>58</sub>: C<sub>s</sub> Symmetry, Pent3 after Relaxation, positive bias, def-SV(P)**

**C<sub>58</sub>: C<sub>s</sub> Symmetry, Pent5 without Relaxation, 2.43 Å, -2.19 eV**

**C<sub>58</sub>: C<sub>s</sub> Symmetry, Pent5 after Relaxation**

---

## Bibliography

- [1] H. W. Kroto, J. R. Heath, S. C. O'Brien, R. F. Curl and R. E. Smalley, *C<sub>60</sub>: Buckminsterfullerene*, Nature **318**, 162 (1985).
- [2] X. Lu and Z. Chen, *Curved Pi-Conjugation, Aromaticity, and the Related Chemistry of Small Fullerenes (< C<sub>60</sub>) and Single-Walled Carbon Nanotubes*, Chemical Reviews **105**(10), 3643 (2005).
- [3] S. Iijima, *Helical microtubules of graphitic carbon*, Nature **354**, 56 (1991).
- [4] M. S. Dresselhaus, G. Dresselhaus and P. C. Eklund, *Science of Fullerenes and Carbon Nanotubes* (Academic Press, San Diego [u.a.], 1996).
- [5] C. Joachim and J. K. Gimzewski, *An electromechanical amplifier using a single molecule*, Chemical Physics Letters **265**(3&5), 353 (1997).
- [6] S. J. Tans, A. R. M. Verschueren and C. Dekker, *Room-temperature transistor based on a single carbon nanotube*, Nature **393**, 49 (1998).
- [7] S. Ami and C. Joachim, *Logic gates and memory cells based on single C<sub>60</sub> electromechanical transistors*, Nanotechnology **12**(1), 44 (2001).
- [8] D. J. Bindl, M.-Y. Wu, F. C. Prehn and M. S. Arnold, *Efficiently Harvesting Excitons from Electronic Type-Controlled Semiconducting Carbon Nanotube Films*, Nano Letters **11**(2), 455 (2011).
- [9] Q. L. Zhang, S. C. O'Brien, J. R. Heath, Y. Liu, R. F. Curl, H. W. Kroto and R. E. Smalley, *Reactivity of Large Carbon Clusters: Spheroidal Carbon Shells and Their Possible Relevance to the Formation and Morphology of Soot*, The Journal of Physical Chemistry **90**(4), 525 (1986).
- [10] Y. Liu, S. C. O'Brien, Q. Zhang, J. R. Heath, F. K. Tittel, R. F. Curl, H. W. Kroto and R. E. Smalley, *Negative Carbon Cluster Ion Beams: New Evidence for the Special Nature of C<sub>60</sub>*, Chemical Physics Letters **126**(2), 215 (1986).
- [11] P. R. Cromwell, *Polyhedra : One of the Most Charming Chapters of Geometry* (Cambridge University Press, Cambridge, United Kingdom [u.a.], 1997).

- 
- [12] P. W. Fowler and D. E. Manolopoulos, *An Atlas of Fullerenes*, The international series of monographs on chemistry ; 30 (Clarendon Press, Oxford [u.a.], 1995).
- [13] H. W. Kroto, *The stability of the fullerenes  $C_n$ , with  $n = 24, 28, 32, 36, 50, 60$  and  $70$* , Nature **329**, 529 (1987).
- [14] T. G. Schmalz, W. A. Seitz, D. J. Klein and G. E. Hite, *Elemental Carbon Cages*, Journal of the American Chemical Society **110**(4), 1113 (1988).
- [15] E.E.B. Campbell, P.W. Fowler, D. Mitchell and F. Zerbetto, *Increasing cost of pentagon adjacency for larger fullerenes*, Chemical Physics Letters **250**(5), 544 (1996).
- [16] E. Albertazzi, C. Domene, P. W. Fowler, T. Heine, G. Seifert, C. Van Alsenoy and F. Zerbetto, *Pentagon adjacency as a determinant of fullerene stability*, Physical Chemistry Chemical Physics **1**, 2913 (1999).
- [17] E. Hernández, P. Ordejón and H. Terrones, *Fullerene growth and the role of nonclassical isomers*, Physical Review B **63**, 193403 (2001).
- [18] R. C. Haddon, L. E. Brus and K. Raghavachari, *Rehybridization and  $\pi$ -Orbital Alignment: the Key to the Existence of Spheroidal Carbon Clusters*, Chemical Physics Letters **131**(3), 165 (1986).
- [19] R. C. Haddon, *Chemistry of the Fullerenes: The Manifestation of Strain in a Class of Continuous Aromatic Molecules*, Science **261**(5128), 1545 (1993).
- [20] S. Petrie and D. K. Bohme, *Enhanced reactivity of fullerene cations containing adjacent pentagons*, Nature **365**, 426 (1993).
- [21] A. Bihlmeier, C. C. M. Samson and W. Klopper, *DFT Study of Fullerene Dimers*, Chem. Phys. Chem. **6**(12), 2625 (2005).
- [22] D.-L. Chen, W. Q. Tian, J.-K. Feng and C.-C. Sun, *Structures, Stabilities, and Electronic and Optical Properties of  $C_{58}$  Fullerene Isomers, Ions, and Metallofullerenes*, Chem. Phys. Chem. **8**(7), 1029 (2007).
- [23] A. Böttcher, *private communication*, 2011/2012.
- [24] W. Krätschmer, L. D. Lamb, K. Fostiropoulos and D. R. Huffman, *Solid  $C_{60}$ : A New Form of Carbon*, Nature **347**, 354 (1990).
- [25] A. Böttcher, P. Weis, A. Bihlmeier and M. M. Kappes,  *$C_{58}$  on HOPG: Soft-landing adsorption and thermal desorption*, Physical Chemistry Chemical Physics **6**, 5213 (2004).
- [26] G. Binnig and H. Rohrer, *Scanning tunneling microscopy - from birth to adolescence*, Reviews of Modern Physics **59**, 615 (1987).

- 
- [27] F. Witt, *Untersuchung des Elektronentransportes über einzelne Phthalocyaninmoleküle*, Diplomathesis, Universität Karlsruhe (TH), 2008.
- [28] A. Bork, *Ladungs- und Spintransport durch einzelne Moleküle*, Dipolmathesis, Universität Karlsruhe (TH), 2009.
- [29] K. Capelle, *A Bird's-Eye View of Density-Functional Theory* (2006).
- [30] P. Hohenberg and W. Kohn, *Inhomogeneous Electron Gas*, Physical Review **136**, B864 (1964).
- [31] M. Levy, *Universal variational functionals of electron densities, first-order density matrices, and natural spin-orbitals and solution of the  $v$ -representability problem*, Proceedings of the National Academy of Sciences **76**(12), 6062 (1979).
- [32] R. Ahlrichs, M. Bär, M. Häser, H. Horn and C. Kölmel, *Electronic Structure Calculations on Workstation Computers: The Program System TURBOMOLE*, Chemical Physics Letters **162**(3), 165 (1989).
- [33] O. Treutler and R. Ahlrichs, *Efficient molecular numerical integration schemes*, The Journal of Chemical Physics **102**(1), 346 (1995).
- [34] M. Von Arnim and R. Ahlrichs, *Performance of Parallel TURBOMOLE for Density Functional Calculations*, Journal of Computational Chemistry **19**(15), 1746 (1998).
- [35] K. Eichkorn, O. Treutler, H. Öhm, M. Häser and R. Ahlrichs, *Auxiliary basis sets to approximate Coulomb potentials*, Chemical Physics Letters **242**(6), 652 (1995).
- [36] K. Eichkorn, F. Weigend, O. Treutler and R. Ahlrichs, *Auxiliary basis sets for main row atoms and transition metals and their use to approximate Coulomb potentials*, Theoretical Chemistry Accounts: Theory, Computation, and Modeling (Theoretica Chimica Acta) **97**, 119 (1997).
- [37] R. Ahlrichs, *Efficient evaluation of three-center two-electron integrals over Gaussian functions*, Physical Chemistry Chemical Physics **6**, 5119 (2004).
- [38] M. Sierka, A. Hogekamp and R. Ahlrichs, *Fast evaluation of the Coulomb potential for electron densities using multipole accelerated resolution of identity approximation*, The Journal of Chemical Physics **118**(20), 9136–9148 (2003).
- [39] R. G. Parr and W. Yang, *Density-Functional Theory of Atoms and Molecules*, 1. iss. paperback edition, The international series of monographs on chemistry ; 16 (Oxford University Press [u.a.], New York, 1994).
- [40] S. H. Vosko, L. Wilk and M. Nusair, *Accurate spin-dependent electron liquid correlation energies for local spin density calculations: a critical analysis*, Canadian Journal of Physics **58**(8), 1200 (1980).

- 
- [41] A. D. Becke, *Density-functional exchange-energy approximation with correct asymptotic behavior*, Physical Review A **38**, 3098 (1988).
- [42] J. P. Perdew, *Density-functional approximation for the correlation energy of the inhomogeneous electron gas*, Physical Review B **33**, 8822 (1986).
- [43] A. Bihlmeier, *Dichtefunktionaluntersuchungen zur Reaktivität von non-IPR-Fullerenen*, PhD thesis, Karlsruher Institut für Technologie, 2009.
- [44] A. D. Becke, *Density-functional thermochemistry. III. The role of exact exchange*, The Journal of Chemical Physics **98**(7), 5648 (1993).
- [45] S. Grimme, *Accurate Description of van der Waals Complexes by Density Functional Theory Including Empirical Corrections*, Journal of Computational Chemistry **25**(12), 1463 (2004).
- [46] S. Grimme, *Semiempirical GGA-Type Density Functional Constructed with a Long-Range Dispersion Correction*, Journal of Computational Chemistry **27**(15), 1787 (2006).
- [47] S. Grimme, J. Antony, S. Ehrlich and H. Krieg, *A consistent and accurate ab initio parametrization of density functional dispersion correction (DFT-D) for the 94 elements H-Pu*, The Journal of Chemical Physics **132**(15), 154104 (2010).
- [48] W. J. Hehre, R. F. Stewart and J. A. Pople, *Self-Consistent Molecular-Orbital Methods. I. Use of Gaussian Expansions of Slater-Type Atomic Orbitals*, The Journal of Chemical Physics **51**(6), 2657 (1969).
- [49] F. Weigend, M. Häser, H. Patzelt and R. Ahlrichs, *RI-MP2: optimized auxiliary basis sets and demonstration of efficiency*, Chemical Physics Letters **294**(1), 143 (1998).
- [50] F. Weigend, *Accurate Coulomb-fitting basis sets for H to Rn*, Physical Chemistry Chemical Physics **8**, 1057 (2006).
- [51] A. Schäfer, H. Horn and R. Ahlrichs, *Fully optimized contracted Gaussian basis sets for atoms Li to Kr*, The Journal of Chemical Physics **97**(4), 2571 (1992).
- [52] A. Schäfer, C. Huber and R. Ahlrichs, *Fully optimized contracted Gaussian basis sets of triple zeta valence quality for atoms Li to Kr*, The Journal of Chemical Physics **100**(8), 5829 (1994).
- [53] F. Evers, F. Weigend and M. Koentopp, *Conductance of molecular wires and transport calculations based on density-functional theory*, Physical Review B **69**, 235411 (2004).
- [54] A. Arnold, F. Weigend and F. Evers, *Quantum chemistry calculations for molecules coupled to reservoirs: Formalism, implementation, and application to benzenedithiol*, The Journal of Chemical Physics **126**(17), 174101 (2007).

- 
- [55] F. Evers and A. Arnold, *Molecular Conductance from Ab Initio Calculations: Self Energies and Absorbing Boundary Conditions*, in: *CFN Lectures on Functional Nanostructures - Volume 2*, , Lecture Notes in Physics, Vol. 820 (Springer Berlin / Heidelberg, 2006), p. 27.
- [56] J. Tersoff and D. R. Hamann, *Theory and Application for the Scanning Tunneling Microscope*, Physical Review Letters **50**, 1998 (1983).
- [57] J. Tersoff and D. R. Hamann, *Theory of the scanning tunneling microscope*, Physical Review B **31**, 805 (1985).
- [58] M. De Menech, U. Saalmann and M. E. Garcia, *Energy-resolved STM mapping of C<sub>60</sub> on metal surfaces: A theoretical study*, Physical Review B **73**(Apr), 155407 (2006).
- [59] S. F. A. Kettle, *Symmetrie und Struktur : eine Einführung in die Gruppentheorie*, Teubner Studienbücher : Chemie (Teubner, Stuttgart, 1994).
- [60] C. Seiler, *Fullerene based anchoring groups for single-molecule junctions*, Diplomathesis, Karlsruhe Institute of Technology, 2010.
- [61] <http://www.webelements.com/>.
- [62] G. Geranton, *Conductance of C<sub>60</sub> between two gold electrodes*, Master's thesis, Université Joseph Fourier, 2011.
- [63] X. Lu, M. Grobis, K. H. Khoo, S. G. Louie and M. F. Crommie, *Charge transfer and screening in individual C<sub>60</sub> molecules on metal substrates: A scanning tunneling spectroscopy and theoretical study*, Physical Review B **70**, 115418 (2004).
- [64] X. Lu, M. Grobis, K. H. Khoo, S. G. Louie and M. F. Crommie, *Spatially Mapping the Spectral Density of a Single C<sub>60</sub> Molecule*, Physical Review Letters **90**, 096802 (2003).